Università degli Studi di Palermo

Dipartimento di Ingegneria

S.S.D: ICAR/04

A thesis submitted to the Department of Engineering and the committee on graduate studies of the University of Palermo in partial fulfilment of the requirements for the degree of the European Doctor of Philosophy

A new approach to Road Pavement Management Systems by exploiting Data Analytics, Image Analysis and Deep Learning

Ph.D. Candidate

Ronald Anthony Roberts

Advisors

Prof. Gaetano Di Mino, Prof. Orazio Giuffre, Prof.ssa. Laura Inzerillo

PhD Coordinator

Prof.ssa Antonina Pirrotta

Cycle XXXIII A.A. 2020/2021

Granny – Hope I continue to make you proud

Preface

Road Networks are key drivers for economic success in any city, region or country. However, globally today there are enormous challenges in trying to ensure the road networks are kept in good and acceptable states throughout their life. These challenges arise from continually decreasing budgets, which now will be further impacted by the current pandemic driven economic crises. The deficiencies often result in ineffective data collection and management practices. This thesis targets alleviating some of these difficulties whilst trying to help road managers deliver better pavement management strategies and systems. Specifically, the concepts of sustainable data collection and analyses are tackled. The study identifies low-cost but accurate strategies and techniques to collect road condition data mainly using simple and readily available devices such as smartphones and drones.

Imagery is collected from smartphones and cameras, and the images are used in two important workflows. The first develops deep learning models capable of detecting where pavement distresses occur to carry out hotspot analyses on road networks whilst providing an idea of the severity of damages. The second uses images in a 3D modelling workflow to reconstruct and segment pavements to pinpoint and analyse the distresses producing metric assessments of damage levels at specific points within road networks. Several case studies are built using different equipment parameters and in different environmental conditions in Italy and France to validate the techniques and the models developed.

To add to the robust workflows developed, historical maintenance data and available statistical geographical and environmental information are leveraged in a novel data analytics approach. This is done to predict timelines for maintenance activities in a network to guide and to be used in conjunction with the work done using the imagery and the related image-based models. This was done to ensure the context of the particular network is understood.

Combined these approaches add key workflows to data collection systems in under-resourced networks and organizations. In the workflows, pavement data can be more readily collected so that they can be analyzed and finally used in the road asset database. This allows road managers to better answer the tough questions of where, when and how to carry out their maintenance to ensure road networks are kept in better states to keep economic activities advancing, all in a sustainable approach.

Graphical Abstract

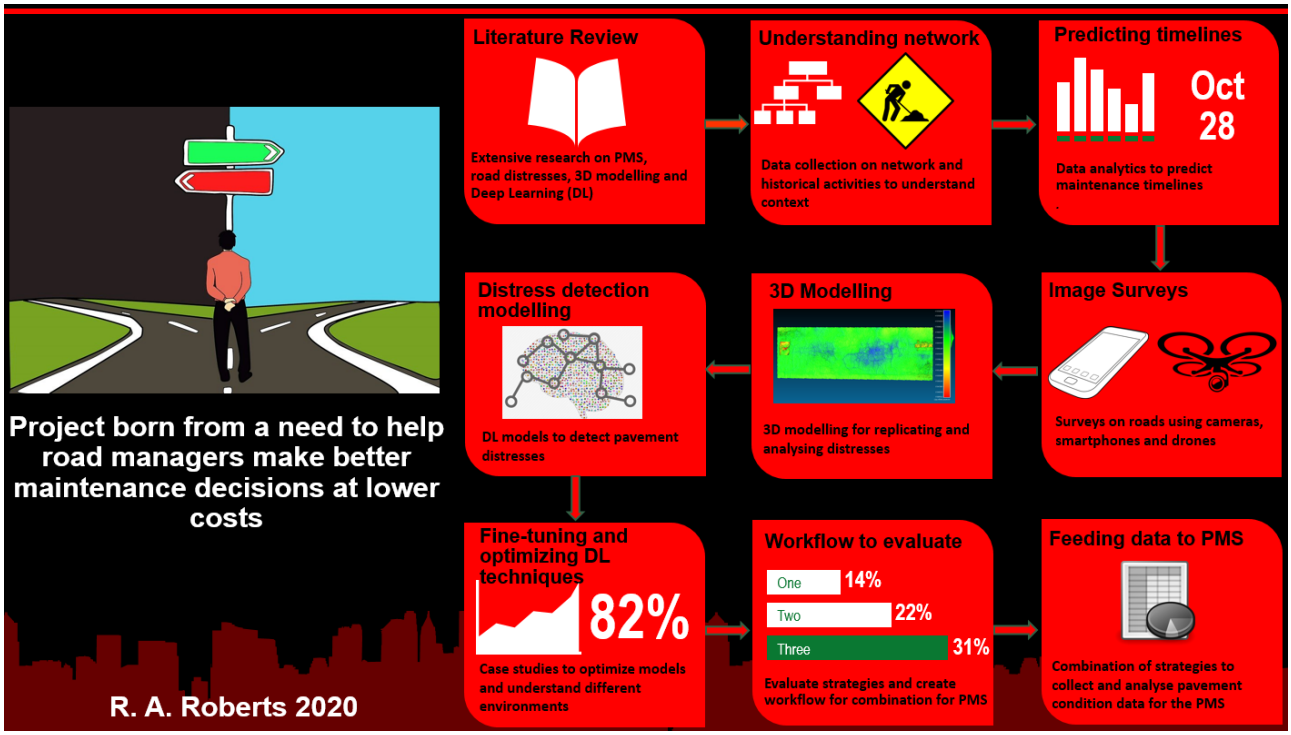

Wordcloud from thesis

Publications included in the current thesis

The Chapters of this thesis have been produced as parts or slightly modified parts of the following international publications:

- **"Image-based 3D reconstruction using traditional and UAV datasets for analysis of road pavement distress"** *published in the international journal "Automation in Construction". [doi:10.1016/j.autcon.2018.10.010].*
- **"Towards low-cost pavement condition health monitoring and analysis using deep learning"** *published in the international Open Access journal "Applied Sciences". [doi:10.3390/app10010319].*
- *"**Exploiting low-cost 3D imagery for the purposes of detecting and analyzing pavement distresses**" published in the international Open Access journal "Infrastructures. [doi:10.3390/infrastructures5010006].*
- *"**Developing a framework for using structure-from-motion techniques for road distress applications**" published in the international Open Access journal "European Transport-Trasporti Europei". [www.istiee.unict.it/sites/default/files/files/2_5_ET_76.pdf].*
- *"**Towards more sustainable pavement management practices using embedded sensor technologies**" published in the international Open Access journal "Infrastructures". [doi:10.3390/infrastructures5010004].*
- *"**Using UAV Based 3D Modelling to Provide Smart Monitoring of Road Pavement Conditions**" published in the international Open Access journal "Information". [doi: 10.3390/info11120568]*
- *"**Exploiting 3D modelling and life cycle assessment to improve the sustainability of pavement management**" published in the international journal "Smart Innovation, Systems and Technologies". [doi:10.1007/978-3-030-48279-4_137].*
- ***"Exploiting Data Analytics and Deep Learning Systems to Support Pavement Maintenance Decisions"** published in the international Open access journal "Applied Sciences". [doi: 10.3390/app11062458].*

The project has also produced the following publications:

- ***"Image-based 3D reconstruction using traditional and mobile phone data sets for road pavement distress analysis".** Conference Proceedings of the 7th Eurasphalt & Eurobitume Congress. [ISBN: 9789080288461].*
- ***"3D Image-Based Modelling Using Google Earth Imagery for 3D Landscape Modelling"** Conference proceedings of Advances in Intelligent Systems and Computing. [doi:10.1007/978-3-030-12240-9_65].*
- ***"3D Modeling of a complex building: from multi-view image fusion to google earth publication"** Conference proceedings of International Archives of the Photogrammetry, Remote Sensing and Spatial Information Sciences. [doi:10.5194/isprs-archives-XLII-2-W15-577-2019].*
- ***"Optimization of Cultural Heritage Virtual Environments for Gaming Applications".** Conference proceedings for Advances in Information and Communication. [doi:10.1007/978-3-030-39445-5_27].*
- ***"Towards more sustainable airfield pavements using Life-cycle assessment of design alternatives".** Conference proceedings of the International Symposium on Pavement. Roadway, and Bridge Life Cycle Assessment 2020. [doi:10.1201/9781003092278-3].*

Acknowledgements

Firstly, I would like to express my sincerest gratitude towards the European Union, from whom funding for my project was realized under the Marie Curie Skłodowska Actions and the Horizon 2020 Programme. My project was conceived within the SMARTI ETN Project and received funding from the European Union's Horizon 2020 Programme under the Marie Skłodowska-Curie actions for research, technological development and demonstration, under grant n.721493. Without this funding, my project and studies would not have been possible.

I would also like to thank my supervisors at the University of Palermo, Professors Gaetano Di Mino and Laura Inzerillo. They placed their trust and confidence in my abilities when they selected me and provided constant guidance throughout my work to ensure my work continued. Their support was not only for my work but also in providing me with a constant mental and emotional backbone to keep going despite the struggles and rigour of the PhD. The two of them became my local parental figures and I will always remember their kindness and persistent support. I thank them for selecting me and I can only hope that I have delivered on the faith they placed in me. I am also thankful to the PhD board of advisors and the members of the Department of Engineering for giving me this opportunity and providing support during the period including especially, the direction of Prof. Orazio Giuffre, Prof. Davide Lo Presti and the consistent support of Antonino Lorello. I would also like to thank Dr Fabio Galatioto, who recommended the position to me and implored me to apply, stressing that the gelato and pizza in Sicily are amazing – he was not wrong!

I would also like to thank my supervisor during my time in France, Dr Fabient Menant. The circumstances under which I was there were difficult, having to cope with the pandemic and the ensuing chaos of the world and it was comforting to know I had the support of someone interested in my research and who was always there if I needed help not only with work but also for any difficulties. I thank him for his kindness throughout the period. He was also instrumental in fine-tuning important aspects of my research, offering critical feedback and suggestions that helped to make the research stronger. Because of all of this, notwithstanding the pandemic situation, I will always have fond memories of Nantes. My gratitude also extends

to the support staff at Ifsttar, especially the MAST department, who openly welcomed me into their staff and made it feel like I was a part of their team.

Whilst it may seem strange, a piece of gratitude must be given to 'memes', which represent a constant social media outpouring of comedy, satire and parodies in visual forms in today's society, and which provided me with comedy relief throughout my struggles in the darkest of times. Whilst 'memes' are not persons, I thank those who developed them and helped me smile even when the world seemed lost.

Thanks must also be given to the big guy above, who looks over us - thank you for giving me life and allowing me to pursue my research and studies. It is something we often take for granted but should not as no day is promised. To close, my deepest levels of thank you's are to my family and friends who have stayed with me throughout my time in Palermo and my life.

To my friends across the world, from Guyana, the UK, across Europe and everywhere else, thanks for the conversations and the laughter we have shared throughout these three years. Special mention must also be given to the friends I have gained from SMARTI and Palermo, with who I'm sure I will maintain contact with beyond the project and my time in Palermo.

To my Palermo brothers – Iain, Kostas and Gaspare – thank you for being my family in Palermo. For all the nights out, the coffee breaks, the walks, the random nonsensical conversations and the serious ones, and of course sneaky princes – it has been a pleasure and I could not have survived Palermo without you.

To my family, especially my brother and my Mom, there is no single thank you that I can say that can cover my gratitude for your support. To my Mom, thank you for waking me up at 4 am, thank you for making sure I got everything I needed and thank you for always believing in and supporting me. Everything I have ever accomplished or will ever accomplish is because of you and the sacrifices you made to get me to where I needed to be. Thank you.

Finally, to Sasha, there is no PhD without you. It is as simple as that. Your support has always kept me going throughout my time in Palermo and your voice in my head believing in me has guided me and is one of the main reasons I am nearly at the end of this journey. Thanks for being my best friend and the best part of my day. Thank you for sticking with me. #tillghostponies.

List of Abbreviations

AASHTO: American Association of State Highway and Transportation Officials
AI: Artificial Intelligence
ANN: Artificial Neural Network
ASTM: American Society for Testing and Materials
C2M: cloud to model
CAD: Computer-Aided Drafting
CatBoost: Categorical Boosting
CNN: Convolutional Neural Network
COCO: Common Objects in Context
df: dataframe
DL: Deep Learning
Faster R-CNN: Faster Region-based Convolutional Neural Networks
FCN: Fully Convolutional Network
FPN: Feature Pyramid Network
GA: Genetic Algorithm
GSD: Ground Sample Distance
IOU: Intersection over Union
IRI: International Roughness Index
LCMS: Laser Crack Measurement System
lr: learning rate
LTPP: Long-Term Pavement Performance
ML: Machine Learning
MR&R: Maintenance Rehabilitation and Reconstruction
NCHRP: National Cooperative Highway Research Program
NN: Neural Networks
NRMSE: Normalized Root Mean Square Error
PASCAL VOC: Pattern Analysis, Statistical Modelling, and Computational Learning Visual Object Challenge
PCI: Pavement Condition Index
PM: Pavement Management
PMS: Pavement Management System
PPN: Pooling Pyramid Network
PSI: Present Serviceability Index
PSR: Present Serviceability Rating
RANSAC: RANdom SAmpling Consensus
RMSE: Root Mean Square Error
SfM: Structure from Motion
SHAP: Shapely Additive explanations
SSD: Single Shot Multi-box detector
UAV: Unmanned Aerial Vehicle
wd: weight decay
YOLO: You Only Look Once

List of symbols/equation parameters

$Y_{i,m}$ = *measured value*
$Y_{i,e}$ = *estimated value*
D = *object distance*
f = *focal length*
px_{size} = *pixel size*
β =*Weibull shape parameter*
η = *Weibull scale parameter*
γ = *Weibull location parameter*
dH = *average height of deformation*
dV = *average volume of deformation*
TP = *True Positive*
FP = *False Positive*
TN = *True Negative*
FN = *False Negative*
AR = *Aspect Ratio*

Distress Labels
LC – *Longitudinal cracking*
TC – *Transverse cracking*
BC – *Block cracking*
GC – *General cracking*
AC – *Area cracking*
VP – *Visco-plastic deformations*
RV – *Ravelling*
MSC – *Miscellaneous distresses*

Table of contents

List of figures

List of tables

Chapter 1- Introduction: The need for Low-cost Sustainable Road Management Systems

1.1 The concept of sustainable pavement systems

In considering the general concept of sustainability, it is useful to first examine the most used definition of sustainable development derived from the Brundtland Commission Report [1] which defines it as *'development that meets the needs of the present without compromising the ability of future generations to meet their own specific needs'*. To meet this goal, sustainability is generally thought to be composed of three main need components which are the environmental, social and economic needs, and are often referred to as the 'triple bottom line'. With respect to pavements, these components affect the sustainability of many different areas of a pavement network and system as evidenced by examples shown in Figure 1-1.

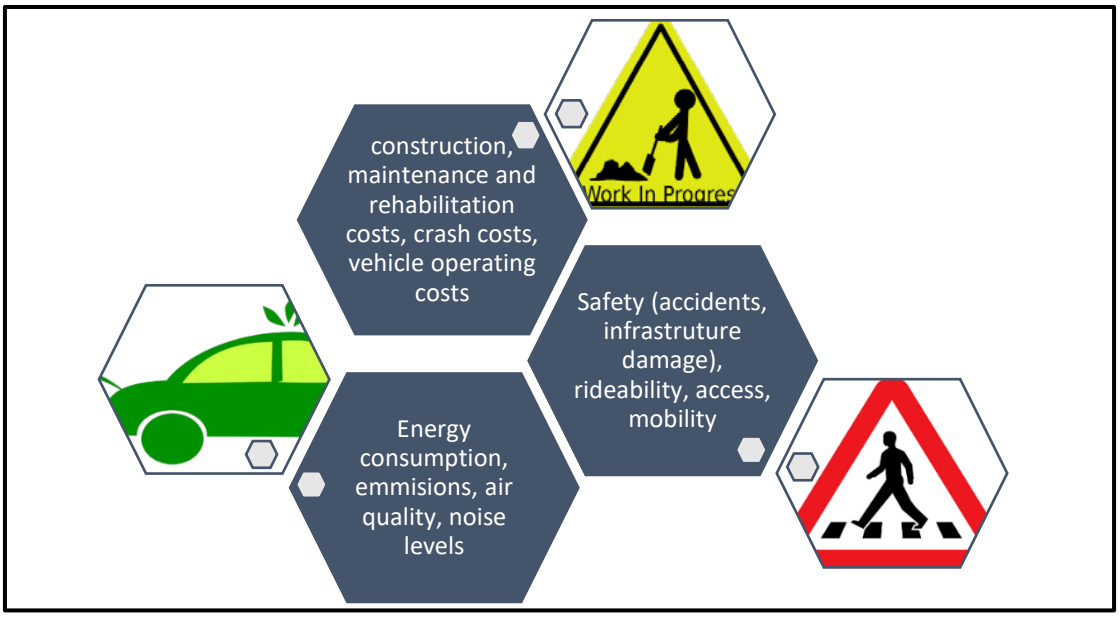

Figure 1-1. Examples of the impact of sustainability on pavements

Whilst in past years the dominant consideration has been the economic one, affecting the various costs listed in Figure 1-1, recently there have been demands for more collective and assertive considerations of the environmental and social aspects. This has been led by

mounting evidence that human activities are endangering the planet's health and thus the prospects of future generations and as a result, the need to implement more sustainable practices has become critical [2].

Universally, transportation can be quite energy-intensive and therefore the associated environmental impacts can be quite adverse. A sustainable pavement can be typically referred to as one that has defined system characteristics that give the pavement the ability to meet the criteria set out in Figure 1-2 [3]. This, however, is not a fixed global definition and a framework for any particular system or organization needs to be context-specific with needs and criteria varying based on the location and circumstance.

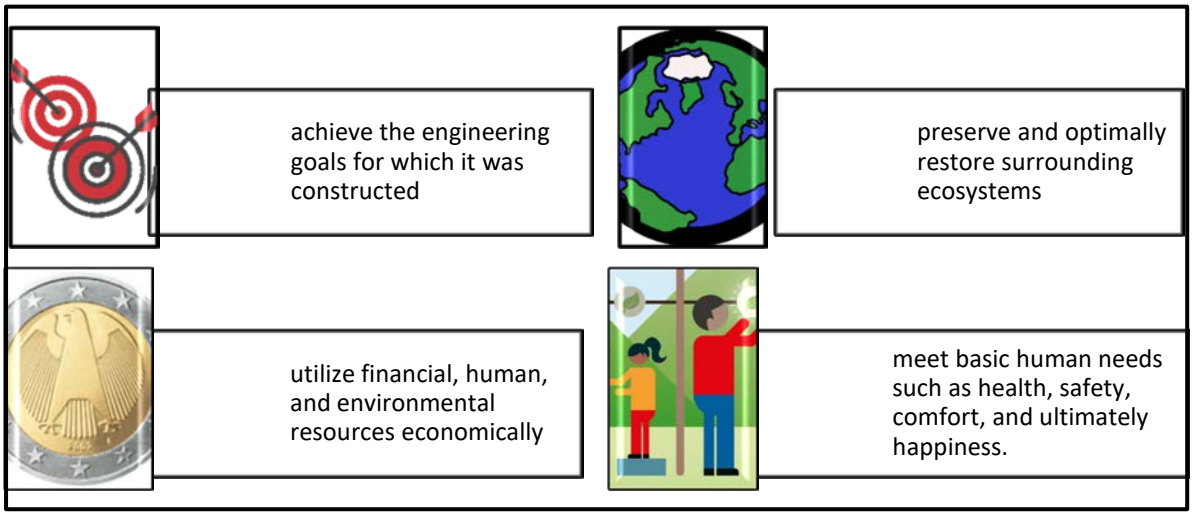

Figure 1-2. Criteria to yield a sustainable pavement

Concerning pavements, the construction, operation and maintenance of the road pavements, or road networks have been previously considered less significant in terms of environmental impacts, when compared to the potential environmental impacts by the vehicles utilizing the specific road or road network during its life cycle [4,5]. However, given the need for more sustainable transportation infrastructures and pavements, it has become apparent that aspects such as pavement construction and maintenance could lead to significantly increased amounts of energy consumption and hence, to higher amounts of emissions [4,6]. To this end, major stakeholders in the pavement community worldwide have begun to embrace the need to adopt maintenance practices that are sustainable and are continually looking for the most up-to-date and low-cost technical information and guidelines to help advance their own practices [7]. It is in this vein that this research project attempts to provide guidance and

solutions on the way forward in producing low-cost pavement maintenance guidelines and techniques to ensure that new approaches help meet the needs of a sustainable system.

1.2 The global perspective on pavement maintenance and preservation activities and programs

Pavement maintenance and its related activities and interventions generally refer to activities that can help to slow the pavement deterioration through the pinpointing and targeting of explicit deficiencies and problems that contribute to the overall deterioration of the structure. In many instances in the past, agencies and authorities have employed a 'worst-first' approach to pavement maintenance wherein the pavements are not treated until they reach a level of high distress and then major rehabilitation and maintenance is required [7]. To curb this, some agencies have stressed the importance of carrying out cost-effective preservation activities, which has spurred the movement towards more preventative and preservative programs that aim to improve safety and mobility to produce longer pavement life cycles [8]. Continually reducing agency budgets and the appreciation of life cycle costing and analyses have begun to motivate practitioners to consider the environmental and financial aspects through practices that lead towards pavement preservation.

Road networks worldwide have seen reductions in budgetary allocations for maintenance with reductions in both expenditures on investment in road networks and maintenance [9] despite the tremendous value of the asset. Considering the European network, the road network has an approximate size of 5.5 million km with an estimated value of over €8,000 billion [10]. This demonstrates the size and importance of the network towards the continual development of the region. Concurrently, The European Union Road Federation has exclaimed that the roads are in danger with issues including the absence of information and awareness on road conditions and the importance of maintenance which leads to *'chronic underfinancing and deterioration'* [10]. In particular, the road network in Italy is very old with many structures having been built decades ago and estimates indicating that as much as 63% of the national roads are in critical need of interventions to prevent further deterioration [11]. With the national network comprising 170,000 km of main roads and 670,000 km of municipal roads, such a large percentage needing maintenance represents a serious problem for road agencies across the country. This has caused increases in required maintenance costs but this has been

simultaneously met with decreasing budgets for maintenance and road networks with decreases of up to 18% per cent in road maintenance spending over the previous ten year period [12]. Therefore, the situation presented is one where there is more maintenance required and less money is available, creating a critical imbalance and stressing the clear need for cheaper systems and optimized plans and tools. Road Asset Management is therefore vital and presents a pathway towards sustainable road management [10].

These issues have also been recently further worsened, with the economic turmoil caused by the COVID-19 pandemic, which will have deep financial impacts on upcoming budgetary allocations [13]. With this in mind, possibly, more than ever, road authorities need to utilize efficient and low-cost maintenance approaches to extend road life cycles and limit excessive rehabilitation activities in the future.

The preservation of pavements is fundamentally a sustainable action as it tries to extend pavement life and reduce environmental impacts at a lower cost. To this end, the project aims to fit directly under the umbrella of sustainability as low-cost tools and techniques will be employed to help preserve pavements. Through this, the project will address issues that cannot be so easily detected and handled by agencies and authorities that do not have a lot of resources at their disposal and would otherwise employ ineffective and unsustainable approaches.

Pavements that are well maintained provide better surfaces in terms of safety, smoothness, and noise, which can, in turn, result in better fuel efficiencies, lower accident rates and lower noise disturbances, which all add positively to the overall sustainability of the pavement [7]. Several systems can be put in place for the preservations to be done, namely, the Pavement Management System (PMS), which will be further described and analysed in chapter 2. The basic idea of what happens when pavement treatments are applied is illuminated in Figure 1-3 [7]. The figure illustrates that the extension of the pavement life cycle is made possible by delaying the need for extensive and costly rehabilitation actions and using preservative approaches.

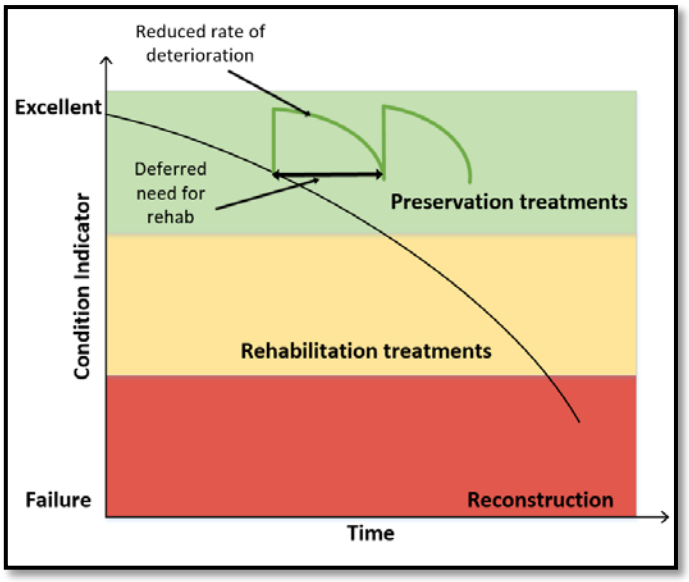

Figure 1-3. Impact of Pavement preservation activities on the Pavement life cycle

In the figure, it is shown that the choice to carry out the preventative maintenance can defer the need for the more costly rehabilitation methods by modifying the performance curve. [14]. The preventative methods can slow the pavement deterioration rates by years, and considering the low costs of preventative treatments, can result in significant cost savings.

For the adequate inclusion of sustainable preservation practices into systems, there has to be a significant effort on the part of the authorities or agencies to re-examine their typical data collection activities, modelling approaches and maintenance programmes. For the integration of the management systems and the pavement preservation approaches it has been established that three critical steps should be involved [14]. These are:

1. Pavement Condition Assessment – the evaluation and documentation of the pavement condition based on the related industry standards
2. Pavement Performance Modelling – developing models to predict future performance, activities and interventions
3. Pavement Treatment rules and impact rules – developing rules for the feasibility of treatments and monitoring these treatments and their performance over time.

Typically, the final selection of treatments and plans has to assess the needs and constraints of the particular project and city/region but these are all based on the input of current and historical pavement performance data along with data on the maintenance and rehabilitation activities that were carried out in the past [15]. This exemplifies the importance of data and

data analysis to the entire process and further shows that without accurate or available data, any decisions made can be flawed and result in poor systems that can end up being costly and unsustainable in the long term. To improve the sustainability of the system it is always considered a positive to choose the correct intervention at the right time [16]. This is where the importance of this research lies - in trying to address issues that agencies have in the general procurement, analysis and modelling of this data. Additionally, the project is limited to the first two steps that are considered requirements for integrating sustainability into the pavement management system (as set out earlier by [14]) that being pavement condition assessment and modelling.

1.3 Assessment of the information needs to implement sustainable road asset systems

As mentioned before, maintaining good road conditions is critical as roads are considered the gateway to mobility and access for citizens which in turn leads to economic and social benefits for cities and their residents [7]. This concern is further worsened by the continuing budget reductions for road authorities for pavement maintenance and rehabilitation programs [9]. These reductions result in authorities not having sufficient financial resources to maintain their networks in an optimal state.

There are numerous attempts to utilize optimization systems but most are highly dependent on the availability of data on the condition of the roads in the network. The acquisition of this road condition data can be quite costly as the most accurate technologies to date largely involve expensive equipment and vehicles [17]. These systems in many cases require significant time and substantial training for the authorized personnel working in the road authorities. As a result of this, agencies quite often rely on the use of manual surveys to obtain this data [18] and as a result, this data can be considered subjective and in some cases, inaccurate. This leads to the development of poor maintenance strategies or in many cases a pre-set strategy with no capacity to adapt to real-time circumstances and challenges. To this end, it has been the goal of many authorities and agencies to find lower-cost solutions for monitoring road conditions for building accurate and robust asset databases.

The information from these solutions can be commonly utilized within a pavement management system for particular needs as shown in Figure 1-4 [19,20]. Within the figure,

the highest need is the determination of the needs of the particular road, which speaks clearly to the need for context-specific data. The full extent to which the information can be utilized within the PMS is not covered within this study but the collection of data and ways in which it can be used for determining needs of the pavement and for planning interventions is the main focus of the work. The use of the data can extend the road service life and improve its safety.

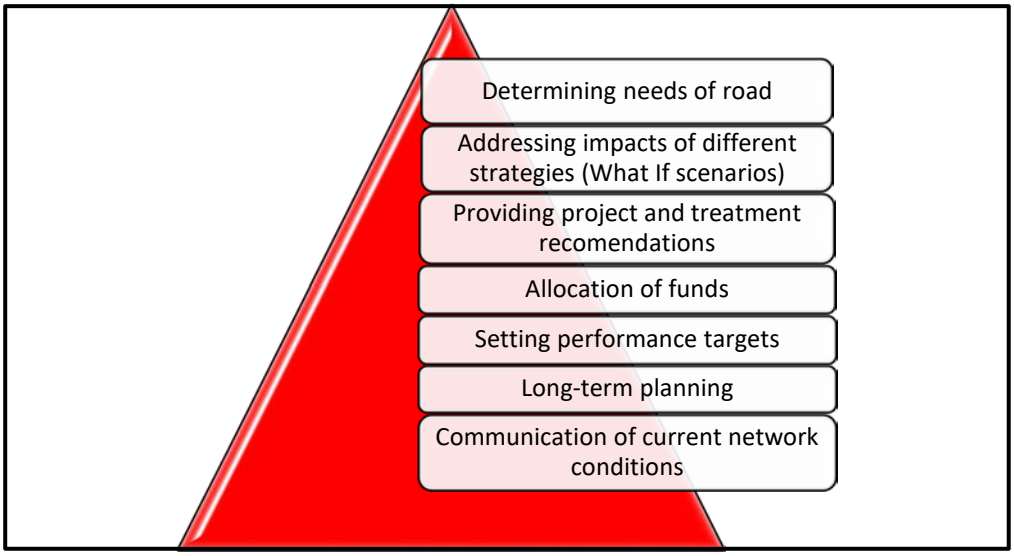

Figure 1-4. Typical uses of Pavement Management Information in a pavement management system

1.4 The importance of understanding the particular needs of the consumer and deploying low-cost systems

Given the growing needs for sustainable practices as so far outlined, it is imperative to stress that systems must be context-specific and understanding the need of a particular agency or city is vital towards a working and adequate model or technique. Consequently, this project will approach the particular needs of areas in the urban road network in Palermo, Italy and also a specific application for secondary roads in mainland France. The project is heavily focused on utilizing data science approaches to provide low-cost data analyses and systems to help to produce sustainable pavement management.

Given the focus of data science approaches within the study, it is useful to consider the typical workflow of a data science project as illustrated in Figure 1-5. In Figure 1-5, four of the steps are also highlighted in red; these are: understanding the problem, understanding the data, preparing the data and model iteration. Based on the work carried out within the study, these are considered the most important for future adaptations to other environments and cities to ensure that the correct context is applied and models are efficient based on relevant

information and sources. These factors are the reason why the study encompasses a wide variety of different data analysis techniques. This was done to ensure that individual models and techniques are not considered in isolation and instead consider the larger holistic view needed to be applied practically and have an impact on the advancement of pavement management systems. The factors will be further expounded on throughout the study but it is considered important to point to them from the beginning to establish their importance.

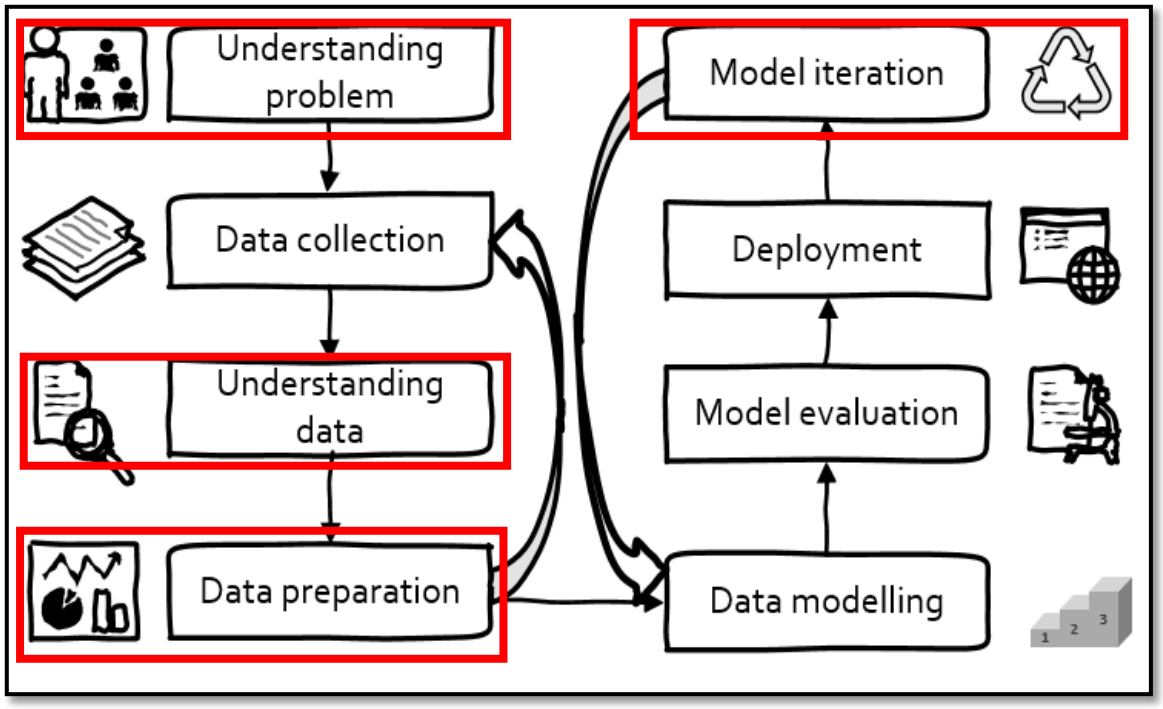

Figure 1-5. Typical stages of a data science project

With all of these factors in mind, it is now important to explain the main aspects of this particular study and identify the areas, which will be analysed to help bridge gaps within the general research area.

1.5 Project Background

1.5.1 SMARTI ETN Project

This research project is one part of a wider SMARTI ETN Marie-Skłodowska European Union funded project [21]. The entire SMARTI ETN project is a consortium of university and industry partners across Europe, including fifteen early state researchers researching various prototypes and guidelines with the aim of creating a shift to sustainable multi-functional automated resilient transport infrastructures. The entire project attempts to deliver a framework for new innovative technologies and strategies for transportation for this and the

next generation. This particular project is one component and has a direct focus on establishing workable guidelines for authorities for aspects of road management and maintenance planning. This specific project under this wider framework focuses on developing sustainable and critically low-cost road management techniques to be configured as guidelines to help road authorities in their quest for better-managed road networks. In this view, the project aims to bridge gaps that exist in acquiring data, understanding various modelling techniques and finally, creating practical workflows that can be readily adapted by road authorities.

1.5.2 Key concepts of the research project

This research project is built around the concept of using low-cost systems and correspondingly using key data sources that are not only easily available but also flexible enough to provide adaptation for future use and implementation. A significant aspect of the project was developed around the concept of utilizing imagery. However, whilst analysing the imagery, the question of where and how to focus the attention of maintenance and interventions on particular points of the network became relevant to the overall understanding and application of tools within a network. To this end, this research project first sets out to understand the conditions within the network being analysed, i.e. Palermo, Italy, through the use of historical data and analytical assessments; then goes on to identify and set up workflows to analyse particular points in the road network. The following are the key applications and methods that have been analysed within the project.

1.5.3 Application of data analysis using limited data sets to understand historical and future road maintenance interventions

Within this aspect of the study, a roadmap was developed to help under-resourced authorities by using low-cost and flexible data analysis and deep learning computational systems to highlight important factors within road networks and construct models that can adequately help planning by predicting future network interventions. A case study was developed to demonstrate how the techniques could be applied to perform appropriate feature selection and prediction models based on limited data sources. Feature selection tools were developed based on the features, found in open-source datasets, to identify which of them are the most important towards explaining the point in time at which intervention activities need to be

carried out. Once the feature selection tool was developed, it was used to pinpoint the most important features in the dataset, which were then used in a deep learning model to help predict the time for an intervention for a particular road in the network.

The process exploits the strengths of both gradient boosting algorithms and deep learning, leveraging their combined power to handle categorical variables and the strength of deep learning to search out connections on a deeper level than traditional approaches. The predicted models can aptly be used to generate schedules of which roads and sections should be prioritized over time. The workflow helps exploit several low-cost element techniques, which would be helpful for many agencies with limited and reducing maintenance budgetary allocations.

1.5.4 Application of 3D modelling and analysis of pavement distresses

Within this section of the study, different pavement manuals, techniques and systems used by road agencies worldwide to evaluate pavement conditions are explored. The commonalities and gaps among them were identified so as to guide new detection methods. Using these, workflows were established to show what these requirements are. Case studies were then subsequently developed to demonstrate how 3D Image-based modelling could be used to both replicate pavement distresses and fulfil manual requirements to determine severities. Using real-world examples, from each associated category, the process was validated, establishing not only the necessary requirements of the manuals but also additional features and measurements along with cross-sectional analyses not possible with visual and manual surveys. Following this, the accuracies of using different devices namely mobile phones and drones were considered and validated.

After the considerations of the accuracy of the 3D models, segmentation analyses were done using the 3D imagery. Models were segmented using different developed algorithms and based on similarly observed features, which allowed for a differentiation of the different pavement distress categories. Segmentation was used to pinpoint occurring distresses and obtain metric information on them and further established the value of the 3D modelling techniques and algorithms that were explored.

1.5.5 Application of distress detection to pinpoint the location of distresses

Finally, the third aspect was aimed at presenting a deep learning pipeline and framework for carrying out a low-cost hotspot analysis of the pavement distresses that are present on a road network. The intention of this was to provide road authorities and engineers with a low-cost platform for quickly understanding not only the type of distresses that are present on the network but also provide an idea of the severity of the distresses. This would, therefore, lead to better planning for interventions to restore the pavement to an acceptable standard.

Artificial Neural Networks were developed based on imagery obtained during several surveys to set up models capable of carrying out this task. To aid in this model development, a harmonized severity classification was also developed based on perceived safety and comfort impact. These classifications allowed the model to produce predictions that adequately can carry out the hot-spot analysis. The models produced showed high accuracies in identifying the distress categories developed and thus the associated severities. Optimization tests and tests in different environments using different model configurations were also tested to establish critical factors when building models of these types. Models were also developed using different camera angles and also in different lighting conditions to understand what would need to be changed if these aspects of the survey were changed. It was also established how models built with these pipelines could be complemented by other low-cost techniques cited before. This includes the 3D image-based modelling with smartphone and drone imagery, which could be used to provide detailed quantitative assessments of the areas, which are considered in need of intervention. The idea of this was to show how each individual workflow explored connects with each other for a better understanding of the network and its maintenance needs.

1.6 Research Gaps

There are several areas, where this project aimed to fill existing research gaps. One important gap is within the connection between the fields of deep learning and the practical application in engineering and in particular, road asset management. In recent times, there has been a significant increase in research into deep learning in the field of pavement engineering. This can be quickly verified by assessing the research works where the two fields (deep learning and pavement engineering) collide as evidenced in Figure 1-6 using an analysis of the

documents archived in Scopus [22]. The pace of research over the last five years, in particular, has advanced exponentially and it can be expected that this will continue as more development into deep learning models continues on a global level.

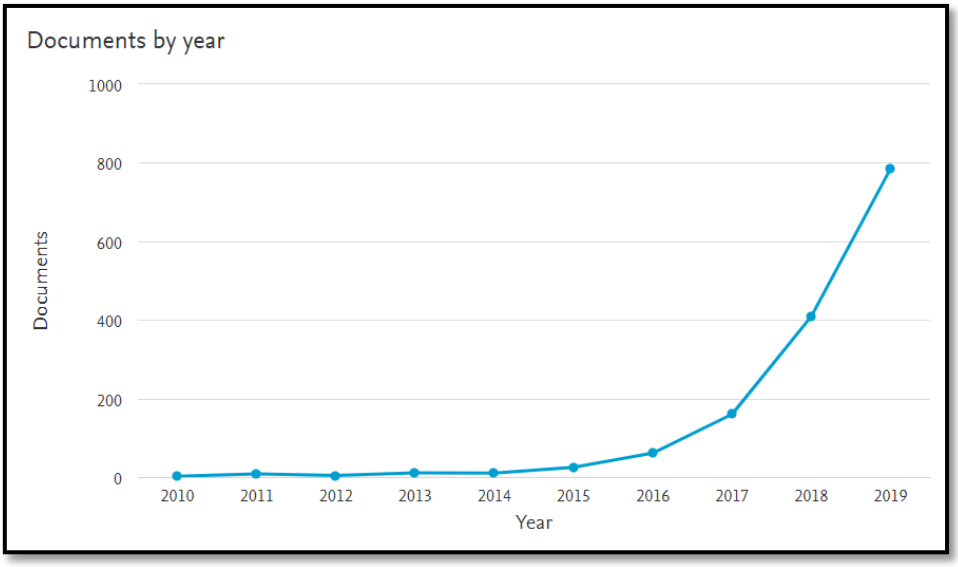

Figure 1-6. Documents archived in Scopus concerning both Deep learning and pavement engineering

However, when looking at the subject area of documents discussed, the focus has been primarily on computer science aspects of the research with many studies focusing on improving the structure and makeup of algorithms and deep learning models rather than on the application of them towards real-world scenarios. This is further exemplified considering a look at the subject fields that are spoken about within the documents archived in Figure 1-7.

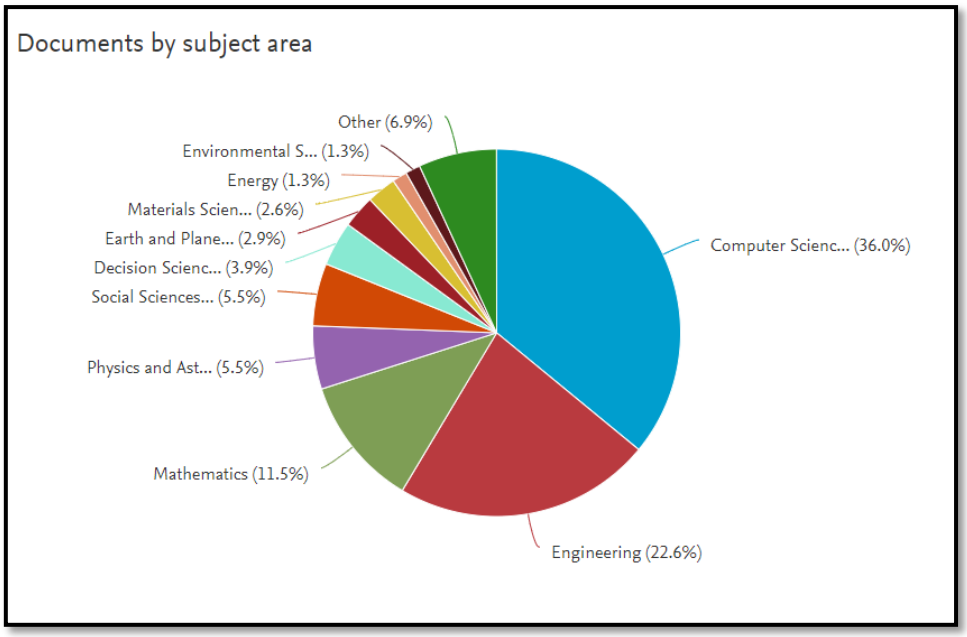

Figure 1-7. The subject area of documents archived focusing on both deep learning and pavement engineering.

Computer Science and Mathematics dominate the subject area (a combined 47.5% of the total) with the focus on engineering aspects only making up 22.6% of the total. This relates to many studies and projects focusing on generating new structures within the computer science models and new types of algorithms that can reduce error rates based on generic isolated datasets.

This is often seen as a problem with deep learning as there is often a disconnect between modelling and real-world applications where the connection of important problems to the larger world of science and society has been lost [23]. The meaningful connections are lost in many instances because deep learning researchers are not experts within the relevant scientific areas and therefore focus more on the models rather than their adaptation. Several models have been developed for detecting and analysing pavement distresses and these will be identified through the course of the thesis. However, the adaptation to real-world implementation is often absent and this is one of the primary goals of the study to bridge this gap to ensure that guidelines developed herein, will deliver models that are context-driven and can be understood by practitioners and not just researchers. Models developed in this project were done so directly from a civil engineering practitioner's point of view and not with the typical idea of generating a mathematically innovative model that may not have practical application. To this end, models and techniques within the research start from the point of asking what is the particular need within the system and solutions are geared towards that.

In addition to the highlighted disconnect between many deep learning models and practical application and implementation, gaps exist in general pavement data collection practices. In many instances, agencies try to create and maintain large information databases that in the long term do not provide efficient systems and cost a lot of time and resources to be up kept. It has been shown that many of these extensive activities and systems do not provide useful data for the authorities [24]. This leaves authorities burdened, either with ineffective databases, or the lack of a plan to handle their inability to build an exhaustive database. To this end, there is a gap, especially for research on small or under-resourced authorities, to understand how to use easily available network information with small datasets to provide sufficient predictions of future maintenance occurrences and understand what is truly important to their networks. The potential of leveraging the concepts of data analytics and deep learning to provide a workflow for mining network features to be used in a model for

the prediction of maintenance activities provides a pathway towards solving this gap. This study creates pipelines using configurations of models that leverage deep learning for tabular analysis and feature selection in a way that has not been done before.

Finally, whilst it is important to help data collection and database systems, it is also vital to have metric information on the distresses present in a network. To this end, the other research gap that is explored within the study is tackling the issue of subjectivity that plagues conditional pavement distress surveys in road agencies that cannot afford or rely on expensive automated survey techniques. Many of these surveys are done utilizing manual methods [25,26] which has led to many studies on ways to use automatic detection and analysis systems. The goals of these systems are to remove the subjectivity and provide accurate information on pavement condition without relying on manual detection methods [27]. The use of manual methods can be considered risky and even dangerous [28] as the results could lead to ineffective and inefficient maintenance plans and treatments. Despite the many studies on the subject, there remain gaps to advance pavement distress detection methods especially in the fields of computer vision and analysis. This has become even more important given recent advancements with cameras and drones, as their resolutions are continually increasing whilst simultaneously becoming more easily available at cheaper costs [29].

Given these main research gaps, the Solutions explored during the project can be broken into three specific sections. At the beginning of the research project and to date, these exact processes and solutions explored within this study have not been done before.

The first of these is the development of models and workflows to understand the environmental/area context of the region under analysis to predict the likely locations of future maintenance interventions. To do this varying algorithms were explored such as gradient boosting and tabular deep learning models. This is tackled in Chapter 2.

The second aspect was on creating a workflow to carry out a hotspot analysis on the specific roads in the network which are considered critical as identified from the first part. To do this, deep learning object detection models were considered using imagery from smartphones and webcams attached/equipped to vehicles traversing the road networks. These concepts are further discussed and analysed in Chapter 6 and 7.

Finally, the third part was on creating workflows and optimizing techniques to generate 3D models of the pavement distresses on the network and both specific points in the network using point and shoot cameras and over a longer section using drone imagery. Additionally, once the models were generated, segmentation techniques were explored to isolate the distresses, measure them and analyse them to feed the information to the asset management system and to make decisions on what type of therapy is required. These solutions are detailed in Chapter 4. The full work can be summarized in Figure 1-8, which details the main stages of the project.

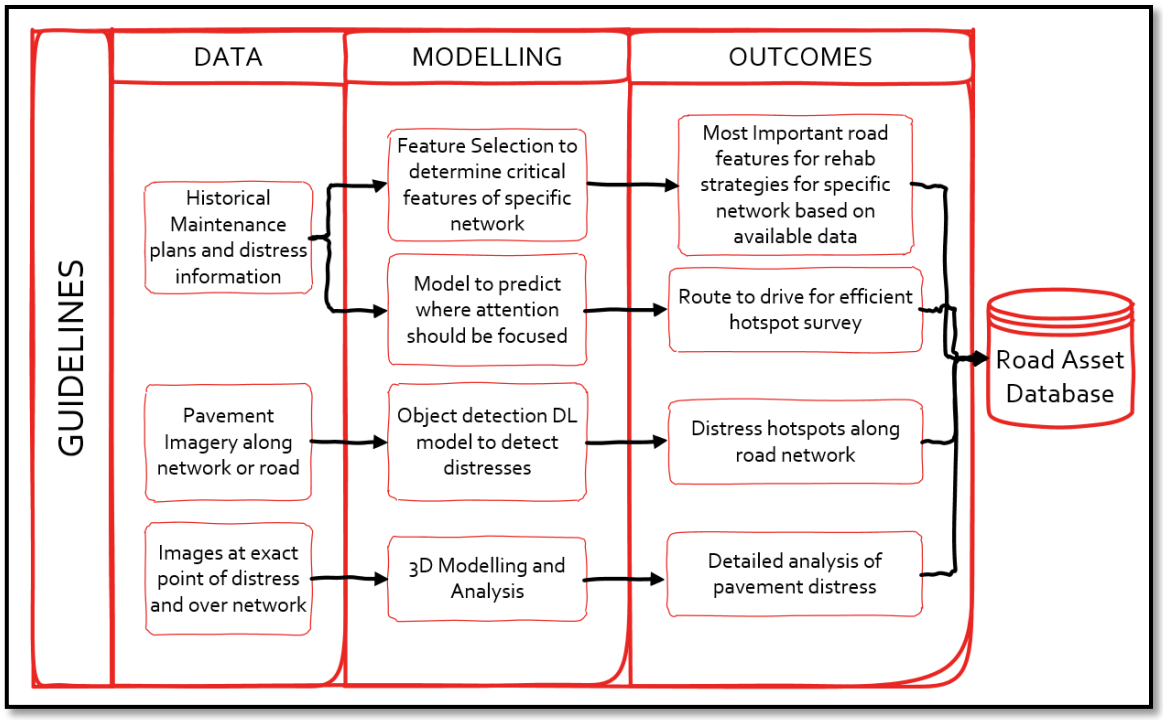

Figure 1-7. Overview of the main elements of the research project

As shown in the figure, three main types of data are used, followed by four different types of modelling processes. The modelling process begins by understanding the network and finishes with a detailed analysis of particular points of interest. The outcomes are all important pieces of data for road managers and as a result, all of them are to be fed towards the asset database of the road authority/agency.

The framework presented within this project, whilst focused on pavements, can also be considered in the advancement of general Intelligent Transport Systems (ITS) applications. An ITS aims to leverage accurate information about conditions to assist decision-makers in the wider transport system [30]. Equally, the information provided at each level of the project helps create a workflow for a better transport system. Better-maintained roads leads to better

transport systems flows, which can reduce traffic congestion and improve the overall movement of goods and services.

Pavements are only one facet of the transport system with other important elements and their condition also playing a major role in the overall development of a region. These include components such as bridges, electrical grids and buildings. Smarter detection and analytical measures help these systems by not only freeing up maintenance funds for these other elements but also producing workflows that can be modified to also sustainably manage them. A positive ripple effect can be created for monitoring these other critical components. As a by-product of having these workflows in place for pavements, other related infrastructure and asset systems will benefit as applications have shown that the techniques discussed in the study can also be used to monitor and analyse these components. Specifically, the use of drones and image analysis can also be used to monitor the condition of other civil infrastructure such as buildings and bridges during construction and for defect detection and analysis [31]. The discussed deep learning pipelines can also be utilized by agencies in other related fields. This includes improving the resiliency of critical infrastructure by monitoring power-related infrastructure such as electrical polls and systems that appear along road networks [32]. Furthermore, deep learning techniques can be used to build smart infrastructure and smart cities by increasing energy efficiency and sustainably improving resource use [33]. Having institutional capacity in this field will go a long way towards exploiting these other possible application points. Therefore, having a road agency and municipality equipped with, and using the deep learning and monitoring frameworks and pipelines, will prove vital in applying similar systems for other areas needed to secure and consolidate sustainable infrastructure across the many domains of a city.

1.7 General Research Objectives

The biggest goal of this research is to develop workflows that simplify aspects of the pavement asset management processes using flexible but low-cost tools and techniques. The major aspects involved scrutinizing how pavement distresses are detected, analysed and used to plan future interventions. To pursue this goal, several data analysis and deep learning techniques are explored using easily accessible data sources that make it easier for road authorities to implement their related strategies. This involved the use of national and local

statistical data on communities and the use of images taken from smartphones, cameras and drones at different points along a road network.

Considering the overall goal, the following sub-objectives are addressed under the research project:

1. **To review relevant pavement management processes and information**

   For this objective, the necessary background information, historical context and existing processes were reviewed. This information was analysed to understand the underlying conditions for pavement management practices in the specific contexts of the research and also to identify how new techniques could and should be adapted using the existing tools. This involved exploring the general structure of the pavement management system and then the structure and practices of detecting pavement distresses in a network or section. This was done to provide a basis for practically expanding the tools using the state of the art practices developed within the research project. Existing manuals for pavement detection were analysed to identify the needs of new detection technologies based on industry standards. Case studies were subsequently developed to show how the new techniques and workflows fit into the existing paradigms to make them practically implementable.

2. **To develop suitable and practical workflows**

   Given the systems and techniques explored in sub-objective one, it was necessary to test and adapt the techniques that were developed in theory in real-world tests. This objective focuses on this, to ensure that the techniques developed are not simply theoretical. Test cases were developed to explore this and set up system designs that can practically use the approaches from this research project. The focus here was on implementing models on external roads and data sets to verify their accuracy and performance. Additionally, models developed to predict activities were similarly verified on external data points.

3. **To evaluate and optimize the developed workflows and processes and combine the techniques explored in a suitable way**

   The final sub-objective involves optimizing the models and techniques developed in the research in an attempt to boost the performance of models to detect distresses, further understand how they could be implemented in different environments and

ensure that they are flexible enough to be used by road practitioners. Computational times and resources are also identified to provide context for future use.

1.8 Thesis Outline

Within the outline, objective one is tackled in chapter 1, 2 and 3, objective two is dealt with in chapters 4, 5 and 6 and finally, objective three is addressed in chapters 7 and 8. The overall thesis is built around eight main chapters and is structured as follows:

Chapter 1 provides an introduction to the research and the reasons why it was pursued. To this end, the research gaps are described along with the objectives that were designed to overcome the gaps and take advantage of the research opportunities.

Chapter 2 offers a background of aspects of the Pavement Management System and highlights points of research opportunity. Following the background, a workflow was designed to understand the features of road networks and where road interventions should be placed. The focus is based on circumstances where the road authority is under-resourced and as a result, does not have access to large extensive databases and historical information.

Chapter 3 presents a background of how pavement surfaced conditions are measured and analysed. This is done in order to set the base for the research on newer advances using imagery and 3D modelling in the subsequent chapters. The chapter also presents a foundation on pavement distress types, which is used, in developing distress detection deep learning models in the later chapters.

Chapter 4 focuses on the use of 3D modelling to recreate pavement distresses and then seeks to establish workflows and systems to adequately isolate, measure and analyse the 3D models through segmentation and geometric modelling.

Chapter 5 sets the stage for work on deep learning using imagery for the detection and analysis of pavement distresses. An overview of work done on deep learning and the connection to the research carried out is depicted. Within it, several tools are identified which were used to create the deep learning methodology.

Chapter 6 focuses on creating detection models to pinpoint the location and sizes of pavement distresses. A workflow is established to show how the methodology was applied and how the hot spot analyses could be carried out with a focus on the needs of the particular context of

the project. The methodology for assessing the results of the models is also considered along with a pipeline for deploying mobile smartphone versions of the models.

Chapter 7 provides an overview of the modelling results and how the models can be used in a practical manner. The chapter then considers several optimization strategies and also demonstrates the effects of changing the environmental context of the models by carrying out case studies in a different city and country and using different image types.

Chapter 8 finally presents the important conclusions and takeaways from the research and synthesizes the future perspectives and recommendations for implementation and application in industry and research.

Chapter 2: Sustainably prioritizing pavement maintenance interventions

Given the importance of sustainable pavement management that was previously outlined in chapter one, the next stage was to understand how current pavement asset management systems are built and utilized. This is vital in pinpointing the points of concern within a network and understanding how the techniques within the project can be practically deployed. This chapter outlines the salient points involved in the components of a Pavement management system, its data requirements and how data is used within the system. After this, the chapter then further advances these concepts to build a low-cost modelling workflow for a road authority to understand the critical needs of their road network and predict timelines for future pavement interventions using flexible data analysis tools and systems.*[1]

[1] This chapter is based on the following paper:
"Exploiting Data Analytics and Deep Learning Systems to Support Pavement Maintenance Decisions", published in the international peer-reviewed journal "Applied Sciences" and which was authored by the same author of this thesis. doi: 10.3390/app11062458.

2.1 What are the key concepts of a Pavement Management System (PMS)?

The overall process of Pavement Management (PM) is hierarchical and is typically composed of four levels or stages of implementation. These are approach, analysis, evaluation and parameter selection, and are detailed in Figure 2-1 [34] showing the different stages.

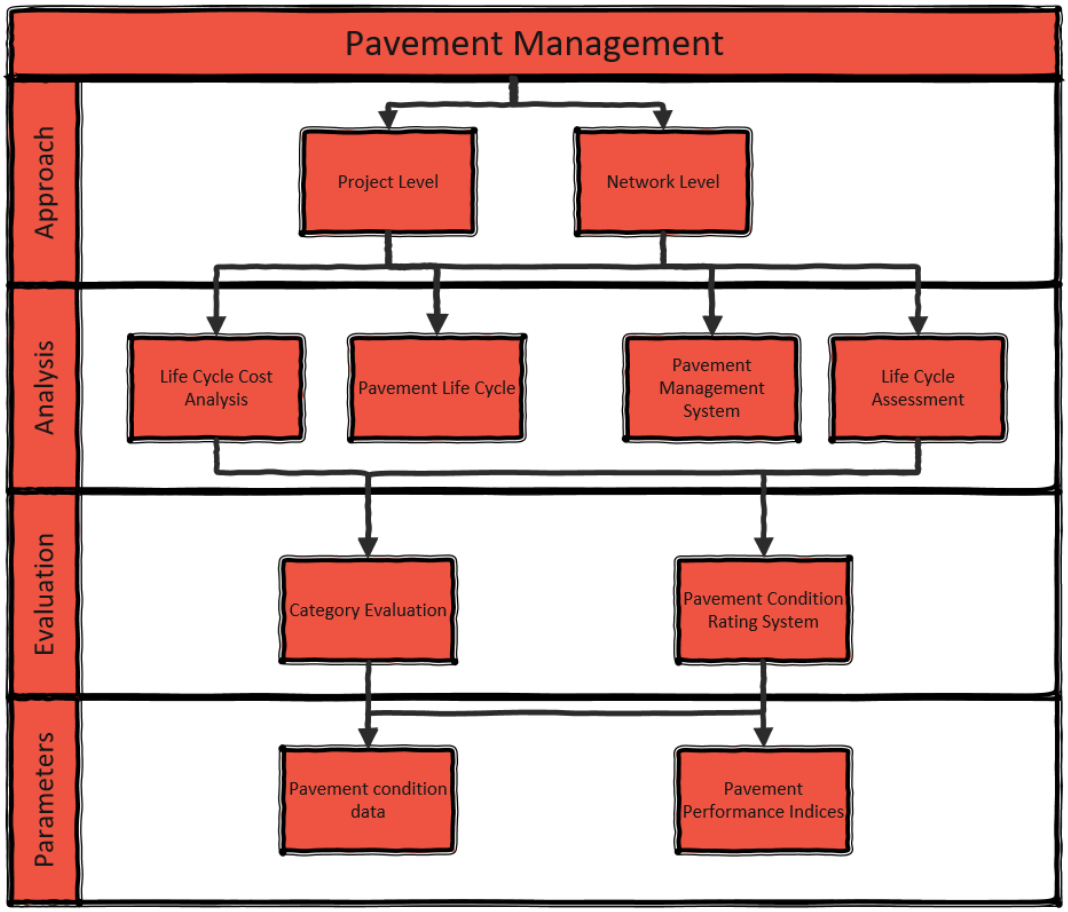

Figure 2-1. Pavement Management: hierarchic process composed by approach, analysis, evaluation and parameter selections

Across the Decision Making Processes, PM is aimed at reaching several technical, economic and environmental goals, through the analysis and evaluation of specific indices and parameters in accordance with the approach depending on the scale of the domain (Project Level or Network Level). As seen in the figure, the process begins with the decision of the level of the approach to be taken. Following this, the analysis is carried out utilizing the appropriate analysis systems. For analysis, the appropriate evaluation systems are identified and the individual parameters to be used. The evaluation systems and their related parameters will be further discussed in chapter 3. For this study, the analysis method that will be discussed is the best-known and applied one, which is the Pavement Management System (PMS). The analysis

is a forward-looking aspect of the assessment of pavement life cycles and is generally carried out on a motorway network, even if some studies have been focused on urban road networks [35–38]. The PMS is an efficient method to get the most value out of available public funds for Road Maintenance and can be described as a coordinated set of activities aimed at matching public funds with smooth, safe, and economical pavements [39]. The PMS was originally developed in the 1970s in the United States and the local and regional highway authorities have played a significant role in the development of the modern-day PMS. A brief overview of the key points of the development is given in Table 2-1.

Table 2-1. Development of the PMS

Year	Development	Remarks
1970s	Early development of the PMS	Development begins in the US in several states including Washington, Arizona, Utah, South Dakota and by the US Army Corps of Engineers
	Research by the largest highway agencies in the US underway	Research by the American Association of State Highway and Transportation Officials (AASHTO) and the National Cooperative Highway Research Program (NCHRP)
1985	AAHSTO guidelines on Project Management	Introduced the PMS concept and defined it outlining development and its implementation for road authorities
1987	Definitive PMS guide by NCHRP	Guide produced by Peterson defining PMS and its use [39]
1989	Development of the US Federal Highway Administration(FHWA) policy on Project Management	Policy introduced to require all states in the US to use PMS updated several times with the most recent update in 2017 [40]
1990	AASHTO guidelines for PMS updated [41]	Additional guidelines by the pavement management task force on pavement management introducing the following: • Description of the basic characteristics • Identification of components of a PMS and role • Description of development, implementation and operation steps • Definition of the role of communications
1991	Intermodal Surface Transportation Efficiency Act (ISTEA) development	Law introduced which required all US states to have PMS to cover all federal aided highways [42]
2005	Safe, Accountable, Flexible, Efficient, Transportation Equity Act- A Legacy for Users (SAFETY-LU) [43] introduced	Focused on spending of money to be directed at the following in the US: • Pavement Management • Bridge Management • Safety Management • Traffic Congestion • Public Transportation Facilities and Equipment • Intermodal transportation Facilities
Present	Continual studies on the optimization of various techniques and systems under the PMS from data collection practices to intervention and maintenance planning	

The milestones described in Table 2-1 show that the system has been used for a very long time and the core concepts of the system have been thoroughly developed. Aside from these major milestones, there have been several studies over the years, which have introduced new and innovative ways of implementing the various steps of this process and research continues on discovering and using different optimization methods. A snapshot of some of the important optimization techniques considered is provided in Table 2-2.

Table 2-2. Different methods used to optimize the PMS

Method of optimization	Description of study
Mixed-integer nonlinear programming	Using an objective function to maximise life cycle costing for treatments at a network level considering both economic and social benefits [44]
Mathematical programming	Using objective functions to minimize agency and user costs [45]
Using thresholds for optimization of performance	Considering optimized thresholds for performance indicators to yield positive cost-benefit return, also considered life cycle costs in the analysis [46]
Genetic Algorithm (GA)	Using Multi-objective Genetic algorithms to maximize work production, minimizes maintenance costs and maximize network conditions. Used a Pareto analysis to compare alternatives. [47]
Combination of GA and Neural networks	Using objective functions to maximize sideway force coefficient and reduce accident rates within GA, then used neural networks to predict future occurrences [48]
Other applications of GA	- Using a GA to identify the best solutions, considering the costs of different rehabilitation strategies and accident rates in a multi-objective optimization method for a PMS for both the project and network-level [49] - Optimizing interventions by considering shorter maintenance sections, developed optimum strategies for short sections using GA [50] - Using a GA in combination with an analytical hierarchical process to prioritize maintenance activities at both the project and network level
Particle Swarm Optimization (PSO)	Considering a test study of different road segments and compared the use of a PSO system and a GA one showing the PSO had a higher performance with lower costs [51]
Use of other factors for optimization	- using the International Roughness Index for maximising the functions [52] - using a network analysis including the indirect operating costs incurred by urban vehicles [53]. - Using a neural network considering structural characteristics of the pavement to optimize intervention planning [54] - Using a neural network considering functional characteristics of the network for optimization [55]

Within the table, it can be seen that numerous studies have tried to tackle the issues of minimizing costs and increasing pavement life cycles for different aspects of the PMS. This aspect of the study focuses on the data side of the PMS and finding innovative ways of delivering the appropriate data to the PMS so that these optimization strategies can then be employed. The data required depends on the category of the PMS.

Specifically within the PMS, the category, evaluation is very important to explaining conditions and providing a context of the particular situation of the road or network. For this, the pavement evaluation is carried out by measuring well-known performance parameters such as the International Roughness Index (IRI), the Deflection, the Skid Resistance or the Friction Coefficient, the Surface Distress Severity, in order to compare every value to the fixed threshold value. Additionally, the evaluation may be undertaken by ranking the pavement according to two peculiar recognized indices: The Pavement Condition Index (PCI) and the Present Serviceability Index (PSI). Both of these indices need reliable measurements of the geometric features of the distresses. There are several distresses manuals [56–63] that provide information and references on the types, severity and extent of the road damages. Nevertheless, no uniform values of geometrical features (for instance the width of the crack) are maintained across the manuals. This, however, is significant as the severity class dictates the necessary remedial actions and is largely based on the geometrical measurements obtained. Therefore, accurate measurements must be taken during the distress inspection surveys to ensure the correct severity class is identified. This highlights the need to verify the metric accuracy of any new techniques. More analysis of the distresses and the manuals is provided in chapter 3.

Moreover, the possible causes of the distress can be identified just by observing the geometry of the defects in detail and, therefore, it is possible to establish an optimized strategy of road pavement maintenance, rehabilitation and reconstruction (MR&R). Furthermore, as most of the evaluations of the pavements are based on visual observations, the resulting descriptions involve high degrees of subjectivity, hazardous exposure and low production rates. Hence, an automated distress identification method has become a fundamental goal for transportation authorities, even if in most instances this is unattainable due to budget constraints [9]. The effectiveness of an MR&R strategy depends on the soundness of the diagnosis of the pavement distresses that, in turn, depend on the reliability of the quantitative analysis of the pavement distresses. Furthermore, well-known pavement design methods such as the mechanistic-empirical (M-E) pavement design [64] methods include distress information such as the rut depth and fatigue prediction as fundamental parts of the estimation of the pavement service life. In the case of rutting, the importance of the detailed geometrical analysis to identify the cause of the permanent deformation has been shown [65]. These

factors, therefore, play a major role in identifying appropriate strategies for maintenance plans and schedules but they are not the only ones as there are several data requirements for the PMS to function efficiently.

2.2 Data requirements for Asset Management within the PMS

In general, the PMS consists of five key blocks: data collection, criteria definitions, analyses including the use of algorithms used to interpret data in meaningful ways, development of decision criteria and implementation procedures [39]. Within the PMS, the database is seen as a vital component. For the road asset database to be effective, the phases of data collection storage and management have to be efficient and cost-effective [66]. Three success factors have been designated for the effective management of databases and these are Relevance, Reliability and Affordability [67]. These factors have remained important regardless of the time that has passed since the introduction of the PMS or the type of new technologies that are now available and or will be available in the future. Therefore, new technologies must adhere to these factors so that their inclusion in the system can be effective. This is critical for this study, as these factors need to be considered and relied on in order to demonstrate the practicality of the new approaches put forward by this study. These are further detailed in Figure 2-2 which highlights how the activities fit together within the PMS.

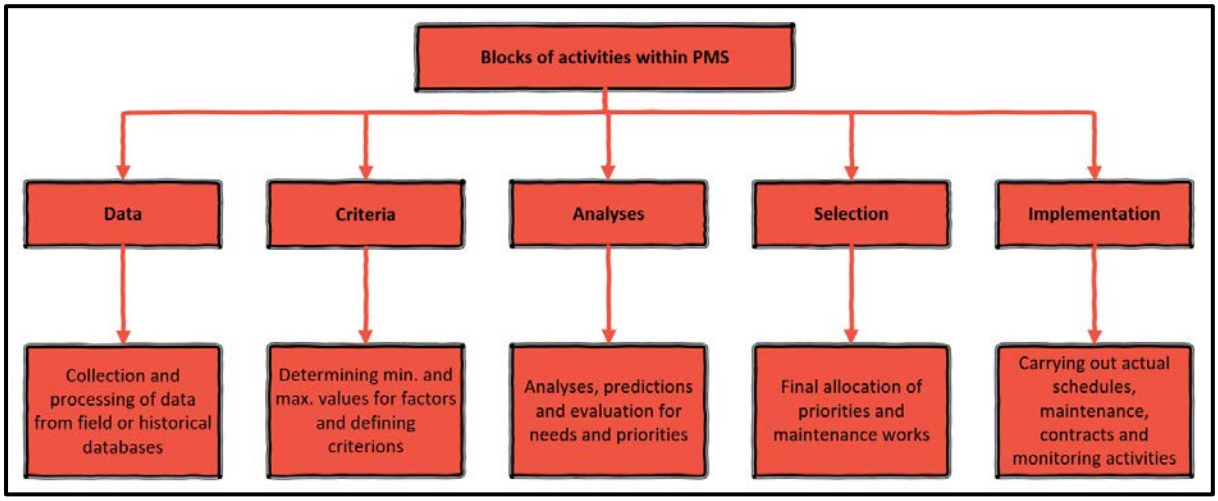

Figure 2-2. Main activity groups within the PMS

The main purpose of the analysis is to evaluate the performance of the pavement and to understand its ability to serve traffic over time in safe, smooth and economic conditions. There are three critical basic requirements for the adequate application of a PMS [68] which are:

1. It serves different types of users within the organization.

2. It allows for good decision making with respect to programs and projects and allows for the timely execution of projects.
3. It makes good use of existing technologies and new ones once they are available.

With this in mind, there are two major categories of pavement data collected, which are inventory data and pavement condition data. The precise data that is required then depends on the level at which the PMS is being deployed, whether it be the network or project level. Based on these inputs, information on pavement distresses forms a very important part in defining the condition of a pavement and in identifying the appropriate treatment. The evaluation is typically made up of three factors: type, severity and extent of the damage. The data used as inputs for inventory data and pavement data along with the uses of the data are summarized in Figure 2-3 below.

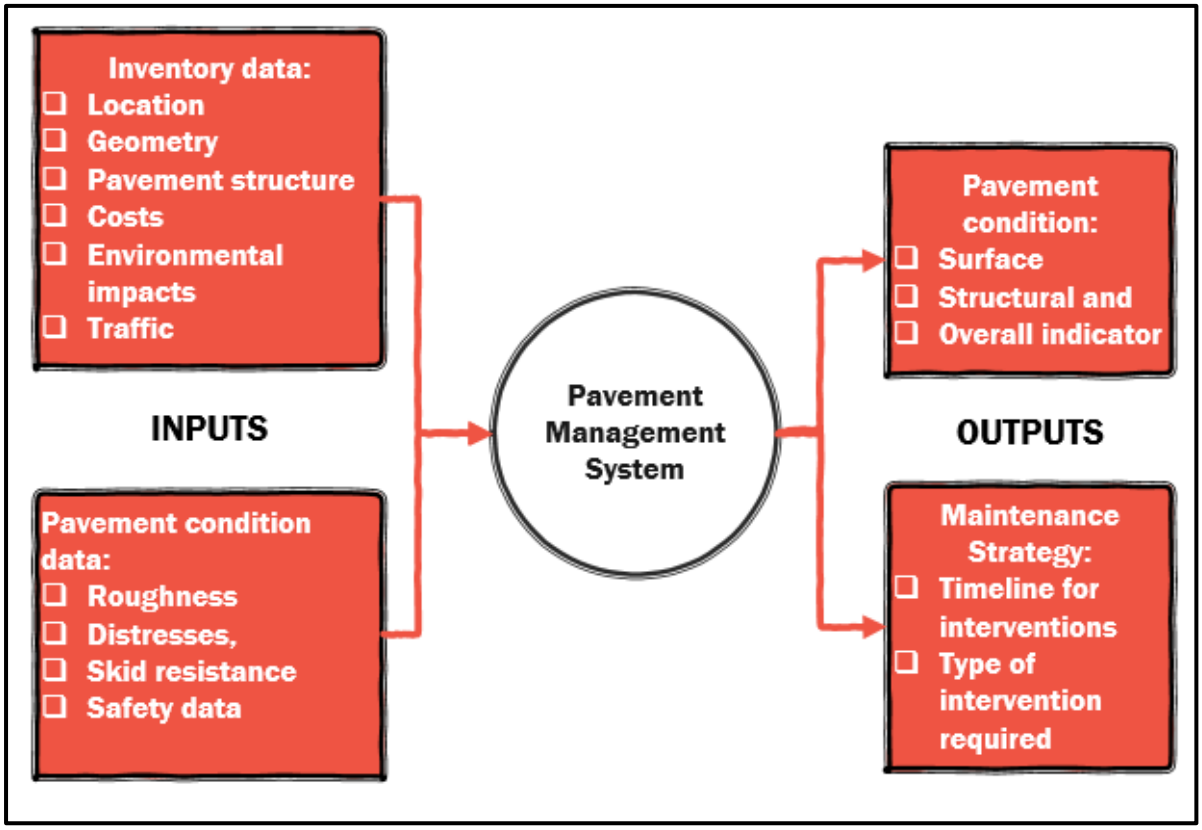

Figure 2-3. Summary of uses of data within the Pavement Management System

Within the figure, it is shown that the input data is fed into the PMS to yield the outputs of understanding what the conditions are and deciding on the maintenance approaches. It is critical to have systems in place that can produce appropriate data. However, in many instances, the collection of this pavement condition data is done manually with some studies

indicating the number to be as high as 90% of the cases [2], which therefore allocates a tremendous amount of subjectivity into the process. This is typically due to the data acquisition process being very expensive, exhaustive, and time-intensive [69]. Data should be collected in a practical and effective manner. Furthermore, it has been rationalized that data collection should be driven by three core-guiding principles [67,70], which are:

1. Only collect the data which is needed
2. Data collection should be done at the lowest level of detail satisfactory enough to make effective decisions
3. Data collection should only be done when it is required.

When these principles are not enforced, there can be an overabundance of data which can lead to abandonment or mismanagement of systems.

2.3 Metrics utilized within the PMS for analysis and prediction of pavement conditions

Whilst the data collected is very important, how it is utilized is equally important to the system. Within the PMS, pavement distress information is typically collected and utilized by agencies to determine an overall road system rating using standardized performance indices. There are several of these indices. The first of these is the Present Serviceability Rating (PSR) which was developed by the American Association of State Highway Officials (AASHO) [71]. The PSR is a subjective rating, which is given based on the experiences and judgement of road users. For a more robust index, the PSR was used to develop the Present Serviceability Index (PSI) with a basis on the road characteristics of pavement roughness and distresses of patching, rutting and cracking. On the premise of smoothness and ride-ability, the International Roughness Index (IRI) was also developed but this index typically requires specialized equipment particularly the use of a profiler, to measure road profiles utilizing built-in algorithms [72]. Using the subjective ratings of distresses the U.S. Army Corps of Engineers (USACE) also developed the Pavement Condition Index (PCI) (American Society for Testing and Materials. (ASTM), 2018). The PCI is widely used and respected and is based on calculating deduct values allocated to each distress type based on its area affected and severity level and subsequently subtracting these values from the total to obtain a rating of 1 – 100 (where 100 = perfect pavement) which is related to a verbal Pavement condition rating ranging from

'Good' to 'Failed'. The PCI has been used as a good parameter for evaluation of urban road networks [73] and recent work on this has been done with respect to the Urban Italian Road Network wherein the PCI has been considered as a good basis for finding a new distress identification system for the Italian Urban network [38].

To establish the priority rankings of any models the models must consider costs, pavement serviceability and condition index, functional classifications and traffic levels [36]. There are several different models, which have been utilized to predict the performance and degradation of the pavement. They can also be applied at each level of the overall PM whether it be network or project. The prediction models can typically be grouped as purely mechanistic, mechanistic-empirical, regression-based or subjective. The Mechanistic-Empirical Pavement Design Guide developed by AASHTO [64] has been seen as a viable and well-established approach for performance predictions.

2.4 Issues when trying to implement a PMS

In terms of implementing a PMS, there are several roadblocks that a road agency faces. These can be grouped according to the following: the formulation of objective functions (maximizing pavement performance and/or to minimize costs), financial network constraints and defining the timeline for analysis and implementation [74]. With this in mind, it is critical for road managers worldwide to have an understanding of the road conditions in their respective networks or regions. However, for every region or network, the conditions are different and different prevailing factors underscore what is important to the region. Therefore, it is vital for any tool or guideline that is being developed to be done so with an overall understanding of the geographical and regional contexts. For this project, the focus is on flexible pavements and on under-resourced authorities and agencies seeking answers to questions of location and timing of pavement maintenance activities so as to minimize costs whilst maximizing the pavement and network performance. To do this, the relationships that exist in a particular location are therefore critical.

2.5 Relationship of factors and features that contribute to Pavement maintenance interventions

The selection of potential sites for pavement maintenance is generally dependent on the pavement age, frequency of maintenance interventions, traffic rates, accessibility and safety [75]. The preference between these sites can then be decided based on performance and distress surveys. In practice, there is a multitude of different performance indicators for roads that can be employed during the decision-making processes [76]. Many PMS's will utilize top-down approaches wherein funding levels required to meet long-term performance goals are estimated but in these scenarios, further steps are still required to prioritize specific segments for maintenance interventions [77]. However, some gaps have been identified within the methodologies utilized for the PMS in effectively considering multi-attribute condition information for modelling processes [74].

Performance indicators are useful and important because they help to efficiently allocate resources amongst options based on the availability of resources [78]. It has been suggested that frameworks for performance indicators for road assets should be divided across two levels – general performance indicators which can provide an overview and can be ascertained from public statistics and detailed objective indicators of service quality and institutional effectiveness [78]. These overview characteristics are important as they can provide a summarized view of the network's situation. Concerning the overview performance indicators, there are typical feature groups that should be assessed to ascertain the summary of the road asset [78,79] which include:

1. Network parameters – geometric configuration and dimensions of roads
2. Asset values
3. Road users – types of users and trip purposes
4. Demography and economic circumstances – population and land area
5. The density of network and roads
6. Use of roads – travel by class
7. Safety – accidents and fatalities

Concerning these indicators, it is possible to retrieve a plethora of this data from local sources such as censuses, therefore making them a viable resource outlet for obtaining data for modelling scenarios for small or under-resourced authorities. The data sourcing can be

complicated based on city circumstances but it is a necessary step to adequately understand particular situations and predict future trends. The use of this approach is pioneering as traditionally extensive data collection systems are put in place. Additionally, it follows a sustainable approach, as explained in chapter 1, given the low-cost of data acquisition and analysis.

2.6 How have Pavement Management decisions and approaches been supported by data analytics?

Once data has been identified in a system, the next important decision is the type of modelling and estimation to be done to make and support maintenance decisions. For this, numerous studies have used different algorithms and techniques to validate decisions. There are several areas within the PMS decision-making processes where artificial intelligence-based systems can help support decisions. These include estimation of pavement condition, assessment of maintenance needs, identification and selection of maintenance actions and prioritization of maintenance programs [80].

Studies have also tried to develop algorithms using techniques such as decision trees to predict Pavement Condition Index (PCI) [58] values, and therefore future pavement conditions of road sections using input data such as historical PCI values, weather, historical maintenance data and traffic [81]. Additional studies have focused on the International Roughness Index (IRI) [72]. Using this index, random forests regressions have been used to predict values of IRI to determine pavement roughness of sections utilizing information on traffic, previous IRI values and pavement distresses [82]. Artificial Neural networks (ANN) have also been constructed using the IRI as an input to identify maintenance strategies with reliance on large national datasets [83,84]. Other studies have tried to predict PCI values using neural networks. Planning of road interventions utilizing Fuzzy based networks has also been considered [75]. In other cases, ANNs were utilized to predict an exact pavement maintenance decision based on inputs of distress data, functional class, traffic and pavement structure [54]. Another method of analysis is the use of Genetic Algorithms, which were shown as an effective tool for predicting maintenance programs and have been combined within neural networks to bolster their effectiveness [48,49,85]. These previous studies all represent attempts at helping to plan maintenance interventions but have commonly relied on large databases.

2.7 Development of strategies for pavement maintenance in agencies with limited data and resources

Data Analytics has been considered as an effective way of handling pavement condition data and relating predicting pavement conditions [81]. However, in many instances, many large databases do not provide particularly useful information to allow for efficient decisions to be made with many of the databases having subjective data [24]. There have been attempts at creating datasets that will help boost deep learning activities in the field of civil engineering where datasets of different infrastructures have been set up [86]. However, these studies have been inclined to focus on image-based datasets. Image-based analysis can be very effective and recent studies have shown how low-cost models can be developed to detect distresses within a network using smartphones [87] and this will be explored as a solution within this study in later chapters. However, even within these systems, the question of where to direct the image survey and how to understand the feature characteristics of the network still needs to be addressed for them to be practically applied. There is one large database that includes pavement features and factors called the Long-Term Pavement Performance (LTPP) database [88]. The LTPP database is an enormous one developed and maintained by the Federal Highway Administration in the U.S and it has allowed for the study and development of many different algorithms and decision-based studies for predicting different future conditions of pavements and developing maintenance strategies. If similar databases could be set up for all agencies, it would be a great help in their planning processes. However, in most cases, road agencies do not have access or funds to create such a large database and the associated algorithms and models developed for road maintenance are therefore not useable. This means the systems and predictions cannot be applied to their situations.

Whilst it can be reasoned that more data can produce higher accuracies in models, the costs of acquiring the additional data must be amply considered by the road authority. Therefore, there should be a balance between available budgets and information pursuit [89]. The use of feature selection has been considered useful to help increase the accuracy of models by utilizing fewer feature characteristics but those of the most significant importance [89]. To this end, machine learning and data analytic approaches have been used to obtain the most important features within a dataset with conclusions that these approaches could potentially be effective for cases where there is limited data available.

2.8 Leveraging data analytical tools to optimize management systems

Given the constraints faced by road agencies worldwide and the expressed importance of data collection and analysis for the PMS, it is vital to consider low-cost methods to solve these problems. To this end, one important goal of this research project, therefore, was to create an innovative workflow for agencies to carry out efficient information mining to understand the important features in their road networks and when interventions should be carried out. To enable this, a case study in the city of Palermo, Italy utilizing historical information on road interventions, network characteristics and census information was used to provide a succinct but effective overview of features as identified by previous studies [78,79] from low-cost and easily available sources.

An innovative aspect of this part of the project is that it considers a relatively small database, which does not have the many descriptive and technical features of large-scale databases. To this end, the workflow highlights important factors that contribute to the road intervention schedule without relying on expensive data collection systems. This entails creating an effective feature selection, following by the development of a deep model constructed using open-source and flexible computing libraries to predict when interventions should be done within the network. The output allows for the optimization of available information at a low-cost and with limited resources, which helps to advance the pavement management planning and implementation process in limited data circumstances.

2.9 Development of models to understand pavement maintenance priority locations

Given the state of the research field and the need to create a pipeline that could be augmented to different agencies based on data availabilities, a general workflow was created that could be adapted based on the particular circumstances of a road agency. This workflow is shown in Figure 2-4. The workflow highlights the sources of data, the type of analysis needed at each stage and the outcome, which is a model to identify times for interventions for various roads within the network.

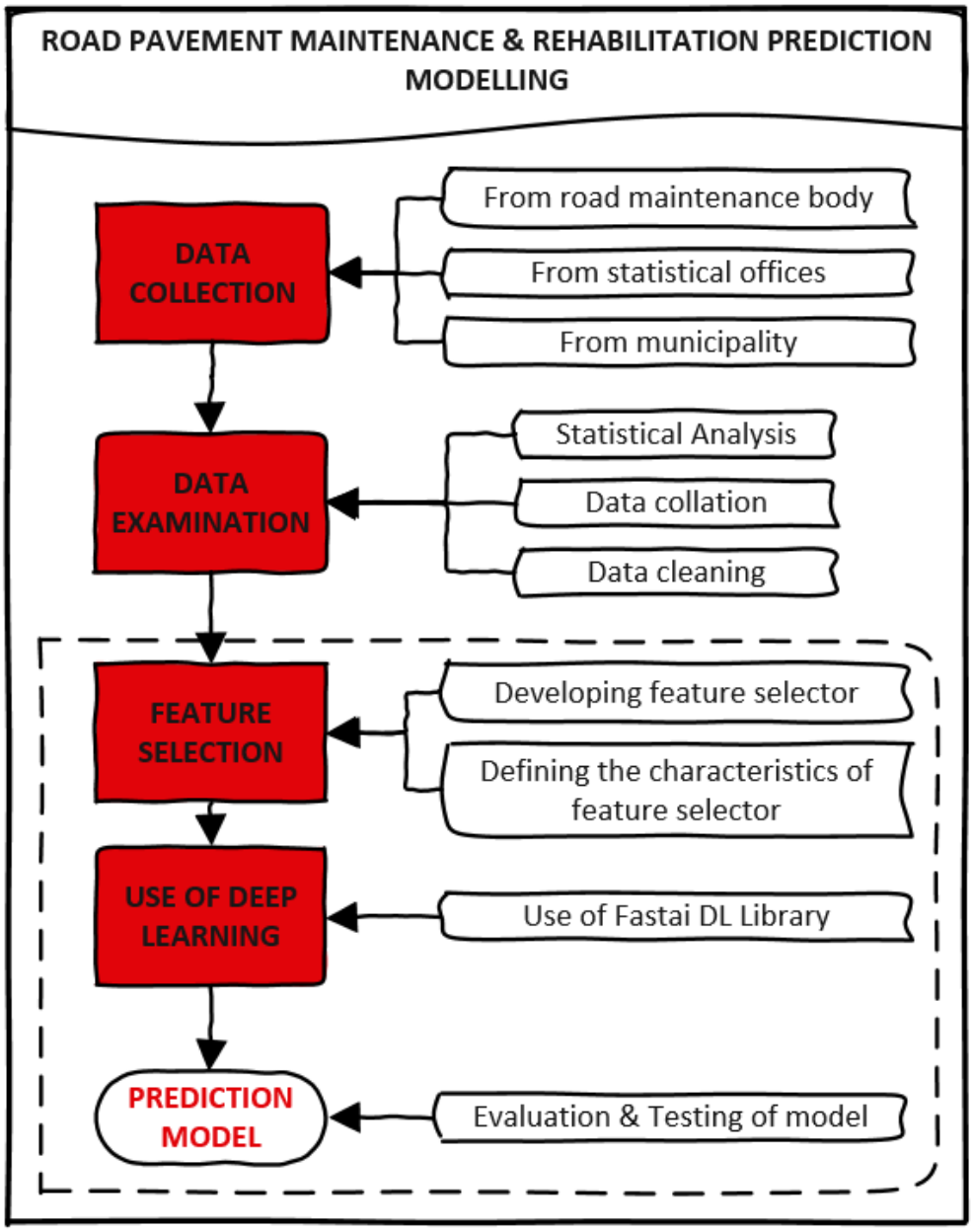

Figure 2-4. Workflow to determine locations to prioritize interventions

Within this methodological framework the use of well-known data analytic tools, including deep learning systems, are particularly well suited due to the intrinsic nature and complexity of the issues addressed.

2.10 Case study pipeline

The data collected was obtained using several open datasets available from government authorities, both locally and nationally, namely the statistical offices in Italy, and locally in Palermo, the local municipality and the road maintenance company. It was very important

given the context of the study to have data that was readily available. Data characteristics are further described in section 2.12.

2.10.1 Feature selection workflow

Once the data was obtained, the first step was a visual overview data analysis to establish relationships between features. To carry this out, a pandas dataframe [90] was set up to explore the dataset along with the use of matplotlib [91] and seaborn [92] for visualization through graphical relationship plots. This process allows for easy visualization of the statistics of the dataset and any necessary data cleaning before processing can begin. Both packages are also open-sourced and therefore can easily be utilized for further works and implementations. A descriptive analysis of the dataset was then performed to highlight distributions and identify relationships between the various features. The data was also pre-processed and sorted to ensure there were no missing values and inconsistencies.

2.10.2 Developing Feature Selector

Once the data was pre-processed, the next step was to prepare a feature selector tool adapted to the particular dataset but whose configuration could be modified based on the type of data typically available by road authorities and agencies. Feature selection involves using only appropriate features that explain the dependant variable and the process helps produce good learners and models [93]. In this instance, the dependent variable is the year of maintenance intervention of a given road within the network. A feature selector is essentially a tool that can be used for producing strong datasets for machine learning purposes. For the study, a feature selector tool was developed considering a selector developed in python utilizing the LightGBM library [94]. For the feature selector for this study, the backbone model of the tool was redesigned to identify feature importances using a gradient boosting machine from the CatBoost (Category Boosting) [95] library instead. This construction was done based on the strength of CatBoost to handle categorical features and the high presence of these features within this study. For the backbone of the feature selector, several ensemble deep learning gradient boosting algorithms were considered.

Gradient boosting algorithms are powerful tools that work by building ensemble tree predictors carrying out gradient descent within a functional space [95]. The algorithms sequentially create base models. The accuracy of these models versus others are considered

higher given the production of multiple models sequentially and the emphasis on training cases that are more difficult to evaluate, making mistakes more evident. In the process, the examples that were considered harder to estimate in the earlier base models are forced to appear more frequently in the training data. The subsequent base models are all aimed at correcting the prior mistakes in earlier models. The boosting process utilizes weak base models that are easier to predict and combines them to get one highly accurate model. The process fits subsequent models that allow for minimization of particular loss function objectives and errors averaged across the training data [96]. The pseudocode for Friedman's gradient boosting algorithm is given below [97]:

Algorithm

Inputs:

- Input data $(x, y)_{i=1}^{N}$
- Number of iterations, M
- Choice of the loss-function $\Psi(y, f)$
- Choice of the base-learner model $h(x, \theta)$

Algorithm:

1: Initialize $\hat{f}_0$ with a constant

2: **for** $t = 1$ to M **do**

a. Compute the negative gradient $g_t(x)$

b. Fit a new base-learner function $h(x, \theta_t)$

c. Find the best gradient descent step-size ρt:

$$\rho_t = \arg\min_{\rho} \sum_{i=1}^{N} \Psi\left[y_i, \hat{f}_{t-1}(x_i) + \rho h(x_i, \theta_t)\right]$$

d. Update the function estimate:

$$\hat{f}_t \leftarrow \hat{f}_{t-1} + \rho_t h(x, \theta_t)$$

3: **end for**

Gradient boosting methods offer a high level of customizable flexibility to any specific data-driven job [98] making it appealing for this dataset. There are several available gradient boosting models that are applied for prediction and regression problems. These include XGBoost [99], AdaBoost [100] and LightGBM [101] with the recent introduction of the CatBoost [95] libraries which provide a new approach, especially for categorical features. As a result of this, the CatBoost library was chosen given its ability to handle categorical features and previous studies identifying a higher performance of this algorithm versus the others previously mentioned [102,103]. This is particularly important to the model given the number of categorical features present in the dataset. CatBoost is different from the other gradient boosting algorithms in the following ways. The library handles categorical features during training as opposed to during the pre-processing time. It also utilizes the entire dataset for training. For each training example, the library carries out a random permutation of the

dataset and calculates an average label value for the particular example with the same category value placed before the one provided by the permutation [104]. The library allows for unbiased boosting with the categorical features and feature combinations wherein all the categorical features can be combined as a new feature [95]. It also makes use of a fast scorer in which CatBoost utilizes oblivious trees as base predictors [104].

The CatBoost library [95,105] introduced two vital advances: ordered boosting, which is a permutation driven alternative to the classic choice and a state-of-the-art algorithm to process categorical features. Most gradient boosting algorithms use encoding for categorical features but CatBoost utilizes an innovative strategy for this. An ordering principle is utilized which feeds training examples sequentially which allows the target values to rely on the historically observed values. For this to be possible, CatBoost utilizes a random artificial time permutation for the training examples for the gradient boosting process. Based on these factors, the CatBoost library was exploited.

2.10.3 Defining the characteristics of the feature selector

Once the backbone model was determined, the hyperparameters of the model were needed. Within the selector, 12 training runs were utilized to lower variances with the CatBoost model itself being run for 500 iterations, and early stopping using a validation set was used to avoid overfitting of the data. Within the implementation, CatBoost gives indices of categorical columns to allow them to be encoded as one-hot encoding utilizing the 'one_hot_max_size' feature. This is based on the number of unique values available for the features considered. This is important for this study as the process can be calibrated based on the number of unique values within the dataset instead of using an assumptive value. A 'one_hot_max_size' of 25 was utilized given the presence of data for 25 neighbourhoods (as is the case in Palermo) which have related categorical features. The use of the 'cat_features' parameter allows the user to pass the column indices for the categorical features through the model for preprocessing and use in the one-hot encoding process. The model utilized within the setup was defined as follows using the CatBoostRegressor model setup:

```
model = catboost.CatBoostRegressor(eval_metric='RMSE', one_hot_max_size=25
,depth=10,iterations=500, l2_leaf_reg=9, learning_rate=0.05)
```

Within the definition of the model, the 'eval_metric' used was the Root Mean Square (RMSE) with an 'l2_leaf_reg' value of 9 used (regularization term used to regularize the objective

function and minimize both loss and complexity of the model) and a depth of 10 (depth of tree used) and a learning rate of 0.05. The Root Mean Square Error (RMSE) metric is a common evaluation metric and is estimated by the function given in equation 2-1 below.

$$RMSE = \sqrt{\frac{1}{n}\sum_{i=1}^{n}(Y_{i,m} - Y_{i,e})^2} \quad (2\text{-}1)$$

where $Y_{i,m}$ = measured value , $Y_{i,e}$ = estimated value, n = number of observations. The parameters used were based on iterations of models and were found to be the most appropriate. Early stopping of the model was also carried out with a test set of 20% to validate and ensure overfitting was not done. During the run of the model, the feature importances were recorded using the 'feature_importances' function of the Catboost library. These were recorded and sorted in descending order to showcase the features with the most impact on the model. Additionally, a SHAP (Shapely Additive explanations) analysis was done to further illustrate the effects of the various factors used in the study. SHAP uses a theoretical game approach the explain the outputs of machine learning models as it tries to connect credit allocations with the local explanations using values from game theory [106]. It was utilized only for visualization purposes of understanding how the interventions could be changed by individual changes in the factors used. Finally, the values were normalized based on the total contribution to the model result and these results were graphically represented.

2.10.4 Using machine learning on tabular datasets

Once the important features were identified, the next step was developing a model that could attempt to predict the year for intervention when roads would reach a similar degradation level as those identified in the dataset, based on the available characteristics. To accomplish this, a deep learning model was developed for the application on a tabular dataset. Deep Learning is a machine learning technique based on the "learn by example" principle. It must also be mentioned here that the application of deep learning on pavement engineering will be further thoroughly evaluated in chapters 5 to 7 but the focus will be on imagery applications. A Deep Learning model commonly uses large sets of labelled data which is processed through neural network architectures built-up with many layers. By exploiting the input data, through synaptic connections between adjacent layers with feed-forward propagation, the output data is computed. The output quality depends on the recognition accuracy, which in turn depends on the consistency of both the neural structure and process

data. Therefore, it is clear that the choice of the input data (features) and the neural network architecture, including the typical training and testing parameters, are important to achieve decision-making targets. Whilst, a significant amount of research has been focused on the utilization of deep learning for image analysis, there is a lot of merit to leverage the power of deep learning for tabular dataset analysis as well. New base architectures have shown a lot of worth in this type of analysis over traditional classification and grouping methods [107] and by considering a deep learning model, this workflow can leverage both the resources of the gradient boosting for feature selection and deep learning for the model development. Deep learning models also have shown advantages over traditional approaches when datasets have a high number of categorical variables. This is as a result of the model using embeddings for these categorical features [108] and this is important given the presence of these variables in the dataset.

For this study, the open-source FastAI deep learning library [107] was utilized. This library was chosen because of its ease of use, therefore, making it easily interpretable and easily replicated for authorities and users. The library was designed around two main goals: to make its implementation and use approachable and productive whilst maintaining flexible configurability. This is important as there is not a significant level of training needed to create the models and therefore explaining its implementation for road professionals would not be difficult. FastAI also offers excellent support for tabular datasets with built-in loaders to handle this type of data. Within the FastAI library, there is high-level API support for tabular datasets which allows the creation of models based on characteristics of the dataset available. Within the tabular data setup, there are also provisions to denote categorical elements, which is an added advantage, considering the dataset at hand. The tabular API is made up of the components shown in Figure 2-5.

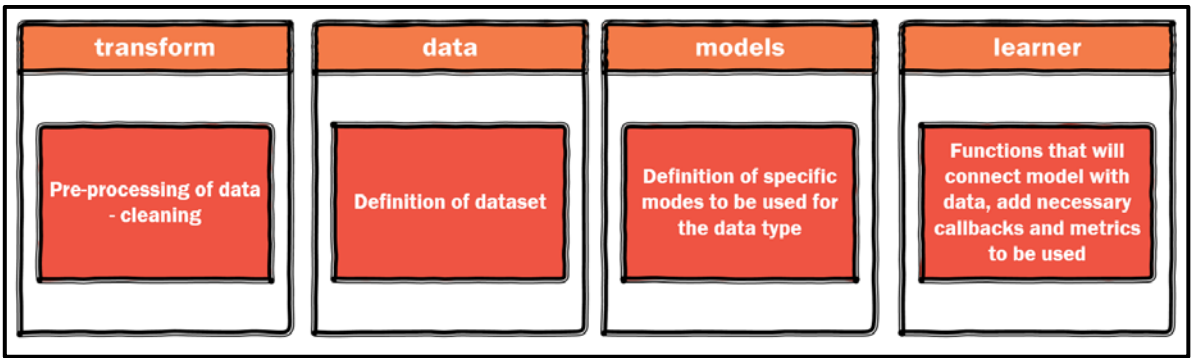

Figure 2-5. FastAI tabular module structure

The library also has model-fitting methods within its structure namely, the 'lr_find' feature, which allows the establishment of a good learning rate to be used rather than going through an iterative process at the training level. Within the model, the training was regularized utilizing dropouts for dense layers and embeddings (0.05). These were features applied to avoid overfitting of the model. A random seed value of 47 was utilized for starting the training of the model. Three preprocessors were also utilized – FillMissing, Categorify and Normalize; FillMissing searches for missing values, Categorify finds the categorical variables and Normalize carries out a normalization for continuous variables within the dataset. The dependent variable ('dep_var) for this study was the year and the features used were grouped based on them being either categorical (cat_vars) or continuous variables (cont_vars). The data was split between training, testing and validation sets with 80% allocated for training and 20% for training and validation. In the model, three dense layers were utilized with different dropout values for each of the dense layers. It is critical to note that only the most important features as set out by the results from the feature importance tool (as discussed in section 2.10.3) were utilized in the FastAI model. The model setup and the code parameters developed and used are further given in Appendix A.

Once these parameters were set up, the learning rate finder was employed to suggest an appropriate learning rate and using this learning rate (lr) the model was trained with 80 epochs (training steps) and using a weight decay factor (wd) of 0.2 to help regularization and to prevent overfitting. All of these factors implemented using the 'learn.fit_one_cycle' function within the library.

2.10.5 Assessment of the accuracy of the predictor model

For the metric evaluation of the model produced, the Root Mean Square Error (RMSE) metric was utilized (as previously explained in section 2.10). This is a common metric used for evaluating regression-based models and is estimated by the function given in equation 2-1.

To further explain the model's results accuracy, the RMSE was normalized based on the mean of the dependent variable, using a metric called Normalized Root Mean Square Error (NMRSE) to allow for a comparison across different scales and one that is more interpretable to users. These metrics are typical and representative of metrics utilized when assessing the accuracy

of machine learning forecasting models [109,110]. This was generated using the function in equation 2-2.

$$NRMSE = \frac{\sqrt{\frac{1}{n}\sum_{i=1}^{n}\left(Y_{i,m} - Y_{i,e}\right)^2}}{\overline{Y_{i,m}}} \quad (2\text{-}2)$$

The evaluation was done utilizing the validation set during the model to establish the accuracy of the model. Additional tests were also run using data augmented data from the municipality to further validate the use of the model and workflow.

2.11 Description of Case Study – understanding the complexities of Palermo, Italy

For the case study, it is important to understand the particulars of the city. The city of Palermo is located on the north-western coast of Sicily, Italy, covering an area of 158.88 sq. km with 663,401 inhabitants [111]. It is a part of southern Italy, where municipalities have been shown to have a lower efficiency when considering the difference between the assessed spending needs given conditions and the actual spending [112]. This is an important factor as the efficiency level is associated with productivity levels. This is coupled with lower spending on information technology (IT) systems and services within the public sector [113] which limits the capacity of agencies to use highly technical systems. Because of this, there is a great opportunity to use the city as a case study given the limited resources these authorities face and therefore the need to implement systems, which do not require significant IT investment and resources.

The municipality's road network consists of approximately 3,800 road axes with a total surface area equal to approx. 9 million sq. meters. This is a significantly large network and therefore having a system in place that could pinpoint particular areas of interest for intervention would be very useful. Data on the commute from the last population census carried out by ISTAT (Italian National Institute of Statistics) [114] show that there are approximately 278,954 individuals who commute every morning, for work and study purposes, of which 96.3% of the movements are carried out within the municipality. It is also important to consider that car sharing is very low with the average coefficient of vehicle occupancy being 1.3 and the majority of trips made by private cars [115]. This is an important consideration as it means

that the number of workers within the city will have a significant impact on the traffic levels and in turn the roads with higher debilitating conditions.

The city was previously divided into 25 neighbourhoods but this was subsequently amended in 2009 to a division of eight circumscriptions [115] (screenshot taken from Google Earth [116]) as shown in Figure 2-6. Circumscription no.1 is particularly important as it houses the historical district of the city and the ZTL (Limited Traffic Zone) area, which has a traffic congestion charge attached to it and additionally is where a lot of tourism is concentrated given the presence of historical buildings, museums and artefacts. Circumscription no. 8 is also important given its central location and proximity to the port.

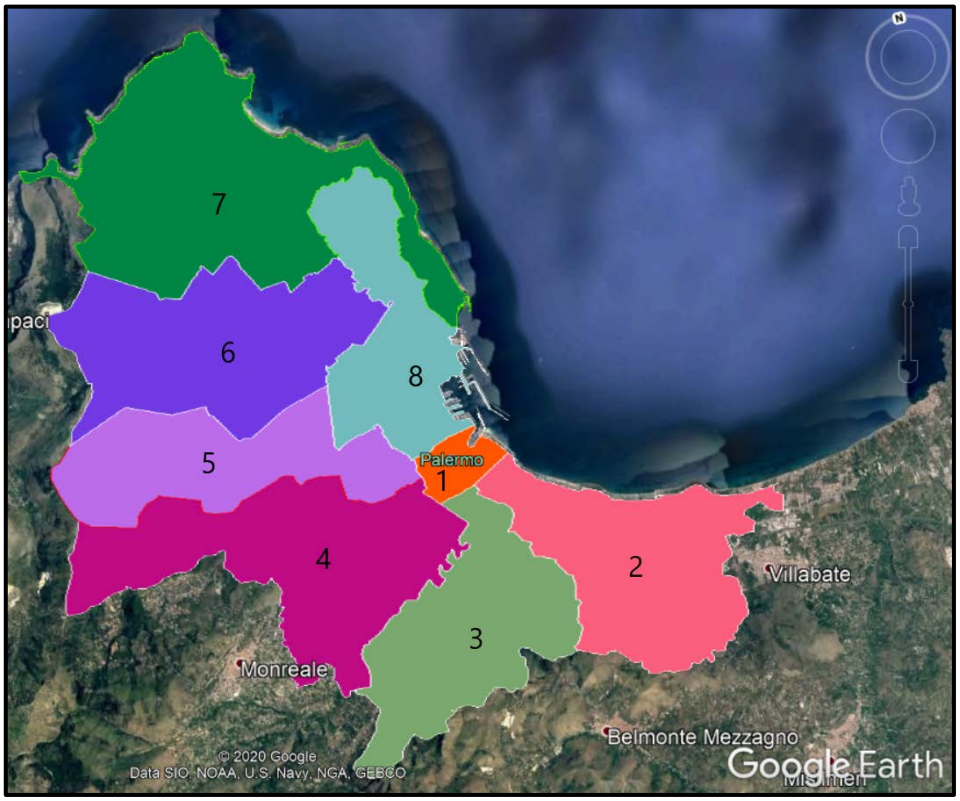

Figure 2-6. Circumscription divisions within Palermo

The circumscription and neighbourhood divisions are very important as population and industrial data has generally been collected and aggregated according to these boundaries. It is critical for any model development to understand the regional and geographical divisions within a city to adequately collate the data collected and therefore this should be carried out in any study of this nature. For traffic analysis, the city is divided into 200 traffic zones ('PUT' traffic zones) across its area and this is shown in Figure 2-7 (Drawing from Palermo Statistics Report [117]). This is particularly important as commute and commercial activity are also recorded based on the interactions between these 'traffic zones'.

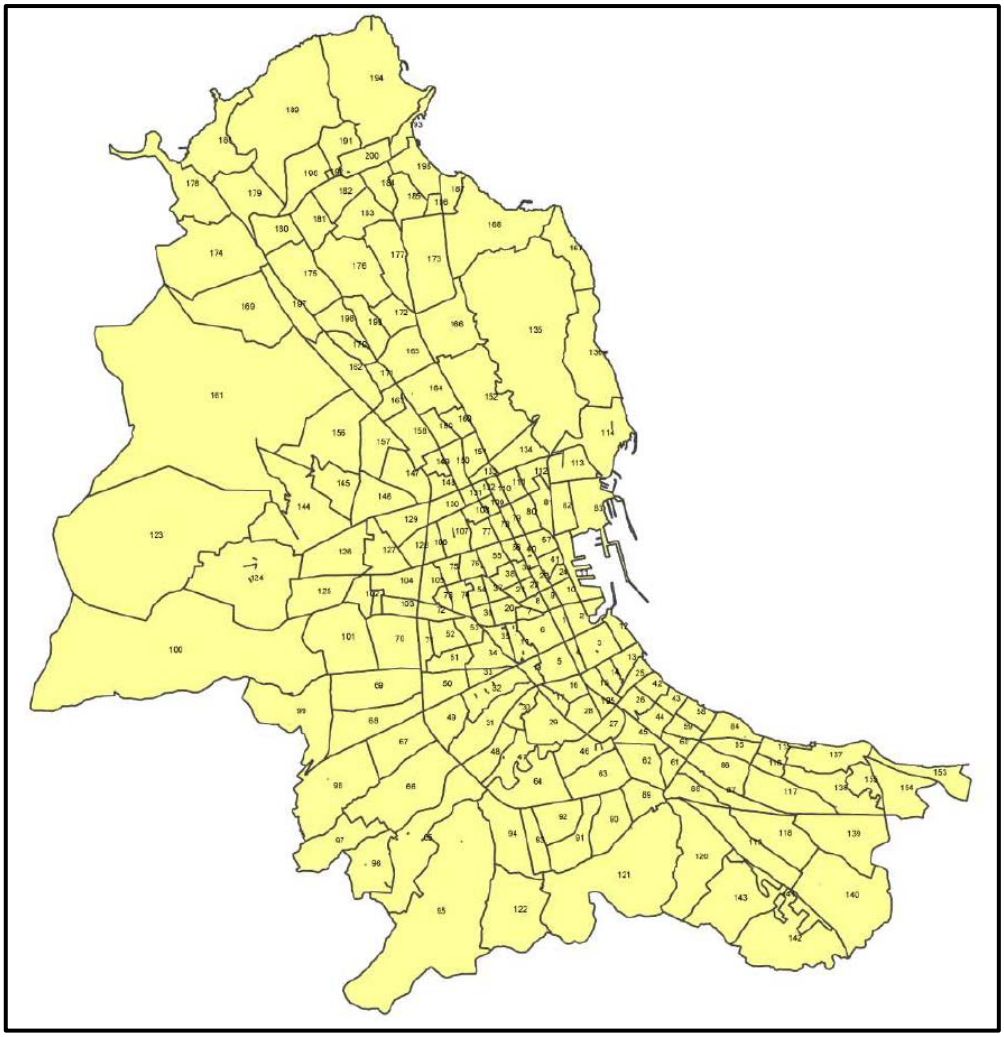

Figure 2-7. PUT traffic zones within Palermo

2.11.1 Characteristics of available data

As previously mentioned, the data collected was obtained from government authorities, both locally and nationally. The data compiled from these sources resulted in a dataset of 1099 maintenance occurrences over 10 years in the city. The local company legally required to carry out these maintenance activities is currently Risorse Ambiente Palermo S.p.A. (RAP) [118]. The data sources are summarized in Table 2-3.

Table 2-3. Summary of data sources

Data Group	Source	Data obtained
Census data	ISTAT [114]	Population of Circumscription,
Traffic and commuting data	ISTAT, Municipality of Palermo [114,117,119]	Employment, commuting statistics, industrial activities, commercial activities
Economic activity data	Palermo Urban Transport Plan [115]	PUT zone activity rate, traffic rate, workers, arrivals and departures, Industrial activities in the zone
Historical maintenance and road network data	RAP and Municipality of Palermo [120]	Year of maintenance, road lengths and area

According to the company's legal requirements, it has to carry out a minimum of 1.8% annual surface area interventions on the road network. For the planning of interventions, the company employs the application of filtering criterion that produces a list of roads to be maintained that are in the worst deterioration state and the process favours those roads with higher traffic intensity. To create this list of roads with grave severities, road inspectors carry out laborious monitoring activities throughout the year to update road conditions. They manually observe conditions, using video and physical surveys [121], and generate reports on the road conditions. Whilst this can be an effective method to collect data, it can also be expensive considering the number of surveys and personnel involved. Therefore, having a model that could assist in predicting which roads are likely to need rehabilitation would reduce costs. Additionally, should physical surveys not be possible, the model could be utilized to produce a non-subjective indication of where interventions should be done.

The instances of intervention were recorded for six time intervals over the period and therefore within the data, the year group is recorded with numerical values with a range of 1-6 where the interventions occurring at year group 6, represent interventions at 10 years beyond the first recording. The roads within the list are those having a high severity rating and therefore requiring full surface depth repair over the area specified in the data. The characteristics of the roads on which these interventions were carried out were compiled and this represented the list of features to be analysed. Unlike large databases like the LTPP database, where detailed technical information on the road condition and monitoring, such as PCI and IRI values, are available, the dataset focused on physical road characteristics, movements of cars and people and economic activities carried out on and near the roads. This issue is evident in many small countries and cities where there is a lack of funds to have extensive databases and therefore the challenge exists to produce reputable data analyses with limited data. The features produced by this research workflow are shown in Table 2-4. It must be noted whilst the data was obtained from several open-source systems, it did involve multiple stakeholders. For the final compilation, a collation of the variables across matching points for each intervention and each road had to be carried out. From this, these factors provide a good representation of the city's situation considering the typical overview feature groups previously discussed in section 2.5, allowing for an accurate portrayal of the network. The task was, therefore, to utilize these factors to provide analyses on road maintenance and

predict the next instances of interventions. Consequently, using this workflow could provide an easier pathway for the road authority to plan interventions.

Table 2-4. Description of features within the dataset

Data Group	Description of data
neighbourhood	neighbourhood where the road is located
circ	Circumscription(circ.) where the road is located
circ_pop	population of circ. where the road is located
street_category	road category classification (labelled 1 or 2; where 1 represents the higher trafficked option)
length	road length (measured in meters)
area	road area covered (measured in sq. meters)
zone	zone where road is located (1-historic centre, 2-main city, 3 – city peripheries)
year	year group of maintenance
pop_den	the density of population in circ.
public_buildings	The presence or lack of presence of public buildings near the road (labelled 1 for yes and 0 for no)
commercial_activties	The presence or lack of presence of commercial activities along the road (labelled 1 for yes and 0 for no)
traffic_rate	rate of activities in traffic zone where the road is located
tz_pop	population of traffic zone where the road is located
tz_pop_den	population density of traffic zone where the road is located
tz_workers	number of workers in the traffic zone where the road is located
unemployment	percentage of unemployment in circ. where road is located
industrial_jobs	percentage of industrial jobs in circ.
circ_road_den	road density within circ. where road is located
t_arrivals	number of trip arrivals in the traffic zone where the road is located
tz_departures	number of departures in the traffic zone where the road is located
tz_perdays_rt	number of total trips made within the traffic zone where the road is located

Within the dataset, it is worth mentioning that a significant number of the features are categorical as they relate to the circumscription or the neighbourhood in which the feature occurs.

2.12 Results and discussions from model development

The first step was the uploading and examination of the data utilizing a pandas dataframe. The first analytical step was a descriptive analysis of the features of the dataset. A snapshot of the features within the dataset is shown in Figure 2-8 which was created in the pandas df setup. Within the figure, it can be seen that there were no missing data entries, which is important to ensure there are no model inconsistencies later in the process. As previously mentioned there were 21 feature categories present in the dataset each carrying 1099 values corresponding to the maintenance activities carried out over the previous 10 years (2001-

2019). This timeline thereby represents a significant period for analysis, which is important to ensure credibility in the process.

```
<class 'pandas.core.frame.DataFrame'>
RangeIndex: 1099 entries, 0 to 1098
Data columns (total 21 columns):
 #   Column                 Non-Null Count
---  ------                 --------------
 0   neighbourhood          1099 non-null
 1   circ_pop               1099 non-null
 2   street_category        1099 non-null
 3   length                 1099 non-null
 4   area                   1099 non-null
 5   zone                   1099 non-null
 6   year                   1099 non-null
 7   circ                   1099 non-null
 8   pop_den                1099 non-null
 9   public_buildings       1099 non-null
 10  commercial_activities  1099 non-null
 11  traffic_rate           1099 non-null
 12  tz_pop                 1099 non-null
 13  tz_pop_den             1099 non-null
 14  tz_workers             1099 non-null
 15  unemployment           1099 non-null
 16  industrial_jobs        1099 non-null
 17  circ_road_den          1099 non-null
 18  tz_arrivals            1099 non-null
 19  tz_depatures           1099 non-null
 20  tz_perdays_rt          1099 non-null
dtypes: int64(21)
```

Figure 2-8. Description of data entries using pandas dataframe

To understand the distributions within the data, histograms were generated for the features to analyse the distributions of the features across the period. Of particular interest were the distributions of the features corresponding to the physical road characteristics (length and area) and the distributions for the occurrences of activities within the different zones, circumscriptions and neighbourhoods over the 10 years. The length and area are directly related to each other with their distributions showing a direct similarity. The distribution for the length feature is shown in Figure 2-9. This figure shows that the majority of interventions were of a road length of less than 500m.

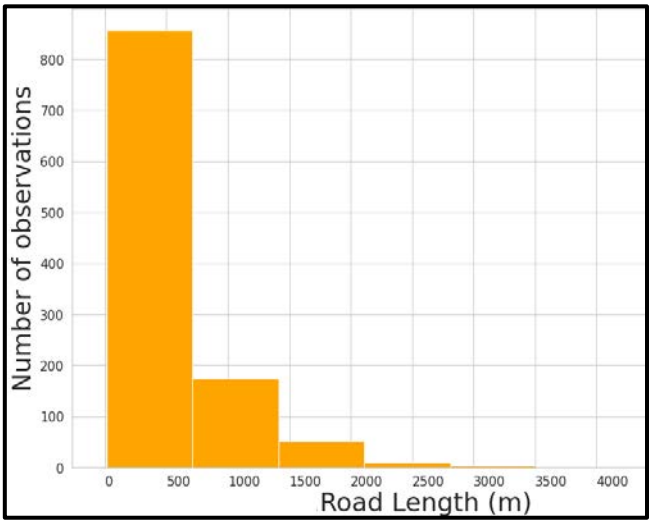

Figure 2-9. Distribution of feature - Road Length

Subsequently, the distributions corresponding to the geographical divisions of the city were examined. The distribution corresponding to the zoning of the city is shown in Figure 2-10 (where the zones are numbered as described in Table 2-4 with 1 representing the historical centre, 2 – the main city and 3 the city's peripheries). This highlights that most interventions do not take place within the historical centre and instead are concentrated outside of the centre and the central districts of the city. This was expected given the traffic levels within the centre and a higher level of foot traffic which occurs within the historical district due to restrictions and congestion charging being in place. Furthermore, zone 3 is larger and therefore has more roads than the other two zones. This provides another key to understanding the necessary intervention scheduling in the municipality.

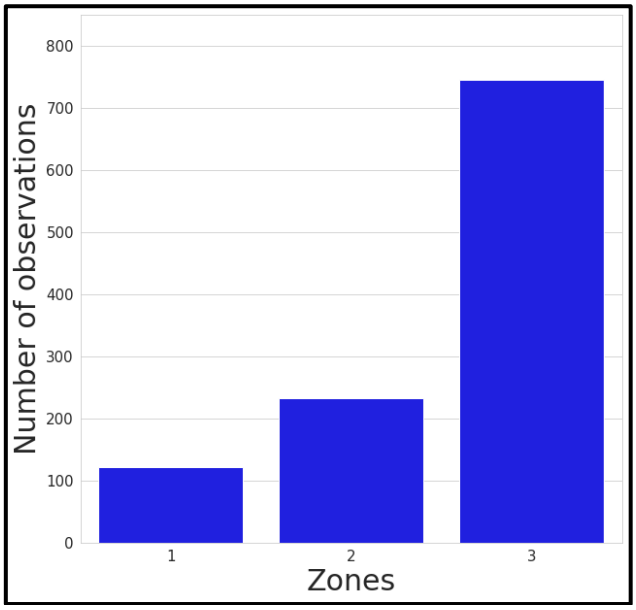

Figure 2-10. Distribution of interventions across zones

Concerning the distributions of the district divisions (Figure 2-11), it was noted that the majority of interventions were recorded in circumscription No. 8 which is near the seaport as previously noted in section 4. The most prevalent neighbourhood was no.10 which is the 'Politeama' area, which has many stores and is highly trafficked therefore validating this statistic. This provides an insight into the priority locations of intervention. Otherwise, the number of interventions across the neighbourhoods is fairly distributed. Whilst these are interesting results, it was also critical to identify correlations between interventions within these districts and the time of intervention to understand the sequences of interventions concerning not only their location but also time.

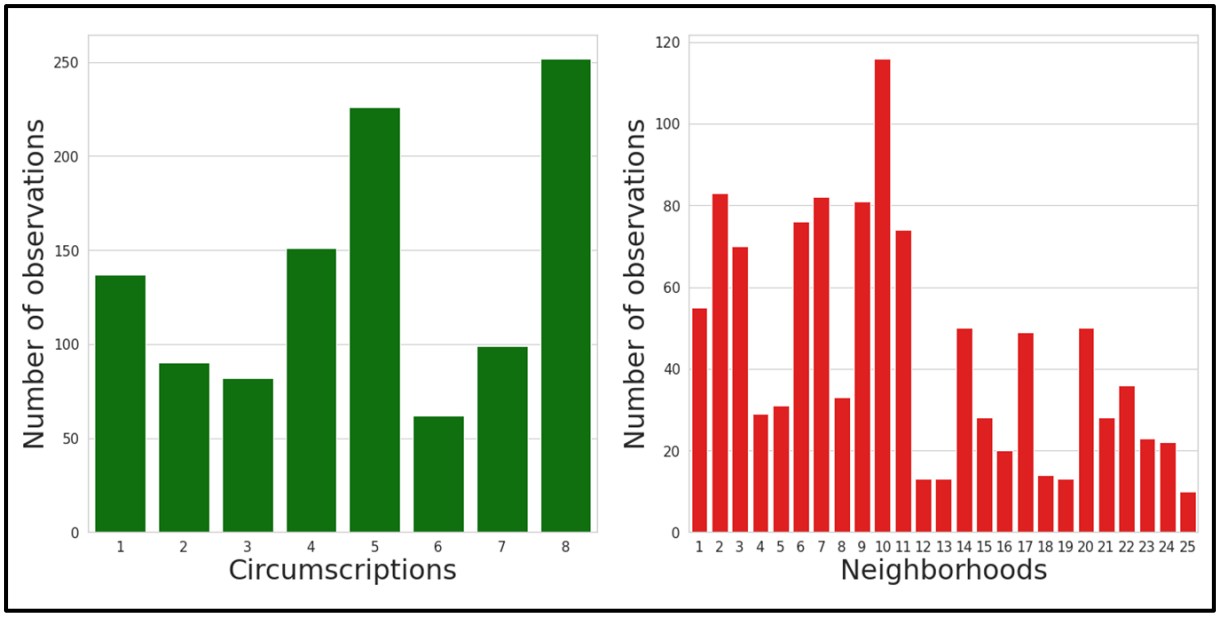

Figure 2-11. Distributions across circumscriptions and neighbourhoods in municipality

To analyse the interventions by time, boxplots were used, within the pandas dataframe, to relate the divisions to the year group of intervention. These boxplots are given in Figure 2-12 and Figure 2-13.

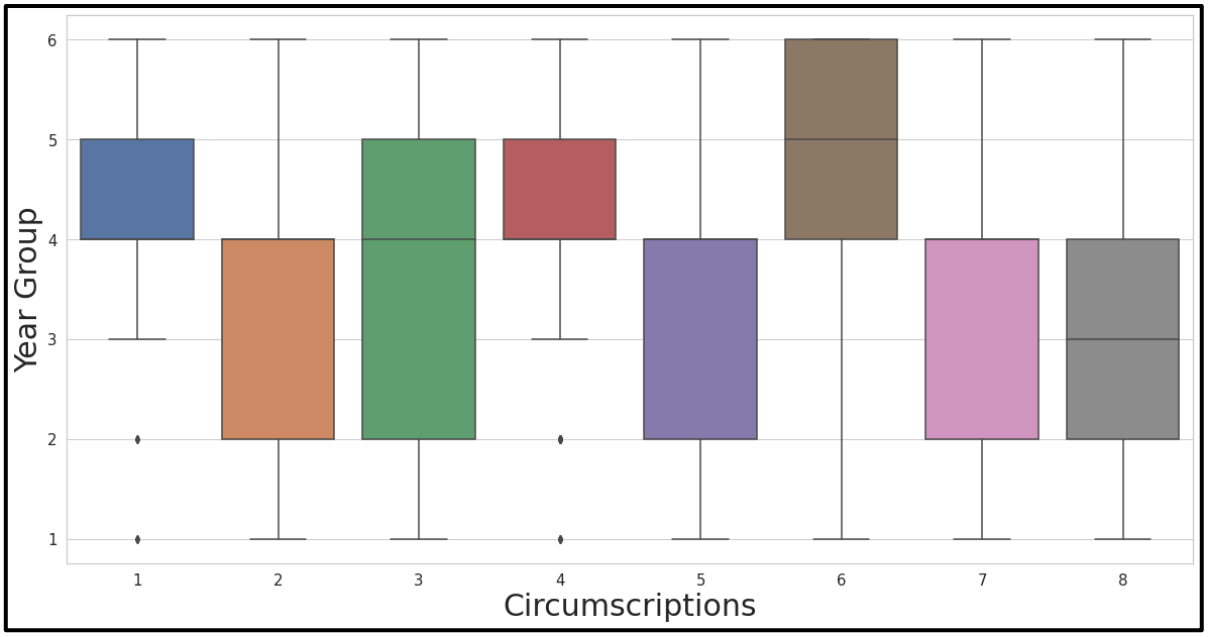

Figure 2-12. Boxplot of maintenance intervention in each circumscription with respect to time

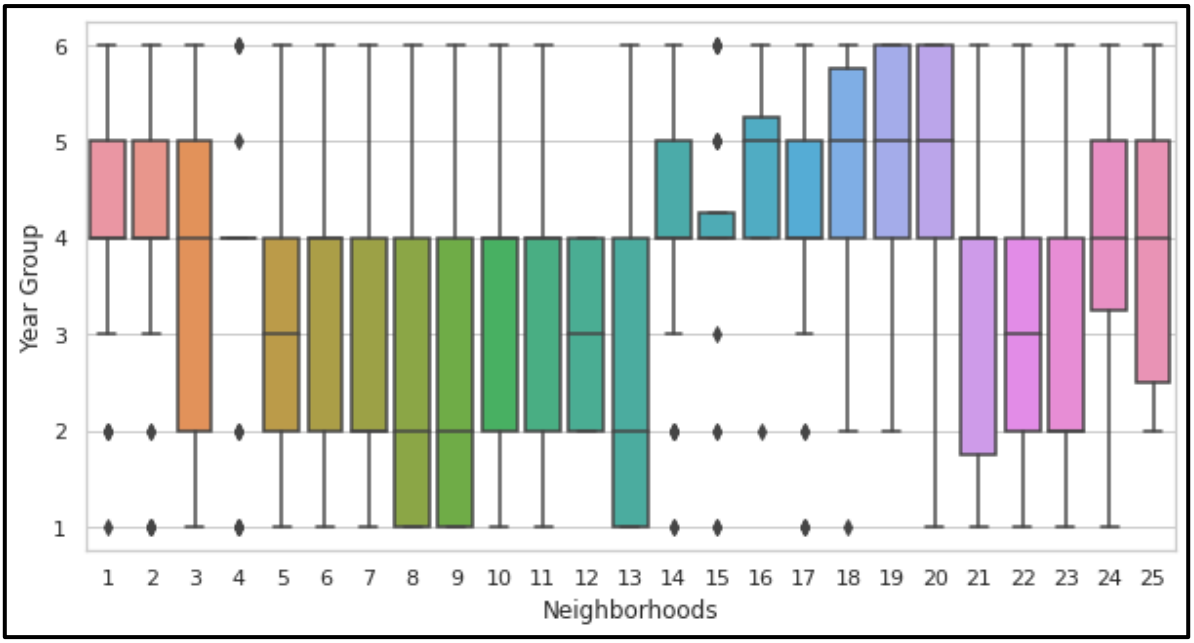

Figure 2-13. Boxplot of maintenance intervention in the neighbourhood with respect to time

The plots allowed for analysis of when the interventions are taking place. For the circumscriptions, the interventions are split in time with the majority of interventions taking place within the first 4 year groups for circumscriptions 1, 5, 7 and 8. On the other hand, activities were concentrated in the later years for circumscriptions 2, 4 and 6; with circumscription 3 being the only one with a statistically significant overlap of activities across the period. This is important because it again gives an insight into time intervals that can be set up for monitoring activities within various districts based on the historical activities. It essentially demonstrates timelines of when neighbourhoods and circumscriptions need attention and thus intervention.

The next important data analytic was the year of the intervention. A violin plot was constructed to highlight when in time the activities were being carried out. This is shown in Figure 2-14. The violin plot is a combination of a box plot and a kernel density plot as it represents a modification of the box plot where the information from the local density estimates are also added and displayed [122]. It was used here because it offers the clear advantage of not only displaying the typical statistical measures (median, interquartile ranges and outliers); but also showing the entire data distribution. This is key in this analysis as it enables the display of multiple peaks as seen in the figure, which could not be seen in a typical boxplot. Within the plot, it can be seen that the majority of interventions occurred in the middle at year group 4, which represents interventions at year 7 but also, gives the smaller

peak at year group 2, which should also be a point of alert for the road agency. This gives the study another important discussion point as it showcases that the interventions are concentrated around these times and thus a larger number of resources could be allocated in the future for these periods.

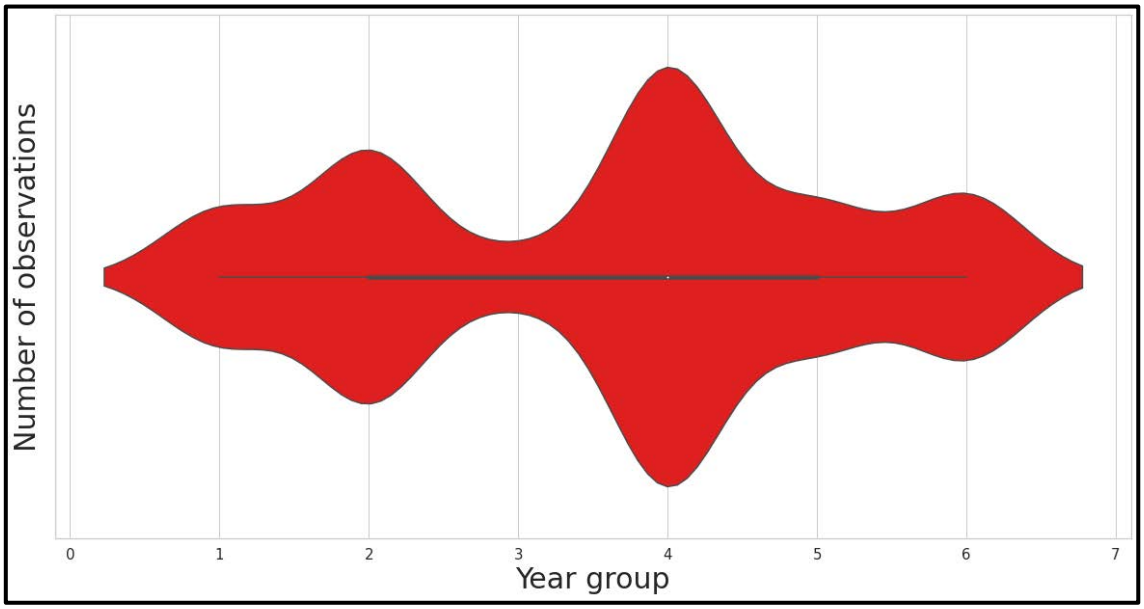

Figure 2-14. Violin plot of the distribution of interventions in time

For the other features within the dataset, another interesting feature to highlight was the presence of commercial activities. This is important as commercial activities are likely to lead to higher traffic and general activity and therefore the roads in these areas are likely to suffer from more damager quicker. A boxplot of this feature versus time was plotted and is displayed in Figure 2-15. This indicates that the areas without commercial activities required maintenance at a later stage than those with the businesses. This was expected but it is important to confirm to validate the use of this data based on typical trends in traffic and road maintenance on pavement deterioration.

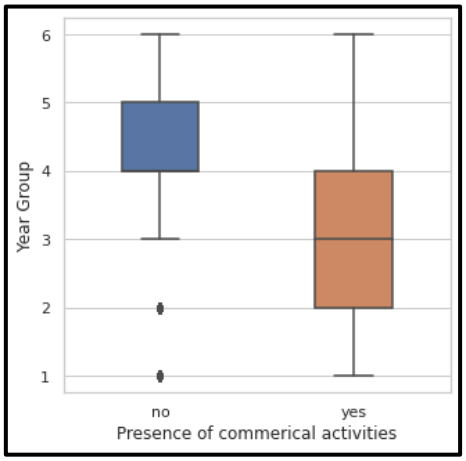

Figure 2-15. Distribution of maintenance interventions by the presence of commercial activities

Once the initial examination of the data was completed, the next phase was the feature selection as it is more difficult to understand which of the other features should be utilized in a modelling framework using only a statistical examination of the distributions of features.

2.12.1 Feature Selection results

With the first examination of the features complete, the feature selection algorithm as constructed in section 2.10.3 was applied. The model was implemented in python and a normalized plot of feature importances was generated. At iteration 408, the best result was achieved according to the model. The top 15 important ranked normalized features are given in Figure 2-16.

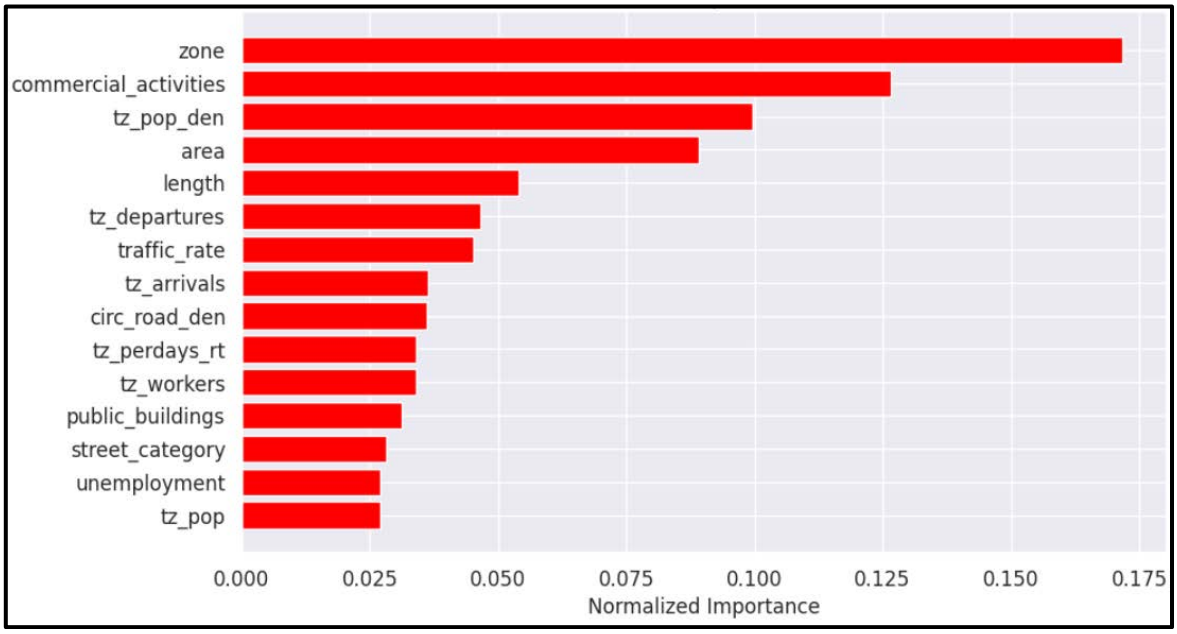

Figure 2-16. Ranked feature importances within the dataset

Within the figure, it can be seen that the most important feature is the zone and this can be further validated based on the data examined in section 2.12 concerning the distribution of interventions within the zones. The next important feature is that of commercial activity and this again can be expected given the propensity of interventions being needed earlier when there are commercial activities as highlighted in Figure 2-15. The next feature on the list is that of the population density within the traffic zone showing how important it is to understand the density of people living near a particular road for maintenance activities. Following these are the physical features of area and length, which definitely should be considered to be important as they represent information on the actual road's dimensions. It is important however to note that whilst the physical characteristics are important they are

not the most important features, which is an important concluding result. The next series of features related to the traffic in the zone and on the type of persons living near a particular road.

Another point of the analysis is the use of the SHAP importance values, which indicate how changing one factor would affect when the model predicts an intervention should happen. These values are illustrated in Figure 2-17. Within the figure, the visualized output value is 4.61 representing an intervention at this time and for this prediction, it can be seen that only the factors of zone and street category are pushing the prediction to be lower whilst all the other features are pushing the prediction to be a higher value. This gives an understanding of the impact of these particular features on the model as particular zones or street categories will push the model to make a predicted intervention earlier. This represents a snapshot of the possibilities of the model and is used here only as another validation of the most important ranked features shown in Figure 2-16 being commercial activities and zones. For each individual prediction, the exact impact will vary but the two most referenced features will be expected to remain the same.

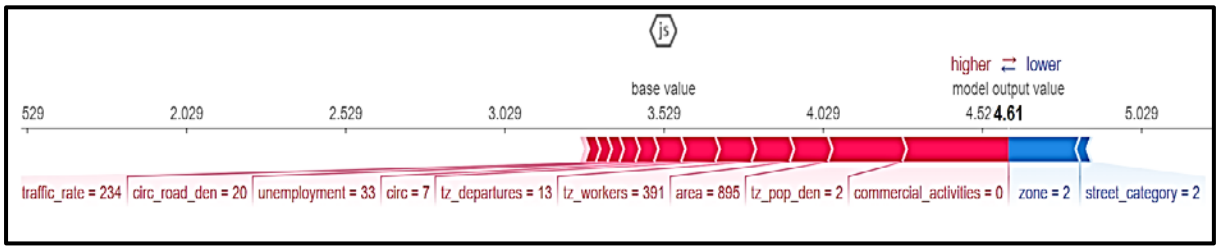

Figure 2-17. SHAP Importance values for factors

It should be noted that these results are about the particular situation within the municipality under question and the same features could result in a different relationship in a different city. As such, it is critical to utilize results from the particular municipality and not rely on feature representations of other cities or municipalities. Therefore, what is important is the modelling process and also the ability to verify whether the results produced by the model can be explained considering the situation in real life within the city. Once these features were computed, the next phase of the study was the use of these particular features within a model to predict maintenance interventions.

2.12.2 Prediction Model results

The model was set up using the hyperparameters as set out in section 2.10.4 and it was run with 80 epochs (model steps) used to reduce variances. For the model, the first step was to utilize the learner within the FastAI library to identify the appropriate learning rate for the training. This was performed within the setup and was based on models carried out to determine appropriate learning rates for machine learning models [123]. This is visualized by the graph in Figure 2-18, showing the point corresponding to this learning rate to be utilized. The FastAI library has a built-in function, which allows for programming a suggested value that can then be utilized directly within the model for more effective training. This process was done with the suggested training rate being highlighted as seen in Figure 2-18. From this process, a learning rate of approximately 0.02 was used for the model.

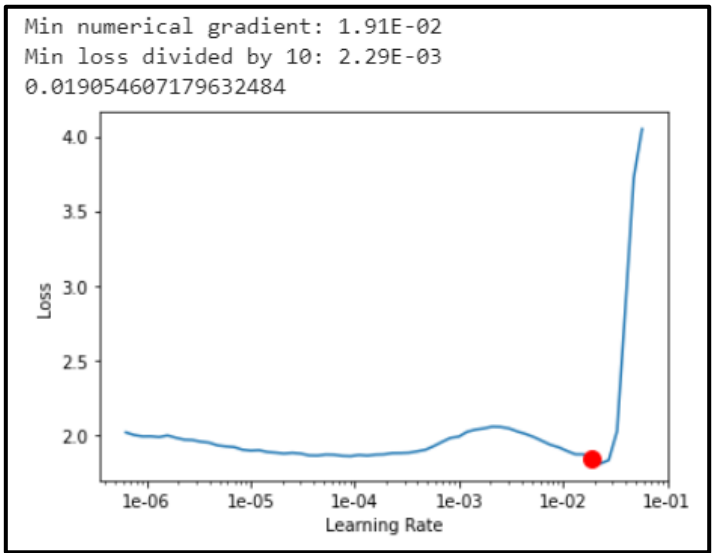

Figure 2-18. Utilization of learning rate finder within FastAI library

This learning rate was subsequently utilized in the training process. During the training, the validation loss was monitored against the training loss to ensure there was no overfitting. Overfitting can typically be assumed to be taking place if the validation loss is significantly higher than the training loss. This was monitored within the setup with the graph shown in Figure 2-18. Within the figure, it can be seen that the values stabilized by the end of the training run and the validation losses were not significantly higher than the training losses. The RMSE values were also recorded during the process as shown in Figure 2-19. The values of RMSE were also stabilized by the end of the training.

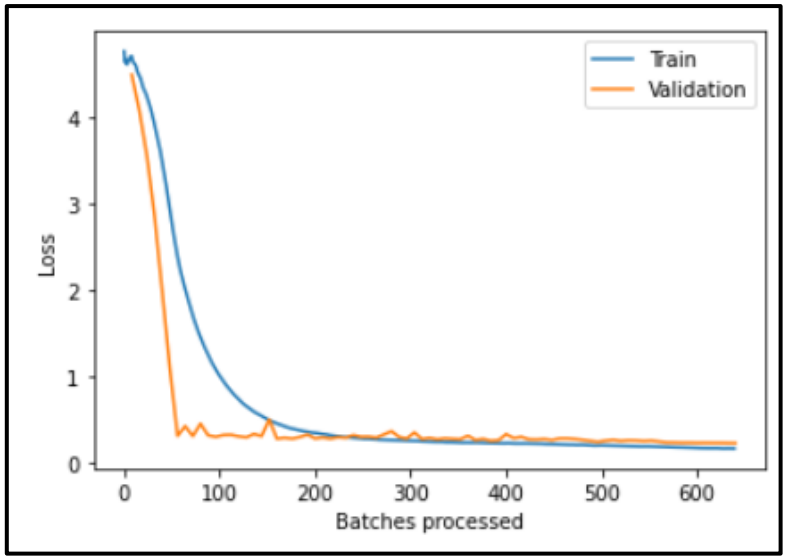

Figure 2-19. Loss observed during the training process

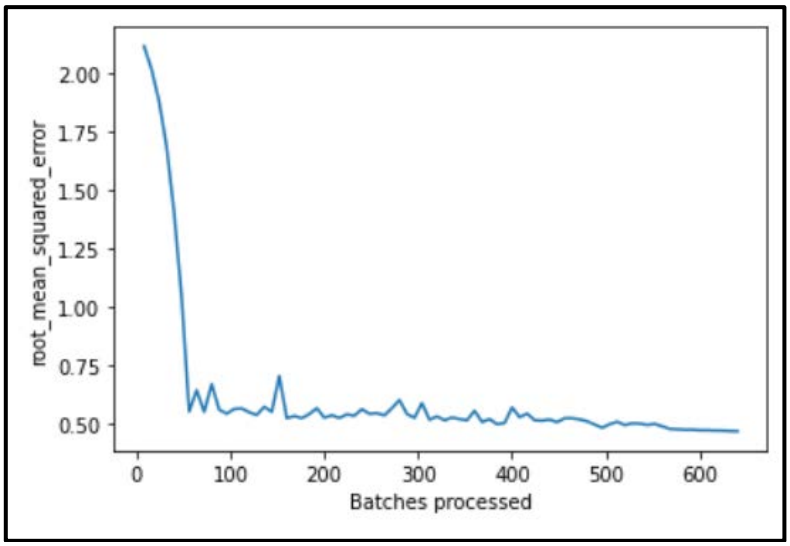

Figure 2-20. Observed training metric during training

Once the model was run, a model summary was generated and this is shown in Appendix A. Within the model summary, it can be seen there are embedding layers for each categorical variable and there are dropout layers provided to help reduce biases and variances as previously indicated. Additionally, all the parameters used for the model were trainable and utilized in the training. After training was completed, the RMSE observed at the final epoch was 0.469. Using the values of RMSE, the NRMSE was computed using the average of the input dataset to normalize the value and make it interpretable on different scales and to provide clearer interpretation. This resulted in an NRMSE of 0.128, which therefore equates to an accuracy rate of 0.872, meaning the accuracy of the derived model is 87.2%.

For validation of the feature selection, the model was also run using all the features from Table 2-4 and this model achieved an NRMSE of 0.196 indicating an accuracy of 80% displaying an

increase of 7% in performance when using the feature selection, which could prove key in carrying out the correct maintenance at the correct time. Whilst it can be thought that this reduction may seem marginal it represents an increase with a very small subset (reduction of 20 features to 15) and the workflow could be adapted for a database with much more features and be able to reduce it to a subset of the most suitable features which could maximize the prediction accuracy. The increase could also be more if more features are eliminated from a potentially larger database, eliminating those features that are not key to the dependent variable. Therefore, the more important result is the workflow to ensure that only suitable features are used. Whilst this does require an additional step in the process, which extends the pipeline, it could help save significant costs and time for authorities unaware of the best features to use in the modelling process. This is important as feature selection has shown to be highly successful when used to filter out redundant data, improve accuracies and help produce more explainable models [124].

Whilst it is important to mention that still represents an error, it is clear that the model is very good considering the inputs. Additionally, in scenarios where there are no models in place because of the lack of data, this would represent a substantial upgrade to their planning processes. Concerning time, the error would represent less than 1.5 months of time of a gap between when the model predicts maintenance should occur and when it does occur. Considering that plans are made on a yearly scale, this error can, therefore, be considered acceptable as opposed to the alternative, where the activity is scheduled in a different year or not at all for a particular road without the model. Additionally, by having a clearer idea of the next areas where extensive rehabilitation activities are needed, preservation interventions can be planned and carried out before the designated ‘worse case’ timelines happen and additional monitoring of these sections can be planned. For a better graphical representation of the possible scheduling, the test dataset of 220 road instances was considered and a hypothetical prediction of the required maintenance intervention was plotted for the next 10-year period, grouped by the respective circumscriptions and is shown in Figure 2-21.

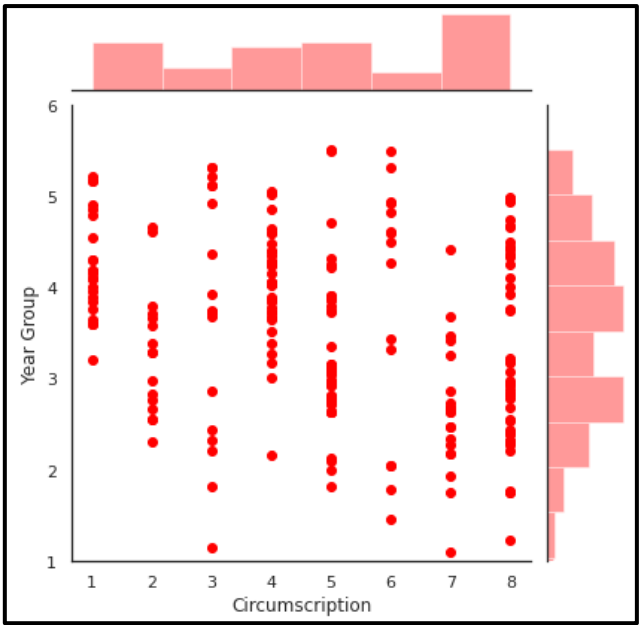

Figure 2-21. Jointplot of predicted future maintenance interventions grouped by circumscription

This figure highlights the time points where the model has predicted that maintenance should occur and should be programmed over the next period of years. Within the figure, it is shown which circumscriptions are critical at which points in time. Using this, a plan of activities can easily be drawn up for the next period and budgets can be planned with a better idea of how much interventions are likely required in a particular year. Additionally, to provide a clearer picture of criticalities, the plot was further grouped to generate a heatmap of points in Figure 2-21 to understand the important periods and circumscriptions. This was generated using the seaborn library and is given in Figure 2-22.

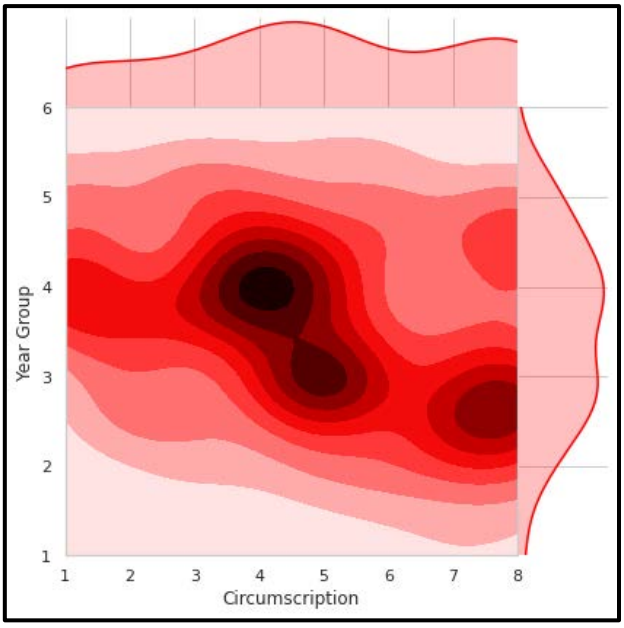

Figure 2-22. Heatmap of Jointplot of predicted interventions grouped by circumscription

As expected from the discussions, the plot shows that the period where more action is required are the mid to later year periods but it also importantly highlights the circumscriptions where more intervention is needed, which is critical for planning and budget allocations. Whilst there is room for improvement in the model, it must be emphasized that given the size of the dataset and the resources available, it is a significantly useful result that could help better plan interventions within the municipality. It is also a pathway towards planning interventions without relying on excessive and expensive databases.

2.13 Consequences of model and workflow development

This aspect of the research project was designed to present a low-cost and flexible framework towards utilizing easily available information on cities and their road network for planning road maintenance interventions. The purpose was to create a workflow that could be replicated by small and under-resourced road authorities who cannot create and access large databases but still have to create effective maintenance and rehabilitation plans and strategies. The analyses and models were developed relying on low-cost data analytics tools, open-source algorithms and deep learning frameworks. These plans would lead to better planning practices utilizing information already available by road authorities.

For the validation of the workflow of the study, a case study in Palermo, Italy was utilized. Within the study, several open-source datasets that are typically available in most cities were utilized from the city's census, road traffic and maintenance history. It must be noted whilst the data was obtained from several open-source systems, it did involve multiple stakeholders. However, this is an unavoidable task to ensure that the characteristics of the situation are understood and additionally it is a step that would only be needed to be done at the beginning of the process in a practical implementation scenario. Feature selection tools were developed based on the features found in the dataset to identify which of them are the most important towards explaining the point in time at which intervention activities need to be carried out. The feature selection tools were based on gradient boosting algorithms that adequately could handle the presence of categorical variables, which commonly exist in these types of databases. Once the feature selection tool was developed, it was used to pinpoint the most important features in the dataset, which were then utilized in a deep learning model to help predict the time for an intervention for a particular road. This process, therefore, utilizes the

strengths of both gradient boosting algorithms and deep learning, leveraging their combined power to handle categorical variables and the strength of deep learning to search out connections on a deeper level than traditional approaches.

The most important features, as observed by the feature selection tool, were analysed and validated based on analyses of feature distributions and the specific situation within the municipality. Once the features were integrated into the DL model, a model with high accuracy was achieved. Though the model is not perfect, it provides a very good assessment of when interventions should occur. This is in line with other studies, which have used different forms of artificial intelligence to predict performance characteristics in pavements. This is validated in recent studies which have achieved accuracies of: 87% when predicting the infrastructure's condition using a neural network with embedding [125], 86% for predicting road surface milling and overlays interventions [126], 85% when using combinations of gradient boosting trees to predict the PCI [127] and 87% predicting global road performance indicators [83]. Given the level of accuracy achieved from this study using the available data and resources, the result represents a substantial advance for the targeted types of road agencies.

The model is also non-contact and does not require excessive physical surveys. The predicted models can aptly be used to generate schedules of which roads and sections should be prioritized over time. Finally, it is worth pointing out this aspect of the study exploits both low-cost investigation techniques on road pavement conditions and indirect data analytics, to establish over time and space, the best network maintenance strategy. This would allow more budget allocation towards effective interventions rather than on complex and expensive systematic investigations. With the techniques combined, they offer another step towards low-cost automation of elements of the PMS.

With a model and workflow in hand that can adequately handle the available data on maintenance and the dimensions of the municipality, the focus of the thesis will now be shifted towards using the identified locations from the model to understand the physical surface conditions of the road. To this end, the next chapter will consider the methods utilized for pavement surface evaluations and the common methods used for the detection of distresses.

Chapter 3: How are Pavement Surface conditions measured and analysed?

Given the work in the previous chapter, the models produced have the capacity to determine which roads in the network should be looked at and the related particular points of time that should be used to guide inspections and interventions. Those models would help authorities to better allocate funds for maintenance activities. This however does not solve the problems associated with characterizing what are the actual distresses at those points in the network. The characterization of the distress is important as it can change the type of intervention and therapy needed. This is another vital component in providing a holistic low-cost system for these agencies, and as identified in the previous chapter, pavement distress data represents a key data input for the PMS. However, before tackling the issues of detecting and analysing the distress it is important to understand how these surveys and detections are typically carried out in industry and research and the current state of the art. In this light, this chapter focuses on the physical surface conditions and tools and techniques which are typically used to quantitatively measure their conditions in order to guide a new technique and workflow towards producing models capable of representing the pavement distresses.*[2]

[2] This chapter is based on "Developing a framework for using Structure-from-Motion techniques for Road Distress applications" published in the international journal "European Transport /Transporti Europei" which was authored by the same author of this thesis. File: http://www.istiee.unict.it/sites/default/files/files/2_5_ET_76.pdf

3.1 Pavement Surface Distress characterization

Within the PMS, pavement distress information is typically collected and utilized by agencies, to get an overall rating of a road system using standardized performance indices. There are several of these indices including the Present Serviceability Rating (PSR), the Present Serviceability Index (PSI), the Pavement Condition Index (PCI) and the International Roughness Index (IRI) as were previously identified in chapter 2. The use of these indices depends on the scale of the PMS and the particular region or country where the system is being implemented. To this end, there are significant differences in the actual interpretation and classification of distresses worldwide. This is relevant as any technique developed must be related to the distress definitions of the road agency and regulations of the particular city or region.

3.1.1 Pavement distress manuals worldwide

Within the context of pavement distress identification, road agencies typically rely on distress identification manuals to attempt to standardize the subjective nature of the results obtained from surveys. There are several distress manuals worldwide that aim to describe the distresses occurring on the pavement and give descriptions on how to identify these and how to measure their severity. For the purpose of this project, several agencies worldwide are considered and analysed to cover a large geographical spread across continents with the focus here being in North America, Europe and Australia. This was done to have a thorough understanding of how different road agencies classify and treat pavement distresses. The manuals that were considered are:

1. Standard Practice for Roads and Parking Lots Pavement Condition Index Surveys - American Society for Testing and Materials (ASTM) – USA [58] (2018).
2. Distress Identification Manual for the Long-Term Pavement Performance Program – US Department of Transportation Federal Highway Administration - USA [62] (2014).
3. Pavement Surface Condition Rating Manual – British Columbia Ministry of Transportation and Infrastructure - Canada [63] (2016).
4. Catalogue des degradations de surface des chausses – Laboratorie Central des Ponts et Chausses - France [57] (1998).
5. Catalogo dei disesti delle pavimentazioni stradali – Direzione Generale Infrastutture e Mobilita - Italy [60] (2005).

6. Guide to Surface Inspection Rating for pavements surfaced with sprayed seals and asphalt – VicRoads – Australia [128] (2009).
7. Manuel d'identification des dégradations des chaussées flexibles - Ministère des Transports du Québec (MTQ) – Canada [129] (2002).
8. Pavement Surface Condition Field Rating Manual for Asphalt Pavement - Washington State Department of Transportation (WSDOT) – USA [130] (1999).

The manuals used were the most recent versions found at the time of the project. Some of the manuals have the severity being defined by specific dimensions of the distress and then have the distress itself recorded as a ratio of the distressed area to the total area (e.g. ASTM) whilst others define the severity directly by this ratio. Generally, distresses can be broken down into five categories based on the cause of the distress: surface texture deficiencies, deterioration, deformation, patching and structural distress [131] and typically, they are measured in one of three ways as shown in Table 3-1[132]. Using these definitions, the understanding of what is important to and required by any new technique can be acquired in order to yield the requisite quantitative data for each of these categories regardless of the geographical location or context.

Table 3-1. Breakdown of distresses by measurement type

Units of measurements used by manuals	Distresses typically covered
Linear meters	Edge cracking, Joint reflection, Lane/shoulder drop off, Longitudinal and Transverse cracking
Number of occurrences	Potholes
Square meters	Alligator cracking, Bleeding, Block cracking, Corrugation, Depression, Patching and Utility cut patching, polished aggregate, railroad crossings, rutting, shoving, slippage cracking, swelling, ravelling, weathering

Given these groups, an analysis of how these types of distresses are defined by the manuals was carried out. An example of each type is highlighted as shown in Table 3-2. A broader analysis of the wider range of distress types found on networks is given in Appendix B.

The types shown in Table 3-2 are Longitudinal/Transverse cracking, Potholes and Rutting. The reason for this is related to both the primary location of the study (Italy) and the importance of the distresses. Cracking was chosen as it represents the largest number of pavement distress on Urban roadways in Italy [38]. Rutting was chosen given its importance to the design of the pavement itself [64] and given the fact that when a pavement begins to suffer this type

of distress its pavement life is in its final stages. Finally, potholes were chosen as this distress represents the only one typically measured based on a 'number of occurrences' method. A comparison of the severity definition in the manuals for the example cases is given in Table 3-2.

Table 3-2. Examples of definitions of distress severity given by distress manuals

Manual	**Longitudinal Cracking**			**Pothole**			**Rutting**		
	Low	Medium	High	Low	Medium	High	Low	Medium	High
1	width< 10mm	10mm≥ width≥ 75mm	width≥76mm	depth: 13 to ≤25mm and ø <450mm or depth: 25 to ≤50mm and ø <200mm	depth 13 to ≤25mm and 450mm>ø>750mm **or** depth >25mm to ≤50mm and 200mm<ø<450mm **or** depth:>50mm and 200mm<ø<450mm	depth > 25mm and ≤50mm and 450mm< ø <750mm or depth:> 50mm and 450mm< ø<750mm	depth of 6 to 13 mm	depth >13 to 25 mm	depth >25 mm
2	Mean width ≤ 6 mm	Mean width > 6 mm and ≤ 19 mm or any crack with a mean width ≤ 19 mm	Mean width > 19 mm or any crack with a mean width ≤ 19 mm	< 25 mm deep.	25 to 50 mm deep.	> 50 mm deep.	Des.	Des.	Des.
3	mean unsealed crack width < 5mm	mean unsealed crack width 5-20mm	mean unsealed crack width >20mm	area > 175 cm² (~150mm ø) and < 25mm deep	area > 175 cm² (~150mm ø) and 25 to 50mm deep	area > 175 cm² (~150mm ø) and > 50mm deep	depth < 10 mm	depth of 10 to 20 mm	depth > 20 mm

Manual	**Longitudinal Cracking**			**Pothole**			**Rutting**		
	Low	Medium	High	Low	Medium	High	Low	Medium	High
4	Des.	Des.	Des.	ø < 150mm	ø > 150mm		noticeable depth of 5 to 15 mm	significant depth of 15 to 30 mm	deep rut depth > 30 mm
5	Width <2mm	2mm> Width <10mm	width> 10mm	ø<100mm and depth <50mm	100<ø<300mm and depth <25mm	ø>300mm and depth >25mm	depth<15mm	depth>15 to <30mm	depth> 30mm
6	affecting < 10% of area.	affecting 10 – 20% of area.	affecting > 20% of area	Measured in terms of the area affected but grouped under current required 'maintenance patching'			affecting < 10% of area	affecting 10 – 30% of area	affecting > 30% of area
7	< 5mm width	5mm≥ width≥ 20mm	>20mm width	< 200mm diameter	200mm≥ diameter≥ 300mm	>300mm diameter	< 10mm depth	10mm≥ depth≥ 20mm	>20mm depth
8	< 1/4 in. width	> ¼ in. width with no spalling	>¼ in. width with spalling	Potholes are considered as high severity alligator cracking and need to be noted in the comments area of field forms.			¼ in. to ½ in. depth	½ in. to ¾ in. depth	over ¾ in. depth

Note: ø = Diameter, Des. = Descriptive definition

As seen in Table 3-2, there are varying numerical definitions of distress types and several differences in how they are measured. There is thus no uniformity amongst definitions and some of these deviations are quite large. As an example; using the definition of longitudinal cracking between manuals, the high severity class is defined as a crack with a width over 19mm for Manual 2 while for Manual 1 it is defined as one with a width over 76mm. This represents just one example of differences observed and this seeks to establish the importance of knowing the scope of the distress evaluation.

Furthermore, it should be noted that these parameters are typically based on the manuals' locale and environmental conditions will play a role in determining what is severe in particular conditions. This further stresses that any definition system should be based on local conditions rather than the arbitrary use of any single distress identification manual or technique.

3.1.2 Differences in requirements and severity assessment

Nevertheless, the important takeaways from Table 3-1 and Table 3-2 are the measurement requirements for practitioners when carrying out a distress survey, regardless of the locations when considering industry used guidelines. Using these analyses, the requirements were grouped and this is depicted in Figure 3-1.

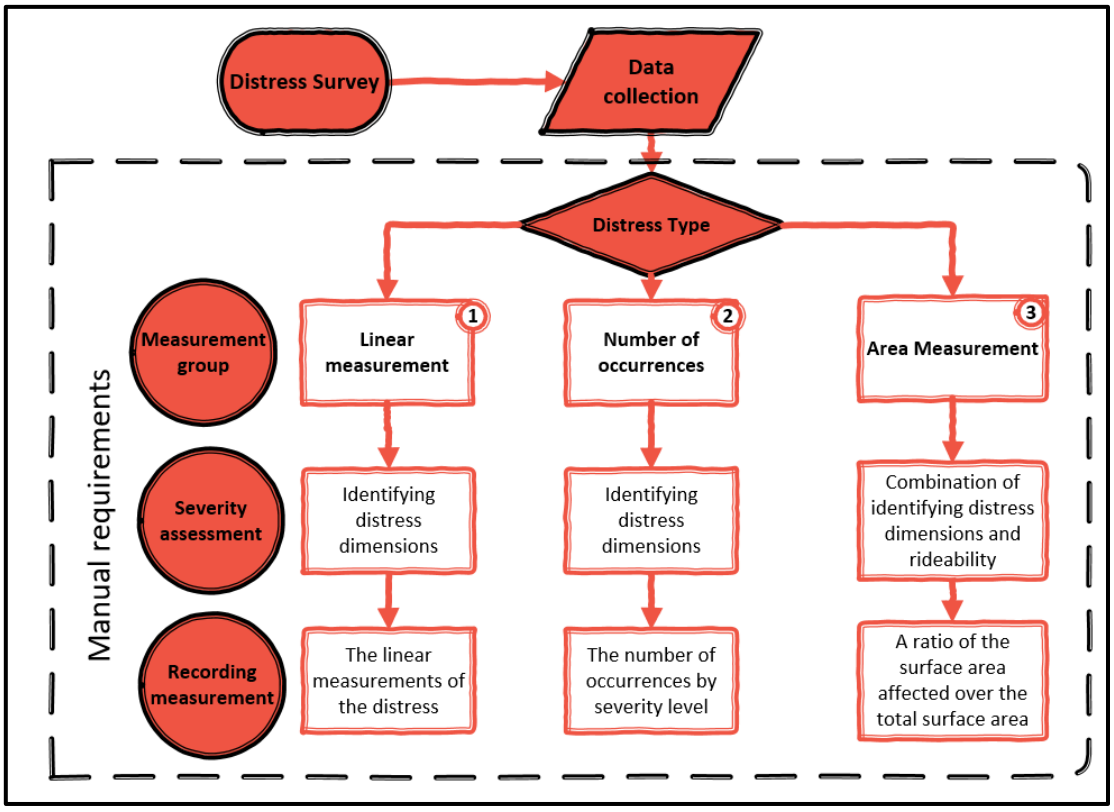

Figure 3-1. Requirements to identify and analyse pavement distressed as defined by manuals

From Figure 3-1, three main measurement groups were noted which are linear measurements, measurement of the number of occurrences, and area measurements. Utilizing these categories, then the manual requirements for severity assessment were also grouped and then finally the measurements that are needed to be recorded were also grouped. For the severity assessments, the main focus of the requirement was on detailing the physical dimensions of the distress. The measurement recorded within the guideline of the manuals relied on these dimensions. The recorded measurements are what is needed for the practitioner to calculate the related performance indices for that particular agency based on the manual used.

These factors are important as any method for carrying out the surveys must meet these criteria to adequately feed information to the agencies towards defining the overall road condition parameters such as the PCI for the PMS.

3.2 Techniques used for distress characterization and surveys

As the requirements for identifying and analysing pavement distresses have been discussed, the next aspect to consider was the techniques that are typically deployed to produce this information. To this end, several efforts have been employed over the years to develop automated distress detection with the aim of reducing the subjectivity of the visual measurements [26,133]. These efforts can be summarized as shown in Figure 3-2. Each subcategory has been vastly studied and some of the equipment used relating to the methods are given in Table 3-3.

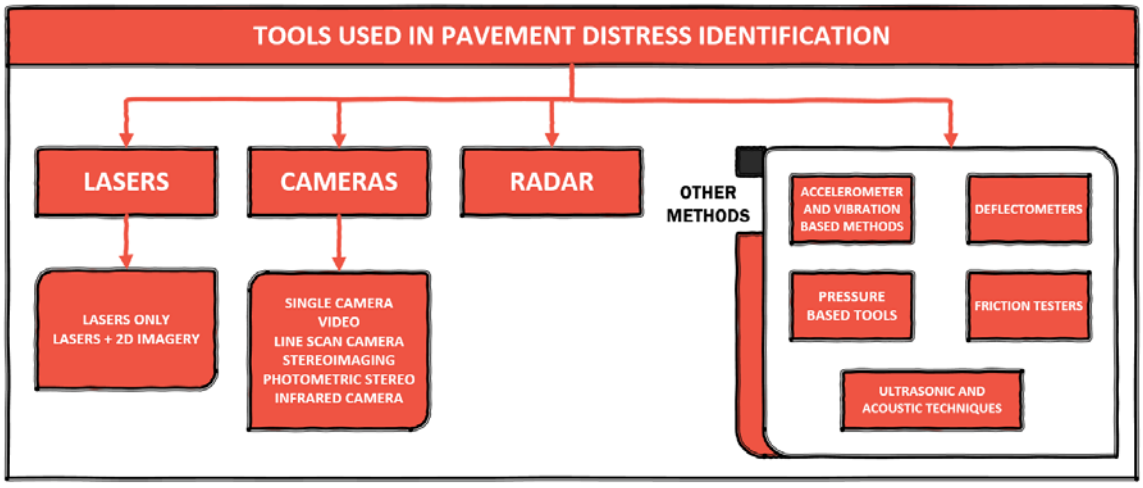

Figure 3-2. Summary of tools used in pavement distress identification

3.2.1 Equipment utilized for pavement distress surveys

The equipment utilized for the surveys relates directly to the methods used and the available funds and resources by the road authority. Devices used and their related studies per category are listed in Table 3-3 [133]. However, despite the global availability of these devices, the main approach for detecting pavement distresses is using manual surveys given the budgetary limitations. Pavement roughness and permanent deformation are typically estimated using static laser sensors that allow the measurement of the longitudinal and transverse profiles of the pavements [134] whilst for all other surface distresses, the most common type of survey is based on the visual evaluation of the defects and the results are affected by subjectivity and high degrees of uncertainty.

Table 3-3. Devices used for detecting pavement distresses

Type of detection	Device
Camera-based Systems	CCD (charge-coupled device) [135–137], Infrared [138], CMOS (metal-oxide-semiconductor sensor)[139,140], Line-scan[141,142] [141], Video[143,144] [145], Black-box [144], smart phone [146,147][148][149], Retroreflectivity meter [150]
Accelerometer	Device on: Smartphone [151], On the wheel, on wheel axis, in-car, in other tool [152]
3D Sensors	Laser Profiler [153], Line projection, Stereo vision [154], Kinect device [155], Ground Penetrating Radar [156], LIDAR [157], Structured light, Photometric stereo [158,159]
Microphone	Device placed: on Tyre, Near the road, beneath car [160]
Sound propagation	Sonar device [161]
Pressure	Pressure sensor [162,163]
Friction	Tyre traction, angled wheel [164]
Deflectometer	Falling Weight Deflectometer – FWD [165], Dynamic Rolling Weight Deflectometer – RWD [166]

When using the current accurate technologies and techniques, the cost of the pavement condition surveys is commonly so considerable, that expenditure due to PMS is usually not sustainable in urban areas as well as for local networks [38]. However, these networks generally have the highest number of accidents [167], while rural networks have the highest fatal crash incidence densities [168,169], making both networks important to road safety. Furthermore, it has been shown that poor road surface conditions caused by insufficient maintenance present a dangerous environment for road users and there are direct correlations between friction rates and crash rates [170], highlighting the need for proper maintenance management systems. Because of this and the continual funding deficiencies, it

is necessary to implement an automated, rapid, safe and low-cost analysis system of the pavement distress with a suitable metric accuracy.

3.2.2 Laser and imagery based methods

Of the many techniques, methods and equipment used for detecting and analysing pavement distresses, the two most researched categories from Figure 3-2 are those that feature laser and imaging technologies and these are the bases for many commercial tools and applications currently used in the industry. With regards to laser technologies, Laurent et al [171], was part of the development of the Laser Crack Measurement System (LCMS) which is now the basis for many laser oriented systems in today's market. That system consists of two high-performance lasers attached to a survey vehicle along with cameras creating a laser profiler capable of measuring road profiles, IRI and road slopes with a resolution of 1mm generating 3D profiles of a pavement. The system utilizes both 2D intensity data and 3D texture data for evaluation and has been used as the basis for many system applications using cameras and profilers. Other systems integrating the use of lasers along with cameras have also been researched including Oliveira and Correia [172], who proposed a specific system for crack detection and classification into several classes using a Laser road imaging system (LRIS) system, composed of two high speed/high-resolution line-scan cameras in conjunction with high power lasers. Wix and Leschinski [153] carried out research comparing four different types of systems for crack detecting using lasers and imagery including using area view cameras, line scan cameras and two automated systems involving layers. The focus of this research was on automated systems. The first automated system for comparison was the LCMS and the second was the Roadcrack system. The Roadcrack system utilized modules that are equipped with high-resolution cameras and a unique lighting system and have been shown to be more effective for cracks on sprayed seal roads than the LCMS. Both of these systems have a focus on pavement cracks and both require the use of survey vehicles. The image-based systems were identified to have issues with quality because of lighting and the conclusion is more work was required on these systems. Laser profiling systems similar to these are used in many commercially available equipment systems including ARAN, ROMDAS, Dynatest and ARRB Hawkeye [133]. A commonly used survey vehicle that combines a lot of these tools is the ARAN one which is displayed in Figure 3-3, showing its various functions including a laser profiler, GPS, ground-penetrating radar and texture detection systems [173].

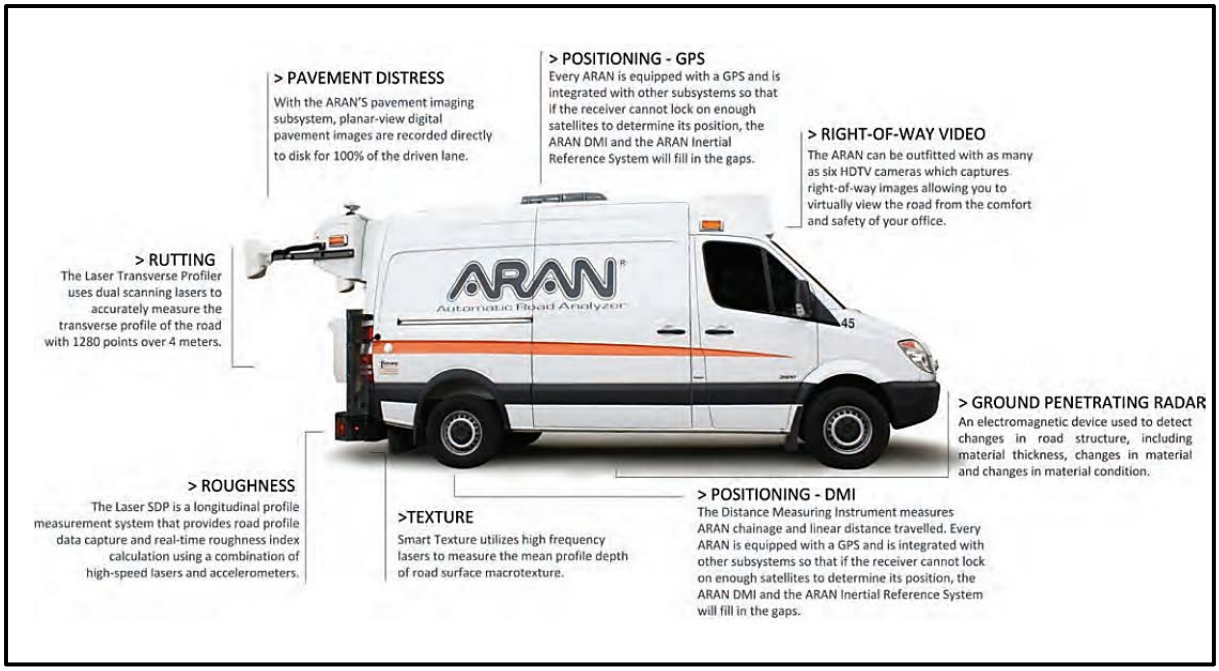

Figure 3-3. ARAN Road Survey vehicle and functions *[173]*.

More recently there have been studies on utilizing data from laser systems and deep learning techniques for automating the process [174]. There have also been attempts recently to integrate mobile lasers for highway data collection and utilizing Lidar systems as more research is being conducted with laser technology [175,176]. Whilst the main research focus has been on the cracking type distresses, there have also been studies involving different types of distresses with the attempt to automate the systems [134]. Overall, lasers have been proven to provide a high accuracy but represent a costly resource. As a result of this, image-based technologies have been widely researched to offer an alternative to laser-based systems. These imaging technologies involve the capture and interpretation of images of the pavement surface. There have also been studies involving the creating of algorithms for the processing of images for distress identification [134,177,178].

Under the branch of camera-based techniques, the use of stereoscopic surveying is incorporated. This includes Structure from Motion (SfM) techniques. Photogrammetry and SfM can be applied using a single image (for example, for applications such as the straightening and the mono-plotting), or couples (stereo) or more images (bundle-block adjustment) [179]. Several applications of photogrammetric techniques have been realized using the stereovision approach [180,181]. SfM techniques have generally been utilized in other fields such as architecture and archaeology for the preservation of artefacts and historical figures [182]. There have also been studies on asphalt pavements wherein the techniques were used for

replicating road surfaces and their distresses [177,183] and other studies have considered using drones to carry out the process [184,185]

Specifically, in terms of pavements, early studies on the subject have suggested potential in the process. One of the early stereo-vision systems was proposed by Wang et al., [134] in which two digital cameras were used (resolution 2048-pixel/camera or 1300-pixel/camera) to capture images of half of a lane-width. Coupling the images and overlapping the common parts it was shown to be possible to reconstruct a 3D model. Therefore, geometric modelling was used to evaluate the pavement condition. The system was subsequently updated including two more cameras to cover the entire lane-width but this has also posed difficulties in implementation with this method.

Further work was also done utilizing the photogrammetric approach for an automated program for cracks with the focus on the development of algorithms able to process the stereoscopic imagery [177]. The use of drones has also been employed with photogrammetric algorithms to reconstruct rural roads [186,187] and for historical purposes [188]. These studies have shown that rural roads could be reconstructed but with issues arising due to shadows, mismatches and the low variation in the road surface and a lack of texture. Sarsam et al [189] utilized the technology for close-range photogrammetry with the creation of ortho and 3D stereo imagery which are then compared to visual inspections of distresses. Ahmed et al [181] suggested the use of photogrammetry for pavement distress surveying and researched algorithms that can be utilized in carrying out 3D reconstruction. Other studies have also focused on algorithm development for pavement texture and evaluation [190]. Mathavan [154] specifically looked at the hardware being employed in imaging technologies for these purposes and identified that there is a lack of available tools for industry for this technology. Other criticisms of the use of SfM systems also include shortcomings in accuracy, high computing processing requirements and scaling issues. The computational stereopsis also requires photographs to appear very similar in order to recover reliable results [191].

However, there has been significant recent advances in image spectrometry but this research on the accuracy of the systems have been focused on architectural and archaeological studies. [192,193]. More recently research has shown that recently available commercial software packages (including Agisoft Metashape, Pix4D Pix4Dmapper Pro and Capturing REeality RealityCapture) can help solve previously occurring issues with higher accuracies, lower

computational times and reliability whilst utilizing complex datasets with different cameras and systems [194]. To analyse the accuracy of these systems these researchers have utilized laser scans as a reference case and have tested various applications including landslides [195], forest structure [196] buildings [197] and several cultural heritage sites, artefacts and collections complex in shape and type [198,199]. The results from these studies show higher accuracies in the techniques and software now available.

The successes of these applications have therefore led to the consideration of the SfM approach, for monitoring surface conditions of asphalt pavements utilizing commercial software that has shown in other applications to achieve high accuracy. As the SfM technique offers the ability to anyone to make 3D models from a photo dataset the potential of verifying its ability to assist in pavement distress applications would help overcome cost challenges and present a low-cost method for Road agencies to utilize. This field of research provides additional opportunities for the analysis of pavement distresses as accurately generated 3D models can provide critical metric information on the distress that can yield effective intervention strategies.

Inzerillo et al., [65] carried out experiments on laboratory samples of rutted asphalt creating an SfM model (carried out by Agisoft Photoscan) which was then subsequently compared with the 3D model obtained with a blue led 3D scanner (Artec Spider) with a metric accuracy in the order of the micron. The 3D scanner Artec Spider was used to define the virtual reference closer to the most realistic reconstruction. When the N-SfM and the Artec Spider models were compared, the N-SfM showed high accuracy in the rutting distress reconstruction. The results of this study led this research project to pursue tests on field pavements to further validate any use of this technology and this will be thoroughly examined in Chapter 4. This is important, as further work is needed in a practical environment to take the research further to validate the use of the modelling process and assessing the practicality and applicability of the processes. The work on testing and exploring different pipelines and techniques of 3D modelling applications for detecting pavement distresses is the focus of Chapter 4.

3.3 Limitations of imaged-based techniques and research opportunity to exploit new techniques

Overall, with all of the techniques discussed, one key objective is to enable automated distress detection, which can reduce subjectivity and variability, implementing high levels of automation without requiring time-consuming personnel training. For this, the survey method should count on reliable devices that provide a high level of accuracy without creating significant constraints due to their difficulty in use and without increasing the cost of the operations.

As evidenced, there have been several research works on automatic pavement distresses [133] but in the existing methods that use the image processing techniques, certain limitations emerge: the distortion of the detection of the distress' location due to the presence of shadows and brightness, different textures, noise and tree leaves. The issue of shadows and image clarity is also a well-known limitation of the image-based techniques and emphasis, therefore, needs to be placed on ensuring the environmental conditions are consistent throughout surveys and that surveys are done in particular lighting conditions to reduce them.

These systems are also affected by inaccuracy due to possible perspective projection and additionally, lens distortions could have a negative impact on the reliability of the survey. The last aspect to be mentioned but not the least important is that in the past these techniques have had tendencies to need special devices e.g. special lights, parallel computers, specific software which increases the costs and the constraints of the methods [181]. This limitation has been reduced with smartphones and cameras showing the ability to carry out the surveys.

Previously there have also been assumptions that there were was a lack of available industry tools to utilize the techniques [154]. However, new developments in processing power and algorithms have made it possible for an application to pavement engineering [200]. Recent studies have shown the accuracy of models by comparing results to those from laser technologies [201]. This verification of accuracy is in line with typical photogrammetry accuracy development cases for buildings and other structures [196,197]. With the comparisons made to lasers, it was established that professional cameras are capable of carrying out the process. However, these cameras can still be quite expensive and establishing a pipeline using professional cameras still requires the procurement of the devices followed

by subsequent training on their use by road agency staff. Cameras are also stationary devices and therefore if a survey was needed over a large section of the network they would be ineffective. However, using a drone could allow for quick identification of the presence of the distresses on the road pavement and the condition of the road on a large-scale. This would be useful to understand the overall conditions of the state of a long stretch of road pavement, identifying the critical areas of the road surface where it is necessary to carry out a more detailed analysis using the stationary cameras. In this way, the distresses that require detailed geometrical investigation, to narrow down the potential causes of the damage, can be analysed to determine their severity.

To this end, if a pipeline could be established using mobile phones and drones then the process can be considered more ready for implementation and the potential for its use would be accelerated. Therefore, whilst other studies and projects have focused on using the techniques with expensive cameras, the next aspect of this study focuses on demonstrating the accuracy of using the techniques with mobile phones and drones to generate 3D pavement distress models. This would help bridge this research gap and provide quantitative results on the accuracy of developing a mobile and versatile pipeline.

Furthermore, whilst other studies have focused on simple metric analysis, using metric parameters typically recovered from distresses such as distress dimensions of length and width, an associated second goal of this aspect of the research project is to establish methods to critically evaluate the distress using segmentation and enhancement strategies. This would therefore provide a sectional analysis. By doing this, distresses could then be easily isolated and at this point then, the common metric evaluation can be done. Sections can also then be made in both horizontal and vertical planes to extract curvilinear profiles and sections. Multiple parallel longitudinal sections can also be created to define distress profiles. Each created profile can be isolated and analysed. This, therefore, leads to the identification of the required geometrical features of maximum depths and widths and area distressed.

To do these analyses and develop these pipelines, case studies utilizing different strategies and distresses were considered for specific distress types and this is further described in the subsequent chapter. The next chapter also further explains how these image-based techniques can be applied and seeks to identify the accuracies of different devices so as to cover a wide range of practical possibilities in applying the techniques in the real world.

Chapter 4: Using 3D Modelling for Pavement distress detection and analysis

In the previous chapter, an overview of how pavement surface distresses are analysed and the requirements of the various pavement manuals worldwide was given. This was done to understand the global perspective on this work. This chapter will now use the guidance of those manuals and requirements, and focus directly on the utilization of photogrammetric 3D modelling and the development of related segmentation methods to model and analyse pavement distresses. Within the analysis, several case studies are used to exploit a 3D modelling workflow using different devices such as smartphones and drones for data collection. The chapter also establishes the accuracies of the methods and outlines a workflow for utilizing the techniques to provide vital information for road asset databases on the streets designated as high risk by the workflow developed in chapter 2. [3]

[3] This chapter is based on the following papers:
"Image-based 3D reconstruction using traditional and UAV datasets for analysis of road pavement distress" published in the international peer-reviewed journal "Automation in Construction" and which was authored by the same author of this thesis. doi: 10.1016/j.autcon.2018.10.010.
"Exploiting low-cost 3D imagery for the purposes of detecting and analyzing pavement distresses" published in the international peer-reviewed journal "Infrastructures" and which was authored by the same author of this thesis. doi: 10.3390/infrastructures5010006.
"Using UAV Based 3D Modelling to Provide Smart Monitoring of Road Pavement Conditions" published in the international peer-reviewed journal "Information" and which was authored by the same author of this thesis. doi: 10.3390/info11120568.

4.1 Overview of the uses of 3D Image modelling techniques and representations

In exploiting 3D data, there are three different types of representations that are commonly used and relied on. These are multi-view[202], point clouds[203] and voxel data[204]. These data types are examined in Figure 4-1 [205]. Each of the three options has been considered as an option for representing pavement distresses with the multi-view and point cloud methods showing a greater classification accuracy. As point clouds can be obtained from low-cost cameras such as mobile devices and unmanned aerial vehicles (UAVs), and also can be utilized to generate 3D structures and their metric dimensions, they were considered as the most viable option for this part of the research project. The concept of photogrammetry falls under this subset and was subsequently utilized for replicating the pavement distresses in the study.

Multi-view	Point Cloud	Voxel data
• comprised of a collection of 2D images of a generated grid which was captured from different perspectives • does not give a thorough 3D spatial representaton of the object	• an array of points in a three dimensional space, with points carrying both coordinates and color information which can then be used to establish the actual shape of the object being observed • can be used to derive 3D model but can also be disordered and sparse	• smallest unit of data in 3D space where each unit can be looked at as a grid having fixed coordinates • voxel grid can be defined as a point cloud with a fixed size with each vozel having its own specific coordinates • can be computationally expensive for memory use

Figure 4-1. Different types of 3D data representations

4.2 The use of Photogrammetry – Key concepts

Considering the use of 3D point cloud data, the concept of photogrammetry and more specifically, that of structure from motion were then examined. Structure from Motion (SfM) is an innovative photogrammetry technique that allows users to create 3D models from a photo data set; its current application in the road pavement domain is limited, as it is mostly used for architectural and archaeological studies [206,207]. After the first step of identifying

different homologous points in the images, the photogrammetric technique is used to determine metric information about the size, shape and position of an object or scene. Exploiting the photogrammetric approach and the algorithms of Computer Vision, the photogrammetric algorithms can reconstruct the internal parameters of the digital camera and the positions of the homologous points in space. When the homologous points between images have been determined, the relative orientation of pictures can be calculated (the spatial and angular position of the cameras in the arbitrary reference system). Afterwards, a scaled reference system, established by ground points, is used to calculate the orientation in its absolute form [208]. Through the correspondence pixel-pixel, the 3D coordinates of all the points are found and the polygonal models are reconstructed. Results obtained in previous studies [65] provided the impetus to experiment with the methodology on further asphalt pavement distresses and other types and sequences.

Whilst utilizing structure-from-motion techniques, the most critical parameter to be considered is the ground sampling distance (GSD). Models are typically interpreted from this parameter. It is a representation of the distance between two consecutive pixel centres, with respect to actual ground measurements. The GSD is considered as a representation of the smallest details that can be accurately observed on an image [194]. The smaller the value of the GSD, the greater the measurable details. This shows the importance of this value as it will dictate the resolution of the replicated models and thus the possible level of observable features. For the GSD, it has been demonstrated that the smallest visible details are two to three times the value of the GSD [209]. Based on the discussions in chapter 2, generally, the smallest cracks and common distress are not smaller than 0.01 m (10 mm) and with resolutions of 3mm these distresses can be accurately identified [210]. Therefore, the technique must be able to produce a resolution less than this. This is in line with other studies examining the resolution of typical 2D imagery used for detection which utilize a resolution of 3mm [26]. Considering that a detection of 3 mm, which would be appropriate for pavement distresses, the GSD should be no greater than 1 mm for it to align with the concept that the resolution would be 3 times the value of the GSD. The GSD is related to specific parameters of the camera used and is given by equation 4-1 below.

, $$GSD = \frac{D \times px_{size}}{f} \quad (4\text{-}1)$$

where D = object distance, ƒ = focal length, and px_{size} = pixel size (defined by the ratio of the camera's sensor height to the image height). The 'focal length' and 'pixel size' are camera attributes camera and the other parameters can be manipulated to produce an appropriate GSD. For this aspect of the study, a target value of approximately 0.5 mm was used within this study but critically anything below 1mm would be appropriate for the surveys.

4.3 Workflow to analyse 3D models and techniques

The modelling process was broken into different workflows as outlined in Figure 4-2. The first of these was to establish the accuracy of using different devices namely cameras, drones and mobile phones. The initial accuracies were tested using a laser as ground truth in the process. Following the establishment of the accuracy of the devices, a workflow was set up to achieve the necessary accuracy level in practice. Subsequently, segmentation and analytical methods were considered to isolate the distresses found to analyse the level of deterioration on the pavement or section.

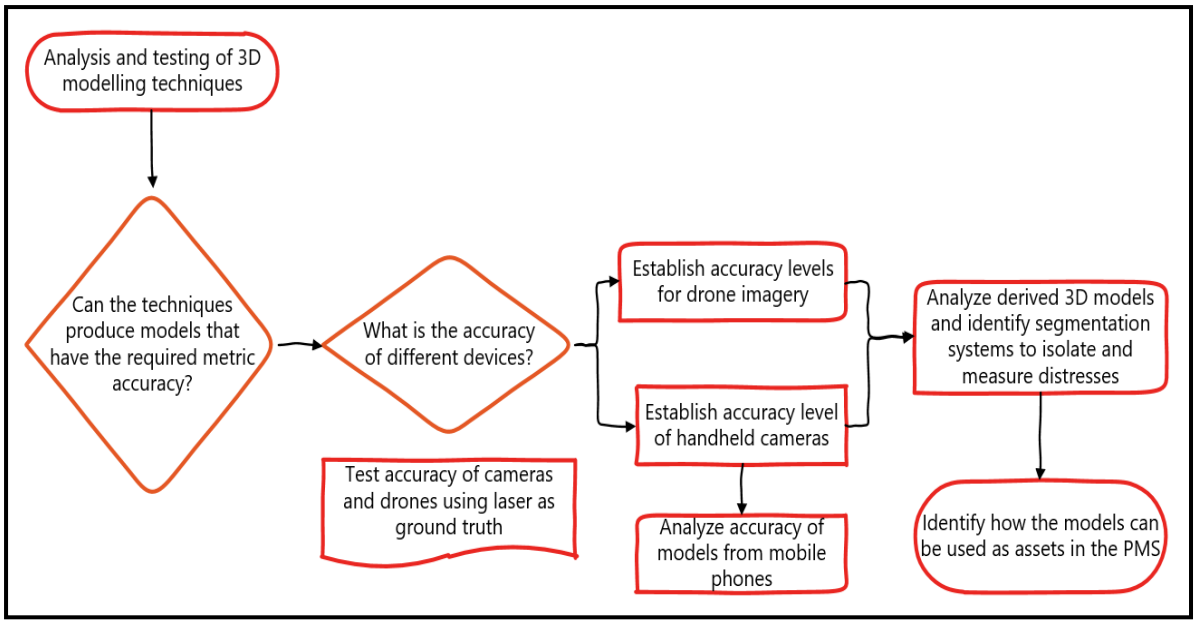

Figure 4-2. Workflow to analyse and determine workflow for 3D modelling techniques

4.3.1 Case study to validate the accuracy of models using laser ground truth

In this case, the SfM technique was considered at two different altitudes. For this reason, the Nikon D5200 camera was used at head-level directly by the operators and denoted as N-SfM and a UAV was used above the pavement surface with this process denoted as UAV-SfM. The resulting models were compared with the dense cloud obtained using the laser scan (terrestrial laser scan 2mm) to analyse the metric accuracy and then the reliability of such

techniques in the distress reconstruction. The camera used to take the data set photo collection was the Nikon D5200 with a resolution of 24 Megapixels. It was set according to the following parameters in Table 4-1:

Table 4-1 Nikon camera parameters

Image Quality	Image Size	Image Size in pixel	ISO Sensitivity
NEF (RAW)+Jpeg normal	Large	6000 x 4000	100

A UAV, also simply called a drone (Figure 4-3), can change the flight altitude, allowing studying with precision, the area acquired by its sensors. UAVs are commonly employed in civil and environmental applications [211,212]. They have also been experimented with for pavement distress detection [184]. They have several technical and logistical advantages such as the ability to obtain high-resolution images, short waiting times for obtaining data, and low operating costs. Nevertheless, their use could be affected by limitations due to the weather conditions (wind, rain, etc.), obstacles (buildings etc.), regulatory aspects (possible presence of "no-fly" zones) and/or instrumental issues (low battery autonomy, low payload, etc.). A GoPro Hero 3 with a resolution of 12 Megapixels was used because of its lightweight which corresponds to the regulations of the Italian laws [213]. In Italy, drones can be flown without special permissions for recreational purposes for heights not more than 70 meters above the ground with commercial purposes allowed up to 150 meters with a license. A direct line of sight must be maintained for the drone during flights. Generally, permission is required for commercial or development purposes. For application in other countries, the legal barriers must be considered as the laws vary based on the region and country of application.

Figure 4-3. Drone equipped with GoPro hero 3

For the ground truth instrument, the FARO Focus3D 120 (Figure 4-4) was used. It is a phase-based laser scanner that captures objects in a range from 0.6 m to 120 m. with a ranging error of ±2 mm. As with other phase-based scanners, it is characterized by a high measuring speed with a maximum of 976,000 measuring points per second.

Figure 4-4. Faro focus3D Scanner

Once the imagery was collected by the various devices, an SfM pipeline as depicted in Figure 4-5 was employed in order to replicate 3D models of each pavement section.

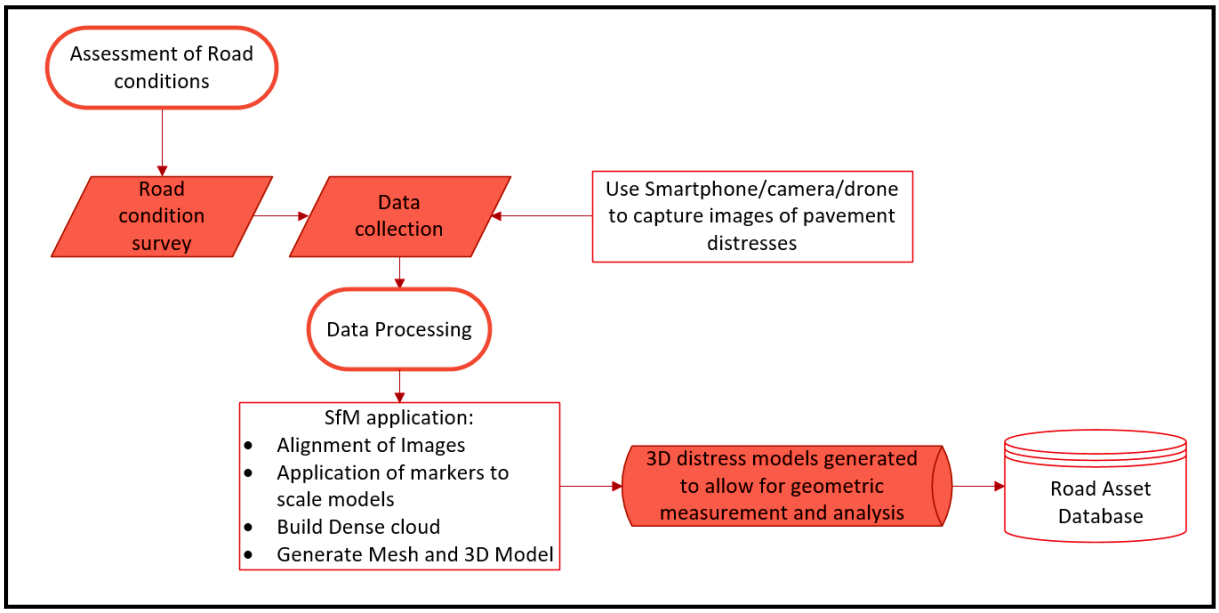

Figure 4-5. Typical SfM pipeline for generating pavement distress models.

Once the calibration of the instruments was completed according to their generic manuals, the following steps were followed:

1. Creation of SfM models.

N-SfM models: Using the previously identified camera, a photographic dataset was taken of the distressed pavement site. A sequence of photos of the pavement defect was captured ensuring that the angle between one shot and the other was between 5 and 10 degrees and the overlapped part was approximately 70%. An example of how the images are taken in the survey and their locations with respect to the image is given in Figure 4-6.

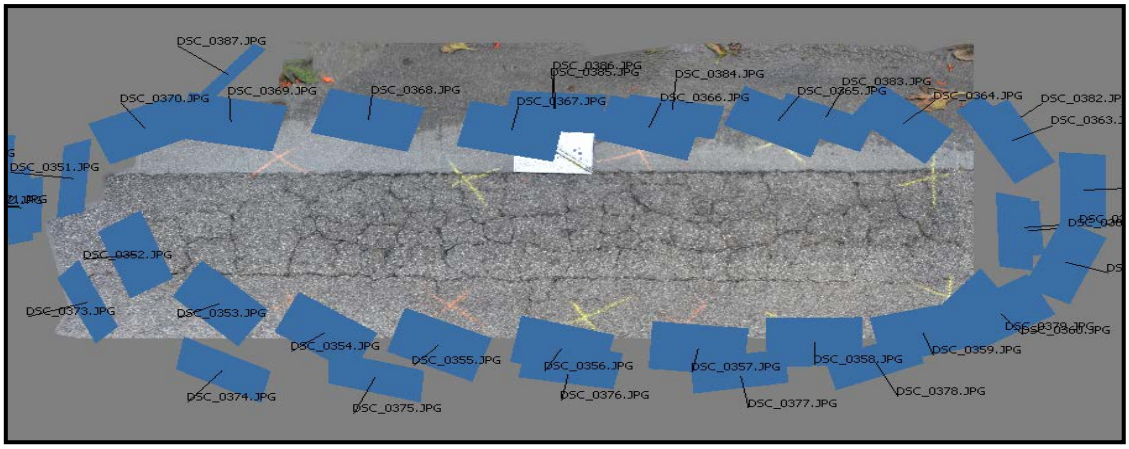

Figure 4-6. Example of a photo dataset around a pavement surface

This dataset was then imported into the SfM software, Agisoft PhotoScan [214], where the typical SfM workflow was used [215,216]. This involved the alignment and orientation of the images followed by the creation of a 3D dense cloud through Bundle Adjustment and then mesh creation and finally, a textured 3D model exploiting the sequence explained in Figure 4-5.

UAV-SfM models: Using the previously identified drone, a photographic dataset was taken of the same pavement site used for the N-SfM. The drone was flown over the site capturing images in the same motion as with the N-SfM but at a higher altitude. The dataset obtained via this method then underwent a similar image elaboration process through the software as explained for the N-SfM;

I. Pre-processing of data – once the imagery was collected a check was made to determine if there were any significant differences in photo quality and lighting exposure. This again represents a limitation of the process and significant lighting changes and shadows can have an adverse effect on the modelling.

II. Estimation of the reliability of SfM through comparison with the laser-scanned dense cloud; this was done utilizing the MeshLab software[217] in which the models obtained through PhotoScan were imported and aligned for comparison computations. This analysis is shown in Section 4.3.2.

III. Geometric /metric analysis of the N-SfM reconstructed model; this was done utilizing the Rhinoceros 3D CAD software [218]. The model was imported into this CAD-based software where the geometric analysis was done on the 3D model;

The experimental survey was carried out within the campus of the University of Palermo, over the area of the Polytechnic School. An asphaltic road segment of length of approximately 100 m, with a carriageway of a width of about 6 m, having an average 3% longitudinal grade. The observed flexible pavement is very distressed as it is likely that maintenance treatment was never performed. On the road surface, several distresses such as longitudinal cracking, block cracking, ravelling, and potholes were the most apparent. (Figure 4-7)

Figure 4-7. Case Study area in the University campus

The survey was performed in a traffic-free condition. To avoid alignment errors due to the dark colour of the asphalt, the uniformity of the material, and the homogeneity of the surface, a few chalk markers were drawn on the road surface. The three different types of survey (laser scan, N-SfM, and UAV-SfM) were conducted in the same conditions of light exposure and radiation at a short distance-time span. Every survey took approximately 10 minutes and it was carried out on the crack-distressed surface of about 90 m².

4.3.2 Assessment of the Accuracy of Models Produced from Imagery

Using the MeshLab software, the models obtained with the UAV-SfM and N-SfM were scaled and aligned with the corresponding model obtained with the laser scanner (Figure 4-8). In terms of visual accuracy, i.e. the visual similarity when comparing the model to a real-life object, the differences between the UAV- SfM and N-SfM are shown in Figure 4-8. On the right side comparison in Figure 4-8, it is possible to deduce the high visual accuracy of the N-SfM with respect to the definition of the crack in terms of the points demonstrated by the 3D coordinates. Furthermore, in the comparisons with the laser-scanned model, the N-SfM is better than the UAV-SfM and in fact, the visual definition is higher for the SfM one than the

Laser scanned model. The metric evaluation was then done by considering the Hausdorff Distance Quality Histogram.

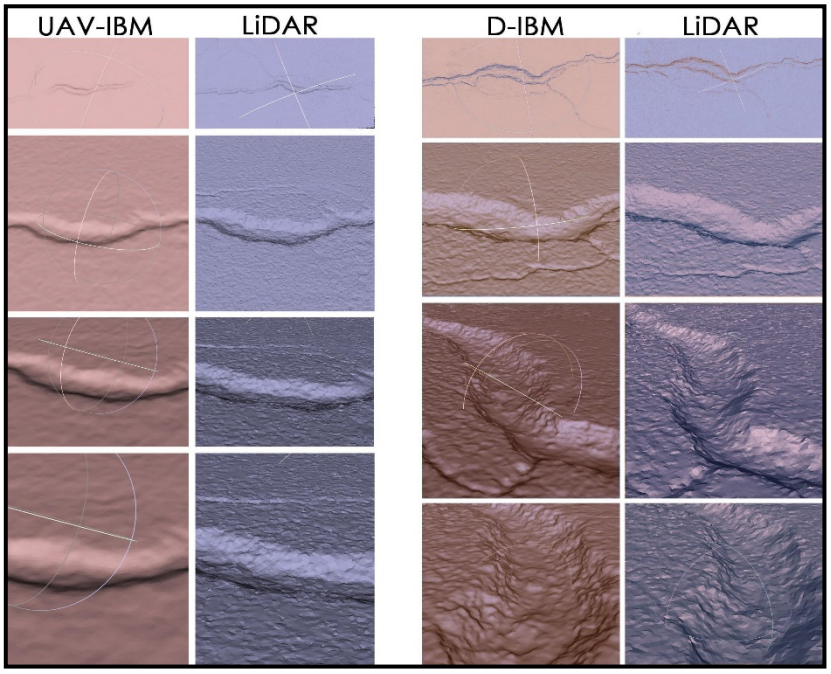

Figure 4-8. Meshlab Alignment UAV-SfM and N-SfM models with the terrestrial laser scanned one

Once the alignment was made, in order to have a metric for the reliability of the SfM models, it was necessary to calculate the differences between the different models produced. There are different ways of analysing this difference and the first method explored was to use the Hausdorff Distance, which represents a measure of adjustment accuracy in object space [219]. The Hausdorff Distance is an algorithm that measures the distance between two subsets of points in a metric space (Figure 4-9 and Figure 4-10).

The metric results were interpreted with respect to the Ground Sample Distance (GSD), i.e. the distance between two consecutive pixel centres measured on the ground. The lower the GSD value, the higher the spatial resolution of the image, i.e. the smallest details which can be seen in an image [219]. There is a direct correlation between flight height and GSD; higher altitudes result in a higher GSD [220]. This, therefore, results in the UAV-SfM having a higher GSD and thus a lower spatial resolution when compared to the N-SfM.

In the Hausdorff Distance histogram, the vertices are coloured using colours that vary from red which corresponds to perfect alignment (deviation equal to 0) to blue which corresponds to a deviation higher or equal to 0.5 mm. The blue colour corresponds to vertices that are outside the calculation range, they represent the points where the scan and 3D reconstructed model are not overlapped. Furthermore, the distribution of the deviations in terms of the

number of vertices per each colour was calculated. In Table 4-2 and Table 4-3, the parameters of the devices used are shown.

Table 4-2. Parameters for cameras used for SfM

	N-SfM	**UAV-SfM**
Camera	Nikon D5200	GoPro Hero 3
Camera resolution [Megapixel]	24	12
Distance from the pavement [cm]	Min. 50 Max. 120	~ 500
Number of photos taken [-]	50	29

From Table 4-2 it can be observed that the camera resolution of the N-SfM is higher and the altitude used for the UAV-SfM is significantly higher as well. For comparison, the specifications for the Laser scanner are shown in Table 4-3 below.

Table 4-3. Specifications of the Laser scanner

	Laser Scanner - FARO Focus 3D 120
Distance accuracy	up to±2mm
Speed	976,000 measuring points per second
Distance range	from 0.6 m to 120 m
Camera Resolution [Megapixels]	Up to 70

Utilizing the camera settings, the models produced, using the SfM software, had differing result characteristics as shown in Table 4-4 below.

Table 4-4. Result characteristics of SfM models

	N-SfM	**UAV-SfM**
Camera	Nikon D5200	GoPro Hero 3
Mesh faces created in SfM software[-]	1 991 999	1 999 998
Processing time	~7h 45 mins	~ 15 mins
GSD [mm/px]	0.0504	0.646

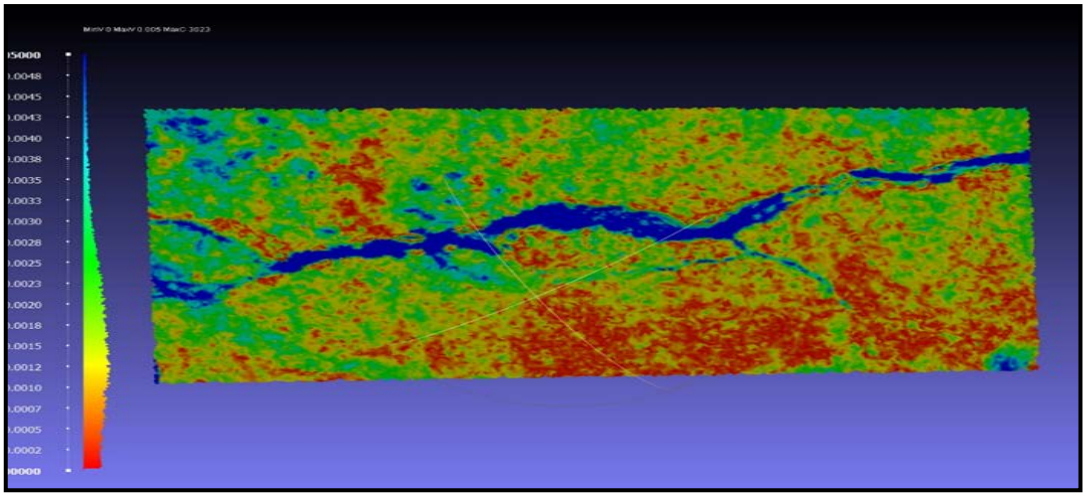

Figure 4-9. Meshlab Quality Histogram of UAV-SfM after Hausdorff Distance with the terrestrial laser scanned one.

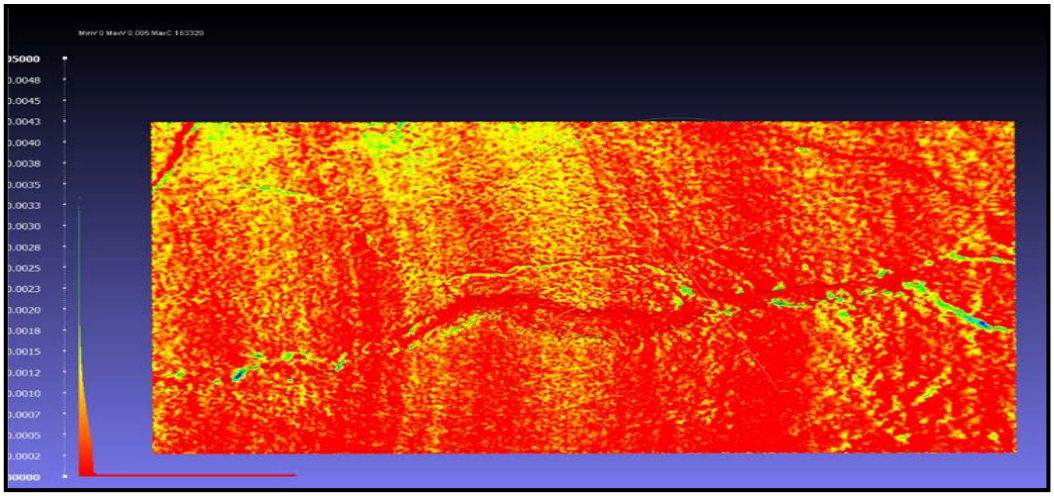

Figure 4-10. Meshlab Quality Histogram of N-SfM after Hausdorff Distance with the terrestrial laser scanned one.

The graphical representation of the Hausdorff distance of N-SfM and laser models shows a small deviation of the homologous points. In the case of UAV-SfM and laser scanner, the deviation of the homologous points is higher as seen in Figure 4-10.

Moreover, this part of the crack is more hidden and the reconstruction is less precise. The metric and visual accuracy depends also on the camera parameters and the altitude of the flight. In this investigation, the resolution of the UAV camera is 12 Megapixels and that of the N-SfM camera is 24 Megapixels; the average altitude of the UAV flight is 7m and the average altitude of the N- SfM data set is about 0.5 m. The different techniques show different metric accuracies in the crack detection as is expected with the variation in the GSDs of the models reproduced. The N-SfM, consistent with the previous work applied on laboratory samples of rutted asphalt, [201] and the accuracy level is also consistent with other recent work in the

photogrammetry field [194], provides higher level of details of the crack if compared to the laser scanner as illustrated visually on Figure 4-9. This is particularly evident when the object is scaled. The laser scan images are significantly grainier than the N-SfM ones. On the other hand, the UAV-SfM instead provides a lower accuracy compared to the laser scan and the N-SfM. This again was expected due to the variation in the GSDs.

With the results presented, the UAV-SfM allows a quick identification of the presence of the distresses on the road pavement and the condition of the road on a large-scale. Therefore, the UAV-SfM results are useful to understand the overall conditions of the state of a long stretch of road pavement, identifying the critical areas of the road surface where it is necessary to carry out a more detailed analysis using the N-SfM. In this way, the distresses that require detailed geometrical investigation, to narrow down the potential causes of the damage, can be analysed to determine their severity. Consequently, N-SfM can be applied when the distress requires a high level of detail to identify the cause and severity, relying on the high metric accuracy of the technique. The realistic model reconstructed with this technique allows gathering important geometrical information of the distress. Multiple sections with variable distances can be created to dissect the model. The capabilities of the model reconstruction can be exploited improving the mechanism of the geometrical analysis to obtain dimensions and this is further examined in section 4.4.

4.3.3 Assessment of Accuracy of Models Created from Mobile Phone Imagery

Given the validation of the accuracy of using imagery from a camera and a drone, it was then important to establish the accuracy of using imagery from smartphones. For this, the control in the experiment was the use of the camera previously specified in section 4.3.1 and this was validated by its results when compared to the ground truth of the laser scanner. The average Hausdorff Distance between the laser and the camera models in section 4.3.2 was found to be 156x10-6 mm, which validates the use of this device as a ground truth because of the small difference between the devices' performance. For a metric evaluation of the differences between models generated by the mobile phones and those generated by a professional camera, a statistical evaluation of the measured geometric differences between the models was done utilizing the Weibull distribution.

The Weibull distribution is a continuous probability distribution and it was applied as it is typically used in reliability analyses and used to determine the accuracies of structure-from-motion models [221].

The distribution is defined by the probability density function given in Equation 4-2 below.

$$f(t) = \frac{\beta}{\eta}.(\frac{t-\gamma}{\eta})^{\beta-1}.e^{-(\frac{t-\gamma}{\eta})^{\beta}} \qquad t > \gamma; \quad \beta, \eta > 0 \tag{4-2}$$

where β is the shape parameter, also referred to as the slope of the Weibull plot, η is the scale parameter, also referred to as the characteristic life parameter and γ is the location parameter, also referred to as the guaranteed lifetime (typically this value is set to zero). The shape parameter indicates the point at which the variable is likely to fail in its distribution. A value less than 1 indicates that failure will likely occur in the item's early life. A value of 1 indicates the rate of failure is constant and a value greater than 1 indicates the rate is increasing. Concerning the scale parameter, this value is indicative of 63.2 percentile of the distribution, which means that 63.2 per cent of the distribution will have failed before obtaining this value. The application of the Weibull analysis was done within the CloudCompare software [222]. The critical Weibull distribution shape and scale parameters were ascertained to have an understanding of the reliability and accuracy of the models generated by the mobile images.

As stated previously, a target value GSD value of 0.5 mm was used so the object distance was manipulated to ensure this value was obtained. Three devices were utilized for the surveys. A professional camera was used and two different common market mobile phones were used to test the accuracy of the technique using mobile phones. The camera was used as a control in the experiment. The specifications for these devices are given in Table 4-5. Mobile phones were utilized within the study because they are typically already in the possession of the average person in today's society and it has been shown that the image quality obtained from these devices are now commonly comparable to even entry-level DSLR cameras [223].

Moreover, the phones used were not the recent versions of the flagship phones. Thrice newer models have already superseded both phones used in the study (Huawei P20 Pro and Samsung Galaxy s9) and it is expected that newer models of both devices will be released shortly. This was done deliberately to show that the process does not require the most recent phones and it further shows that as time progresses the then 'older' models will still be able to accurately

carry out the process without heavy costs of new models. It is expected that the specifications of cameras on mobile phones will keep increasing as demonstrated by market trends and therefore even the average phone used by anyone will have the capacity to carry out the process. Additionally, by using mobile devices as opposed to cameras, there is no need for the purchase of other devices and the process would then therefore be possible with the typically used phone device by any user. Mobile imagery data also has an advantage over drone data in that higher resolutions can be yielded given that distance to the object is smaller and also surveys can be made in areas where drone use is forbidden.

Table 4-5. Specifications of devices used for SfM surveys.

Device	Nikon D5200	Huawei P20 Pro	Samsung Galaxy S9
Camera resolution [Megapixel]	24	40	12
Image Size [pixel]	6000 x 4000	3648 x 2736	4032 x 1960
Focal length used [mm]	24	3.95	4.3

For the surveys, three different sections in Palermo were chosen for the case study. The sections chosen had distresses comprising longitudinal and transverse cracking, alligator cracking, block cracking and depressions. The predominant distress type covered within the sections is cracking. Sections with a lot of cracking were considered as cracking is the most frequently occurring distress in the geographical region of study [38]. Images of these sections of pavements are shown in Figure 4-11, Figure 4-12 and Figure 4-13.

Figure 4-11. Distressed section 1

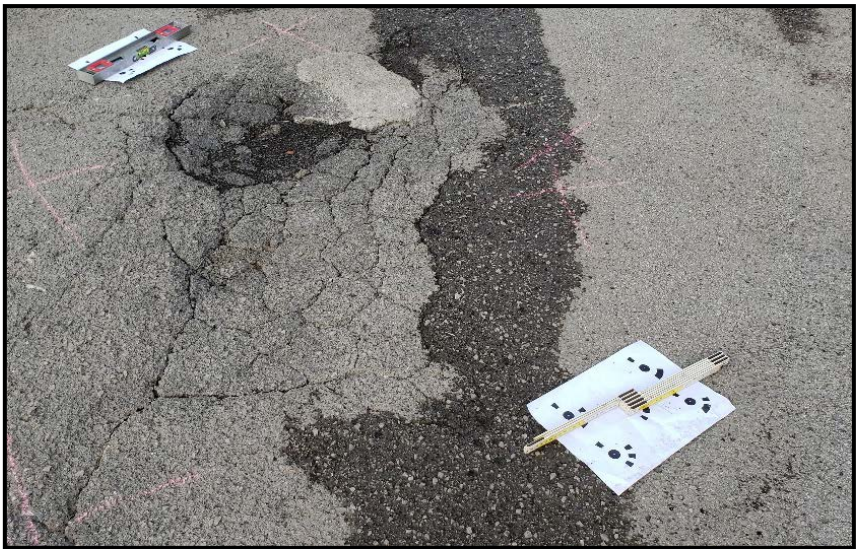

Figure 4-12. Distressed section 2

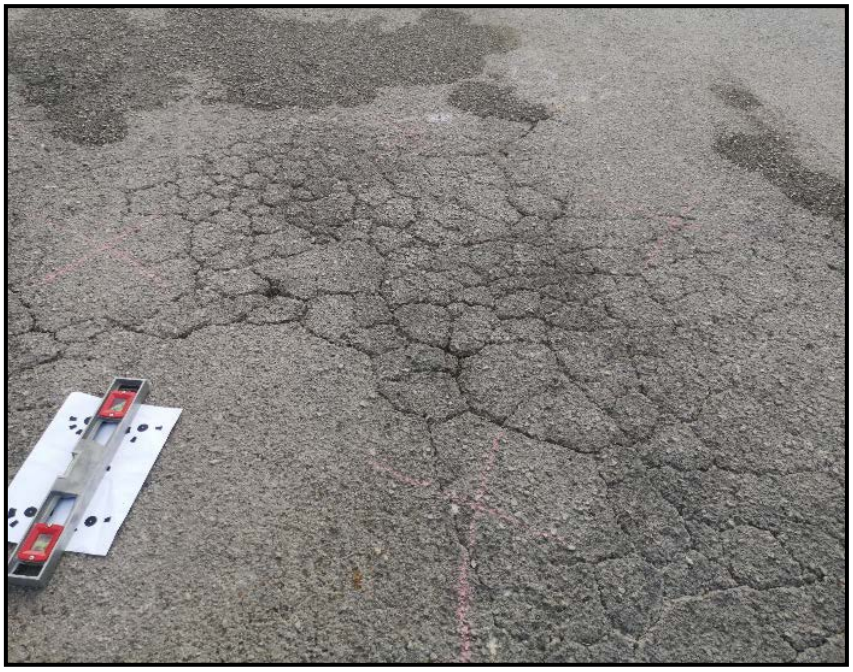

Figure 4-13. Distressed section 3

During the survey, images were taken in sequence and with the use of coded markers on the pavement, which allowed for scaling of the models. The images were also captured with an estimated overlap of 70% and slightly varying angles around the pavement distresses. Each distressed section was surveyed by each device and this was done consecutively to replicate similar environmental conditions to ensure the results were comparable.

The survey was carried out with users operating the devices by hand. The images were taken from varying inclined angles in a rotational manner around the distressed section. This was done to capture details at the crevices of the distresses that are hard to be seen if the image is taken directly vertical above the object. This methodological choice of using inclined

imagery is typical in photogrammetry to allow for the registration of the small minor details on the object being analysed. By carrying out the survey at angles, the minor details along these crevices are easier to collect and the 3D model generated can be more accurate.

For each section, the survey took approximately ten minutes per device. It should be noted here that whilst this length of time can be considered as more than that of a manual survey of a particular distress section, this type of survey has the potential to yield results that are not subjective as is often the case with manual surveys. This is as a result of most used pavement condition indices having input parameters that rely on a subjective interpretation of the condition by the surveyor. Additionally, this type of 3D survey will yield results that are not possible as with common manual surveys as a full 3D metric evaluation is possible with the SfM approach. The time needed for model processing should also be considered. This would be based on the level of details required by the authority and the equipment utilized. For a drone survey over pavement sections of approximately 4km, the processing can be done within two hours per section whereas, for a model directed at one distress, the model and processing can be done in a much shorter time. These times are based on the computing power of an average PC workstation with 32GB of ram. It should be noted as well that the workstation described is not a high-end one. In both instances, models and results can be generated within 1 day, once the workflow is followed as described in section 4.3.1.

Following the completion of the 3D model generation, the point clouds of each model were transferred to CloudCompare to establish the accuracy of the models derived from the mobile imagery and to segment the models to analyse the distresses occurring in each section. Before the segmentation strategies can be employed, the accuracies of utilizing the techniques using mobile phones needed to be established, and this was done comparing models from imagery mobile devices against the models generated using imagery from a professional camera.

- Analysis of Pavement Section 1

For the first section, the visualized differences along with the plotted distribution and Weibull plot are shown in Figure 4-14 and Figure 4-15. The two important resulting parameters from this distribution are the Weibull shape and scale parameters and the values for these are given in Table 4-6 where the scale parameter would be measured in meters and the shape parameter has no dimension. The scale value typically specifies that 63.2 percentile of the distribution will fail before reaching this point [224]. Given the values in the table, this signifies

that for all of the models this value was less than 0.003 m (3 mm). Furthermore, the value of the shape parameter was also close to one, which signifies that within the distribution it is more likely that the majority of the values will occur early in the plot. Therefore, it can be inferred that for a random point on the model, it is likely that it would have a small measured difference, as the small differences are the values that occur early in the distribution plot. This helps to validate the hypothesis of using low-cost mobile imagery for this section. The visualizations provided also depicted the locations on the pavement where the most change is present. This was generally along the inside of the cracks as can be demonstrated in Figure 4-14 and Figure 4-15.

Table 4-6. Weibull parameters observed from each model comparison for Distressed Section 1

	Weibull parameters	
Phone	Shape (a)	Scale (b)
Huawei P20 Pro	1.186156	0.002275
Samsung Galaxy s9	0.981589	0.002794

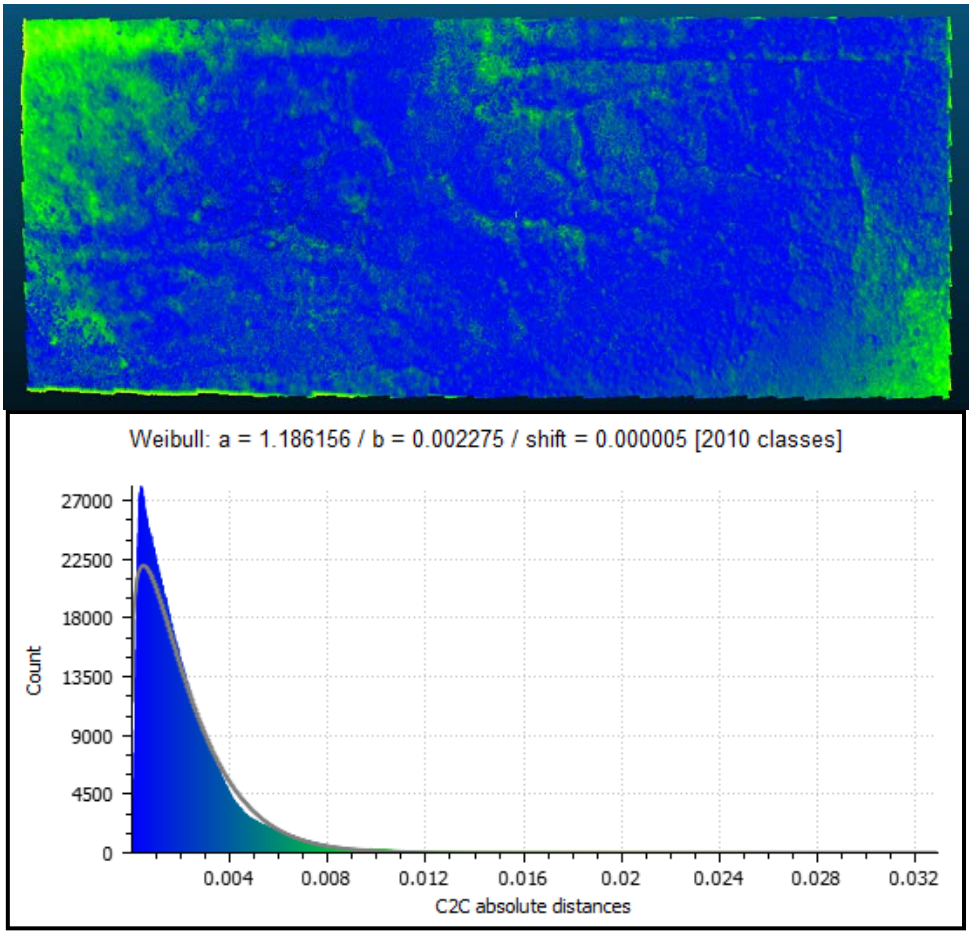

Figure 4-14. Measured differences between model generated by the camera and Huawei phone, (top)—visualization of differences projected on the model, (bottom)—distribution of measured differences.

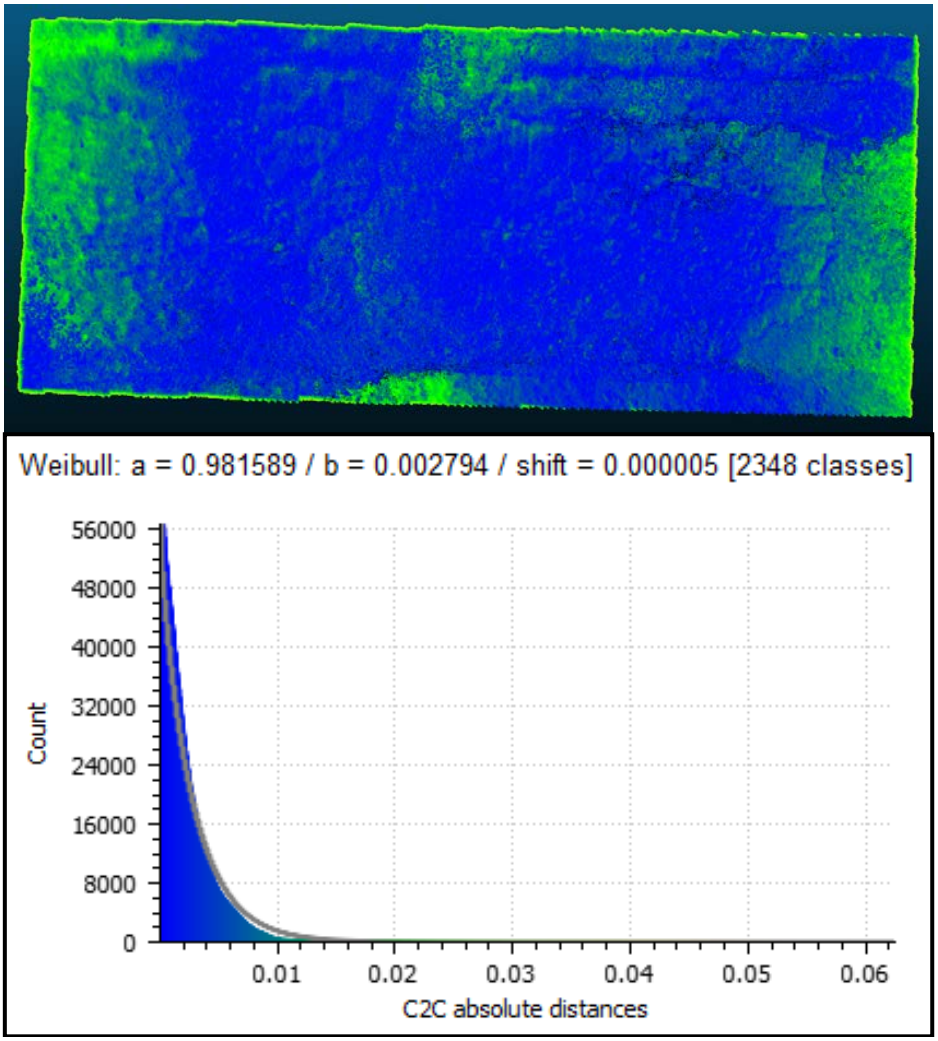

Figure 4-15. Measured differences between model generated by the camera and Samsung phone, (top)—visualization of differences projected on the model, (bottom)—distribution of measured differences.

- Analysis of Pavement Section 2

For the second section, the visualized differences along with the plotted distribution and Weibull plot are shown in Figure 4-16 and Figure 4-17. The Weibull shape and scale parameters are shown in Table 4-7. For this section, the values for the scale were again less than 0.003 m (3 mm). The shape parameter value was again close to 1, which once more signifies that within the distribution it is more likely that the majority of the values will occur early in the plot. This helps to reinforce the validity of the methodology for a different section, this one with depressions and cracking. The visualizations for these two comparisons showed that the most change occurred along the crack but also in the interior of the depression in the section.

Table 4-7. Weibull parameters observed from each model comparison for distressed section 2

	Weibull parameters	
Phone	Shape (a)	Scale (b)
Huawei P20 Pro	0.941246	0.001772
Samsung Galaxy s9	1.005422	0.001528

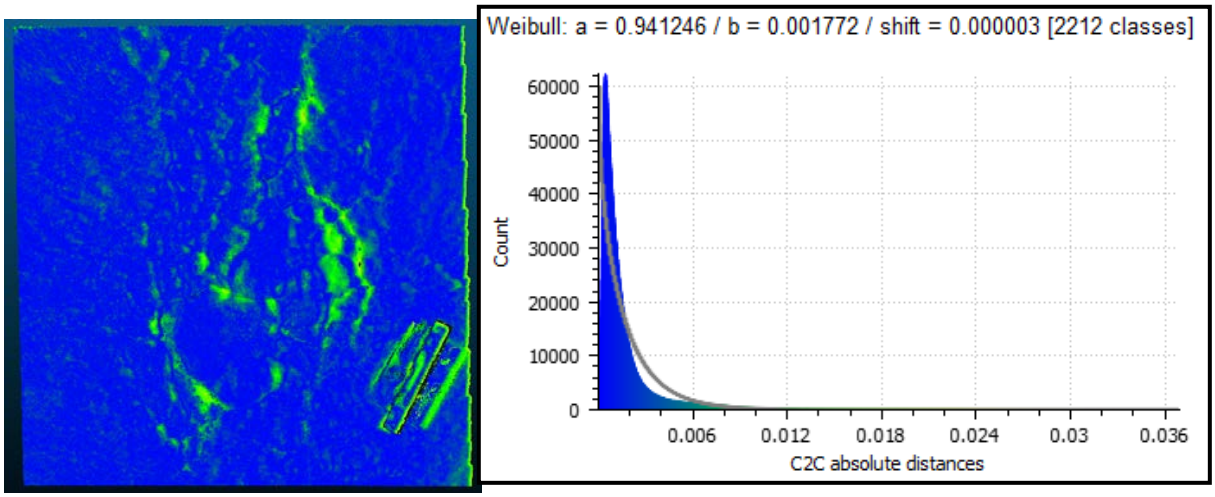

Figure 4-16. Measured differences between model generated by the camera and Huawei phone, (right) — visualization of differences projected on the model, (left)—distribution of measured differences.

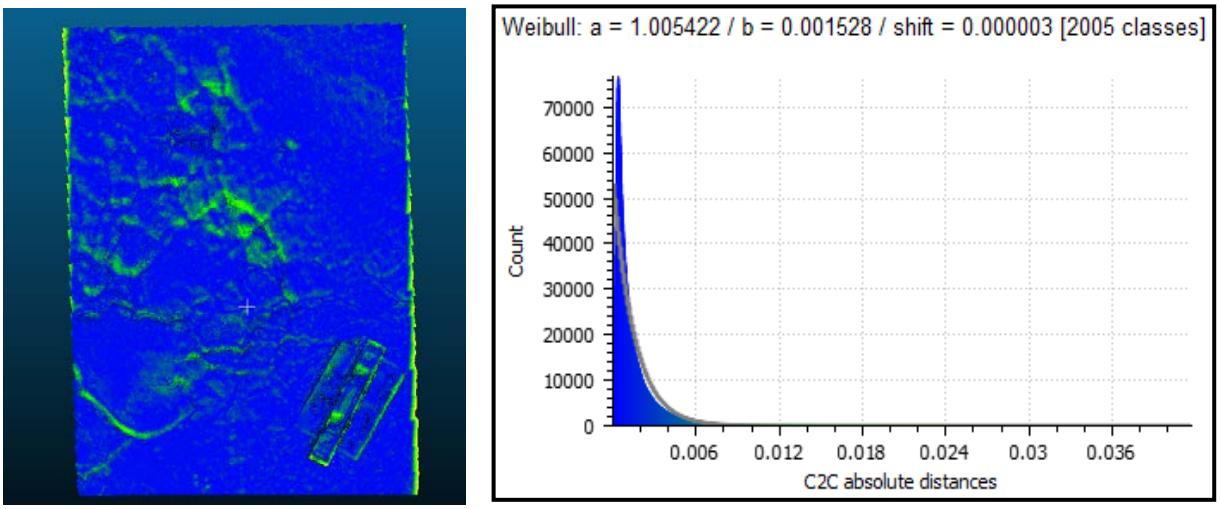

Figure 4-17. Measured differences between model generated by the camera and Samsung phone, (right) — visualization of differences projected on the model, (left)—distribution of measured differences.

- Analysis of Pavement Section 3

For the third section, the visualized differences along with the plotted distribution and Weibull plot are shown in Figure 4-18 and Figure 4-19. The Weibull shape and scale parameters are also given in Table 4-8. For this section, the scale values were again less than 0.003 m (3 mm). Additionally as was the case with the two previous sections, the shape parameter was again close to 1 which once more signifies that within the distribution it is more likely that the

majority of the values will occur early in the plot. Once more this reinforces the validity of the methodology for a different section, this one with area-wide cracking that is block and alligator-like. The visualizations for these two comparisons showed that the most change occurred along the interiors of the blocks of the crack.

Table 4-8. Weibull parameters observed from each model comparison for distressed section 3

	Weibull parameters	
Phone	Shape (a)	Scale (b)
Huawei P20 Pro	0.725207	0.002148
Samsung Galaxy s9	1.183398	0.001785

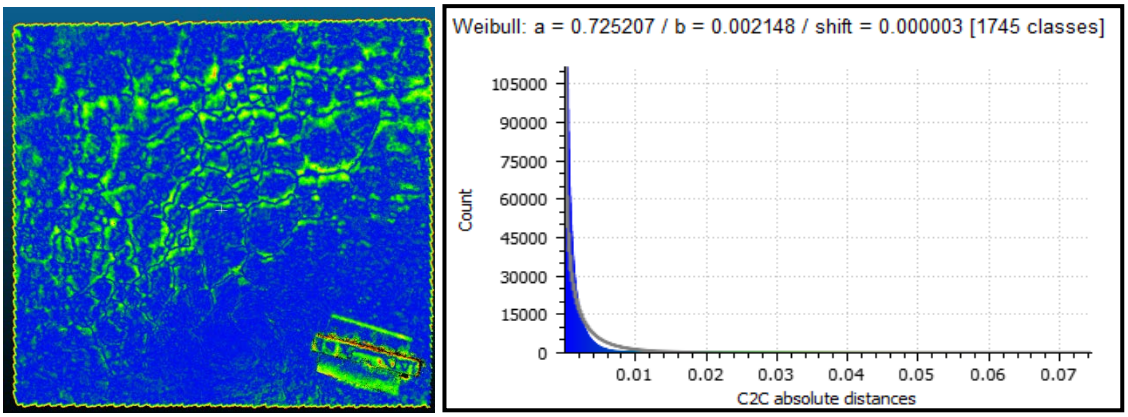

Figure 4-18. Measured differences between model generated by the camera and Huawei phone, (right) — visualization of differences projected on the model, (left)—distribution of measured differences.

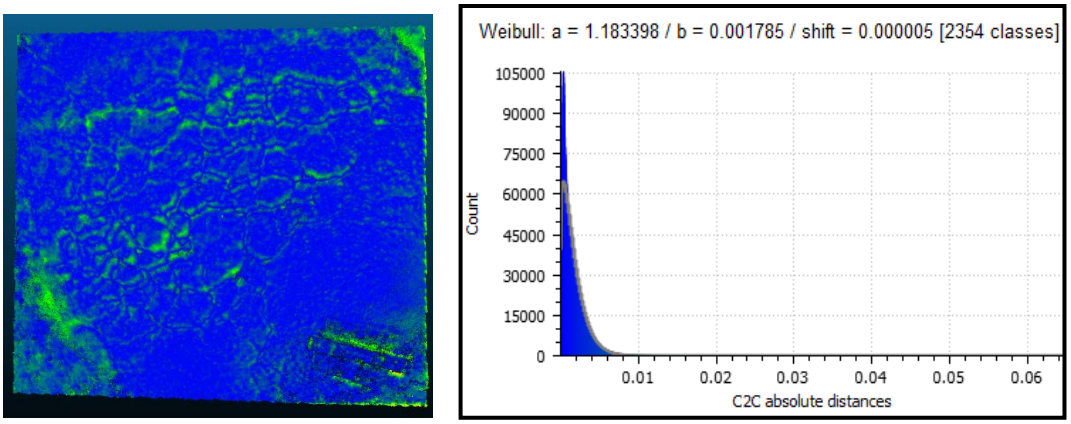

Figure 4-19. Measured differences between model generated by the camera and Samsung phone, (right)— visualization of differences projected on the model, (left)—distribution of measured differences.

Based on these results using the statistical analyses, it was proven that the SfM techniques discussed can be utilized with the mobile devices used in the study with accurate models being generated that can sufficiently detect the presence of pavement distresses within the sections. Additionally, as previously stated, the use of mobile phones that were not the latest flagship models from their respective companies means that newer phones and those in the future would likely have better cameras and therefore, would likely yield models with greater

resolutions. This demonstrates the capacity of the pipeline moving forward. Furthermore, it must be mentioned that the use of mobile devices poses advantages to other methods of obtaining imagery such as drones that have legal restrictions in many countries.

4.4 Characterization of distress type and severity

Given the replicated models, the methodology adequately obtains the required dimensions and therefore a workflow can be drawn for each. Also of interest are the additional measurements that can be obtained, which provide further information for distress analysis and can be used to generate greater assessments of damages. These additional details are not possible through visual inspections and can be used to further bolster the PMS input data and create a new metric for assessment in the future. The workflows developed are shown below in Figure 4-20. Within the workflow, the measurements that can be utilized for each of the main examples of distresses is shown which will lead to a severity determination for each.

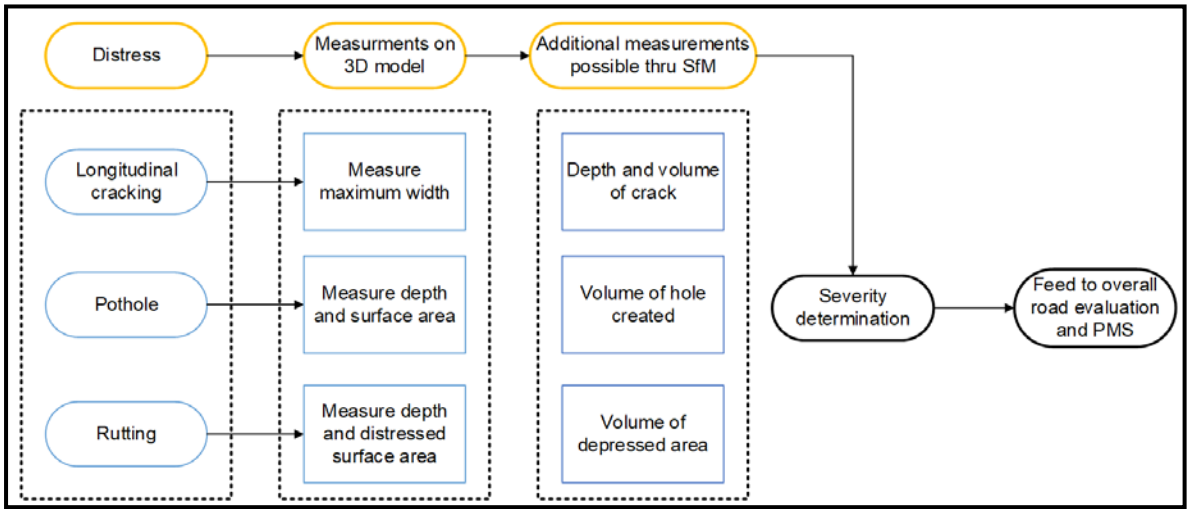

Figure 4-20. Workflow for utilizing SfM Image-based modelling.

4.4.1 Geometric analysis of 3D distress models

To emphasize the potentials of reconstructed models, geometrical analyses were carried out, which allowed important aspects of the distresses to be highlighted. Computer-Aided Drafting (CAD) tools allow the measurement and evaluation of deformations and deviations of the model's surface. Models can be imported into the advanced modelling software and for this, NURBS (Non-Uniform Rational B-Splines), Rhino3D [218] was used. The acquired 3D models can be scaled and rotated in order to align them in an absolute reference system. An initial integrated review of the network polyhedral mesh topology (faces, vertices, edges) was

conducted to identify and correct the possible occurred errors: the elimination of the abnormal and irregular faces, the identification of intersections, gaps, and open edges shared by more than two faces.

Once these preliminary steps were completed, horizontal and vertical planes were defined to intersect the mesh and extract the curvilinear profiles of certain sections. Multiple spaced planar curves (i.e. parallel longitudinal sections) were then created defining several profiles of the crack. Every profile can be isolated and analysed. This process leads to the identification of important characteristics of the distress such as the maximum depth and width of the crack as well as the profile shapes in every section of the distress. A geometrical investigation of the models allows obtaining important information regarding the severity and the possible cause of the distress. To analyse the distress and extrapolate the maximum amount of information, a series of spaced planar curves, i.e. parallel multiple sections 5 mm and 1 mm distant from each other were created. An example of this process is shown in Figure 4-21.

a)

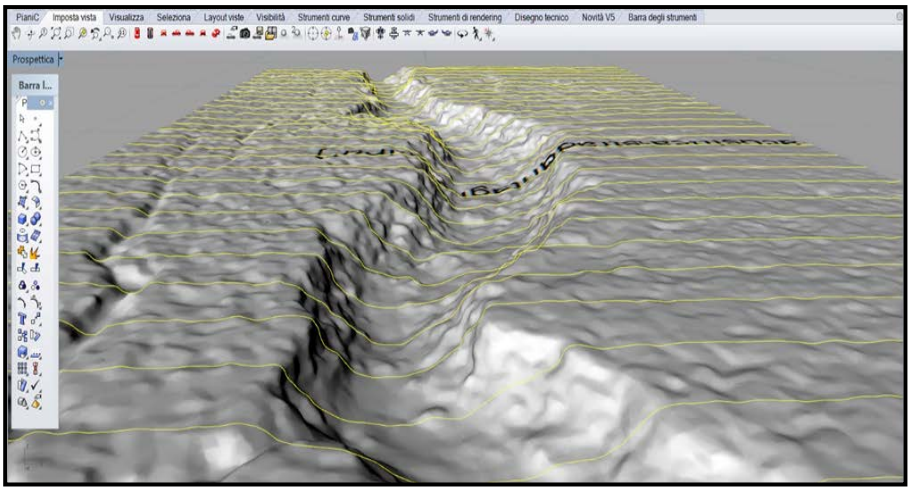

b)

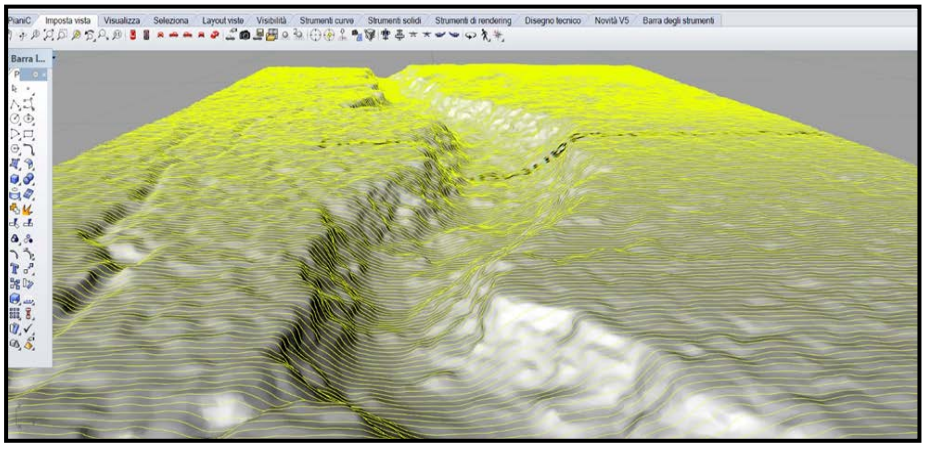

Figure 4-21. Profile curves on the N-SfM reconstructed model spaced at a) 5 mm and b) 1 mm

Once the 3D model is removed, the profiles of the multiple sections could be isolated. An example is shown in Figure 4-22.

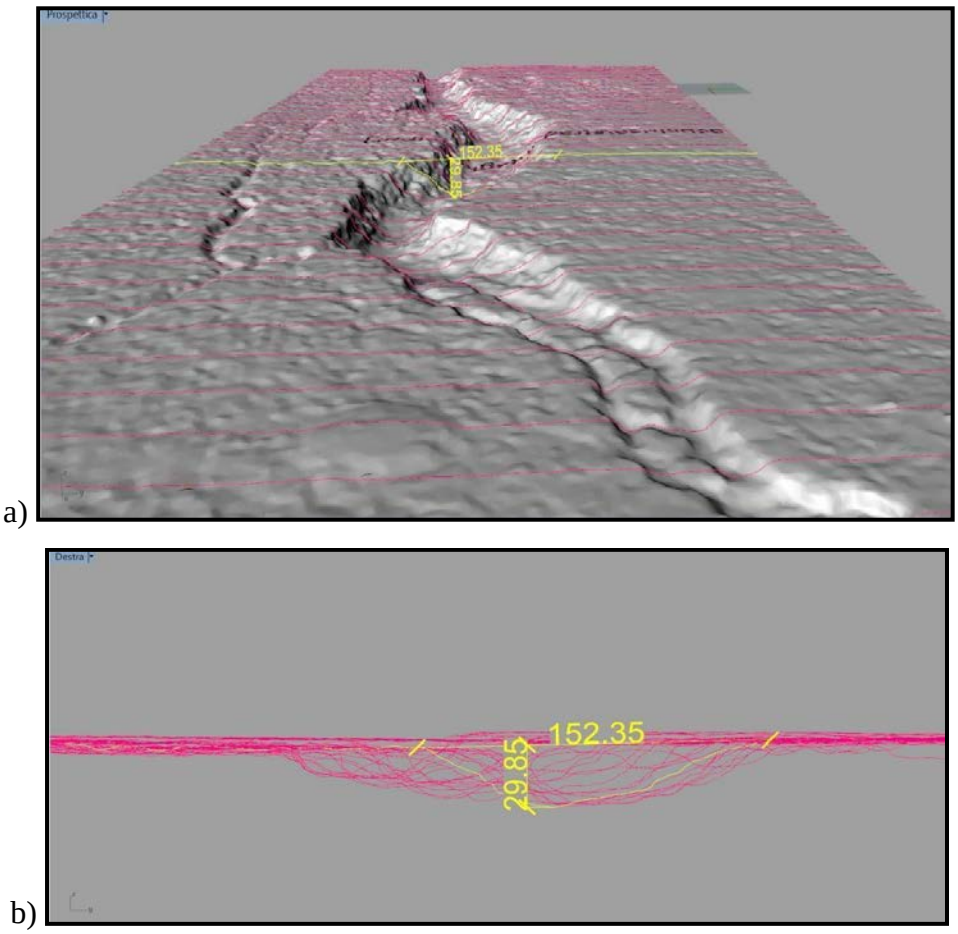

Figure 4-22. a) Identification and b) extrapolation of the maximum depth profile curve.

Every profile curve gives the possibility to measure the depth and the width of the pavement crack at a specific point. Therefore, it is possible to identify the maximum depth and width of the crack (value shown on the yellow line in Figure 4-22.) It is relevant to underline at this point that in general; the distress manuals classify the severity of the cracking according to the amplitude of the crack only, neglecting its depth, which also has considerable importance in defining the gravity of the distress. Therefore, this distress analysis adds a new parameter to the process of analysing the distress, providing further data for the PMS.

It should be noted also that the accuracy also leads to an analysis of other distresses patterns. Based on the processed GSD levels, a wide range of defects are covered, which can be measured in terms of distance measurement. Concerning those defects that are not recognizable in terms of distance measurement, the method also allows for analysis of the colour and the model's radiometric accuracy which can then be utilized to determine the

severity of the distress. This is in accordance with other studies which have conducted radiometric analysis on photogrammetric generated surface models [225].

4.4.2 The Use of Image Segmentation in Pavement Condition Evaluations

Whilst it is useful to recreate the pavement distress with 3D imagery, it is also useful to identify features on these models. Image segmentation was considered for this, which is the process of dividing an image into smaller related segments to analyse and isolate particular features. With regards to pavements, the purpose of image segmentation would be to isolate pavement distresses to quickly pinpoint the location of the distress and also for analysing the type of distress. There have been several attempts over the years to carry this task out utilizing different datasets. Studies have tried to extract useful features from drone image data [185], LIDAR point cloud data [226], Google street view image data [227], 3D laser profilers [228,229], 3D laser images [230]and normal 2D images [231]. There have also been attempts to utilize convolutional neural networks to segment pavement images using annotated masks on the images [232].

There are challenges to the acquisition of this data and the processing power required for analysis. To this end, this aspect of the study focuses on using the low-cost image acquisition pipeline investigated earlier in the chapter. When coupled with the SfM techniques, mobile imagery can be utilized to create point clouds of a distress and these point clouds can be segmented without excessive processing power. Point clouds have previously been classified to produce depth maps and smaller more useful models within the original model in other fields of study [233]. Generally, the process functions as depicted in Figure 4-23.

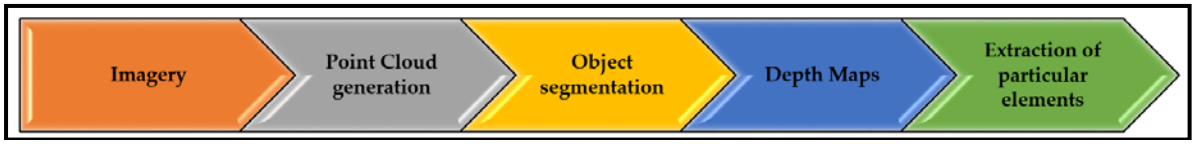

Figure 4-23. Pipeline for image segmentation

Given these factors, this aspect of the study aimed to generate depth maps and extract and isolate critical elements from 3D models generated by the mobile phone and drone imagery.

4.4.3 Application of Random Sampling Consensus (RANSAC) segmentation

The first application investigated was using the RANSAC segmentation algorithm. The RANSAC algorithm is utilized to extract shapes from a derived model. This is done by assigning sets of

points that can define a particular geometric feature type and then extracting shapes that fit this feature type based on the number of points in the category [234]. The algorithm functions by taking a given point-cloud $P = \{p_1, \ldots, p_N\}$ with associated normals $\{n_1, \ldots, n_N\}$ giving an output of a set of primitive shapes $\Psi = \{\Psi_1, \ldots, \Psi_n\}$ with corresponding disjoint sets of points $P_{\psi 1} \subset P, \ldots, P_{\psi n} \subset P$ and a set of remaining points $R = P \setminus \{P_{\psi 1}, \ldots, P_{\psi n}\}$. For every iteration of the algorithm, the primitive with the highest score is sought after. The algorithm iteration will conclude as soon as the defined minimal shape size is achieved for the point cloud. The definition of this minimal shape size can be controlled and for this study, this value was based on the size of the point cloud being analysed. This process can be visualized in the pseudocode for the algorithm shown below as created by [234]:

Algorithm – Extracting shapes in point Cloud P
$\Psi \leftarrow \emptyset$ {extracted shapes}
$C \leftarrow \emptyset$ {shape candidates}
repeat
  $C \leftarrow C \cup$ newCandidates()
  m ← bestCandidate (C)
  if $P(|m|, |C| > pt$ **then**
    $P \leftarrow P \setminus P_m$ {remove points}
    $\Psi \leftarrow \Psi \cup m$
    $C \leftarrow C \setminus C_m$ {remove invalid candidates}
  end if
until $P(\tau, |C| > p_t$
return Ψ

The implementation of this algorithm was done within CloudCompare, utilizing the H-RANSAC plugin. This process can isolate several different shapes from the model including planes, spheres, cylinders, cones and tori. For this study, the focus was on the planes to generate a profile for the pavement to deduce the distressed areas. The purpose, therefore, would be to identify an appropriate plane to be used as a baseline for creating a road profile and to generate depth maps of the section, which can be metrically referenced. Once the maps are created, the particular points of interest on the model can be established and isolated.

- Implementation of RANSAC

The first step for the implementation was assigning a value of the minimum support points per primitive. For each of the models being analysed the total number of points was between 1.4 to 4.5 million points. Additionally, each model assumed a physical distance of about 2 to 4 m^2 on the ground. Given these factors, a value of 50,000 was assigned as this would split the

object into no more than 90 segments, and given the fact that only one plane was required as a reference case, this number would limit the algorithm from producing planes cutting through the model at different mismatched angles. To ensure this value was correct the algorithm was applied for smaller values of 500, 5000, 10,000 and in each of these scenarios, inappropriate planes were generated as shown in Figure 4-24. This process was tried for each model and it was shown that with 50,000 points the result would yield an appropriate reference plane as shown through an example of one of the applications in Figure 4-25. On this, the plane appropriately cuts through the model to create a valid reference plane.

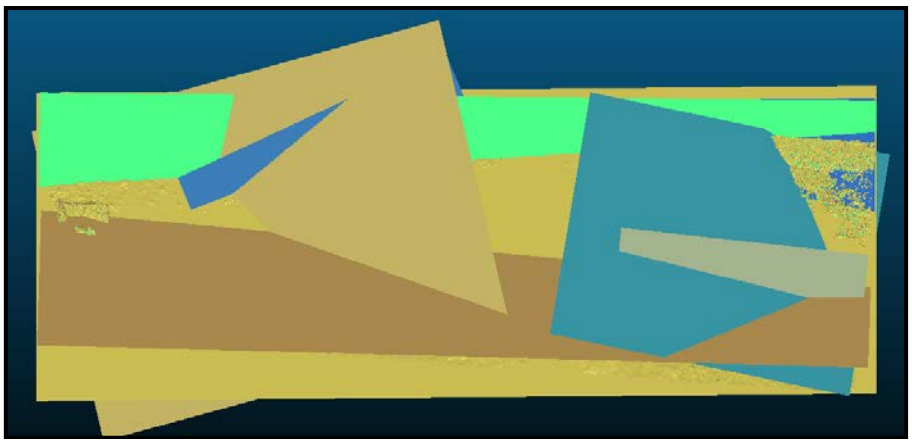

Figure 4-24. Application of RANSAC algorithm with too small of a value for the number of minimum support points.

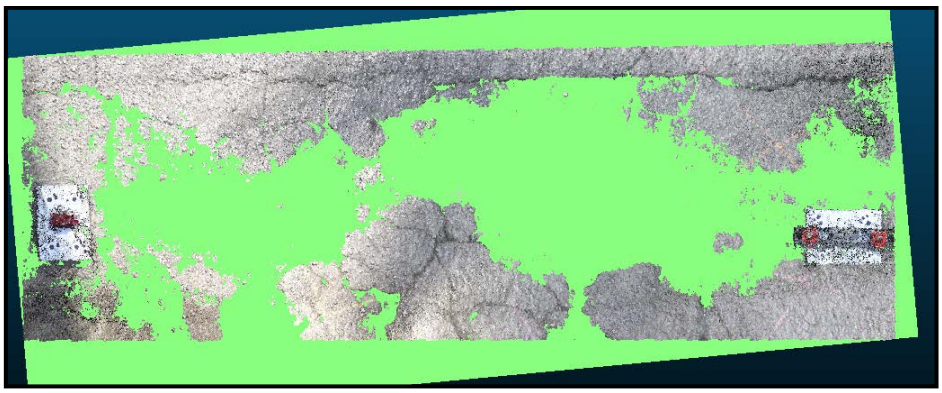

Figure 4-25. Application of plane shape through the RANSAC algorithm.

Once this plane was adequately assigned, a distance computation between the plane mesh and the point cloud was done utilizing the C2M distance computation in CloudCompare to produce a depth map for each distress. The C2M distances represent the depths and filtering that can result in the segmentation of the model. This is illustrated in Figure 4-26**,** Figure 4-27 and Figure 4-28.

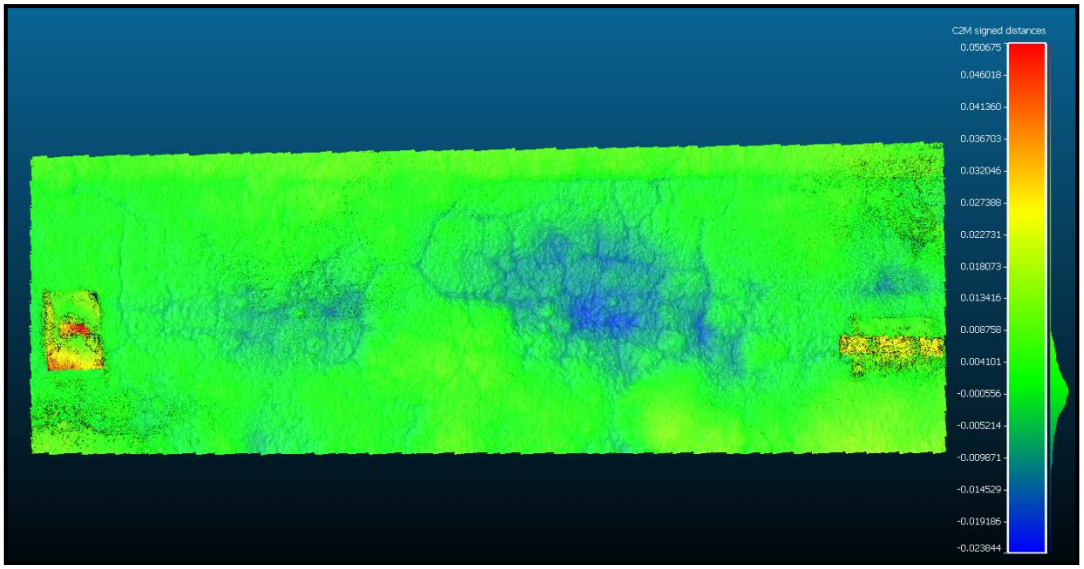

Figure 4-26. Pavement section 1 with the depth map created.

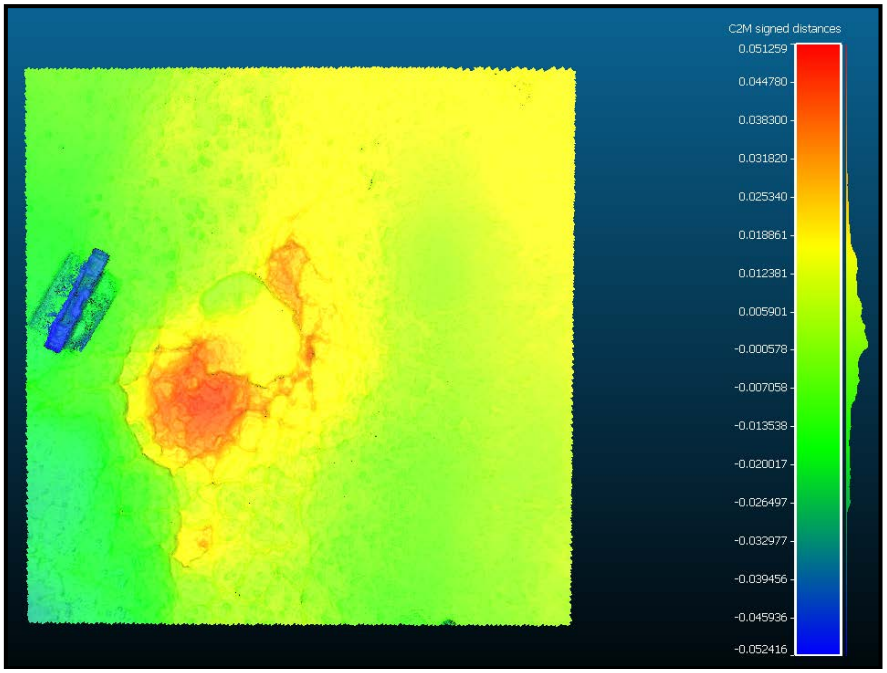

Figure 4-27. Pavement section 2 with the depth map created.

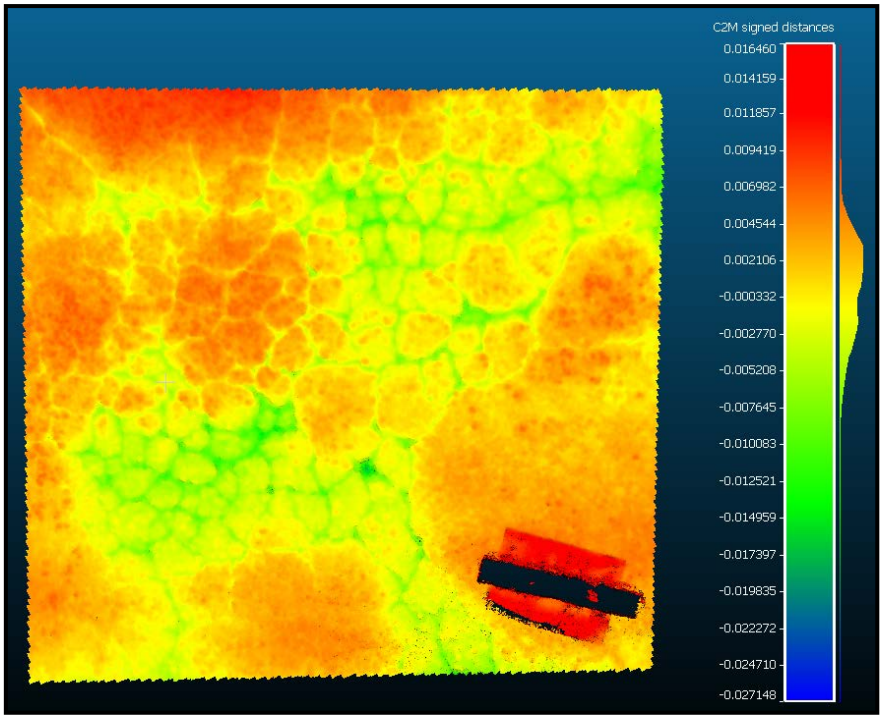

Figure 4-28. Pavement section 3 with the depth map created.

These depth maps now allow filtering to be done by depth and section and allow the model to be segmented for the sections to be analysed. This is easily done by controlling the range of the depth map and this is illustrated in Figure 4-29, Figure 4-30 and Figure 4-31. From the current segmentation result, the process can detect typical distresses where there is a change in surface deviation of the pavement. As the major groups of pavements distresses are cracking distresses and visco-plastic deformations (which both feature this type of deviation), this process and segmentation can account for most distresses. Visco-plastic deformations include bumps, sagging, rutting, corrugations, depressions, potholes, swelling, lane and shoulder drop off, shoving, and stripping. In Figure 4-29, Figure 4-30 and Figure 4-31, the depth maps for the pavement sections are shown at three different levels of segmentation.

In the first image, the entire section is visualized with the hotspots of the distressed sections highlighted. Given that in this depth map one can see the particular points of interest, the depth map was then further segmented to remove the parts of the pavement without distress by using a smaller range on the depth map values. The final image of the three further adjusts the range of the depth map to then only illustrate the distressed section with the deepest distress. In Figure 4-29, the third image highlights the section suffering from not only cracking but also a significant depression.

The same process was carried out for each section and the visualizations as shown in Figure 4-30 and Figure 4-31 follow the same methodology to allow visualization of the exact points

of distress and to isolate these sections. In Figure 4-30, the exact section suffering from a pothole is isolated and in Figure 4-31, the exact section suffering from excessive cracking is isolated. The semantic colour choice of the depth map is up to the user for the visualizations, in terms of which colours signify positive or negative deviations. Once this segmentation is done, metric assessments of the segmented portion can be found such as the area and volume of the segmented region, which can either be the distressed section or the section that is not. By doing this, a ratio of the distressed section to the non-distressed section can be established and inserted into the asset database for the road authorities, which is critical for establishing appropriate pavement management strategies. These critiques are possible as all of the models are scaled and the previous sections have established the metric accuracy of these scaled models. Additionally, features such as the depressed section and the crack section can be filtered by simply changing the range of the depth map as shown in the images. From this segmentation, a differentiation of the types of distresses occurring can be made as well as the particular features of the distress can be more easily identified as the depth maps shown in the figures establish isolation of sections that have related features. At this point, the user would be able to identify the particular distress type. This will provide a road agency with exact measurements of the distress, which can be utilized for severity assessment and to trigger times for maintenance and rehabilitation interventions.

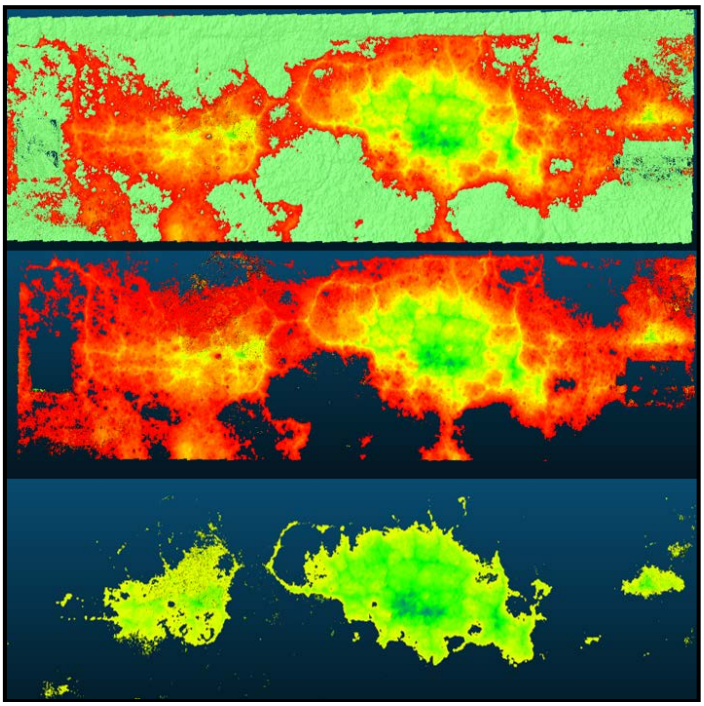

Figure 4-29. Segmentation of pavement section using RANSAC.

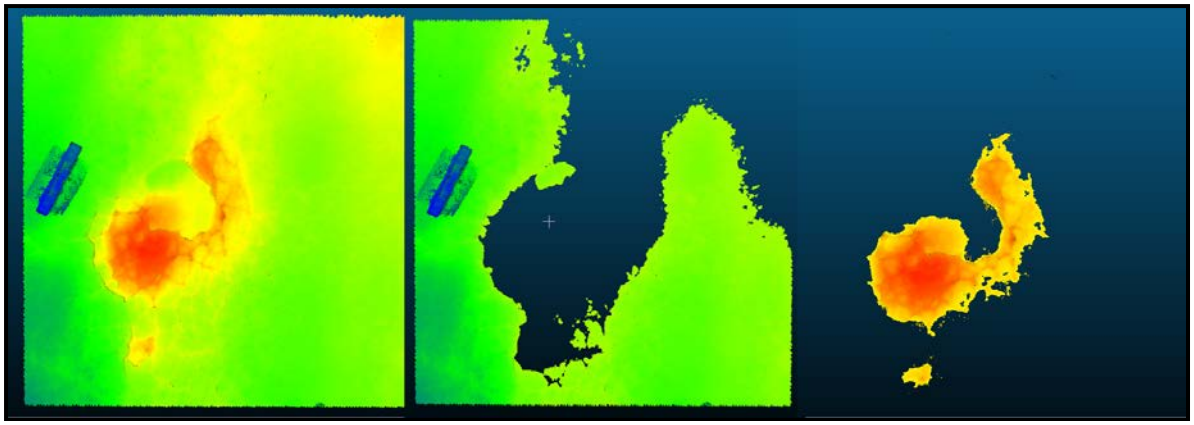

Figure 4-30. Segmentation of pavement section 2 using RANSAC.

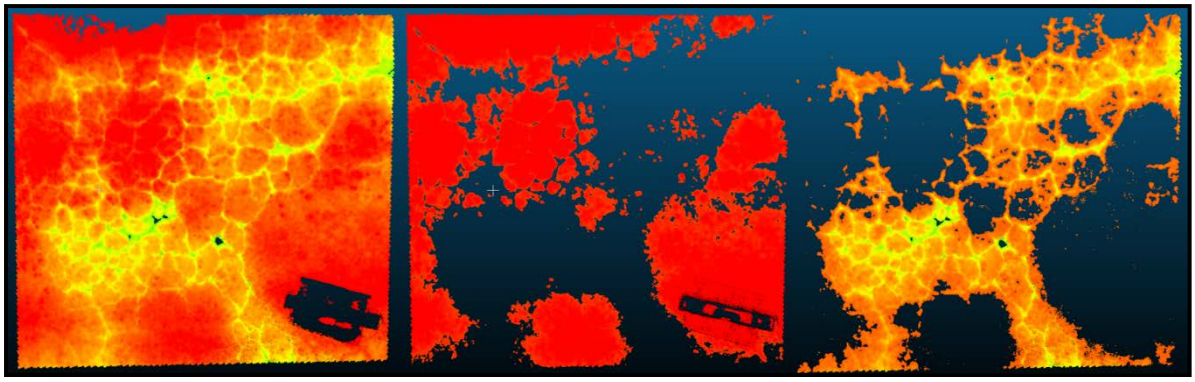

Figure 4-31. Segmentation of pavement section 3 with RANSAC.

4.4.4 Application of 'Fit' Segmentation algorithm

As an alternative to the RANSAC segmentation pipeline, another possible way of segmenting the pavement was explored, which involved utilizing the fit algorithm within the CloudCompare suite. The fit tool creates a plane based on the points within the point cloud. It, therefore, considers the entire point cloud under analysis. To do this, the process utilizes a standard least-squares fitting methodology of the points within the point cloud. This is based directly on the eigenvalues and vectors of the covariance matrix of the cloud so it can be considered as an efficient process. Once this tool is applied, the distance of this plane from the point cloud can again be utilized to create a profile of the measured differences which will generate a depth map to understand the conditions of the pavement section. The depth maps generated from this simple methodology were compared to those from the RANSAC.

- Implementation of fit segmentation

For the application of the fit algorithm, a similar process was followed to that of the RANSAC wherein a plane was generated considering the collection of points within the point cloud. This application can be considered as a simpler method given the fact that it relies on a

standard least-squares fitting methodology. The application of the fit tool was carried out on each model and this is demonstrated in Figure 4-32.

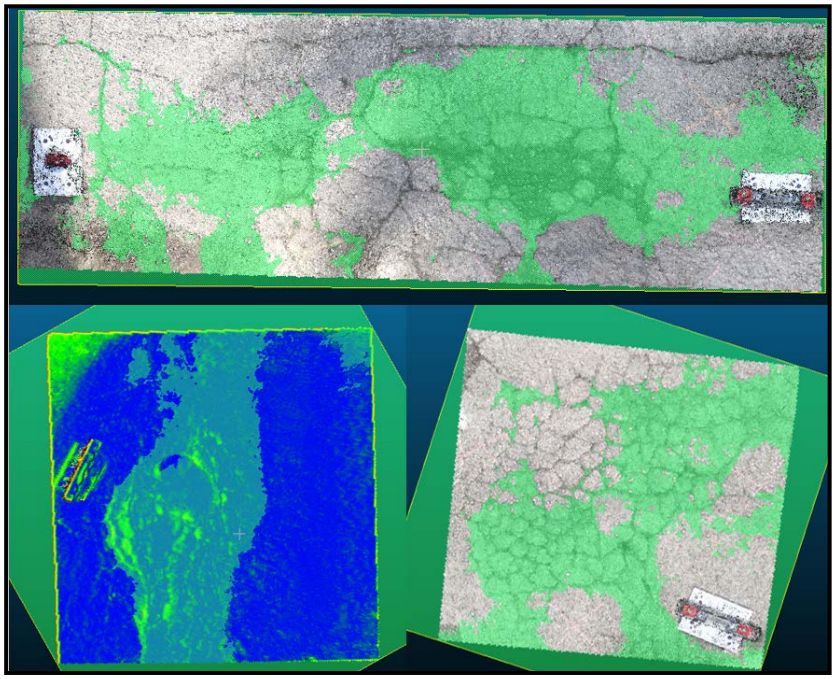

Figure 4-32. Application of 'fit' plane to each pavement section.

Following this plane application, the depth maps were generated on each model similar to the application of the RANSAC. This was done for the same purpose as previously stated to allow for segmenting particular sections of the pavement sections. This is illustrated in Figure 4-33, Figure 4-34 and Figure 4-35. Similar to the segmented images of the sections by the RANSAC algorithm, these images represent three levels of segmentation for each distress and highlight the possibility of isolating particular points of interest by altering the range of the displayed depth map. The segmented images depict particular points of interest. Each isolation can be measured and the metric value recorded to collect asset information and store it within the database of the road authority or agency.

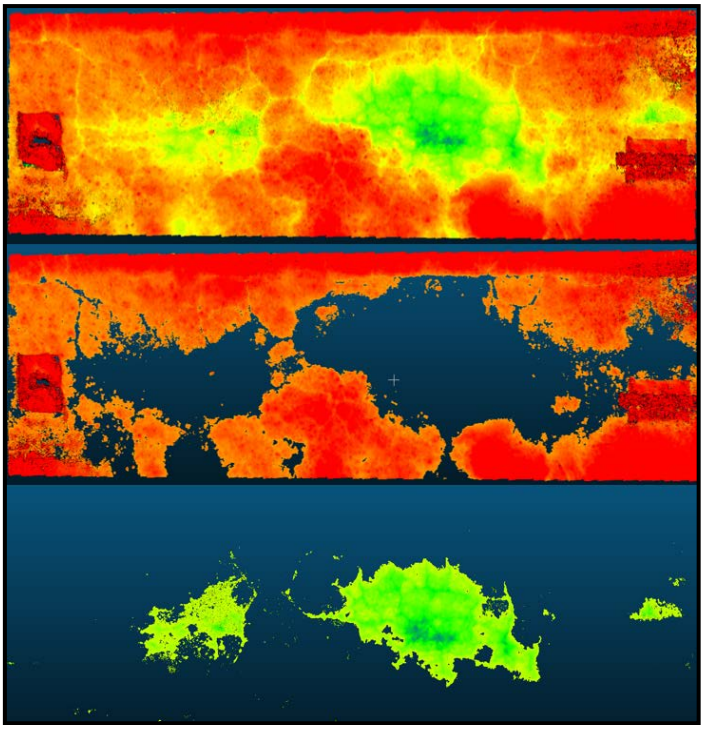

Figure 4-33. Segmented pavement section 1 using the fit plane.

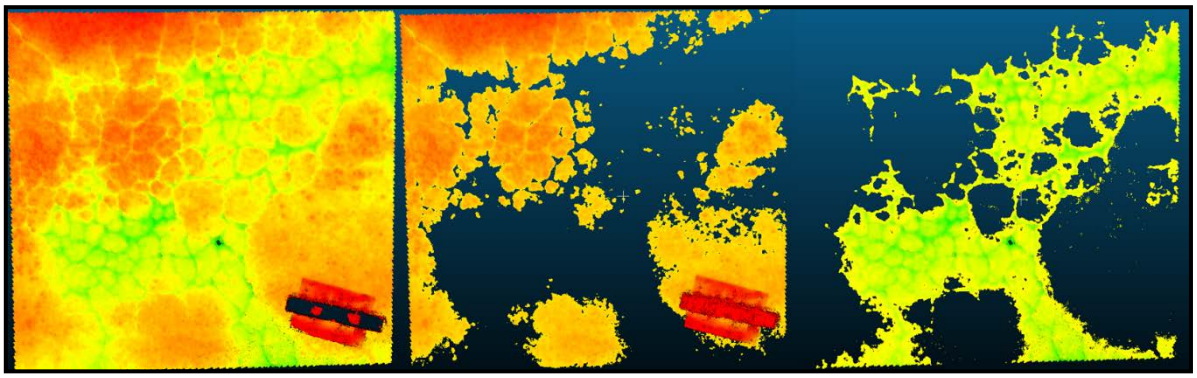

Figure 4-34. Segmented pavement section 2 using the fit plane.

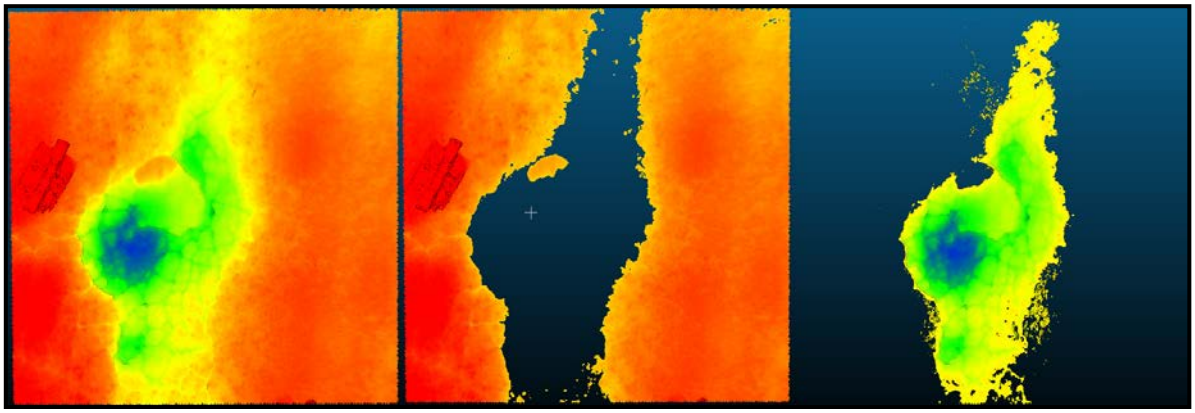

Figure 4-35. Segmented Pavement Section 3 using the fit plane

The figures demonstrate the capacity of using the fit plane. In each segmentation particular sections can be isolated. The sections where there is cracking can be isolated or the sections where there is a depression. The same can be done for the sections which are in suitable

conditions. The results are similar to those obtained with the RANSAC. The essential conclusion from both segmentation applications is that the process can produce the resulting isolated sections of the mobile imagery-based 3D models. These isolated segments can yield critical metric information as seen in section 4.4.1 as they are scaled and the accuracy of the derived models was shown to be sufficient for detecting pavement distresses. The methodology of segmenting the imagery and thus exploiting it for further analysis is the important outcome of this aspect of the study. Additionally, this process was done with user-friendly algorithms that can be practically repeated and do not require substantial processing power or exhaustive timelines utilized by other pipelines. The segmentation strategies used were potent enough to isolate the pavement distresses and this establishes a path forward towards the full low-cost automation of road condition data acquisition and analysis for the pavement management system.

4.4.5 Application of segmentation techniques using UAV based models

Whilst the techniques used in section 4.4.4 examined how to isolate and analyse 3D models, the focus was only on imagery obtained from handheld devices such as cameras and phones. Therefore, it is also important to consider segmenting imagery from a drone as the drone can generate network imagery even if it is of a lower resolution as shown before. To this end, a case study was also considered over a road section where a drone would be used to capture imagery and then the 3D modelling pipeline carried out to identify any differences in methodology needed and to establish how this type of data could be used. For the survey, a different UAV was used from that in section 4.31 so as to provide a different perspective on application. The commercially available DJI Mavic 2 Pro drone was used for the surveys (Figure 4-36). The cost of this drone or one with similar specifications is negligible in comparison to the cost of a survey vehicle equipped with lasers and other tools.

Figure 4-36. DJI Mavic Pro 2 Drone used for surveys

The device specifications are given in Table 4-9, including the exact camera specifications utilized for the surveys. The weight is particularly important as this is a dimension that is consistently mentioned in regulations and must be adhered to to allow for flights.

Table 4-9. Specifications of the camera on the UAV used for SfM surveys

Device	DJI Mavic 2 PRO
Drone weight [grams]	907
Camera resolution [Megapixel]	20
Image Size [pixel]	5568 x 3648
Sensor size [mm]	13.2 x 8.8
Focal length [35 mm eq.]	28
ISO Sensitivity	100
Exposure time	0.001 (shutter speed of 1/1000)
Aperture	f/2.8

Given the specifications of the camera, the object distance was calculated. This resulted in a required object distance of 11.81m to produce the associated GSD value. Given this value, it was a maximum flying height of 10m was used to ensure that at no point the object distance exceeded the recommended value. This was done by monitoring the altitude of the drone throughout the survey with respect to the ground at the beginning of the survey. The main survey was taken over a distance of approximately 1km on a roadway that was relatively flat and contained sections suffering from cracking, depressions and rutting. These distresses represent key distresses that appear on roadways and are typical of the most common distresses practitioners have to deal with in real situations. It was especially important to have a road section with cracks in it, as this is the distress that occurs the most in the region of the study [38]. An image of the overview of the pavement studied is shown in Figure 4-37.

Figure 4-37. Overview of the roadway used for the study

The survey roadway was straight and surrounded by trees and open greenery areas. The survey was also carried out during a time when there was minimal traffic to avoid cars blocking the view of the roadway. As mentioned previously, this is a limitation of the process and it would be difficult to survey a heavily trafficked section, as the drone would not be able to visualize the road and the distresses. The survey was also done during a period where there was minimal wind. The drone itself has a maximum wind speed resistance of 29–38 km/hr so this also represents a limitation that must be considered during surveys. With heavy winds, getting stable images could be a problem and would result in poor models. The trees that are present in the section also present a challenge to the process as they will cast shadows across the road section and the colour of the resulting model will have a different colour at those points. However, for the metric evaluation, the presence of the dark points will not have an effect. For the survey, a typical SfM workflow was utilized as was previously illustrated in Figure 4-5. The survey itself took approximately twenty minutes and GPS points on the ground were used as ground control points for the metric scaling of the subsequent models.

During the survey of the pavements, the flight was pre-set using specific flight settings of the drone. One trip was made across the surface. Whilst multiple trips across the surface could produce more images and possibly a higher accuracy with more details, the survey is limited by the drone battery, which limits the time possible for one survey. If an additional battery pack is utilized during the survey, approximately 8km of a road could be investigated in one trip with images transferred after the survey is completed. Additionally, by using one strip, the workflow becomes more practically applicable and more easily adapted for practitioners. The use of one long burst of images across the surface could produce a deformed 3D model so care must be made to use control points along the surface. This was done using eight coordinated points in every 200m section of the pavement, which can be considered appropriate based on previous studies [235]. Furthermore, by controlling the camera specifications and settings, the settings would not change per image and therefore there would be consistency in the image dataset. This is important because if an automated camera setting is used for the camera, images would have different environmental effects and matching images could cause issues for the 3D replication. The images were taken in sequence moving horizontally across the pavement with the camera focusing at an angle downwards at the pavement surface allowing for an estimated overlap of 70% by an image with the GPS of

the drone being utilized for location assessment. Within the settings, the drone was instructed to automatically take images every 2 seconds to allow the overlap of images needed for the process. The images were also captured in their RAW format to take advantage of the number of colours and complexities that can be represented in this format as opposed to the typical jpeg format which has sixteen times less colour and uses lossless compression which allows them not to suffer from image-compression artefacts. The images captured could then be transferred to the software maximizing the colours available in the original files.

Following this, the images were transferred to the SfM software, Agisoft Metashape [236] where the SfM pipeline was used to replicate 3D models of the surveyed pavement section. Within the software, there are options for calibration and compensation for the rolling stock using pre-calibrated value but these would not be applicable for such a low-level camera and survey and could result in worse results. Any self-calibration would also result in an elongated and difficult workflow that would affect the practicality of implementing it in a road authority. The use of ground control can be considered satisfactory for this type of workflow. In the process, images and corresponding point clouds were filtered to ensure that the model would only depict the pavement and not the side elements of the pavement such as the sidewalk or trees. Once the 3D models were generated, the models were transferred to the open-source software, CloudCompare [222] to examine the defects and identify the distresses existing on the pavement sections. This methodology employed to examine the defects is examined next.

- Application of 2.5D Quadric fit algorithm for UAV models

In the previous section, the segmentation was done on smaller pavement sections, which have a more flat planar reference shape, but for sections over larger lengths, it is likely that there will be some slope on the road and a direct planar reference could be difficult to achieve with the first RANSAC segmentation method. To combat this, an alternative approach was also considered using a 2.5D quadric algorithm. The 2.5D Quadric would be fitted onto the 3D model. This is done to find the flattest dimensions within the model but unlike a fully planar fit, the 2.5 shape more closely mimics a 3D structure and therefore would more adequately handle the road slope. The quadric is then visualized as a triangular mesh and this allows the computation of the deviation of the plane from the actual 3D model. This deviation would therefore represent the deformations that are present in the model and correspondingly the road section forming the depth map similar to the process outlined for the RANSAC

segmentation in section 4.3.3 and using that to isolate and analyse the distressed sections of the pavement. The implementation of the algorithm was again done within CloudCompare. A comparison between this methodology and the RANSAC one was subsequently done to understand the differences and identify when to apply either algorithm.

- Assessment of level of distress

Once the models are segmented and the depth maps are generated the next step is to analyse the level of deformation present on the road section. To do this the distribution of changes in height between the generated 2.5 quadric surface and the actual pavement was considered. The differences are measured across points across the model's surface and can be extracted as a CSV file for analysis. Using this information, equations 4-(3 – 5) could then be applied to give a metric on the level of distress across the pavement section.

$$\text{Average height of deformation(dH)} = \frac{\sum \text{individual deformations}}{\text{Number of points on surface}} \tag{4-3}$$

$$\text{Volume of distressed pavement (dv)} = \text{dH} \times \text{Surface area} \tag{4-4}$$

$$\text{Average Level of distress over section} = \frac{\text{dv} \times \text{total surface area}}{\text{Total volume}} \tag{4-5}$$

Given that the models obtained are scaled and metrically accurate enough to detect distresses, the information can give a practitioner a quick understanding of the level of distress over different sections and thus prioritize particular sections for intervention.

- Generated UAV 3D Pavement Models and segmentation results

The complete surveyed section was first generated before any subsections were done. In Table 4-10, the specifications and results of the complete pavement section model are shown. Additionally, the RMSE values for the ground control points are given in Table 4-11 along the three directions. The RMSE values are adequate considering the level of details required and are in line with expectations of error based on the pixel size and the points used [237].

Table 4-10. Survey specifications for Full section

Device	DJI Mavic 2 PRO
Distance from the pavement [m]	~8
Number of photos taken [-]	554
Ground Sample Distance(GSD) [mm/pixel]	0.97
Number of points created in SfM software [-]	90,508,878

Table 4-11. Total RMSE values for Ground Control and Checkpoints

Direction	Control points RMSE (m)	Checkpoints RMSE (m)
X error	0.0078	0.0095
Y error	0.0082	0.0112
Z error	0.0079	0.0119

The first important result is that of the GSD, which has a value that is less than the required value, as previously identified. Therefore, this allows for the appropriate metric evaluation of distresses within the model. The number of mesh faces as mentioned within the table describes the level of detail within the model and the high number is indicative of the large model that was generated given the section length. A visual inspection of the model would yield a better understanding of the details. Images showing the generated 3D model are given in Figure 4-38. Within the figure, the position of the drone through the survey is also shown illustrating the overlapping images captured from above the pavement's surface.

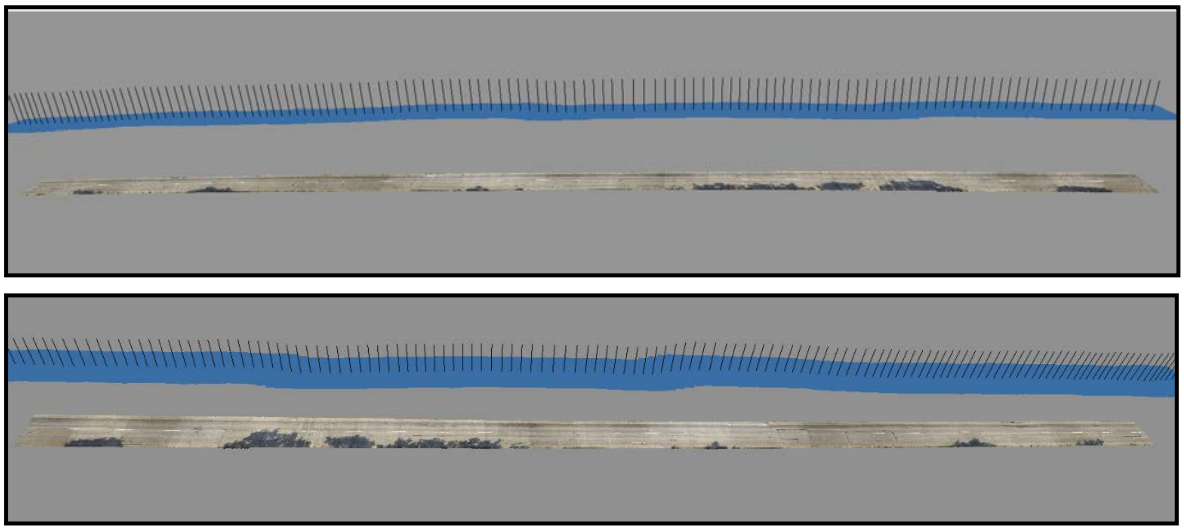

Figure 4-38. Full Model produced by drone imagery

As the pavement section is quite large, to have a better understanding of the level of details, sections were cropped and these are displayed in Figure 4-39. Within these images, the distresses are more clearly seen which include cracking, rutting and depressions. It is also important to note that the models are scaled and therefore a metric evaluation of these particular distresses is possible.

Figure 4-39. Cropped sections of the pavement model's surface (top image shows a cracked and rutted sub-section and the bottom image shows a sub-section with depression, cracking and rutting distresses)

Following the generation of the 3D model of the entire pavement section, the subsequent step was the analysis of the models using the previously mentioned segmentation strategies. The first employed strategy was the utilization of the RANSAC algorithm, which allows the extraction of shapes from the targeted point clouds. In this implementation, the assignment of the value for the minimum support points is needed. For the largest model under analysis, the total number of points in the point cloud was 90 million points. This represents a sectional area of approximately 8,000 m^2 of the ground surface. Using this and parameters previously used to segment pavement models using the RANSAC algorithm, a value of 50,000 points was initially assigned for splitting the object to produce the reference plane. However, when using this value too many planes were created and this is visualized in Figure 4-40.

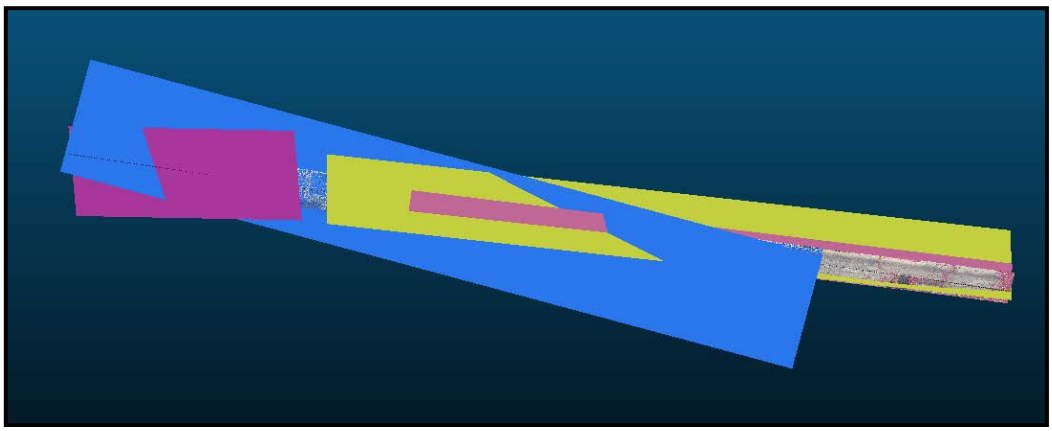

Figure 4-40. Visualization of RANSAC algorithm using inadequate minimum number of support points

Following this, trials using 70,000 to 120,000 points were considered. However, the slope of the road was an issue as planes were generated using the angles at either side of the pavement as shown in Figure 4-41.

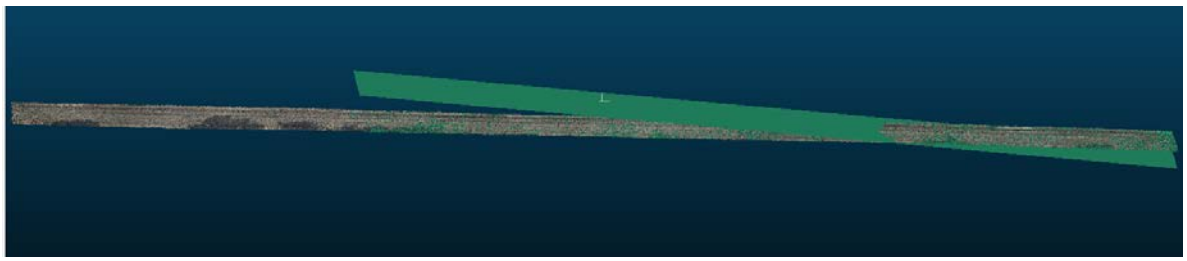

Figure 4-41. Errors in using RANSAC application

Therefore, this proved to be an inappropriate methodology for the full section. However, when applied to subsections where the slope was close to zero it was possible to generate adequate reference planes as is shown in Figure 4-42.

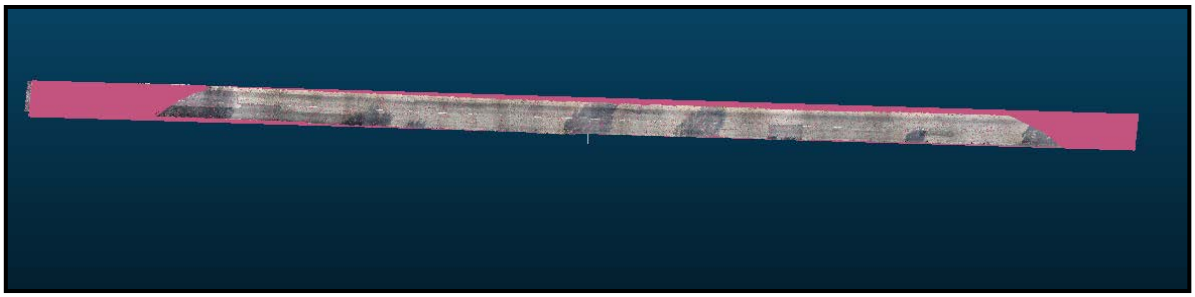

Figure 4-42. Application of plane shape through RANSAC algorithm

Therefore, it can be surmised that this application only works when small sections of roads are considered and therefore for a network or longer road it is not useful to apply this segmentation strategy. Given this, the consideration of the 2.5 Quadric was very important.

- *Application of quadric plane and subsequent segmentation*

For the application of the quadric plane, the plugin was utilized within CloudCompare where the plane was generated upon the surface of the 3D model. With the quadric application, a Root Mean Square (RMS) of 0.0084m was achieved. The RMS value is a good indication of the closeness of the fit between the newly created reference plane and the actual model. A visualization of the plane on the model is given in Figure 4-43.

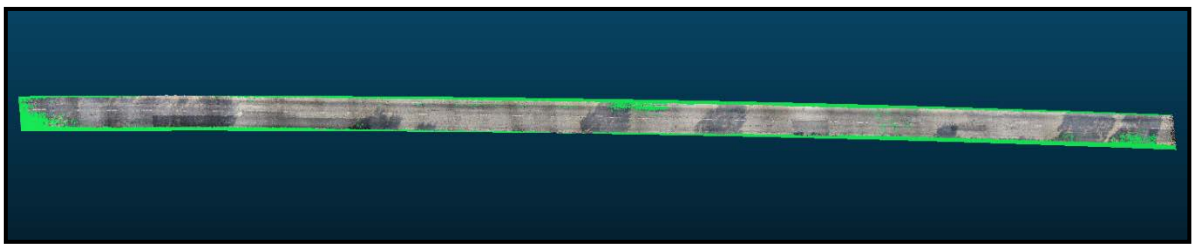

Figure 4-43. Application of quadric plane to model

After the plane was adequately assigned to the model, a computation of the distance between the plane and the model could then be calculated using the 'C2M' distance computation within CloudCompare. This could then be used to establish a depth map of the road section depicting points of deformation and degradation. An overall depth map illustrating the differences between the reference plane and the model is shown in Figure 4-44.

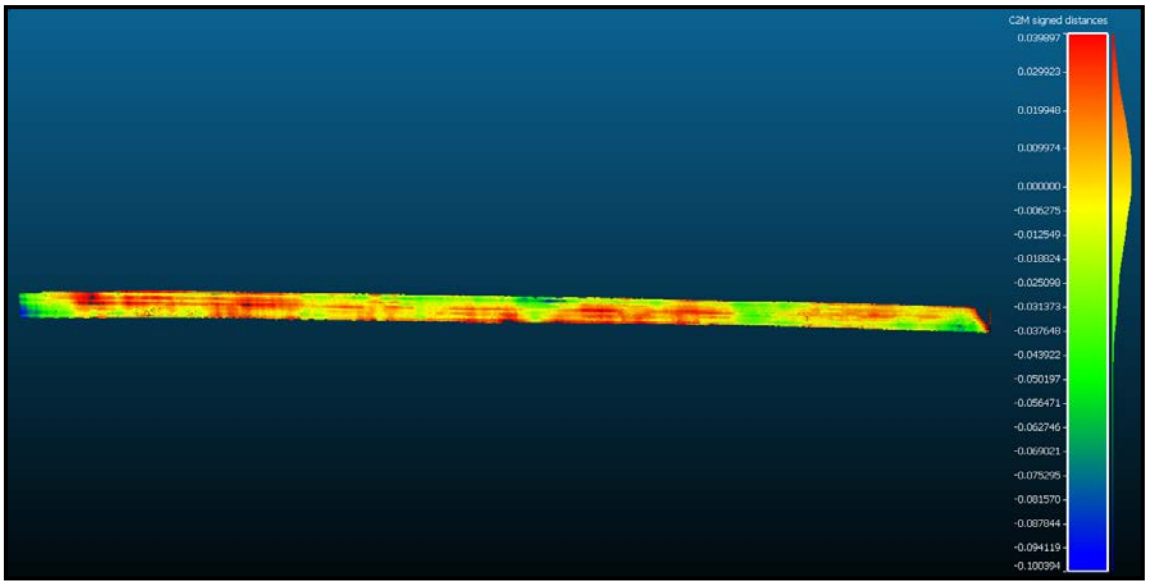

Figure 4-44. Application of quadric plane to the pavement section

Using the depths measured within this overall model, further segmentation can be made at various points of analysis along the model. Examples of particular points of emphasis along the model are given in Figure 4-45 and Figure 4-46.

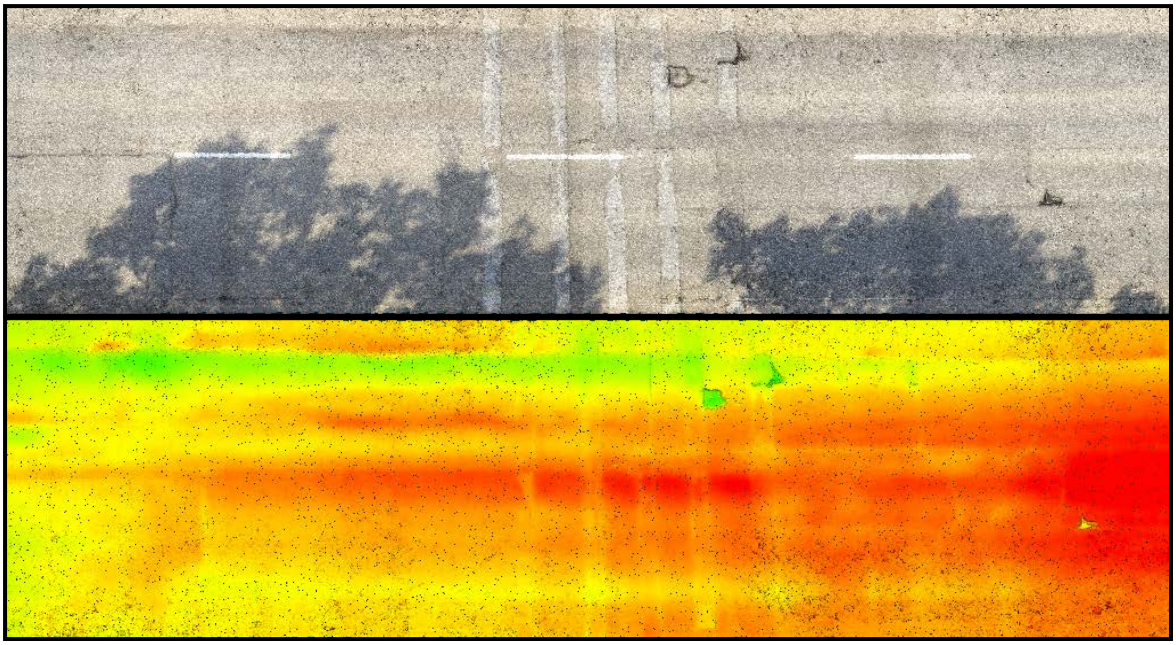

Figure 4-45. The first example of a Segmented Pavement Section

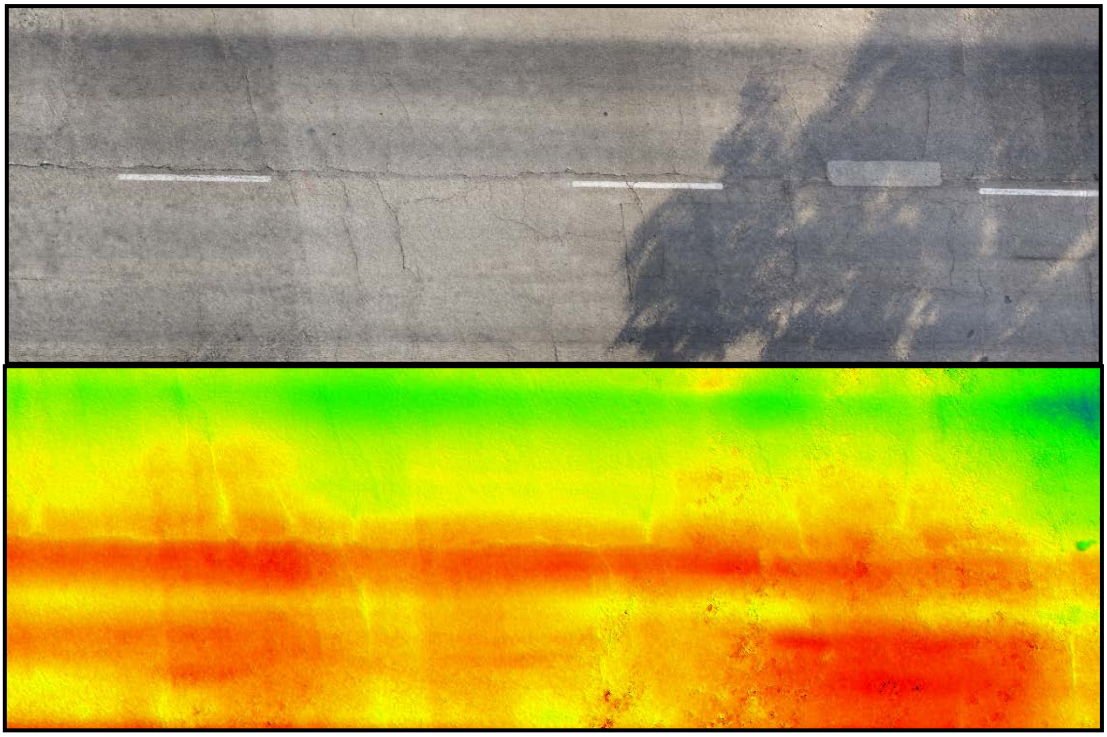

Figure 4-46. Second Example of a segmented pavement section

Within the examples, the points along the crack are visualized and can be isolated from the remainder of the model as well. Using the segmentation applications, the isolated sections will generate important metric analysis and information for road authorities. Metric assessments of any sections would be able to output area and volumetric measurements, which in turn can result in values of the volume or area of the cracks, depressions and other deformations, which are key to the evaluation of the pavement and the overall network. The metric evaluations and analysis can also be made at cross-sections along the model. An example of this is depicted in Figure 4-47 where the 3D model was transferred to Rhino 3D [218] and cross-sections implemented at 0.5m intervals along the model. Within the section shown, rutting and surface roughness are shown and using the model, the exact metric values of deviation can be established. Whilst it is possible for the model itself to display roughness, a check using the original images validated that the rough sections on the model were indeed from the pavement and not from a malformed 3D model.

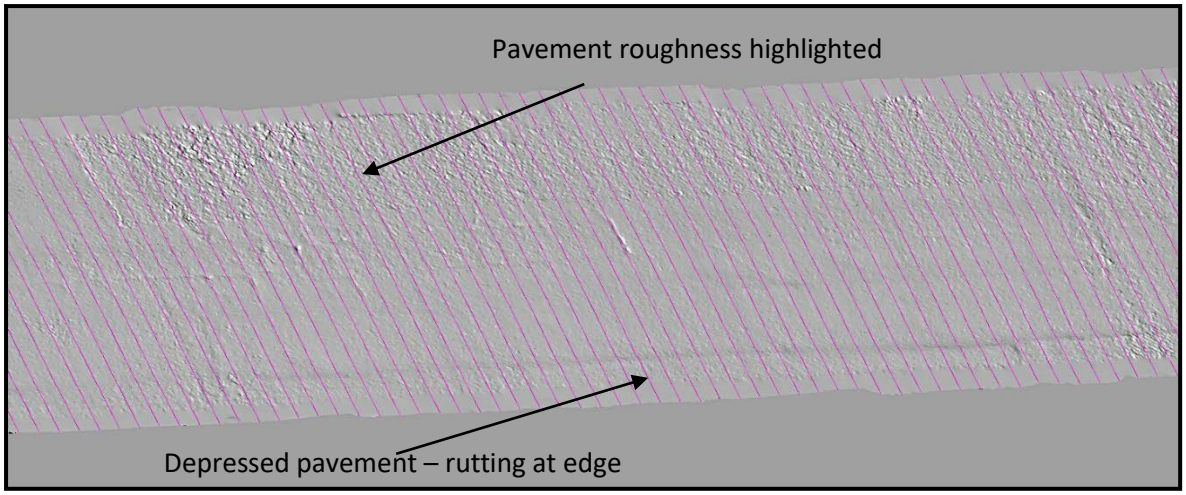

Figure 4-47. Cross-sections drawn on model with CAD at a prescribed distance

To understand the overall levels of distress at different sections, the model was then split using the cross-sectional tools available in CloudCompare as illustrated in Figure 4-48. Using the tools, three subsections were created and using these sections, analysis of the deformations were done to understand the average level of distress on the various sections.

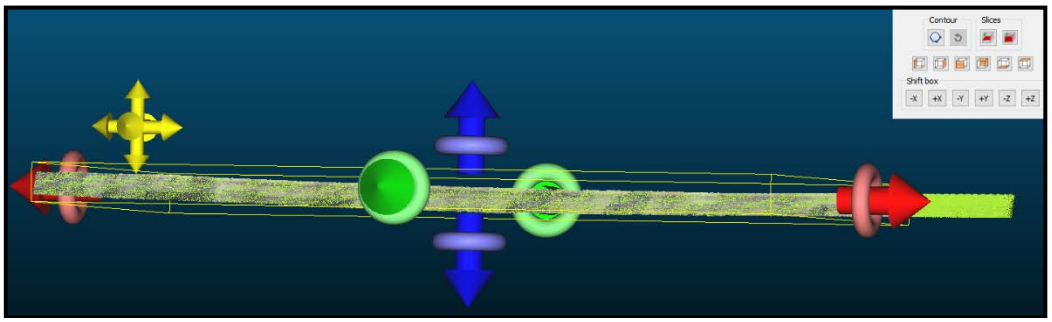

Figure 4-48. Generating cross-sections of model

- Analysis of the level of distress over pavement sections

With the segmentation complete, the formulae to assess conditions were used to understand the general road condition and the deformations present on the road. The results from these calculations are given in Table 4-12. This was done using the outputs from the CSV file expressing the deviations of the surface of the model from the established reference planes.

Table 4-12. Distress results of pavement models

Measurement	Full Section	Subsection 1	Subsection 2	Subsection 3
Length of section (m)	1000	200	250	300
Average height of deformation (m)	0.020	0.043	0.032	0.025
Volume of distressed pavement surface (m^3)	160.80	69.02	64.50	50.20
Average level of distress over section (%)	20.35	43.14	32.25	25.10

From the figures, it can be seen that the overall section has an average level of distress of 20% of its pavement surface. In the other three sub-sections considered the distress is greater with subsection 1 having the largest degree of distress of over forty per cent degradation. A closer examination of this section reveals tremendous cracking, patched areas and highly rutted areas as shown in Figure 4-49.

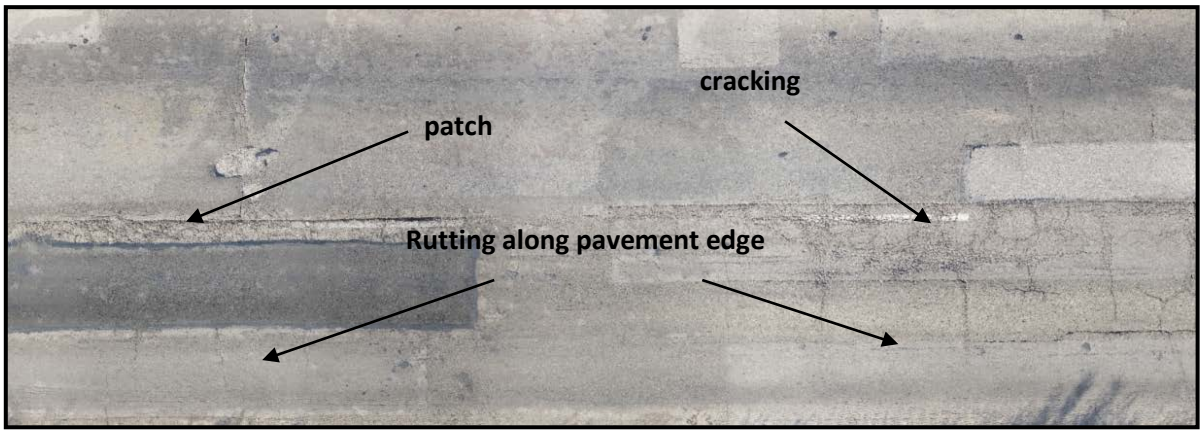

Figure 4-49. Cropped section from subsection 1

This was done to illustrate how the information can be utilized by the road authority. If surveys are carried out using the same methodology for a large number of road sections, then the average level of distress can be generated per section and the road authority would have a clear idea of which sections are in the poorest conditions. The list would then be kept in the road authority's database and can be continually updated at various time intervals to schedule and plan future road interventions. Within the workflow, the techniques would be used to rank road sections within a network based on the average distress levels. This would help users to understand the overall conditions of the network. Additionally, the UAV models will highlight particular points, where additional information may be needed and at these points, similar SfM techniques can be applied using mobile imagery instead as adequately demonstrated by the other aspects of the chapter. With the systems combined the road authority would have vital road condition data to plan their maintenance programs.

4.5 Key Limitations and conclusions of using photogrammetry in the context of distress detection and analysis

Whilst the process of photogrammetry has undergone major expansions with the rise of better algorithms for key phases of the process resulting in unified approaches for photogrammetric applications [238] there still remains significant limitations and challenges to the process. For many applications, there is a trade-off between real-time performance and

accuracy along with the available computational resources [239]. For modelling pavements, real-time processing would only be required if immediate information is needed on a distress. Instead, the building of the database for monitoring and long-term use is more valuable. The issue of correspondence between images also remains [239] which results in the process performing poorly for surfaces that lack texture [240]. However, for objects where this is good surface texture, accuracies are much higher with minimal errors of less than 1% reported [241]. For the purpose of pavements, this would not be an issue for the replication of most models where there are distresses as the major distresses (such as cracks, ravelling and rutting) result in significant textural and deformation surface differences. However, for distresses such as bleeding and polished aggregate, this represents a challenge as the surfaces in these instances suffer from a loss of texture. Therefore, for the detection of these types of distresses, the methods are limited and different techniques need to be incorporated into the system to adequately measure and detect these distresses in a network.

For the use of mobile photogrammetry as well the application refers to only a section of pavement or one particular distress sequentially. This, therefore, means that for the process to be utilized for monitoring it is better adapted when incorporated with UAVs. For this reason, the project also aimed to show how UAVs can be appropriately used for the process.

Whilst these limitations do present challenges to the incorporation of photogrammetric techniques into pavement management systems, there are several advantages to its use. The ability to obtain metric 3D information of a distressed pavement provides a road manager with vital information to answer key questions concerning therapy decisions at a low cost. This information is simply not available in most instances so it serves as a welcome addition to databases where there is zero information and maintenance decisions are made ad-hoc and blind with no true understanding of the actual situation and condition of the pavements in their networks.

Given the framework set up to this point, the next chapter will now begin to focus on detecting the locations of where the distresses are in the network. This will allow the 3D techniques to be adequately be used as the 3D techniques are useful when the general locations of the distresses are known. Whilst the study has adequately demonstrated the accuracy and use of the 3D methods in replicating the distress, for the holistic project and road authorities, it is also important to quickly pinpoint where the distresses are. Therefore, as a precursor to these

methods, it is useful and vital for the workflow to have a low-cost system able to determine the specific locations of the distresses, which would then be followed by detailed assessments. Together these would form a low-cost pipeline ready to be used by road authorities. To quickly perform a hotspot analysis of a road network would be very useful for any road authority. To this end, the use of Artificial Intelligence and deep learning technologies have gained traction in this automated process and towards this type of distress hotspot analysis. The ideas behind these concepts and how they can be exploited for use in pavement engineering will be examined in the subsequent chapters.

Chapter 5: The rise of Artificial Intelligence and Deep Learning and their use in Pavement engineering

While the two previous chapters focused on 3D modelling and characterizing distresses at particular points along a road, the question of where to focus those techniques along the network remains relevant and must be considered as part of this study. To tackle this problem, deep learning techniques are explored to quickly identify the weak points along a network. However, before these techniques can be applied, it is imperative to have an overall understanding of the state of the art of this particular field of application in image processing and pavement engineering. This better enables an appropriate application and exploitation of the field to the particular context of this research. Given this, this chapter seeks to highlight the general area of artificial intelligence and deep learning and the common applications of it within the field of pavement engineering. By doing this, the particular research gap for the technology is identified which will be followed by the actual application of the techniques in case studies in chapters six and seven.

5.1 What exactly is Artificial Intelligence and Deep Learning?

Recently, there has been a universal rise in the research and use of deep learning applications to solve complex and different problems across varying research fields [242]. This has been due to the increases in the accuracy of these methodologies. The accuracies in some instances are now considered even better than those of human abilities. This can be demonstrated by the ImageNet Large Scale Visual Recognition Challenge [243] in which the human benchmark for recognizing objects was beaten in 2015 by a developed deep learning framework [244] and whose accuracy mark has continued to be improved upon every year of the challenge, as new frameworks and algorithms have been developed. Deep learning, however, is just one application under the broader landscape of Artificial Intelligence (AI), which essentially refers to the field of building machines that have the capacity to carry out tasks that are normally done by humans (the larger framework is shown in Figure 5-1).

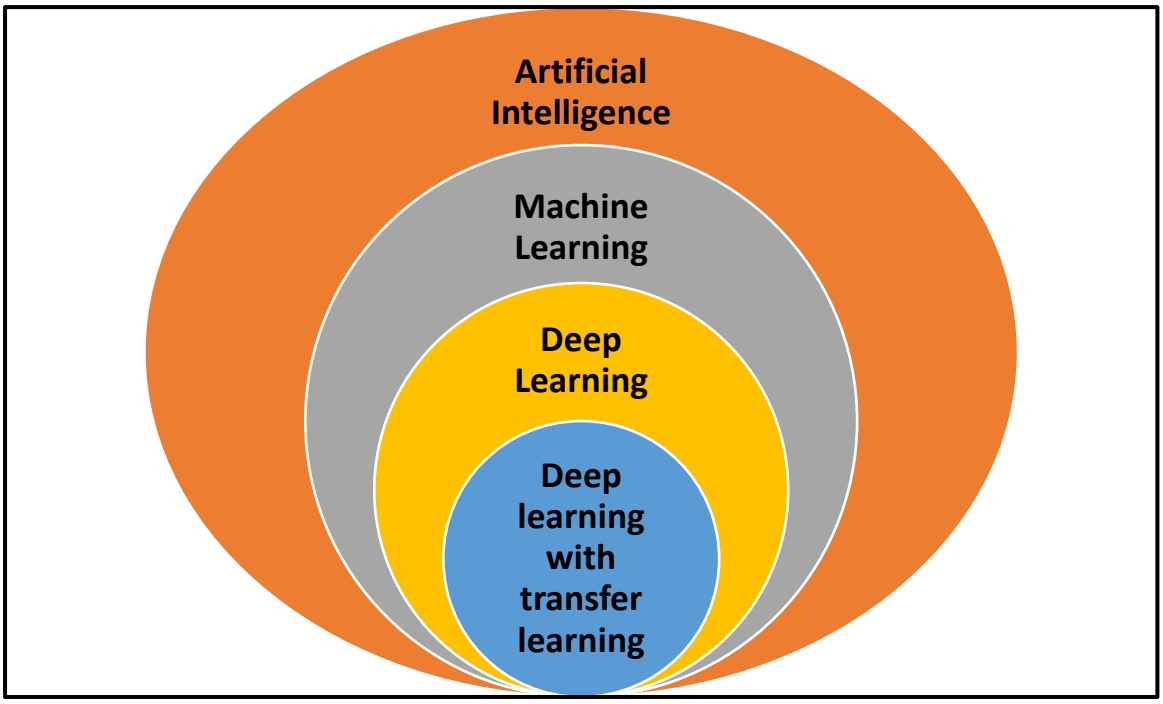

Figure 5-1. Fields of Artificial Intelligence

Within the field of AI lies machine learning. The basic concept of machine learning refers to building computer applications and systems that can automatically carry out tasks such as object detection, image classification and speech recognition based on supplying it with datasets centred around the individual task. Work in this area has been thoroughly researched through the years with many algorithms being developed to help automate critical tasks and assist in key activities for pavement engineering [245]. Machine learning has been considered

the foremost option for any automation or detection challenge until the rise of deep learning and neural networks (details on machine learning shown in section 5.2). It, however, requires a substantial amount of handcrafting by the developer and this can be time-consuming.

Deep Learning is a subset of Machine Learning, which utilizes neural networks rather than traditional handcrafted features. Deep Learning involves the use of computationally based models which are made of several processing layers which learn data representations with several layers of generalization [246]. Artificial Neural Networks (ANN) are based on the biological neural network and consist of input layers, hidden layers and finally the output layers. Deep learning networks figure out the complex structures within datasets by the utilization of backpropagation algorithms, which alert the computer how to alter its internal parameters to yield the best representation of the next layer and eventually the final model. Neurons within the network receive inputs then process them and feed them forward to other neurons in successive layers. The hidden neurons take outputs from previous layers, compute new outputs with the use of activation functions which are then fed forward to the next layer with the use of different weights applied during the applications. A simple graphic of this is demonstrated in Figure 5-2.

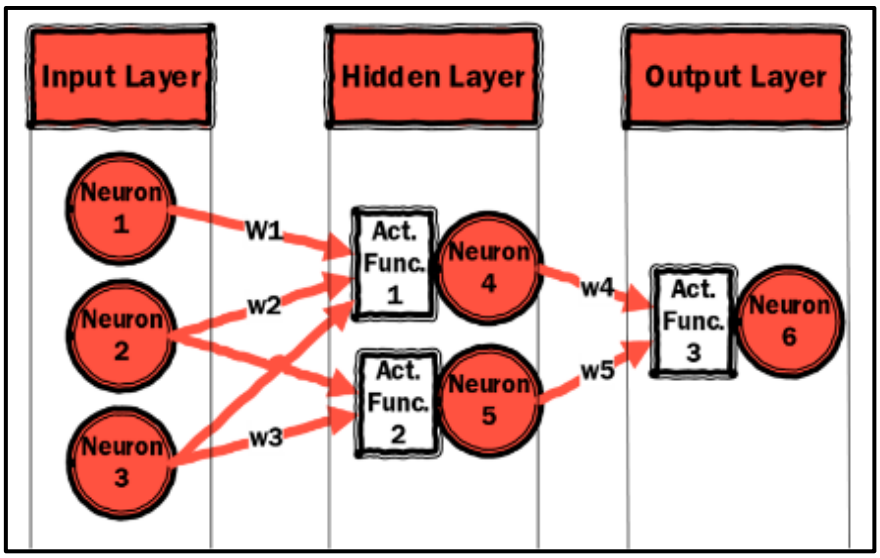

Figure 5-2. Basic structure within a neural network.

They essentially work to understand how the data is built up and thus how to identify, predict or classify future similar but unknown datasets. For image processing, convolutions are utilized. Convolutions utilize filters that help extract different features from the image such as edge information. In neural networks, features are extracted using filters with weights that undergo learning during the training process. The retrieved features are then summed

together to make choices. The spatial relationship of pixels within an image is also considered in the convolution, which helps to identify particular objects that have defined spatial relationships with other objects. The most common type of system is called supervised learning wherein a convolutional neural network is fed annotated datasets and learns to make similar predictions based on the learning data. Convolutional Neural Networks (CNN) have been vastly utilized for this and they are designed in such a way to process data in the form of arrays. CNN's are generally utilized for detection, image segmentation and classification and identifying objects and regions within an image. A typical depiction of the workflow for deploying one of these models and network is shown in Figure 5-3.

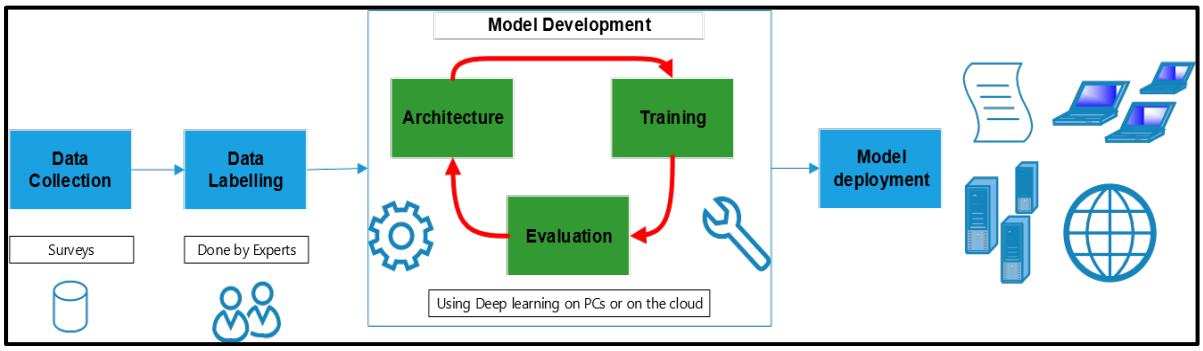

Figure 5-3. Typical model development setup.

These workflows are typical in application development but still rely on the core principles examined in the data science workflow shown in chapter 1 (Fig. 1-2). However, before the use of these techniques is explored and exploited it is important to understand the previous machine learning approaches. This will be further explained in section 5.2.

5.2 Traditional handcrafted Computer Vision techniques

Whilst the area of AI and deep learning is vast including applications in everyday life such as voice recognition and language translation, the scope of this work is limited to image analysis under the area of computer vision. The general aim of computer vision is to allow a computer system to automatically carry out image identification and understanding tasks typically carried out by a human [247]. Computer vision has been utilized for years using traditional machine learning algorithms and development. Whilst the rise of deep learning techniques has caused more research and focus to be shifted from traditional algorithm development, it is still very important to understand the basics of handcrafted techniques. This is because they still represent viable solutions to problems based on the context of the situation and available resources. Additionally, there are possibilities to merge techniques between deep learning

and traditional ones thereby highlighting the importance of them. Below is an assessment of the main traditional techniques used and critiques of these techniques along with examples of the many studies carried out for each. There is generally a lot of hand-tuning required within these techniques as is explained in the following sub-section.

5.2.1 Thresholding

The simplest of the algorithm groups is Thresholding. Thresholding has many different subsets and applications. The simplest form is supervised thresholding. In this application, each pixel within an image is replaced with a black pixel if the image intensity is below a set threshold value and if it is above it is replaced with a white pixel. The method seeks to find a distinct boundary between the object and the background. This is done manually in several instances until a satisfactory threshold value is obtained and applied to the images. The Histogram of the image intensity can be used to identify the threshold value. A more advanced and popular thresholding method is Otsu's Method [231] which can be utilized to reduce grey level images to binary ones. The method seeks to automatically obtain the threshold value and therefore removes the manual application previously mentioned. It carries out an exhaustive iteration through values calculating the pixel level variances on the various sides of the threshold and searching for a value that will limit the variances for the separation.

In general, the method is utilized for images where there are simple images needed to be separated into two segments as in these situations it works best. There should also be a clear gap between the background and foreground within the image. Noisy images do not perform well with the algorithm. If within the image the foreground or background is not proportionate to each other the Otsu method will also not be effective as the intensity histogram will not be bimodal. Another form of the method is adaptive thresholding. Within this method, the image is split up into sections carrying differing thresholding values that are calculated for the various sections of the image under examination [248].

In general, the method is limited but can be considered useful as it is simple to implement. Additionally, thresholding is used in conjunction with the other segmentation methods especially in the use case of pavement distress detection [249]. Typically thresholding has been used for the study of pavement cracks [250,251] with a wide array of thousands of available thresholding algorithms for consideration [252]. The Otsu method in particular has

been used in conjunction with other methods to establish thresholds in the early stage of the detection system [172,253]. The methods can require a lot of tuning and can also be difficult to fit for pavement distresses given their complex nature.

5.2.2 Clustering

Clustering is a more powerful technique, which can be applied for image segmentation. It is however more computationally intensive than thresholding techniques and as a result, it is not widely used [135]. The technique aims to divide the image dataset into a number of groups or clusters. It is also an unsupervised method as it does not require pre-training. Within the image, the cluster can be made around any number of properties, particular features, specific object colours or other RGB values. The typical clustering techniques readily utilized are K-means, Fuzzy C-Means (FCM), expectation-maximization and related techniques [254].

K-means can be utilized for both classification and regression situations. It is a simple method with good computational efficiency. The method divides N observations into K-clusters, in which each observation is a member of the cluster with the closest mean. The assignment of values is done using a distance function, which represents the distance of each observation to each cluster. The Euclidean distance is typically used as this function. Essentially, you choose 'K' points to begin and assume these as the initial cluster centres and run iterations to reduce the distances to a point where there are no noticeable changes in the cluster formations. Two common initiation methods are the forgy and random partition methods. Forgy randomly identifies K-observations from the dataset and begins the process with this and Random partition initiates by randomly assigning a cluster to each observation and starts to compute the initial means to the centroids of the clusters. Within K-means normalization of the variables should be performed or variables of a higher order can produce bias. Limitations of the algorithm include the difficulty in predicting the value of K, production of different final clusters based on initial groupings and the dependency of the initial seed number chosen to the final values. Fuzzy C – means and expectation-maximization algorithms help reduce these limitations by using feature vectors to create multiple memberships to multiple clusters but this comes at a higher computational cost.

Clustering algorithms have been used for crack extraction where two clusters are used (crack and background) and using the distances between points on the image, the algorithm

identifies the crack and extracts this [255] [256]. The Fuzzy C-Means algorithm has also been utilized considering crack enhancement and artificial ants [257]. The ant colony algorithm was utilized to analyse the spatial differences in the area and to extract crack features. Other studies have also used the clustering algorithm to extract the cracks by assigning the pixels to arbitrarily assigned clusters and sifting out the crack related clusters based on their related elongated shapes [258,259]. The algorithm utilizes surface geometries to split the object and group sections of the crack into a cluster. As previously mentioned, the clustering algorithms tend to require a lot of computational resources and time for handcrafting and as a result, their application has been limited. There is more merit in applications in other machine learning domains such as data mining.

5.2.3 Region-based systems

This group includes the use of region merging, growing and splitting algorithms. As opposed to the thresholding systems, in these groups, the particular grouping of a pixel and the characteristics of neighbouring pixels are used for thresholds to decide how to segment the image [252]. The goal of these algorithms is to use the image characteristics to map individual image pixels to predefined and important sets of pixels, referred to as the regions. For the purpose of pavement distresses, the region may correspond to a part of a crack of another distress type. Regions should have no overlapping 2D areas or pixels that belong to two different regions, which can be a problem for distress detection as distresses often overlap each other within the image.

The concept of the region-growing algorithm, in particular, is to grow out from some particular seed pixel starting point within the image with the aim of finding all the related pixels of a particular object or feature and thus the object in totality. With a chosen starting labelled pixel, the algorithms move out looking at neighbouring pixels and if the neighbours are adequately similar then the pixel is added with the same label and the algorithm continues to grow outwards carrying out the same process until there are no more pixels remaining. The watershed algorithm is a popular type under this branch that is used for image segmentation. It functions by identifying common image elements like colour intensity. The algorithm creates a ‘watershed’ barrier between segments of the image where there is a different feature or element detected to segment the entire image. It performs well for images that have touching or overlapping objects, instances in which thresholding usually fails. Images are typically

converted to greyscale and then the process is applied. However, if there is noise within the image, there can be over-segmentation. This, therefore, requires the process to usually undergo a de-noising pre-processing step when applying the algorithm [260].

Superpixel algorithms are also utilized under this branch of techniques in which pixels are grouped to arrive at superpixels which can invariably carry more meaning in terms of understanding the scene and segmenting objects of similar features within the image [261]. This process can also suffer from over-segmentation with complex images but is again adequate for simple images where there are overlapping or touching objects to be segmented. However, these algorithms have shown to have poor performance in detecting cracks in particular as the cracks are typically linear and will blend into the background of the image, making them difficult to separate into regions. As a result, they need to be applied with other techniques for any application in pavement detection to be possible [262].

5.2.4 Edge and corner detection and matching

In any image, the edges and corners represent two of the most useful features for image processing techniques. Edge-based techniques revolve around detecting contours and are easy to implement. As a result of this, blurs in images makes it difficult for the algorithms to connect broken contour lines. They are also weak with noisy images. There are several types of available edge detection algorithms including Sobel, Laplace, Cany and Hougline [263].

The use of a single algorithm is however not the only thing needed when applying the process. The algorithms typically utilize columns convoluted in the original image to calculate for horizontal and vertical changes in the image and thus horizontal and vertical edges. You can adjust the size of the kernel used based on the image and the edges present within the said image. With respect to corner detection, corners are considered as intersections of two edges. Algorithms under this branch function by considering that there are large variations of intensity in more than one direction at an image corner. The algorithm will move around the image in regions trying to see how similar the pixels are in different directions. If there is little to no difference the region is considered flat, if it differs in one direction it is considered an edge and if it is different in two directions it is considered a corner. Examples of this are the Harris Corner Detection algorithm which has been utilized to automatically detect contours on the pavement surface [178] and to identify images with cracks within a complete database

[264]. The Hough transform algorithm has also been used for detecting crack edges and their locations [265] with combinations with other detectors used for performance boosting [266], once again establishing the need to have multiple algorithms used for adequate performance for distress detection.

The edge detection and matching algorithms are commonly used for crack detection [267] [143] given the typical linear shape of cracks and their formations. They are also utilized in conjunction with other algorithms as a base to start searching for similarities within an image for a more complete pavement distress detection but again require substantive handcrafting and this can be time-consuming.

Deep learning can help solve these problems as the networks can be effective at discovering the edges on their own, which can be more effective and less time consuming than coding an algorithm to solely carry out this function.

5.2.5 Templating and Feature selection/matching

Templating is a technique, which makes uses of a template image to find similar patterns that match within other images. Templates can be very simple with features such as edges or corners or they can be complex with faces and multicolours. The template is stepped across the image in a small number of pixels. The template or the image itself can be scaled up or down to maximize the probability of finding the pattern within the image. The process is run several times across and down for each template and a correlation score between the part of the image being processed at each position of the run and the template itself. With this process, an 'image pyramid' is generated. The sections of the image showcasing correlations cores above a decided threshold are considered as a match to the template. The process itself can require a significant amount of computational power. Other drawbacks include the possibility of occlusions and the process is also weak when confronting rotations and reflections. Newer forms of template algorithms have divided templates based on features such as edges and having correlations between the sub-templates. Whilst this can help with the limitations mentioned before, this also increased the time needed and the computational resources needed.

The process can be very useful if the images can be easily picked out by a template. With regards to distress detection, features are detected on cracks and other distresses such as

potholes using spatial dimensions and characteristics. The algorithms then try to extract the identified feature using various mathematical approaches such as support vector machines [268,269]. Cracks with similar widths can be highlighted and their severity levels thereby produced by the detection [270,271].

5.2.6 Justifications for considering Deep learning systems

Given all of the aforementioned traditional techniques, there is a general consensus that no one traditional machine learning technique can be applied for distress detection because of the complexities appearing on pavement surfaces [272,273] and instead hybrid approaches are needed to have a workable system. In comparisons made between the segmentation strategies, it was established that an optimized adapted system is better than any one technique [274]. This is one of the reasons why a deep learning approach offers significant value as a DL system can more readily adapt to the pavement surface complexities without the need or the excessive computational and time resources needed with the traditional approaches. This is due to the difficulties traditional methods have in generalizing different images in a dataset.

Nevertheless, the techniques explained have an influence on the formation of a workflow for a detection system and some of the techniques, namely edge detection and thresholding are used components within some DL combinations and they also feature in the base models of many complex DL frameworks. Additionally, in some instances, there may be simple road networks or systems where only low-level information is needed such as the location of cracks or detecting only cracks and the traditional approaches may be more applicable.

5.3 New approaches using Deep Learning

Given the methods previously explained, deep neural networks were developed to help solve some of the issues with the traditional techniques whilst trying to increase accuracy levels and reduce computational requirements. In deep learning, the major areas of research and breakthroughs in computer vision are image classification, object detection and image segmentation. A brief overview of these sectors is presented in the following sub-sections.

5.3.1 Image Classification

Image classification is a task involving the classification of an image into one particular pre-defined class. This task has been studied for a very long time. The biggest breakthrough in the field with respect to deep learning was the development of the ImageNet Large Scale Visual Recognition Challenge in 2012 [243]. In that contest, AlexNet won the challenge beating out handcrafted features and spurring the notion that deep learning could achieve better classification results than the traditional methods. It is a deep CNN with several convolution layers, pooling layers and fully connected layers with sixty million total parameters. A summary of the most important models developed over this time is shown in Table 5-1 below.

Table 5-1. Development of deep learning models

Model	Year	Accuracy – top 1	Number of parameters
AlexNet [275]	2012	57.2%	60 M
VGGNet [276]	2014	71.5%	138 M
GoogleNet [277]	2014	69.8%	6.8 M
ResNet [278]	2015	78.6%	55 M
DenseNet [279]	2017	79.2%	25.6 M
SENet [280]	2017	82.7%	145.8 M
NASNet [281]	2018	82.7%	88.9 M
SqueezeNet [282]	2016	57.5%	1.2 M
MobileNet [283]	2017	70.6%	4.2 M
ShuffleNet [284]	2018	73.7%	4.7 M
ShiftNet-A [285]	2018	70.1%	4.1 M
FE-Net [286]	2019	75.0%	5.9 M

Each of the models in Table 5-1 feature a different orientation of convolutional layers and parameters and research continues in this field. The models can be used for image classification, object detection and segmentation in different forms. A further examination of key models is presented in section 5.32 where the models used in the study are defined and scrutinized.

5.3.2 Object detection

The second major focus of study in computer vision is object detection and it is under this branch that the subsequent models for the study will be developed. This involves the determination and location of an object from either a large set of predefined categories or a

particular object [247]. Object detection is considered a more difficult task than image classification as the location of the object must also be identified. This makes it useful in situations where there is more than one particular object in the frame and the image cannot be classified as one particular class. Additionally by localizing the object with the technique, the shape and structure of the model can be studied which can be key for monitoring purposes.

For the object detection tasks, two major multi-class datasets have been used to spur the development of new models, structures and frameworks. These are the Pascal-VOC (Pattern Analysis, Statistical Modelling, and Computational Learning Visual Object Challenge) 2007 [287] which has 20 classes and the MS-COCO (Common Objects in Context)dataset [288] with 80 objects. Evaluations on these datasets are done using two common metrics: Average Precision (AP) and Average Recall (AR). Both metrics are in reference to the bounding boxes created by the models within test cases. Precision can be classified as the results within a test that are relevant to the classification problem whilst Recall refers to the percentage of relevant results which are in turn correctly identified by the model. These parameters will be further described in chapter 6 with direct references to pavement distress detection. The two parameters are determined by the following equations:

$$\text{Precision} = \frac{\text{True Positive}}{\text{True Positive} + \text{False Positive}} \tag{5-1}$$

$$\text{Recall} = \frac{\text{True Positive}}{\text{True Positive} + \text{False Negative}} \tag{5-2}$$

There are several available open-source models within the TensorFlow Object Detection API [289], which is an open-source framework developed by Google, which was built upon TensorFlow [290] that allows easy construction, training and deployment of object detection models. Within the Google API, there are prebuilt architectures and weights such as the Single Shot Multi-box detector (SSD) [291] using MobileNet [283], Inception V2 [292], Region-based fully convolutional networks (R-FCN) [293]as well as the Faster R-CNN networks [294].

These models are all publicly available through the TensorFlow object detection API zoo. Each of these models provides a quick model creation pipeline, which can be used for development without the use of heavy computational resources needed for completely new model building.

The two main backbones of networks utilized, and those that will be exploited within this study, are the Faster R-CNN model and the SSD model. Within the Faster R-CNN base model, the same convolutional network is used for both region proposal generation and the object detection task. This model essentially proposes regions, extracts features from these regions and classifies the regions based on the features. This enables the detection to be faster. This is depicted in Figure 5-4 based on the architecture of the model [294].

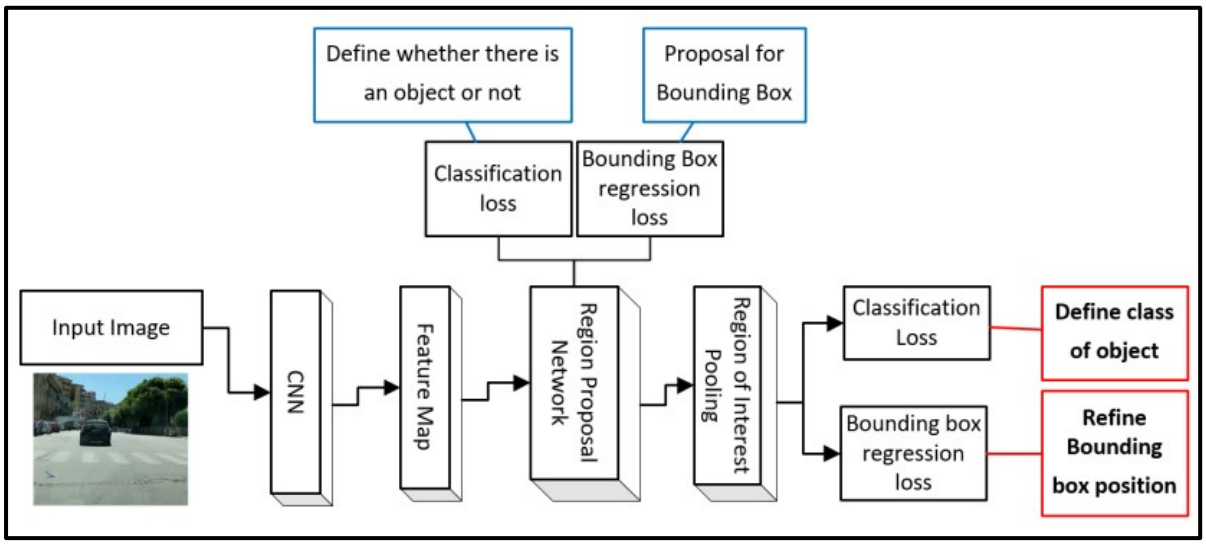

Figure 5-4. The architecture of Faster R-CNN model.

For the Single Shot Detector (SSD) base network, only one single shot is required to detect multiple objects within an image. It is faster when compared to Region proposed networks, which require two shots, one for region proposal generation and then the second for object detection. Within the SSD, the input images are passed through several convolutional layers to produce several feature maps at varying scales. Then for each location in each map, a convolutional filler evaluates a small set of bounding boxes and for each bounding box, it predicts the offset and the class probabilities. The SSD is a feed-forward CNN, which yields a static size of bounding boxes and scores which is followed by a non-maximum suppression step that yields the final detections of the model. This framework for the network is depicted in Figure 5-5 which shows the architecture of the model [291]. It is similar to the other model but essentially avoids the region proposal step and considers all possible bounding boxes in every location in the image whilst simultaneously carrying out the classification.

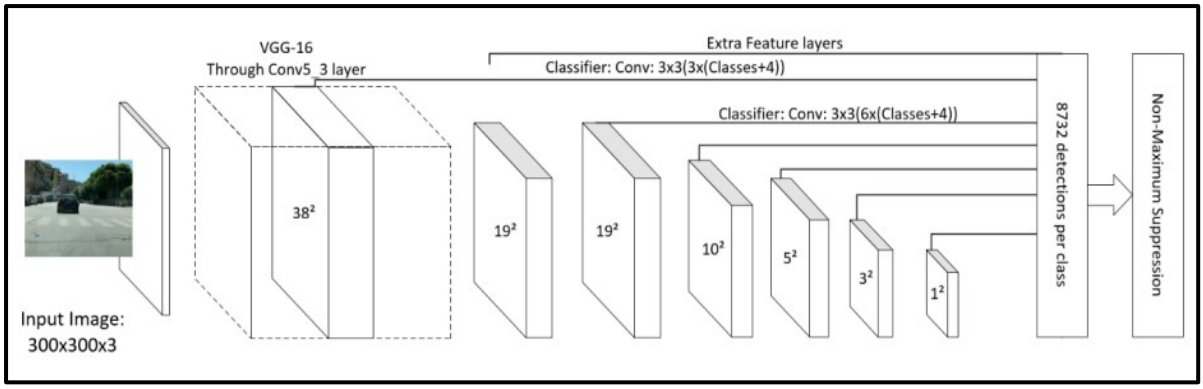

Figure 5-5. The architecture of SSD model.

Other common and available models for object detection from the TensorFlow detection zoo are shown in Table 5-2. Within the table, the speeds given are with respect to the models' inference time.

Table 5-2. Properties of object detection models.

Model Name	Speed (milliseconds, ms)	COCO Mean Average Precision (mAP)	Outputs
faster_rcnn_inception_v2_coco	58	28	Boxes
ssd_inception_v2_coco	42	24	Boxes
ssd_mobilenet_v2_coco	31	22	Boxes
ssd_resnet_50_fpn_coco	76	35	Boxes
faster_rcnn_resnet50_coco	89	30	Boxes
ssd_mobilenet_v3_large_coco	119	22.3	Boxes
ssd_mobilenet_v3_small_coco	43	15.6	Boxes

These models represent a fraction of the available models for use in developing object detection applications. One widely used model that should be mentioned however is the Yolo – You only look once [295] model which uses a single convolutional network for predictions and is the backbone of many applications. The network does not look at the entire image. It splits the model into a grid and then bounding boxes are generated within that image. For each box, the network then outputs the class probabilities and offset values. Boxes that have a class probability above a set threshold value are identified and used to pinpoint the location of the object in the image. It does have issues detecting small objects because of this pipeline and its spatial constraints and as a result, the decision was made not to use it in the analysis within the study.

Furthermore, aside from the general architectures of the models that have been mentioned, it is also important to consider the individual building blocks that are also key to the makeup of the models. The key ones are examined here:

- Inception module

The inception module is a typical building block that was essentially based around the technique of making a model wider rather than just deeper. Previously models were stacked depth-wise which was computationally expensive. Inception proposed the idea of having multiple sizes that could function on the same level – thereby increasing the width of the network. The 'naïve' inception module performed convolutions on inputs using 3 different filter sizes (1x1, 3x3 and 5x5), with a max-pooling operation and outputs being concatenated and sent to the next module [277]. To further help with computational flexibility, a dimension reduction was also introduced wherein smaller convolutions were introduced before the 3x3 and 5x5 convolutions, which helps to limit the number of input channels. This is shown in Figure 5-6 and forms the basis for several neural network models.

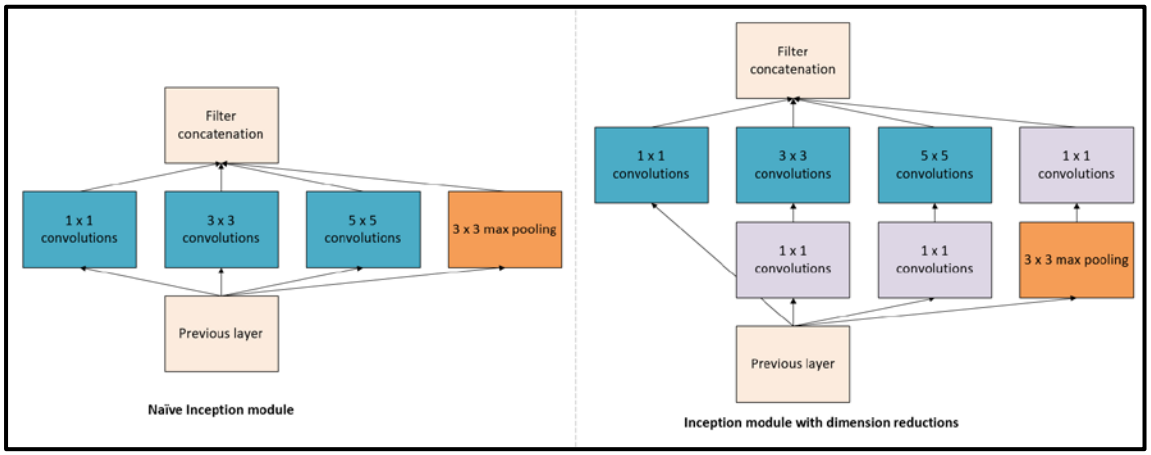

Figure 5-6. Inception modules Mobilenet

Mobilenet is a now-common model architecture used specifically for the purpose of mobile application deployment. It uses depthwise separable convolutions to decrease the model size and complexity [283]. As a result of this, there are fewer number of parameters multiplications and additions. Depthwise separable convolutions deal not only with spatial dimensions but also with the depth dimension. It splits a kernel (the computation) into two separate ones to handle the depth-wise (handling the depth channels of the image) and pointwise convolutions (handling every point). This allows the model to significantly reduce the number of computations.

- Feature Pyramid Network - FPN

This model network uses a pyramid-like structure where predictions are essentially made at different tiers of the pyramid. It uses a region proposal like structure to make predictions. It is made of a bottom-up and top-down pathway that carries out detections at the various scales. It essentially replaces the feature extractors of other models such as faster-rcnn and uses a generation of multiple feature maps layers [296]. This is shown in Figure 5-7.

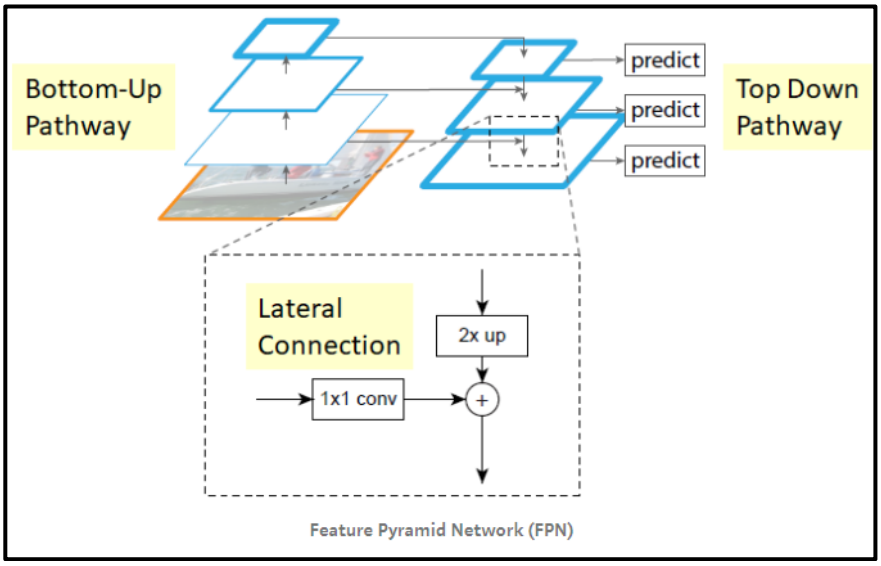

Figure 5-7. Structure of feature pyramid network (taken from [296])

- Pooling pyramid network - PPN

Pooling Pyramid Networks are a single-stage convolutional object detector, which is similar to the SSD network structure. The two critical changes to that of the SSD are that a shared box predictor is used across feature maps with different scales (SSD uses independent predictors for the feature maps) and max pooling operations replace the convolutions between feature maps [297].

This was done to help solve imbalanced datasets with objects of varying sizes that could produce lots of predictors that would not be useful to many objects in the database. For this reason, this was chosen in the study to see if it could help with unbalanced sets.

5.3.3 Image segmentation

The third aspect utilized in computer vision within deep learning is image segmentation. This refers to recognizing how and where the objects in the image are presented. The process typically divides the image into meaningful regions with classifications into a specific class or

type [247]. This is particularly useful to understand a particular captured scene. The classification can be done using pixel-level segmentation – semantic segmentation or instance segmentation which refers to object instances. Both Pascal VOC and MS-COCO challenges also provide competitions for segmentation on their datasets.

Fully convolutional neural networks are implemented for pixel-level segmentation purposes in an end-to-end CNN structure [298]. These systems reproduce heat maps indicating classification scores and areas. This use of FCNs has shown tremendous results as compared to traditional techniques [247]. There are several other network models developed to help solve problems of sematic segmentation on 2D and also 3D imagery [299]. However, the focus of the project will not be on developing semantic segmentation of the 2D pavement images. Nevertheless, the concept is important as it can be used to extend the study's pipeline in the future as work on this would yield more information for the road authority. It can be considered for the future perspectives of both the 2D and 3D image analysis within the study.

5.4 Using transfer learning for low-cost model development

As previously discussed, there are existing networks, which have been trained on millions of images and utilizing high-performance PC systems, which are very deep with complex convolutional layers. Using these as building blocks, Transfer learning can be utilized as a quicker way to develop models without starting over the process, thus reducing time and computational costs. It is the last field of AI as depicted in Figure 5-1. It is an approach wherein knowledge developed in one task is transferred and used to improve the learning of different target tasks using a pre-trained model as a baseline [300,301]. Within the CNN, each layer extracts features from an image and successive layers further extract more complex features. As the initial layers are essentially used for low-level features such as curves and edges these layers can be used for new tasks with training being done on the classifier of the network or the fully connected layer specifically for the new task. This process has been readily used over the last few years given its efficiency [302].

Even in scenarios where there is a large database it has been shown that the utilization of pre-trained weights as opposed to random ones can yield benefits to the new model [303,304]. It has also been proven that even in networks with objectives that are vastly different the use of pre-trained weights and starting points are better than the random initialization used in

models from scratch [305]. The use of transfer learning and hyperparameter tuning has therefore become common in the development of new models for different purposes and is seen as the most effective solution [299,306]. As a result of this, the concept of transfer learning will be used within this study to leverage the power of the models previously discussed.

5.5 Trends of utilizing DL approaches to pavement engineering

As the advances in deep learning have been described, it is now critical to pinpoint the significant research done using these techniques for Pavement Engineering applications [307–310]. These applications can be assigned to the following areas:

- Pavement condition and performance predictions [75,84,311,312] where networks are used to predict future pavement conditions using historical data
- Pavement management systems [54,55,313] where models have been developed to optimize the functioning of the PMS
- Pavement serviceability forecasting [314–316] where models are used to monitor the ability of the pavement to serve its users need (e.g. comfort)
- Structural evaluations [317–319] where models are used to evaluate the physical structure of the pavement
- Modelling pavement materials [320–322] where models are used to simulate the performance of individual materials within the pavement structure and how they will react to different conditions
- Pavement image analysis and classification [308,323–326] where models are used to analyse images of the pavement and where the focus of this aspect of the study lies.

Pavement Image analysis and classification is the most researched area, where the focus is split between image classifications, where images are classified based on the distress occurring in the image; and object detection, where distresses are located using bounding boxes or masks within the image. There are however issues with image classification as distresses regularly occur in a grouped manner thereby making it difficult to label a particular image with just one distress type. This is important as information on connected distresses and the locations of areas where there are multiple distresses are vital for the asset

management system to accurately monitor the road conditions. With object detection, it is possible to have multiple overlapping objects within an image and therefore it is possible to detect multiple overlapping pavement distresses.

A significant proportion of previous studies has been focused on developing models and networks to determine whether there is a presence of a distress or not and also the general detection of pavement distresses [323]. Of the distress types, the main focus has been crack detection and analysis. This is due to the fact that pavement cracks are seen as the most predominant distress type [38] and they are also easier to measure, with the typical requirements being simply to measure the crack's width and length. There are a tremendous number of studies on developing specific neural networks for crack detection and analysis using both 2D and 3D imagery [259,323,324,327–331] and with comparisons made to results from image-based toolboxes for crack detection and analysis such as CrackIT [332]. CrackIT is a Matlab based toolbox developed to detect and characterize cracks. While the detection and monitoring of cracks are important to road agencies, this represents only one main category of distress. There has not been a lot of focus on standardized distress categories as accredited by international manuals on the subject [321]. A few studies have tried to analyze multiple distress categories and generate datasets of multiple types. A research team in Germany developed a CNN for pavement distress application based on imagery obtained through surveys across the German road network using a mobile mapping system attached to a vehicle [333,334]. Their team developed the German Asphalt Pavement Distress (GAPS) dataset which was utilized to generate classifications based on six different distress categories based on the German road manuals with research ongoing utilizing their developed Neural network, ASVINOS. The dataset was also recently updated to have better annotations with a larger database [335]. Other teams have considered the use of street images where DL models are used to isolate images that have distresses, particularly cracks [336] showing higher accuracies than the CrackIT model. Using google street view images, another team also developed models to detect a number of distresses [337] and then further used image segmentation to detect the size of the cracks from the first level of detections [338].

Studies have also been carried out in Italy in which fourteen different categories of distresses were analysed with the application of semantic segmentation and object detection algorithms on a dataset within Naples, Italy [339]. This was done to formulate a decision support system

based on the occurrence of the predicted distresses within the datasets which further highlights the importance of the detection of multiple distresses. There is also a large dataset of road surfaces that exists called the KITTI dataset [340] but this dataset was created primarily for the purpose of assisting with automated driving research. Other studies have considered the use of transfer learning using models that were initially trained in the ImageNet database previously mentioned. Using these models, new models were developed to detect the presence of cracks [323].

The use of mobile phones for capturing datasets has also been considered with one of the earliest applications being the use of a CNN on patches of images collected from a smartphone to detect the presence of cracks [341]. There has also been the development of a database of road distresses in Japan through a mobile application [342] in which eight distresses were annotated within the dataset. The work has led to technical challenges such as an IEEE Big Data challenge based around the database where different models were submitted to obtain higher accuracies based on different network and hyperparameter configurations. This led to several different network configurations using different base networks and models for the same goal of detecting the distresses within the dataset [343–345]. Whilst these developed models represent a significant step forward in pavement distress detection and analysis, the models do not yield any information on the severity of the distress, which would provide an understanding of not only the distress type present but also a trigger for interventions.

This study further explores this by using models built around the specific context of the location and an affiliation with the severity determination therefore adding an important component to the current research field. Different distress assessments and model configurations will be used to develop a low-cost methodology and tool to enable road agencies to monitor the road structure and enable the establishment of points for road maintenance intervention.

5.6 Limitations of DL and object detection model development

While the use of deep learning has increased accuracies for classification and detection systems, they are not perfect and have deficiencies in both their use and implementation. Models developed rely heavily on the data collected and the labelling of this data. Therefore, this process has to be done efficiently as if the model is trained on poorly labelled data, the

resulting models will be poor regardless of the computational efficiency of the model's framework. As a result of this, there is still some human interaction with the process in the early stages of development and this must be carefully monitored.

Deep Learning models require a lot of data for training and this could be costly and time consuming depending on the availability of the source equipment and images. For images, smartphone surveys can help avert this issue but the images taken from a smartphone will have a lower quality and this could, in turn, affect the model performance and this will be discussed further in chapter six and seven. Additionally, DL models need to be developed based on the environmental conditions present in their networks. Models can not be transferred to different locations even if the models are detecting a similar distress as the surrounding road and environmental conditions will be different. Furthermore, models developed based on imagery will suffer from some of the same deficiencies as handcrafted ones when dealing with elements such as shadows and brightened images.

Finally, depending on the models used and the number of distresses being analysed the initial training and modelling could require significant computational resources. However, this is only required at the beginning of the process and once the models are adequately trained, inference time and needed computational power are negligible.

Despite all of these limitations, the possibility of using deep learning systems especially using low-cost data collection systems presents a very viable option for road authorities to gain vital data on the condition of their networks and the locations of pavement distresses.

Chapter six will focus on the development of the models, identifying the exploited workflow and examining the context of the models being developed.

Chapter 6: Setting up DL detection systems for pavement distress detection

Given the context and overview of utilizing deep learning for pavement engineering provided in chapter five, the challenge of the project was then to utilize available resources to create object detection models capable of detecting pavement distresses to feed towards the road asset database in the research environment. This chapter examines the steps used to do this and the important innovations that make it viable. The methodology and reasons for choosing different parameters in the process are given in this chapter and the results and further examinations and optimizations will be featured in chapter 7.[4]

[4] This chapter is based on the following paper:
"Towards low-cost pavement condition health monitoring and analysis using deep learning" published in the international peer-reviewed journal "Applied Sciences" and which was authored by the same author of this thesis. doi: 10.3390/app10010319.

6.1 Overview of the modelling process

Given the state of the research field and the importance of automating pavement detection systems, to allow for effective condition monitoring, the ability to create a system that could automatically detect the presence of distresses on the network would significantly help an authority in their decision-making processes. To this end, the most integral part of the work was the development of object detection models to carry out this task. For the development of these models, the first major decision is the deep learning framework to be used. The framework is the platform from which the models will be trained, evaluated and validated in the work. There are several different deep learning frameworks that are widely available which include TensorFlow, Keras, PyTorch, Caffe and CNTK which represent the frameworks supported by the biggest tech companies of Google, Facebook and Microsoft to name a few. For this project, the decision was made to utilize the open-source TensorFlow framework (developed by Google) [290]. This decision was made in part based on a ranking of the frameworks that considers the number of studies and applications that have used the framework, the available books on the framework and usage surveys. This was important as the framework needs to be one that could be easily practically implemented for use in a road authority. Using these categories and a few others, a ranking of the frameworks was done in 2018 [346] and this is shown in Figure 6-1 below. In the ranking, it can be seen that TensorFlow has the highest rank in comparison to the others with the second and third most highly ranked frameworks being Keras and PyTorch.

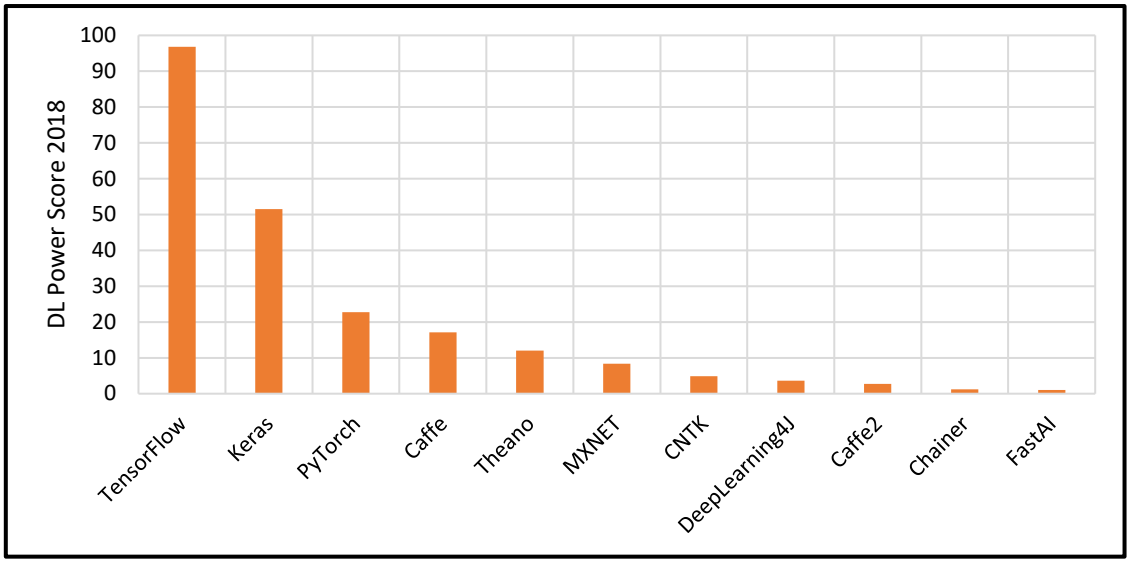

Figure 6-1. Deep learning framework scores for 2018

In the most recent update of the scores, for 2019 [347], the gap between frameworks scores has reduced with the top three shown in Figure 6-2. TensorFlow remains the highest-ranked option and given this, it was utilized for the work and the setup was done to ensure compatibility with the framework.

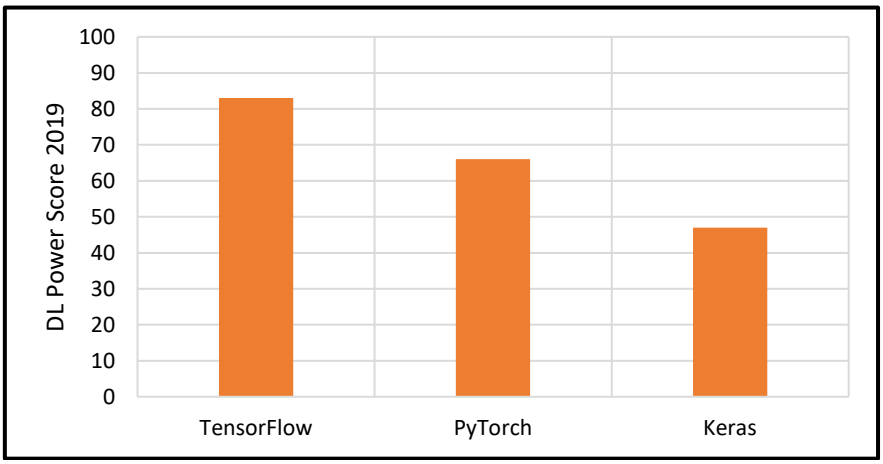

Figure 6-2. Deep Learning framework scores for 2019

The workflow to do this is shown in Figure 6-3, wherein the steps are shown from data collection to final model deployment.

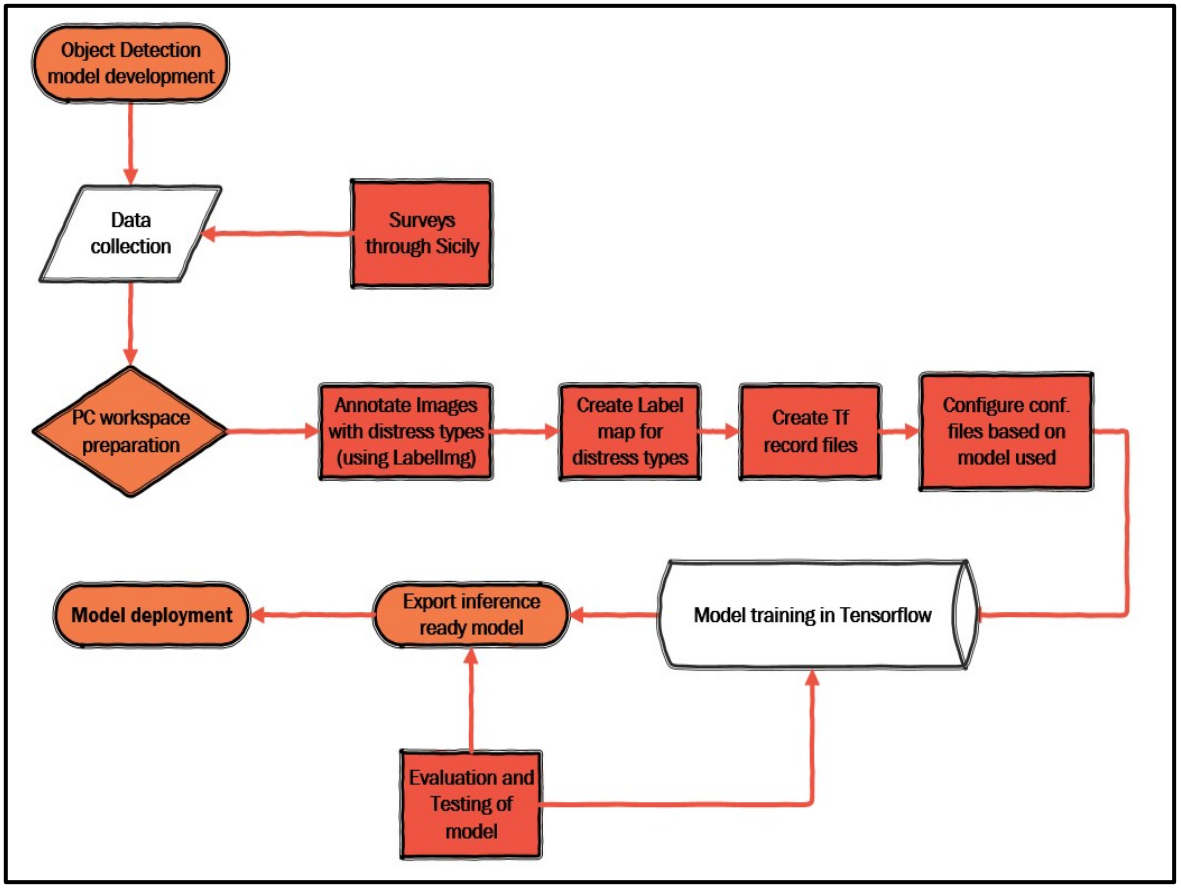

Figure 6-3. Pipeline utilized for the development of object detection model

This workflow is further explained in Sections 6.2–6.4. It is replicable for other datasets and can be utilized for generating models for different cities or regions to enable creating a model based on particular conditions that exist within the road authorities' environment.

6.2 Data collection – Imagery and base model selection

It was important for the exercise to establish a model that could be used in the specific local conditions in Sicily, Italy. Given this challenge, it was necessary to obtain a collection of images from the Sicilian region. To overcome this challenge, the application, My City Report [342], was utilized to capture images from a smartphone that was mounted in a car driven along the Sicilian urban roadways. This setup is depicted in Figure 6-4. The application has the ability to capture images at an approximate distance of 10m ahead of the positioned phone with photographs taken every second. The application was relied on solely for data collection purposes. For the purpose of this study, several trips were made across urban road networks in Sicily generating over 7000 images. The weather and area were diverse within the dataset so as to offer a robust training dataset of urban road networks within the region. However, only the images that were taken during the day and when there was no rain were used. This does identify a limitation of the process, as it is difficult to accurately identify distresses during inclement weather conditions. Additionally, only images of flexible pavements were used. The same camera phone, the Google Pixel 2XL, was utilized for all trips to ensure all of the images had similar image qualities and dimensions.

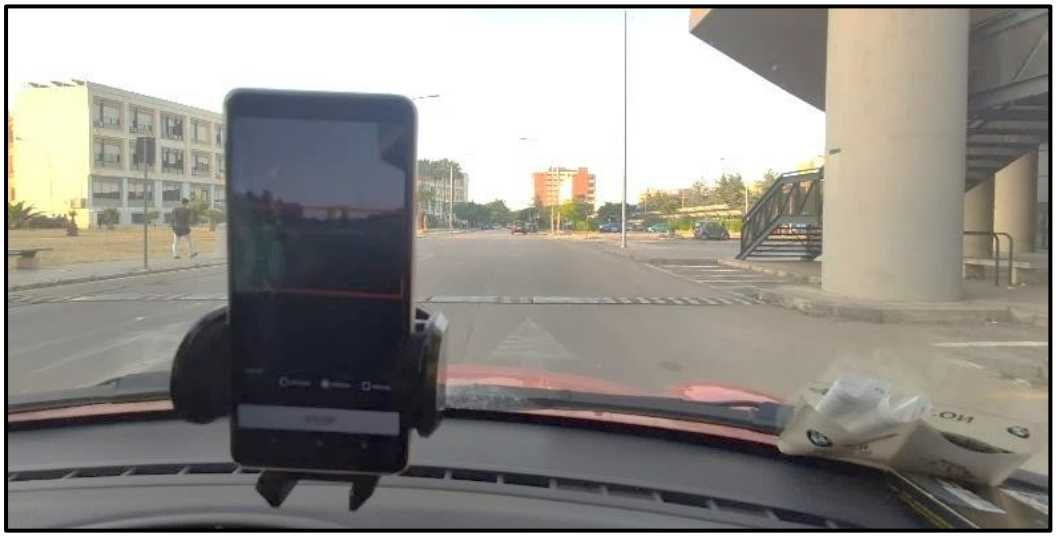

Figure 6-4. Image depicting smartphone setup during surveys.

For the neural network setup, it was decided to use transfer learning given the size of the dataset and the available base networks and the reasons established previously in chapter five. Several different base models were considered given the available networks within the TensorFlow Object Detection API [289], which was built within TensorFlow [290] that allows easy construction, training and deployment of object detection models. Within the Google API, there are prebuilt architectures and weights such as the Single Shot Multi-box detector (SSD) [291] using MobileNet [283], Inception V2 [292], Region-based fully convolutional networks (R-FCN) [293]as well as the Faster R-CNN networks [294] which were previously described.

For the purpose of this study, several models were initially considered but the final base models that were used for development were: Faster R-CNN using Inception V2, based on COCO dataset [288], Single Shot Detector (SSD) using InceptionV2 model based on the COCO dataset and the SSD using MobileNetV2 also based on the COCO dataset. These were chosen as they've shown accuracies in previous model evaluations [289]. The properties of the chosen models are given in Table 6-1.

Table 6-1. Properties of object detection models.

Model Name	Speed (milliseconds, ms)	COCO Mean Average Precision (mAP)	Outputs
faster_rcnn_inception_v2_coco	58	28	Boxes
ssd_inception_v2_coco	42	24	Boxes
ssd_mobilenet_v2_coco	31	22	Boxes

These models are all publicly available through the TensorFlow object detection API zoo. Each of these models provides a quick model creation pipeline, which can be developed without the use of heavy computational resources. The two main networks utilized for the work are the Faster R-CNN model and the SSD model with the utilization of the inceptionv2 and mobilenetv2 CNNs (previously described in chapter five).

6.3 Data preparation – pipeline of model development

6.3.1 Data Annotation

For this study, the open-source labelling software, LabelImg [348], was utilized to individually manually label images based on the type of distresses present. An example of this work is shown in Figure 6-5. This was done by the study team, which comprised trained civil engineers

with experience in asphalt pavement engineering and conditional surveys, which are typically used to define and detect pavement distresses.

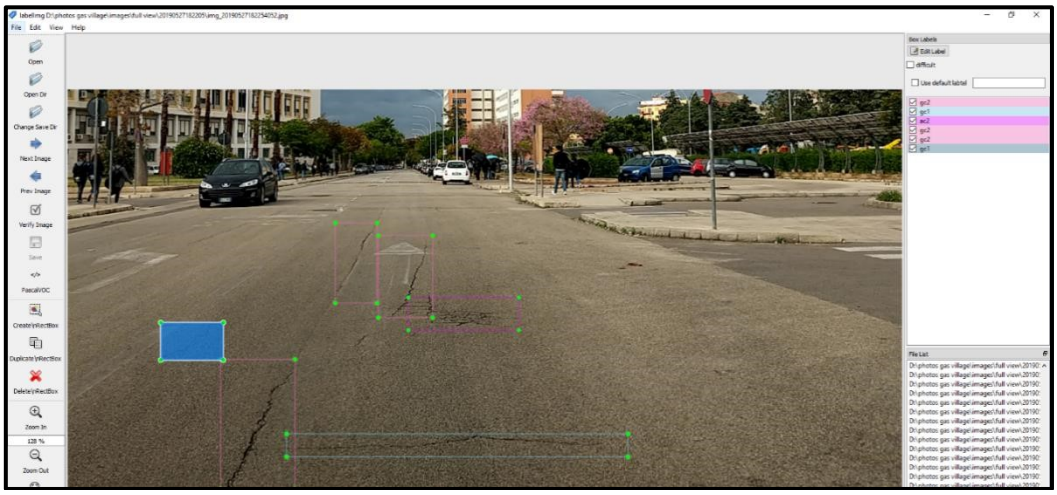

Figure 6-5. Annotation of images using LabelImg.

The software allows for the distress to be captured in two different formats – yolo [295] txt file or a Pascal voc [287] xml file format. Each format is related to the type of deep learning system to be employed but both contain the same information – the annotated class label and the location of the distress identified using a bounding box of which the coordinates are embedded into the annotation files. It is estimated that an annotation takes about 30 seconds per image considering rechecks on the image to verify that the correct bounding box was used. For the deployment in TensorFlow, the xml format was used. An example of the information embedded within the files is shown in Figure 6-6. The other format (txt) embeds similar information.

```
<annotation>
	<folder>distress images</folder>
	<filename>000977.JPG</filename>
	<path>D:\Ronald_Roberts\Releves_2019_06_21_09_29_58
\distress images\000977.JPG</path>
	<source>
		<database>Unknown</database>
	</source>
	<size>
		<width>640</width>
		<height>480</height>
		<depth>3</depth>
	</size>
	<segmented>0</segmented>
	<object>
		<name>TC</name>
		<pose>Unspecified</pose>
		<truncated>1</truncated>
		<difficult>0</difficult>
		<bndbox>
			<xmin>1</xmin>
			<ymin>127</ymin>
			<xmax>577</xmax>
			<ymax>168</ymax>
		</bndbox>
	</object>
	<object>
		<name>LC2</name>
		<pose>Unspecified</pose>
		<truncated>0</truncated>
		<difficult>0</difficult>
		<bndbox>
			<xmin>525</xmin>
			<ymin>118</ymin>
			<xmax>594</xmax>
			<ymax>478</ymax>
		</bndbox>
	</object>
</annotation>
```

Figure 6-6. Example of xml file showing embedded information

The critical and novel step in this process was the development of the distress categories for the model. Typically, pavement distresses can be broken down into four major categories namely: cracking, visco-plastic deformation, surface defects and other miscellaneous types [26]. The grouping is shown in Table 6-2.

Table 6-2. Generalized pavement distress categories.

Distress Category	Distresses
Cracking	Fatigue cracking, Block cracking, Edge Cracking, Longitudinal and Transverse cracking, Joint reflection cracking, Slippage cracking
Visco-plastic deformations	Bumps and Sags, Rutting, Corrugations, Depressions, Potholes, Swelling, Lane/Shoulder drop off, Shoving, Stripping
Surface defects	Bleeding, Polished Aggregate, Raveling
Others	Patching/Utility cut patching, Railroad crossing, Manholes

Of these categories, other studies have shown that there is a direct relationship between the impact each distress has upon safety and comfort per level of severity [26]. Based on this each distress has an impact based on the severity of the occurring distress. This is further depicted in Figure 6-7 and Figure 6-8. From these figures, it can be seen that the most impactful severity level, as expected, was the High severity cases whilst the medium and low severities in most cases have fewer impacts upon safety and comfort.

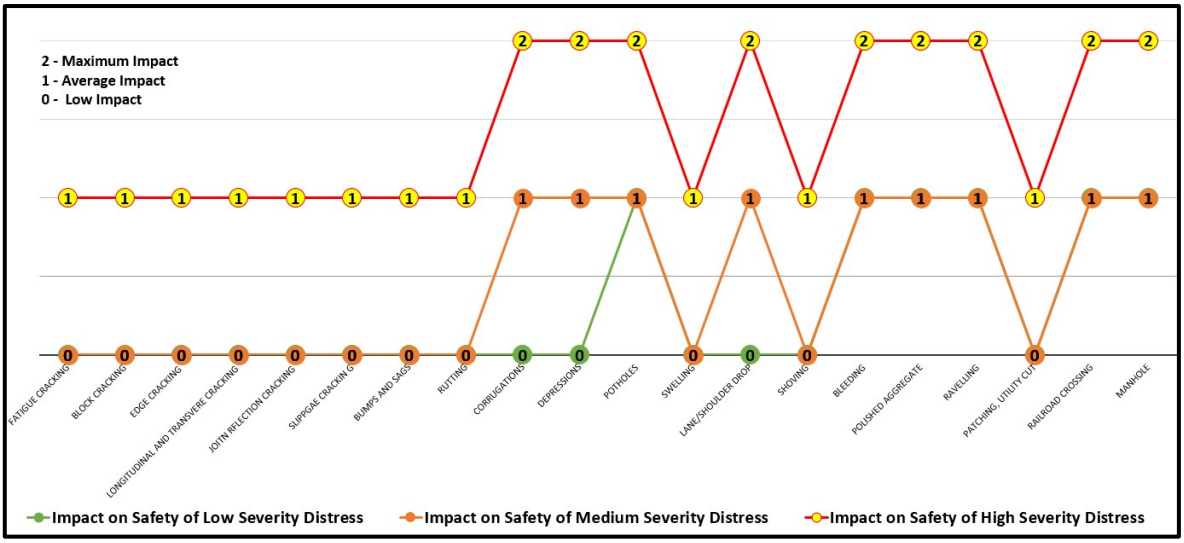

Figure 6-7. Impacts of the severity of pavement distresses on safety.

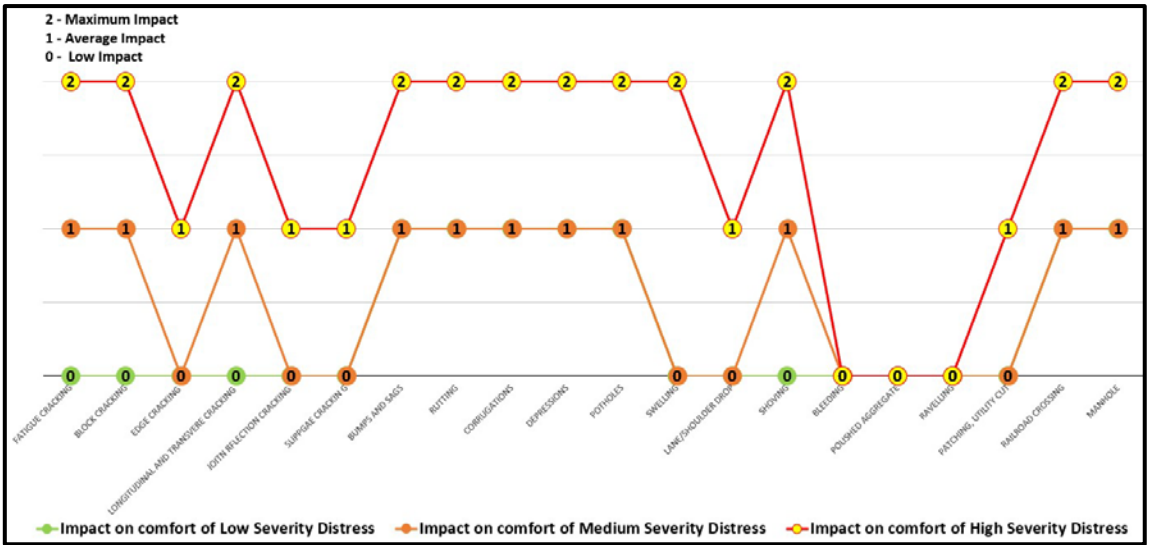

Figure 6-8. Impacts of the severity of pavement distresses on comfort.

The severity level is usually then derived based on data from manual surveys and based on regulations implemented by pavement distress manuals [58,60,63]. Different ratings are then utilized to determine the overall condition of the roads based on the presence of the distresses and other factors such as roughness which are correlated in typical performance indices such as International Roughness Index (IRI) [349] and Pavement Condition Index (PCI) [58].

Based on this, the decision was chosen to have only two severity levels (level 1 and 2), wherein the first represents situations wherein remedial action is not a necessity and the second where it should be done. Using the four general groups as a base case, annotations were made for each with the exemption of Surface defects (such as Bleeding and Polished aggregate) where it is difficult to accurately pinpoint the distress and its associated severity level from a 2D image. The cracking group was also split between general cracking (gc) and area cracking (ac) (as defined by cracking made over a section, such as alligator cracking, as opposed to instances of cracks that are formed at specific points on the road surface or along its surface). With these categories, the developed model should be able to predict different instances of cracking, instances of visco-plastic deformations (vp) and miscellaneous distresses (msc) such as manholes whilst also providing a quick analysis of their severities. There are limitations using this approach as no precise metric measurements would be done on the distresses and having only 2 severity levels does not provide information on cases where intervention action may be required in the near future as could be interrupted by a medium level severity assessment.

However, gaining a general understanding of where these groups of distresses occur and their frequency can provide practitioners with valuable information and allow for an adequate

resource for continuously monitoring the overall health of the road structure. From these groupings, annotations were manually made only on images where there were was a clear view of the distress and it could also be clearly marked. This resulted in a total of 4862 distress annotations to be used for the model as split as shown in Figure 6-9.

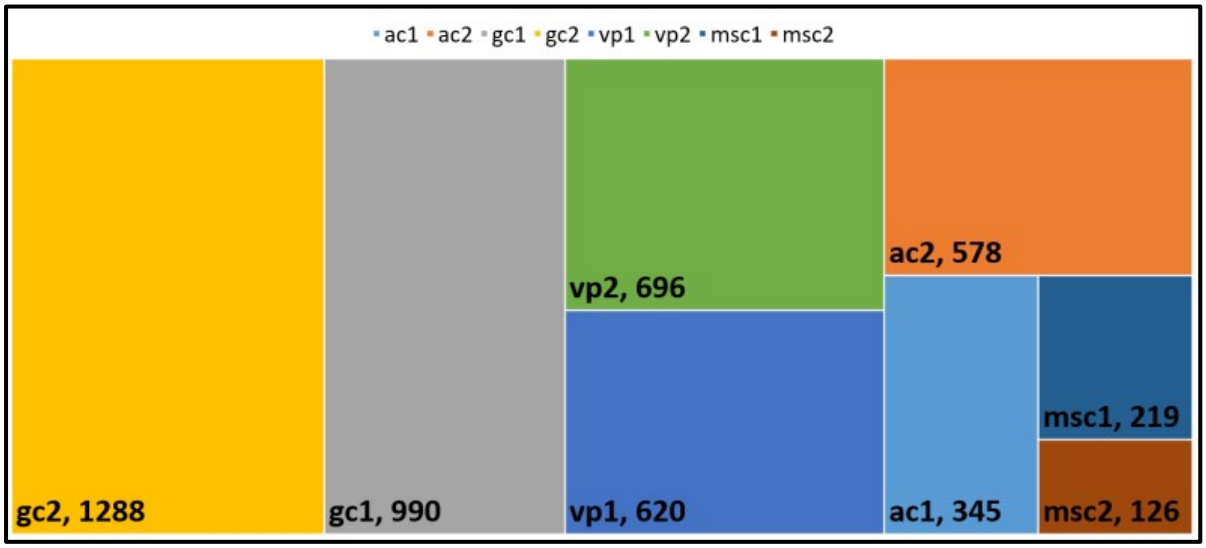

Figure 6-9. Treemap diagram showcasing the distribution of annotated distresses.

Note: ac: Area cracking, gc: general cracking, vp: visco-plastic deformations, msc: miscellaneous distresses 1: Low severity, 2: High severity requiring intervention.

Within this distribution, the most observed distresses are general cracking followed by viscoplastic deformations and then area cracking, with the least being the miscellaneous category. This is expected given the nature of distresses on most urban Italian road networks [38]. Using these distress types, a label map was generated for the previously identified TensorFlow pipeline. Subsequently, the annotated files were converted to the record format to be used within TensorFlow and the datasets were randomly split (in a ratio of 70:20:10 with respect to training: evaluation: validation). This was done for training the model and for testing to ensure the model is not overfitted to the dataset and would therefore not be able to effectively perform on unseen real-world data. Data augmentation was also applied wherein each training image horizontally flipped with a probability of 0.5 (further information and examination of data augmentation will be shown in chapter 7). This allows the study to utilize a smaller dataset as well.

6.4 Experimental and model setup

6.4.1 Hyperparameters utilized

As the data was now in place, the next important phase was the formulation of the hyperparameter values to be used. The hyperparameters are the individual characteristics of the models to be used during the training. For the Faster R-CNN with Inception v2, the parameters used were as follows. An initial learning rate of 0.001 was used and then reduced by a decay of 0.95 every 10,000 steps. The learning rate was in line with that used by previous studies on pavement distress images [58] whilst other rates were experimented with but this rate proving to be effective. A decay was also utilized for the learning rate which helps the model develop momentum and create a quicker convergence as well as reducing opportunities for overfitting with one constant rate. The input images were also resized to 300 × 300 pixels. For the SSD using Inception V2, an initial learning rate of 0.002 was used and then reduced by a decay of 0.95 every 10,000 steps. The same approach of using a time decay for the learning rate was utilized. The input images were also resized to 300 × 300 pixels. The same hyperparameters were established for the SSD using the MobileNetv2 model for comparative purposes. These configurations were set within the configuration files of each prebuilt model.

6.4.2 Workstation Setup

For the training and evaluation, a Windows 10 PC was utilized with an NVIDIA Quadro P4000 GPU (8 GB ram) and total CPU memory of 32 GB. Within the evaluation state, the Intersection Over Union (IOU) evaluation metric was used. This metric is defined by dividing the area of overlap between the bounding boxes by the area of union between them and for this exercise, the threshold was set to 0.5. The IOU essentially provides an estimation of the accuracy of the bounding box as compared to the ground truth labels. More inspection of the effect of the IOU is provided in chapter 7. The general speed of the models utilized was 0.6 seconds per training step in the modelling process. The faster of the models, as expected, is the mobilenet one, which is a model that was developed with the clear purpose of mobile deployment.

6.4.3 Performance Metrics utilized

For models, performance is typically evaluated based on the metrics of precision and recall. Precision can be classified as the results within a test that are relevant to the classification problem whilst Recall refers to the percentage of relevant results which are in turn correctly

identified by the model. These metrics evolve from an evaluation of the confusion matrix of detections which details the occurrences of false and negative positives and negatives as shown in Figure 6-10 [350].

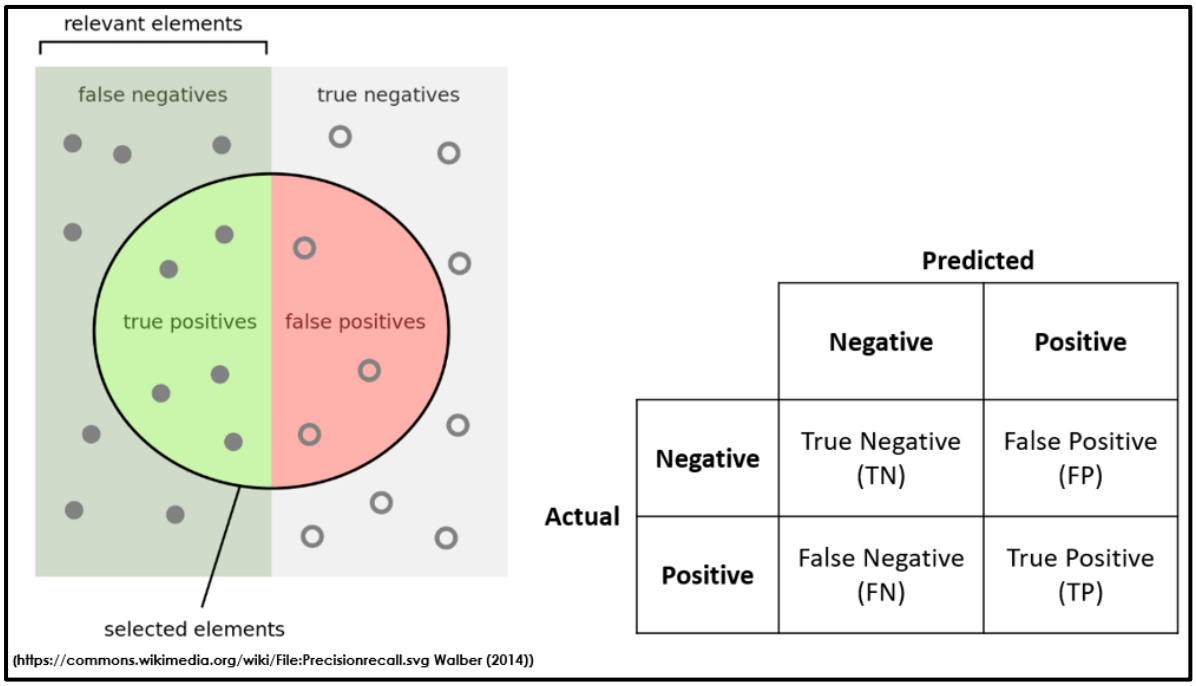

Figure 6-10. Visual representation of confusion matrix and related predictions

Table 6-3 below highlights the commonly used metrics and offers an explanation with respect to the case of detecting pavement distresses.

Table 6-3. Analysis of commonly used metrics

Metric	Description	Formula
Precision	The proportion of accurate distresses that are detected against the total number of predicted distresses	TP/(TP + FP)
Recall	The proportion of accurate distresses that are detected against the total number of actual distresses	TP/(TP + FN)
Accuracy	The proportion of accurate distresses over the entire set	(TP+TN)/(TP+FP+TN+FN)
F1 score	A combination of precision and recall where the two are treated equally	2((1/Precision) + (1/Recall))

Wherein, precision speaks to the relevance of the positive distress results and recall speaks to the ability of the model to detect the distresses. There is also a combined metric, referred to as the f-measure/f1 score, which is a harmonized metric, which weighs precision and recall equally. Accuracy is also a metric that can be considered but the metric itself places a lot of dependency on the total number of negatives and therefore can offer a skewed performance examination that does not identify the possible flaws of the model that can better be

interpreted with precision and recall. Additionally, there are other metrics, which are not as commonly utilized but can provide a succinct overview of the model's performance [351]. These are given in Table 6-4 describing what the metrics imply for distress detection.

Table 6-4. Analysis of metrics used for pavement distress detection

Metric	Description	Formula
Specificity (True Negative Rate)	The proportion of distresses that are classified as not being present in the image and are not there	TN/(TN +FP)
Negative Predictive Value	Can be considered as the opposite of Precision	TN/(TN+FN)
False Positive Rate (fallout)	The chances of having a false positive amongst the total number of images that are considered without a distress	FP/(FP+TN)
False Negative Rate (miss rate)	The chances of missing a distress detection	FN/(TP + FN)
False Discovery Rate	The proportion of false distress detections with respect to the total number of images with distresses	FP/(FP+TP)
False Omission Rate	The proportion of missed detections with regards to the total number of images without a distress	FN/(TN+FN)

The use of these metrics largely depends on the motivation of the study and model. The critical element that must be considered is what is important to the designated stakeholder. The metrics that detail the chances of a false positive or false negative occurring are particularly interesting as they offer a clear view of how a model handles these occurrences. It should be further stated that if a stakeholder emphasizes that there should be limited false positives then precision is considered a good metric for performance evaluation. With regards to pavement distresses, this would mean that the stakeholder does not want a large number of falsely detected pavement distresses. However, should the stakeholder have a higher value on simply identifying the distress and missing a distress is not acceptable then recall is a better metric. If both of these are important then the harmonized f1 score should be the preferred metric.

6.4.4 Workflow for Validation and testing of models

As previously indicated, each model was run using the TensorFlow environment and during the training, the evaluations were observed and followed until the model achieved an acceptable loss level below 1. This, however, does not represent an accuracy level of the model and evaluation needed to be carried out on the model regardless of the loss value. The evaluation relates to the values achieved by the models when estimating the performance

metrics shown in section 6.4.3. This was observed through the TensorBoard environment on as shown in Figure 6-11.

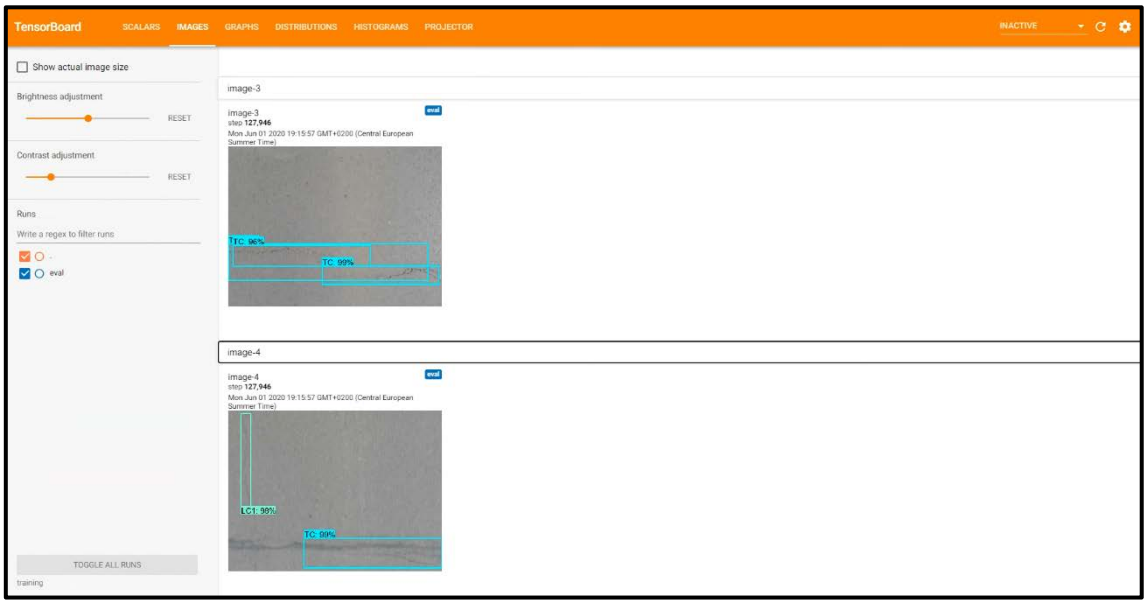

Figure 6-11. Example of TensorBoard environment utilized during the training of the network.

By utilizing the TensorBoard system, it allowed the user to monitor the progress of the model throughout its training. Of particular importance to monitor in this case was the loss which is shown in Figure 6-12. The graphs display the loss over the training iterations time with respect to different characteristics of the model i.e., object detection, localization, and classification. Within the figure, it can be observed that this loss reduces over time and it is important for the model to have a sufficiently low value for the total loss. The platform also allowed the user to monitor the progress of the model on test data during the training which is also helpful as the training could be stopped if it was seen that the model was not producing appropriate results.

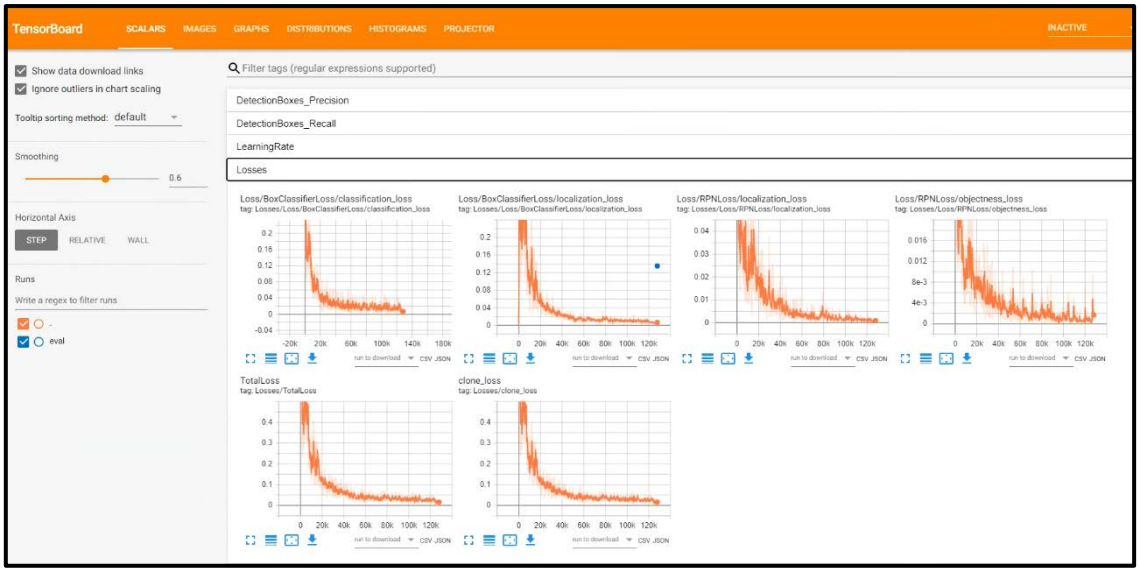

Figure 6-12. The use of TensorBoard to monitor the loss and check on accuracies within the models during evaluation.

Each model was run on the same dataset. After training, the models produced were tested on prediction images run from the test data set and examples of these can be seen in Figure 6-13, Figure 6-14 and Figure 6-15. The model produces a bounding box on the image of the distress type and severity along with a percentage assumption of how accurate this bounding box is based on the calibrations of the model. This value would provide users with an overall assessment of how good the network's condition by generating a hotspot analysis based on the sum of the total possible errors on a survey over a road network. When the model is run within a mobile app, the location of the bounding box (using the phone's GPS) would also be given thus providing the location of the distresses detected within the network. Whilst the accuracy of this location is limited to that of the phone being used, it sill represents a key piece of information. Future adaptations of this can use alterations to the GPS to enable a higher location accuracy.

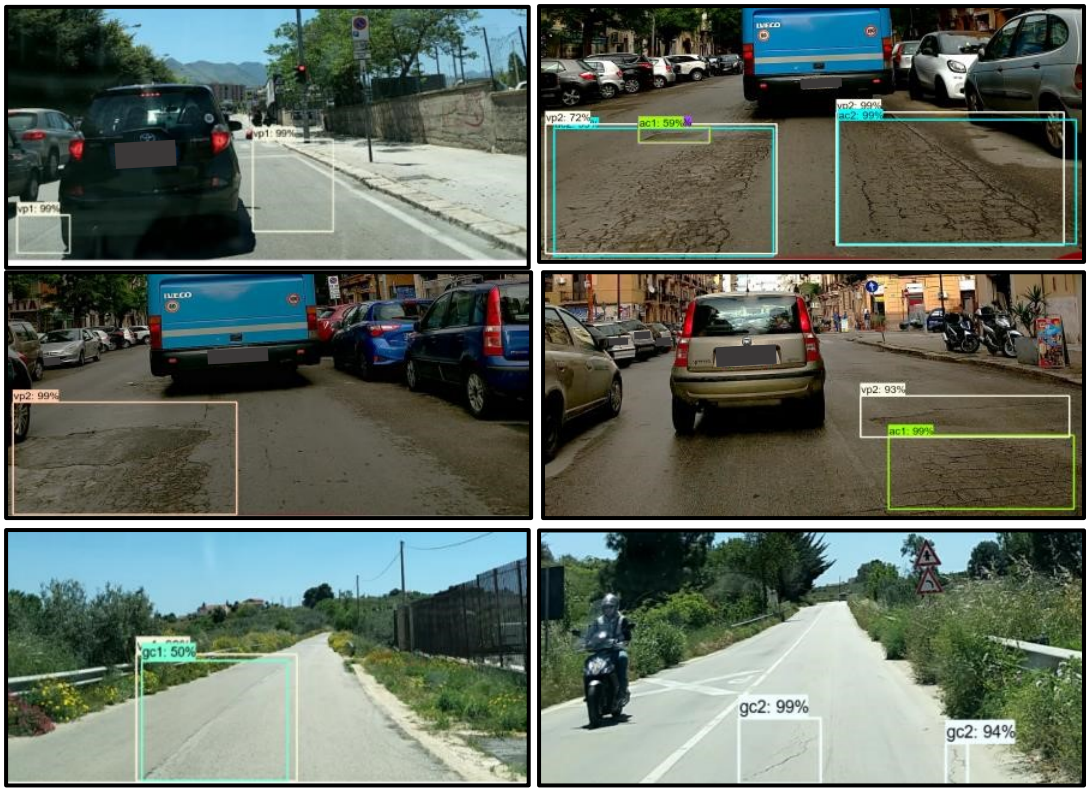

Figure 6-13.Faster R-CNN with inceptionv2 model predictions on test data.

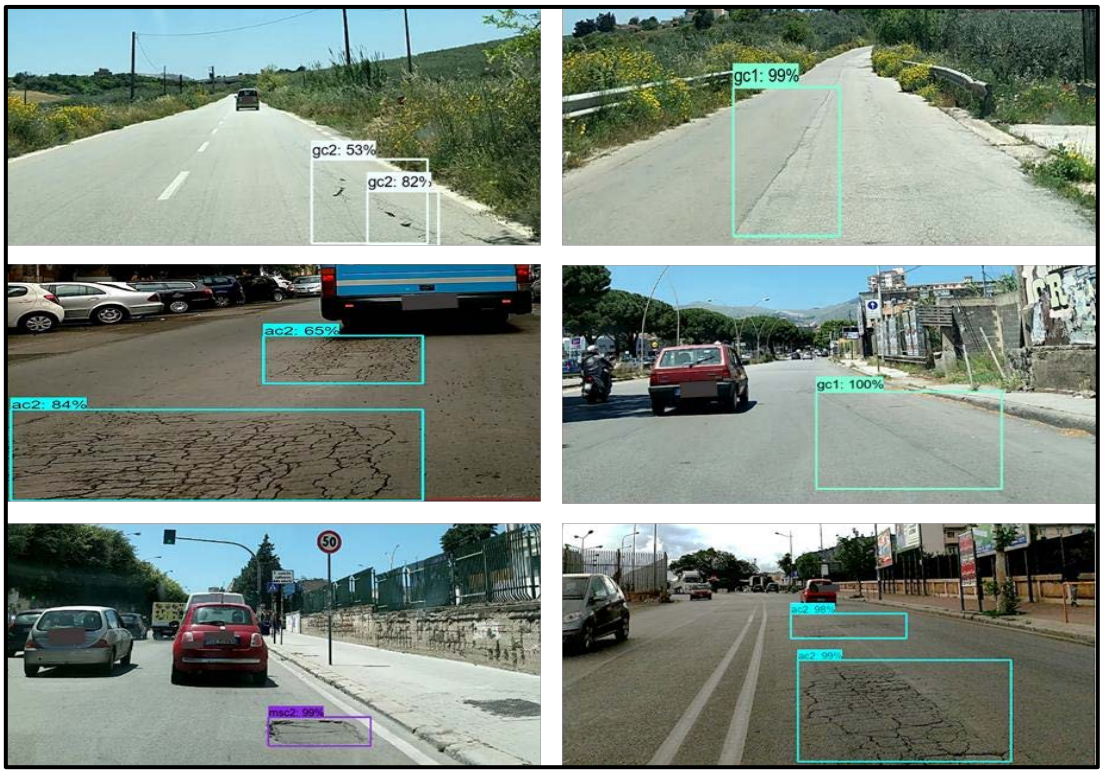

Figure 6-14. SSD with Inceptionv2 model predictions on test data.

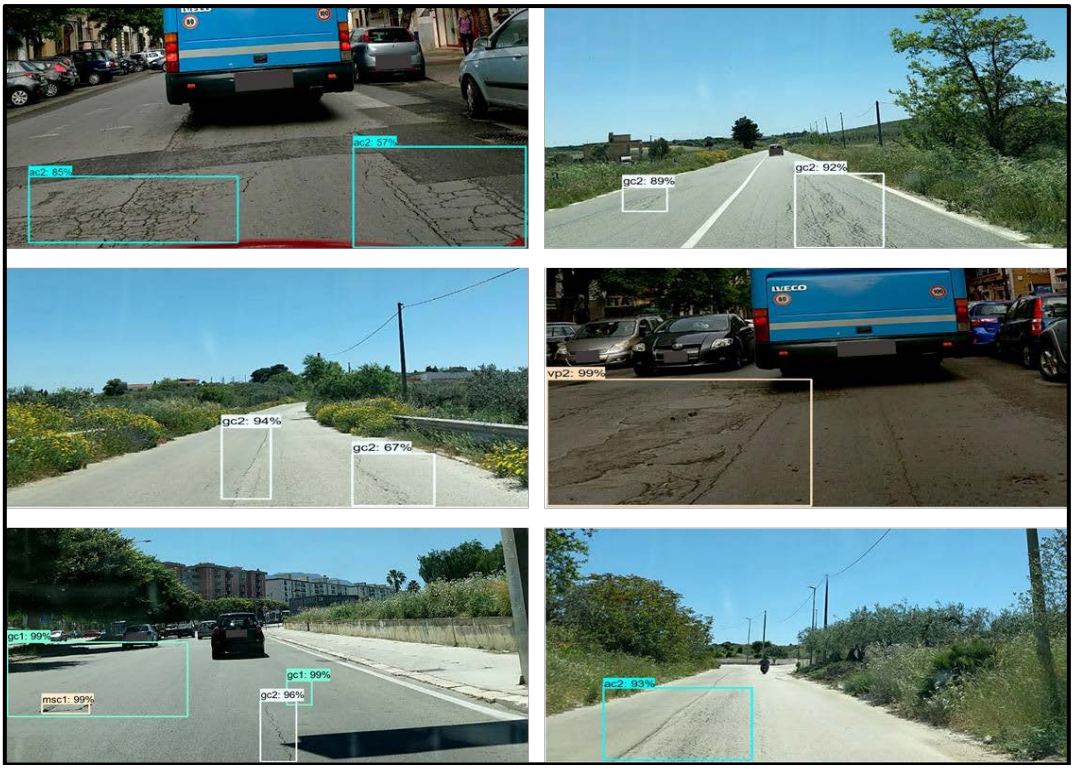

Figure 6-15. SSD with mobilenetv2 model predictions on test data.

6.4.5 Workflow for Inference and deployment of models

After the training, each model was exported to create a graph file that is able to run inference and possibly be deployed to an application or mobile app. This was successfully done for each model at the last given checkpoints of the models, where results displayed the highest accuracies when considering the basic performance metrics. This is important and this step is needed for the model to run on a mobile device and thus be ready for use in a mobile application.

To deploy the models, the TensorFlow Lite system was utilized. TensorFlow Lite is the application used by TensorFlow to execute models efficiently on mobile and other embedded devices with limited computational and memory resources. To use the power of this, TensorFlow models need to be converted to this format before they can be used by TensorFlow Lite. It must be noted also that whilst the conversion process does reduce the file sizes and optimizes its configuration for mobile deployment there is no effect on the accuracy of the model. The conversion makes use of the graph and saved checkpoints that are created once the model has reached a satisfactory level of performance. The graph is frozen, then optimized and finally converted to the TensorFlow Lite format. This produces a ‘detect’ file which can be embedded into a mobile, web or computer-based application to infer detections

based on the classes of the model. For this study, this process was carried out and the models were embedded into a TensorFlow lite object detection application for model testing in real-world conditions. The exploration of these tests are not a part of the work presented in the thesis as the important outcome for this work was the ability to embed the models within an application. The use and testing of the application can be considered in future studies and works. This workflow used for the conversion is shown in Figure 6-16. The mobile models developed in this pipeline can also be used to run the models on images already procured in the past and stored in a road authority's archives. The model could be run on the library of images outputting the location of distresses present in the library, their classification and a confidence level of the prediction. This is important as road authorities could have images already procured and this will provide a quick way of carrying out the analysis of these images as inference on any one image will take less than 0.5 seconds.

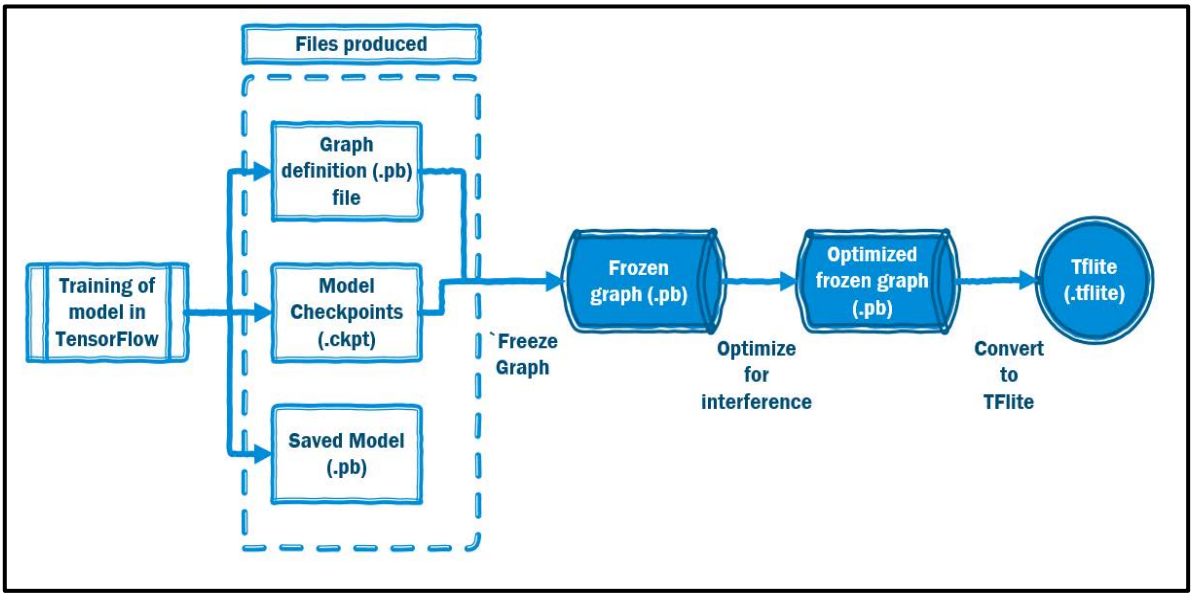

Figure 6-16. The process to convert a model to Tflite version for mobile deployment

The results of these configurations along with the tuning of the models for other situations will be further discussed in chapter 7 to provide a holistic view of the techniques and their strengths in different situations.

6.5 Workflow limitations

The deep learning object detection systems still suffer from some of the issues associated with traditional systems such as difficulties in identifying distresses in shadows. These are difficult to overcome but the results still offer a very good overview of distresses appearing in a network. Additionally, whilst augmentation helps to create larger databases, a lot of data is

required for better model results. To more astutely answer the question of augmentations, this topic will also be further examined in chapter 7.

In the process of preparing the data for data modelling, the pre-processing stages can be time-consuming but they are important to ensure that the correct images, labels and parameters are used. It is also important to stress that the background context is important and needs to be clearly understood when deciding on model particulars and this will be explored further in chapter 7. The modelling process can also be time-consuming but once an acceptable model is achieved, the inference time for use in practical situations is negligible.

Given the workflow and methodology presented within this chapter, the next chapter depicts the results of the models from Italy and further shows how the data can be practically used. Additionally, using case studies in France, the techniques are further experimented with to understand the effects of tuning different model parameters and optimizing the workflow.

Chapter 7: Tuning and evaluating DL distress detection model performance

Based on the methodology described in chapter six concerning setting up the models for detecting pavement distresses, this chapter details and discusses the results of the models within Italy and how they can be practically applied for road management practices. Following this, discussions are made on how to set up models in a different country with different environmental conditions. For this, a new case study was done in France and different image types were considered. By analysing the workflow in a different environment, better assessments on the practicality of the modelling can be made and the guidelines describing how to build these types of models in any situation. Using the case study, different optimization techniques are explored for the training of models and conclusions on the uses of images and the detection pipeline are drawn. [5]

[5] This chapter is based on the following paper:
"Towards low-cost pavement condition health monitoring and analysis using deep learning published in the international peer-reviewed journal "Applied Sciences" and which was authored by the same author of this thesis. doi: 10.3390/app10010319.
It also describes work done during a period of secondment made at Université Gustave Eiffel, which was done in order to meet the requirements of the EuroPhD degree by spending a research period of more than three months at another European university outside of Italy, whilst working on the thesis.

7.1 Performance of models from Italy

7.1.1 Model results

In the first instance, models were evaluated based on the outputs of each model against the test datasets using the final graph. As the base models used for the development of the new model were generated on the 'COCO dataset' it was, therefore, instructive to first consider the 'COCO metrics' for firstly evaluating the performance of the model. These metrics involve the use of Precision, denoted as Average Precision (AP) and recall, denoted as Average Recall (AR) with regards to the bounding boxes within test cases. These values are obtained by running python scripts on the model using the test dataset for the study. These results for all the models are shown in Table 7-1**.** These values are indicative of the mean values obtained after the scripts run several queries at different percentage values of IOU across all the categories in the dataset.

Table 7-1. Average Precision and Recall values for models utilized.

	SSD with Inception v2	**Faster R-CNN with Inception v2**	**SSD with MobileNet v2**
Mean Average Precision	0.909	0.933	0.880
Mean Average Recall	0.929	0.938	0.867
Average f1 scores	0.924	0.933	0.873

Given the numbers showcased, it can be surmised that all three models are capable of solving the problem at hand with the model utilizing the Faster R-CNN base being the most effective. However, these values only depict the average across the categories and for different thresholds, so it is more important to understand the results across the individual categories. Therefore, considering the best model (Faster R-CNN one), the individual values for precision and recall were highlighted for the three main distress categories and their associated severity levels for IOU values of 0.5 and this is shown in Table 7-2.

Table 7-2. Precision and Recall values of individual categories

	AC1	**AC2**	**GC1**	**GC2**	**VP1**	**VP2**
Recall	0.915	0.926	0.968	0.967	0.971	0.932
Precision	0.862	0.800	0.745	0.759	0.799	0.763
f1 scores	0.868	0.858	0.877	0.850	0.878	0.839

Within this table, it can be seen that the individual f1 scores for the main categories are less than the average values given in Table 7-1. This is important, as the individual results of the detection of the categories are key to understanding how the model works and the capacity of detecting the important distress categories. The values are still considered acceptable and the model satisfactory for detecting these categories. For the purposes of this study, however,

what is critical is not only the accuracy of the model but also the simple capacity to recognize that the type of distress and its associated distress category are present within the image and subsequently within the network or road section under analysis. This creates a tool that allows for low-cost hot spot analyses of points on a given road network where there are structural defects and as a result can provide an overall condition estimation of the road network being assessed. The tool would be realized by using the mobile application of tflite as expressed in chapter 6, which produced a model to be deployed in a smartphone application.

Once a survey is carried out using the model, it would also provide a baseline, which can then be utilized for future continuous overall condition monitoring of the pavement structure by simply rerunning the model in a new survey and comparing the defects between the different surveys. This would be without the need for expensive equipment or elaborate survey mechanisms. This is key for road managers and allows for integration within the PMS system. The road authority would be able to determine the location of the specific types of distresses covered by the model, its severity (and thereby an idea of whether an intervention is necessary) and the location and frequency of specific and important types of distresses. This can also then be integrated with techniques that can provide the specific or more detailed measurements required for further actions. More analysis of the use of the model is provided in the next section.

7.1.2 Application of the Model for Monitoring the Health of a Road Network

Whilst the work to this point has shown success in developing deep learning models for the purpose of detecting road pavement distresses, it is also critical to have an idea of how the models can be practically applied in the real world and within practical management systems. To this end, a pipeline was created to show how the information from the deep learning model can effectively be utilized and integrated within the asset database and subsequently the management system. From the discussions of the study, it was demonstrated that the model developed generates a bounding box for each observed distress within the image as well as a judgement on the severity based on the annotation parameters (a level of 1 or 2 for each distress type). This is coupled with the accuracy of the detection. With this information, a database displaying and storing the location of the distress per image in a road network can be generated and be kept for monitoring comparisons and purposes. For this to be done, each image captured during a survey has to be accounted for, highlighting not only the detection of

the distress but also a relationship of this to the length and area of the road segment being surveyed. For this to be possible, a pipeline was developed and is illustrated in Figure 7-1.

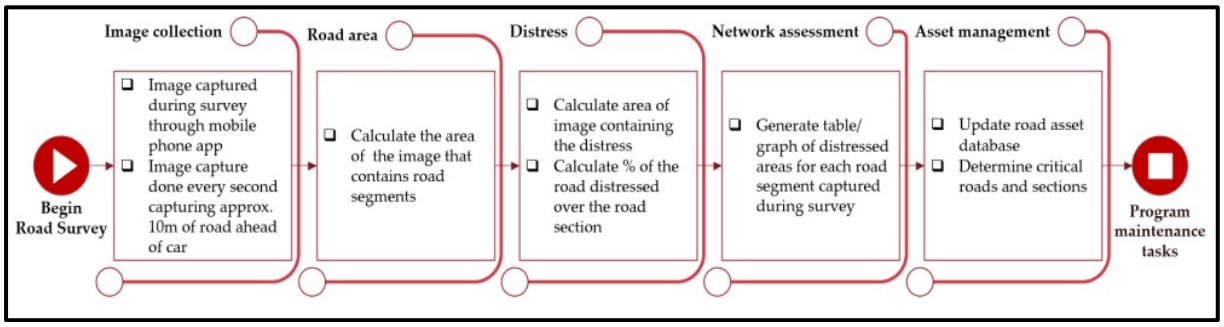

Figure 7-1. Pipeline for applying the model in real-world conditions for health monitoring.

In the pipeline, the area of the road being surveyed is taken into account to have an approximation of the area that the distress covers and as a result, the total distressed areas along a road segment. This is an approximate calculation based on the length of the road segment which is clearly visualized within an imager during the survey (10 m utilized for the survey and case study). Given this pipeline, an example road section during the survey was utilized as a case study to demonstrate the practicality of carrying out these tasks. A random section of approximately 2.6 km was identified to test the pipeline. The area of the road distressed at each 10 m interval was determined and this was plotted for the full section. This is depicted in Figure 7-2.

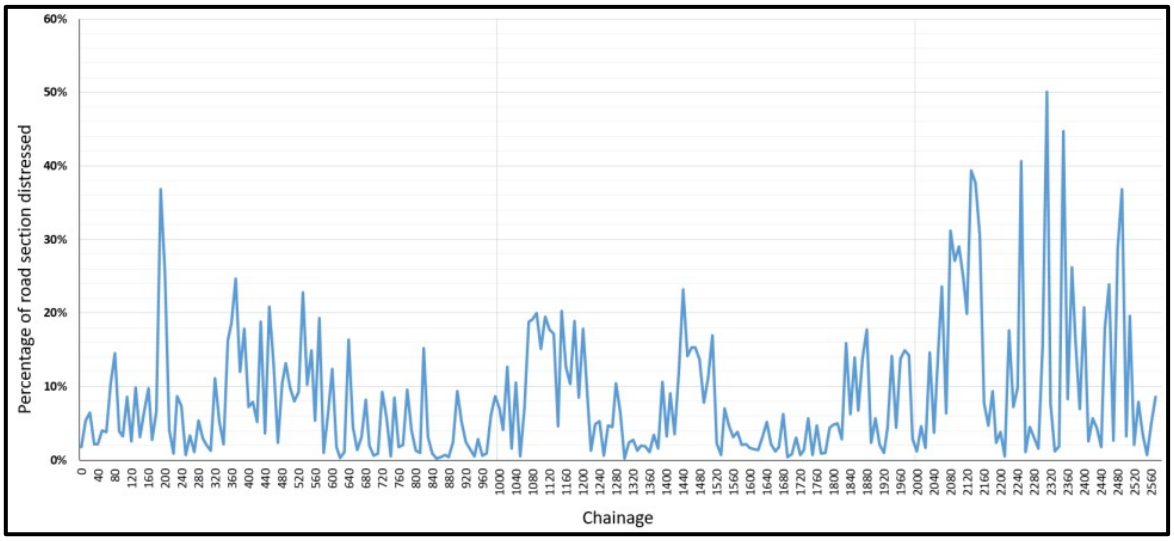

Figure 7-2. Level of the distress on the road across the test section.

From this figure, you can visually identify the sections of the analysed road that are more distressed. For the section under analysis, it appears that between the road chainage of 2000m to 2600m the distressed area is greater than the other sections of the road, which

means that this section could be attributed with a classification of 'critical' health. Therefore, this gives the road practitioner a quick overview of the section under analysis and can allow the agency to pinpoint the area most in need of rehabilitation and maintenance. More critical examinations can be made over this section to determine metric analyses of the distresses, and the pipeline utilizing more advanced visual and metric 3D modelling explored in chapter 4, can be utilized for this. Furthermore, the sections with less distressed areas can be noted within the database and monitored over time. This creates the possibility of monitoring the health of the road network as the survey with the mobile phone can easily be replicated over time creating a timeline of events to monitor.

Another use of this information is to create comparisons of different roads along a network with the goal being to determine which roads should be prioritized for interventions. This can be used in conjunction with the workflow in chapter 2, where the roads projected as necessary for intervention are highlighted. The detection models will add another layer of validation of the other techniques by identifying the level of distresses on the designated roads. This is also critical for road agencies as it is typical for an agency to be faced with a scenario where there are several roads that have many distressed areas but there are only sufficient funds for rehabilitations to be done on a selected number of the roads. To this end, the data can be utilized to create a histogram displaying the number of sections with different levels of distress. Using the same distress information from Figure 7-2, a histogram highlighting the frequency of distresses along the road section was plotted and this is visualized in Figure 7-3.

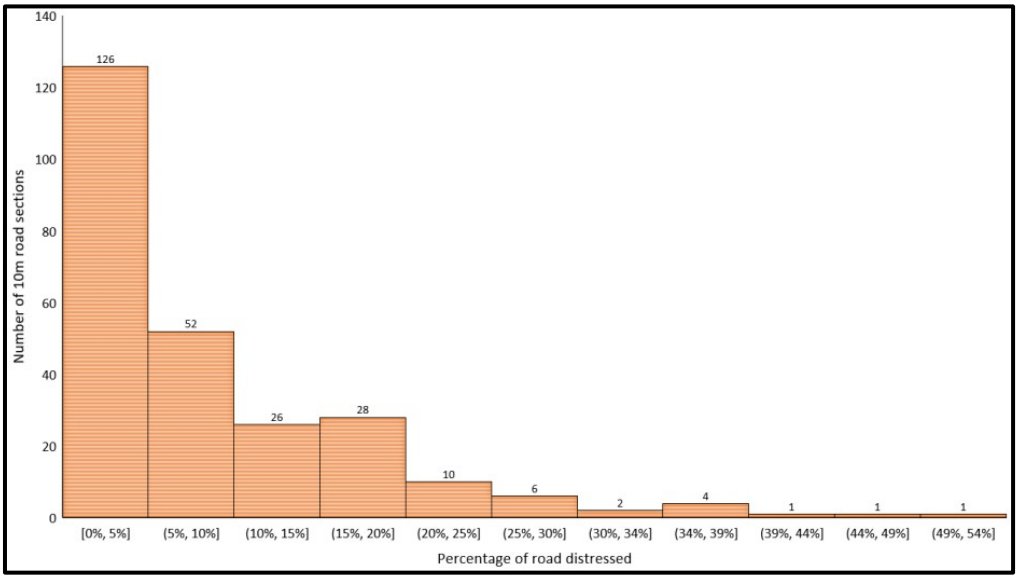

Figure 7-3. Histogram displaying of sections of the road and the respective percentages distressed. (Using distress detection model discussed in chapter four)

For the road section under analysis in Figure 7-3, most of the intervals have damaged areas with distressed levels of 0 to 5% with only a few intervals having sections where most of the road has suffered damage. Similar representations can thus be made for each road section that is surveyed over a network. After this, comparisons could be made between them to see which roads have more distressed sections and therefore which should be prioritized for interventions. This will lead to a further channel for monitoring the health of road networks and optimizing maintenance activities. For the methodology proposed, the computational power would be relatively high at the point of model creation as dictated by the deep learning methodologies developed and the power needed to run the TensorFlow model. Once the model has been validated for a given network, an application can then easily record the points of interest, their location and the percentage of damage incurred on the pavement. This is as a result of the application producing grouped georeferenced data on the damaged points and sections with the definitions of severity already defined within the model. This data can essentially be put in the form of a logged CSV file which is not computationally difficult to interpret. Whilst it should be noted that this could produce a very large file based on the size of the network, the data can be manipulated within a simple statistical programming environment to produce figures such as Figure 7-2 and Figure 7-3, which visually depict the points of interest along the network and thus the points for maintenance. The data analysis can be further streamlined to highlight other practical examinations considering other environmental factors and testing on larger networks.

The case study presented and illustrated represents a snapshot of what is possible with the developed models in hand. Based on the overall results of the models developed in Italy, it was instructive to consider a similar pipeline but in different environments. This was done to understand the differences in developing models under different circumstances. To this end, the pipeline was tested in France.

7.2 Testing pipeline in a different setting – Case study in France

7.2.1 Background of the case study

For the case study in a different environmental context, France was chosen with the aim to build upon previous research done in Italy. However, the conditions present in France and Italy vary significantly and even vary based on the type of road network considered. Therefore,

the subsequent modelling processes needed to be adapted. This adds to the current research by providing an idea of what is needed to adapt systems in different environments. Consequently, it was critical to establish the context and background of the situation in France and the particular road network to be studied. The road network of France is broken down into several different tiers, as depicted in Figure 7-4 [352]. Beside this hierarchy, there are also over 10,000km of highways managed by private operators.

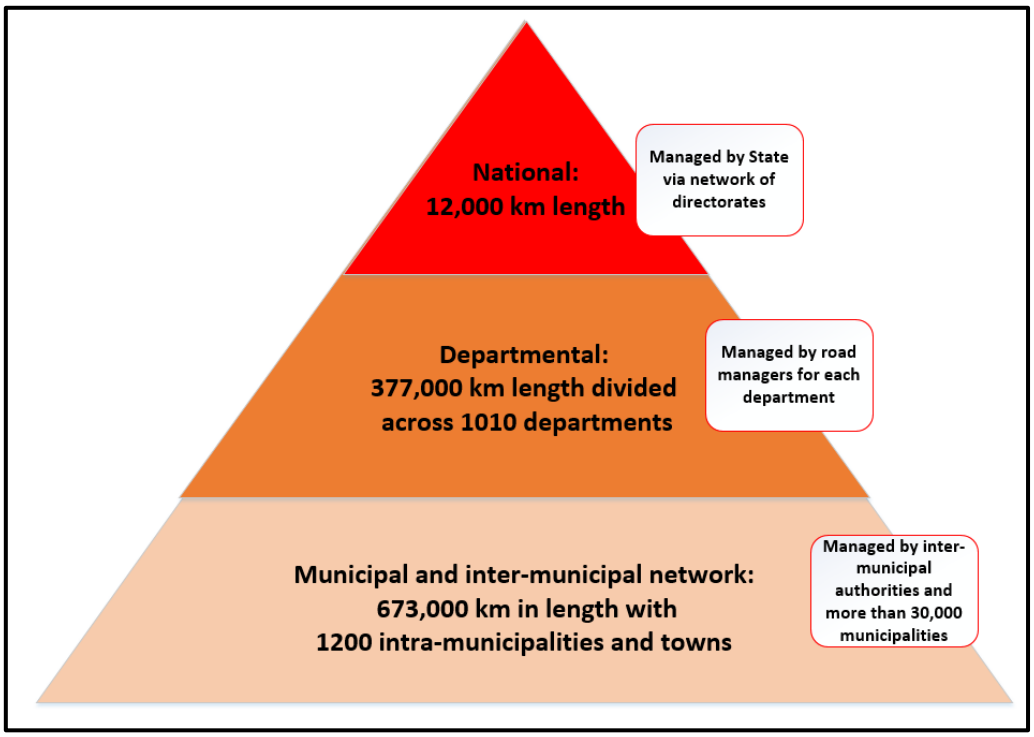

Figure 7-4. Breakdown of how roads are managed in France

Of particular concern and focus are the secondary departmental roads, which are managed by different road managers in the various cities. The cause of concern and the impetus of the work in this case study is that there is little to no available information on the road conditions of these secondary roads. Recent reports have shown that in their networks, visual surveys are relied on with automated methods being reserved for more trafficked networks. Systems and performance ratings are built on consolidated systems of noting degradations with only approximately 40% of departments using automated methods [352]. As a result, maintenance programs are built on ad-hoc pre-planned systems with renewal rehabilitation typically carried out after 14.4 years for local roads. Whilst this is also a major problem in Italy, particularly in the south, where the original case studies are focused, the distresses on these roads are not similar to those in Italy. The general size of the distresses are smaller and further complicating the situation is that a different measurement system is utilized in France based

on their standards. Based on these factors, it was necessary to consider the model pipeline from its inception. The models in this case study, therefore, would focus on local secondary roads and the aim would be trying to achieve a system that could reliably garner information on the roads to feed towards the various road managers. It is very important that models are context-specific and whilst models developed in one country could be used for another, the road networks would have to be similar with similar geographical and environmental characteristics. For the French secondary roads considered, the French regulations require inspections to be done where only the detection of a few number of distresses need to be recorded and the severity level recorded being either significant or grave – 'M3' survey level [353]. This means that just the simple detection of some categories of distress on these roads is very useful, and models delivering this would be highly welcomed. As a result, the categories used for developing the detection models were based on gaining information that would satisfy these data requirements. Higher trafficked roads require more information on distresses with a wider severity detection needed. Once again, this emphasizes the importance of understanding the environmental context of the road network and system.

7.2.2 Data collection and description of the dataset

The first step was detailing the types of distresses that would be considered in the images. A database containing 56,783 images captured across secondary roads was used. The images in the database were taken from a webcam affixed to a road survey vehicle and aimed directly at the pavement's surface in a top-down perspective as shown in Figure 7-5.

Figure 7-5. Webcam set up for capturing images in France

This database represented images from an entirely different perspective from the previous analysis. This, therefore, produced the opportunity to create models with different challenges and the output would lead to a more comprehensive assessment of generating different image detection pipelines. After an overview of the database, it was determined that six distress categories would be considered. These categories were in line with descriptions of the categories according to the French Manual for distress collection and identification [354], which is critical to do as previously highlighted in chapter three. The categories were:

1. Ravelling (denoted as RV)
2. Transverse Cracking (denoted as TC)
3. Longitudinal cracking outside of wheel path (denoted as LC1)
4. Longitudinal cracking within wheel path (denoted as LC2)
5. Alligator/Block cracking outside of wheel path (denoted as BC1)
6. Alligator/Block cracking within wheel path (denoted as BC2)

These distresses are more specific than the categories previously used and therefore represent a different way of analysing a pavement network. Once the description of distresses was decided, the next step was an analysis of the complete dataset of images to highlight and pinpoint images that contained the relevant distresses. This was done manually and the distresses were identified and recorded using the LabelImg open-source software as used before in earlier modelling [348]. The number of distresses identified are detailed in Table 7-3.

Table 7-3. Annotated Distresses in the first dataset

Distresses	Number of occurrences	% of occurrences of the total dataset
RV	904	1.59%
LC1	676	1.19%
LC2	545	0.96%
TC	565	1.00%
BC1	347	0.61%
BC2	243	0.43%

Based on the available labelled dataset it was observed that the number of BC1 and BC2 distresses were significantly lower than the other distresses and therefore a decision was made to combine BC1 and BC2 as both were the same distress type except for the location of the distress relative to the wheel path. It is useful to avoid types of categories with low numbers of occurrences, in relation to the other categories in the training, because it is more difficult to ascertain a model with smaller training numbers and it is more likely that the model will overfit and be practically unusable. The combined class would be referred to as BC1. They

were initially separated because of the distinction made in the French distress category manual as is the separation with LC1/LC2 which is different from the Italian setup. This resulted in a final dataset to be applied as shown in Table 7-4. The original dataset including both categories was also tested and the results are given in section 7.3.

Table 7-4. Annotated distresses using only 5 categories

Distresses	Number of occurrences	% of occurrences of the total dataset
RV	904	1.59%
LC1	676	1.19%
LC2	545	0.96%
TC	565	1.00%
BC1	590	1.04%

This dataset amounted to 2325 images with 3280 annotations (1.4 per image) out of the complete set of 56,783 images (4.09% of images). In an attempt to increase the dataset size to try and produce better results (given the tendency of deep learning to function better with more data [301]), augmentations were considered and applied before the training of the model. Augmentations can also be considered during training but by carrying out the processes before, it would save memory and allow for faster data processing during the training.

7.2.3 Object detection models considered

For model development, the Tensorflow [290] library was utilized in the same process as depicted in chapter 6 for the Italian models. Several of these models were utilized in this case study from the open-source TensorFlow object detection API zoo [355] and these were:

- ssd_mobilenet_v2
- ssd_inception_v2
- faster_rcnn_inception_v2
- ssdlite_mobilenet_v2
- ssd_mobilenet_v1_fpn
- ssd_mobilenet_v1_ppn

These models were chosen based on earlier work [87] and the examination of the backbones of the models as explored in chapter five.

7.2.4 Model workflow

For the training, the workflow given in chapter 6 (Figure 6-23) was used wherein the files necessary for the training are developed using various scripts to be used in the TensorFlow environment. Additionally, it is important to point out that the dataset was split for training, valuation and testing in the same ratio of 70:20:10 used previously for the other models. The

valuation set was used to evaluate the model during the training processes. Finally, the test set was used after the model was deemed to be completed to simulate a real-world test as the images used in this test had not been previously revealed to the model in the earlier stages of the process.

7.2.5 Computational times

Two different workstations were utilized for modelling. The faster of the two was a Windows 10 PC with an NVIDIA Quadro P4000 GPU (8 GB ram) with a cuda compatibility of 6.1 and total CPU memory of 32 GB. The second one was also a Windows 10 PC with an NVIDIA Quadro K420 graphics card, which has a cuda compatibility of 3.0 and a total CPU memory of 16GB. The cuda compatibility of the second workstations limits the use of TensorFlow GPU, which requires a minimum CUDA compatibility of 3.5. This is important as the GPU version of TensorFlow allows the workstation to take advantage of the advanced graphics card and memory within the system. Given the large differences between the systems, the computational processing times clearly show the impact of pc memory and speed on the process which is an important consideration for initial model development. The general speed of the model on the faster workstation is approximately 0.6 seconds per training step with an average of 200,000 steps utilized in the modelling process. The faster of the models, as expected, was the mobilenet one, which is a model that was developed with the clear purpose of mobile deployment.

7.3 Case study Model testing and optimization

In the first instance of testing, the full dataset with five different base models and utilizing the six previously referenced classes. The results of these initial models are depicted considering the three base metrics and are shown in Figure 7-6, Figure 7-7 and Figure 7-8.

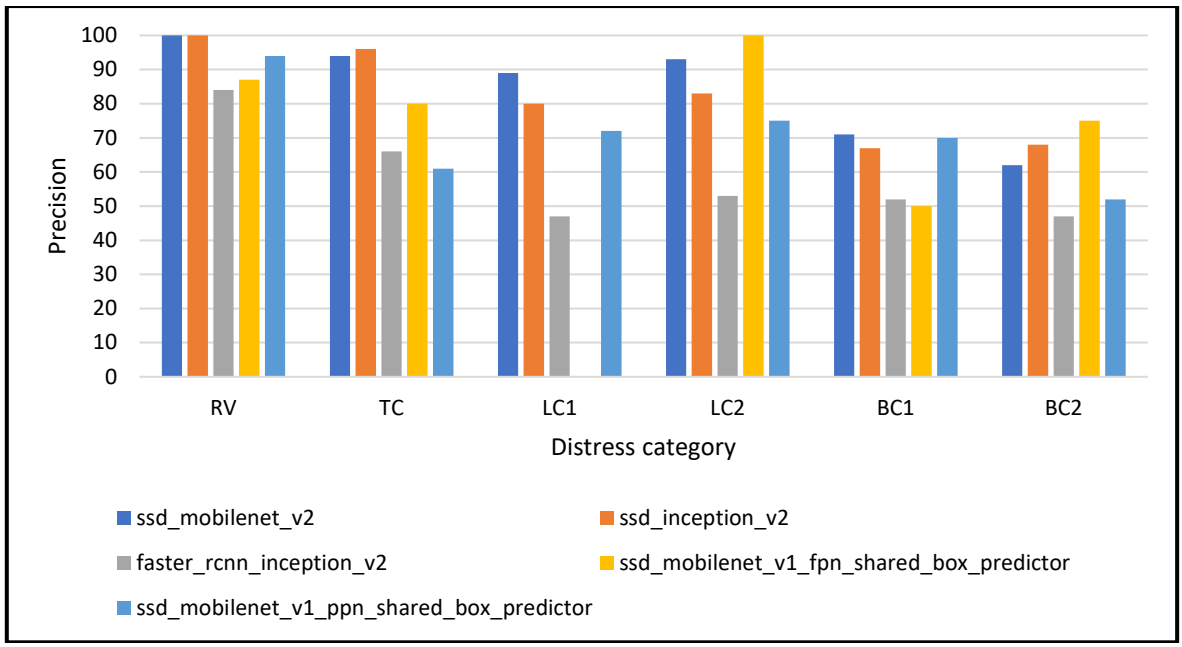

Figure 7-6. Examination of the Precision metric across models

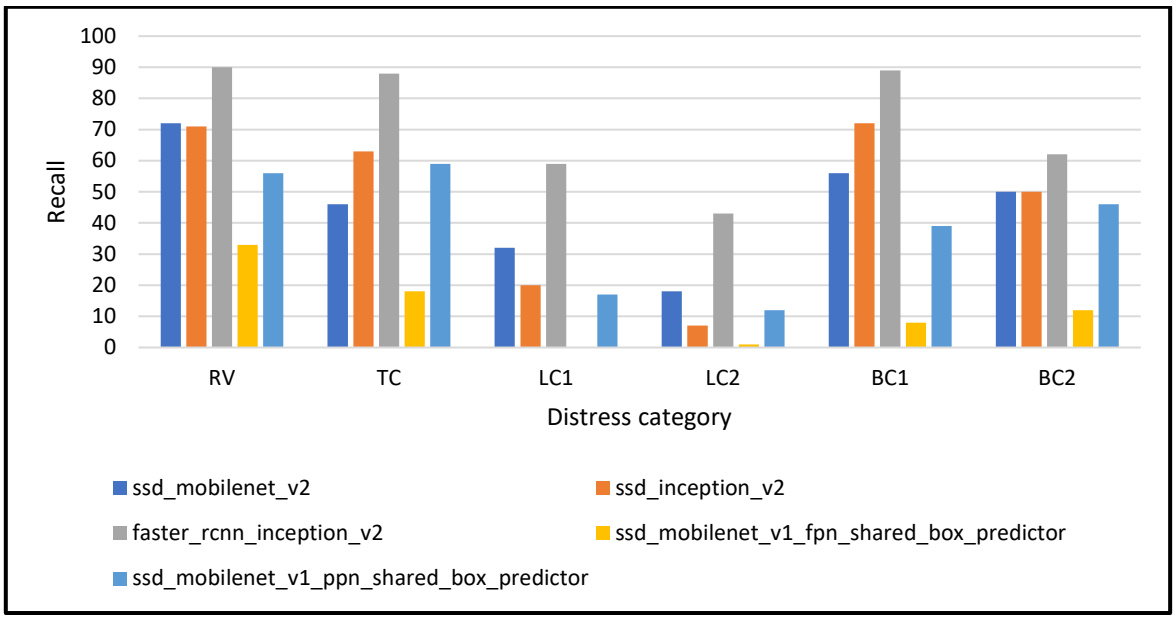

Figure 7-7. Examination of the Recall metric across models

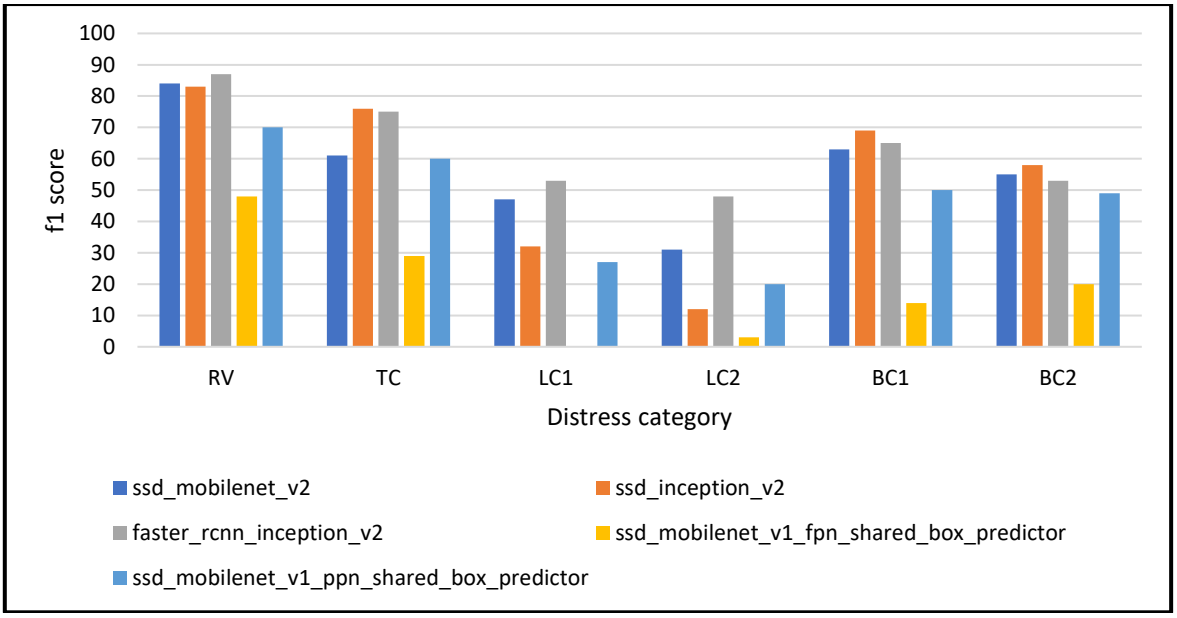

Figure 7-8. Examination of the f1 score metric across models

Considering an overview of the results of these models, there were high levels of precision achieved for the majority of distresses but lower levels of recall, particularly for the longitudinal cracking and block cracking categories. It was also noted that the base models of the 'ssd_mobilenet_v1_fpn_shared_box_predictor' and the 'ssd_mobilenet_v1_ppn_shared_box_predictor' both performed quite poorly with the former of two seemly seemed unable to produce usable results at least under the used configurations of the models. It should not be ruled out that other configurations could yield usable results and therefore further investigations into these models could remain an option. From the figures, it was shown that the models generally were able to detect the distresses of ravelling and transverse cracking the best. The poorest performance was seen with the longitudinal cracking category. To this end, augmentations and changes to the configurations were subsequently carried out using the base models of mobilenet, inception and faster-rcnn, which are the same base models from the Italian models. Additionally for this testing, the database used was reduced to produce a more balanced set as shown in Table 7-5.

Table 7-5. Annotated distresses in 'balanced' set

Distresses	Number of occurrences
RV	672
LC1	670
LC2	569
TC	566
BC1	540

7.3.1 Augmentation considerations

Several different augmentations were considered and applied using Python, namely:

- A random augmentation of brightness
- A random augmentation of exposure applied (note - brightness applies to all pixels, exposure intensifies highlights in image)
- A random augmentation of a Gaussian blur

Additional augmentations were also considered during the training process. The augmentations considered at this point were:

- Random horizontal and vertical flips
- Random crops
- A random augmentation of contrast adjustment
- A random augmentation of pixel normalization

The augmentations done were used so that the dataset was essentially tripled to provide a larger database and theoretically better results. In theory, the augmentations should provide better modelling results but this study aimed to explore the actual effects. To determine the effects of the added augmentations, a base case without the use of any augmentations was considered and results were measured against this model's results. When analysing the results and changes of the augmentations, the changes varied across the distress types and with reference to precision and recall. As the f1 score represents a combination of these two metrics, the impact of the augmentation changes on the f1 score is highlighted in Figure 7-9.

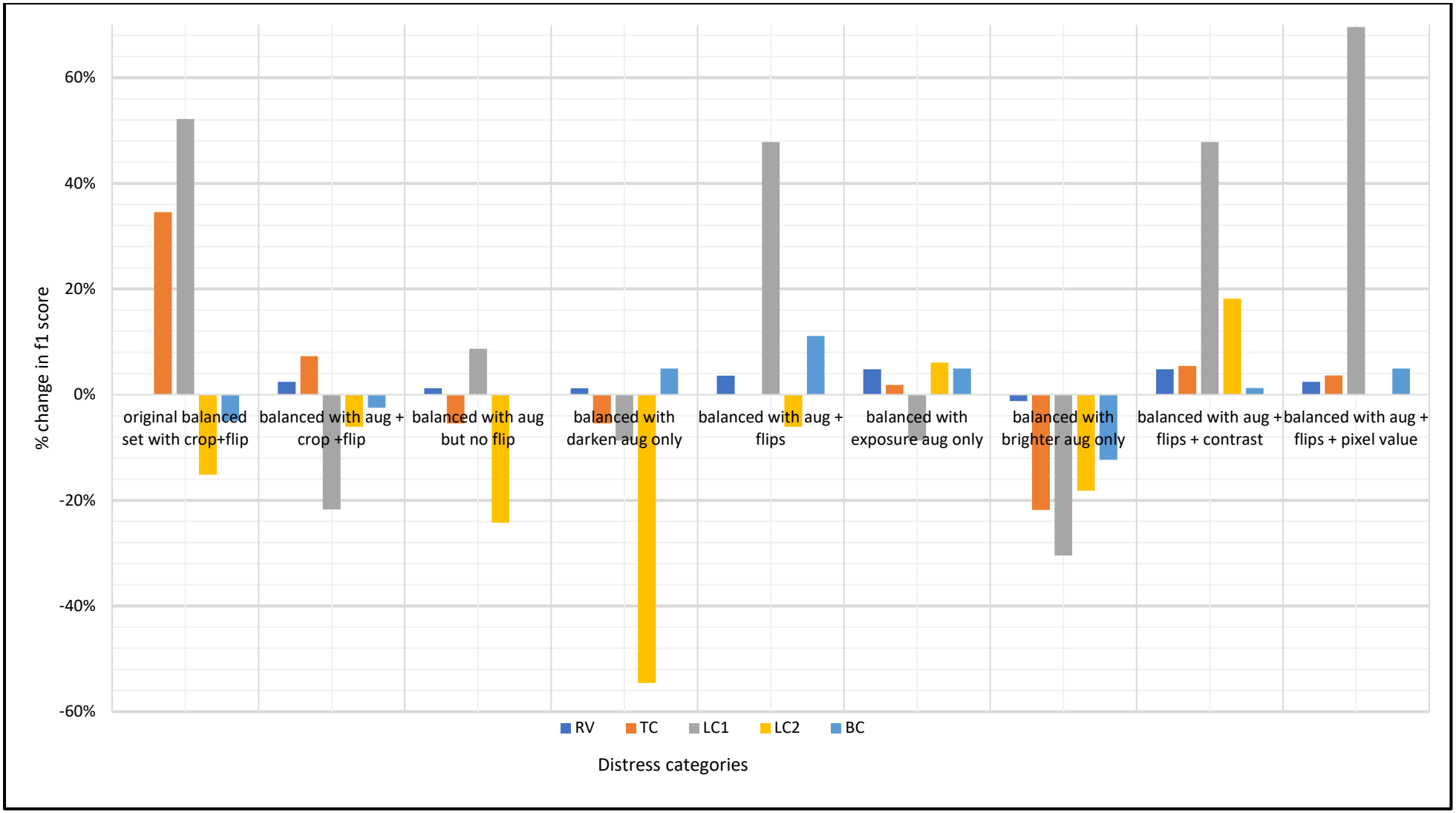

Figure 7-9. Changes in f1 scores using different augmentations vs. reference case with no augmentations

In Figure 7-9, it can be seen that some augmentations had very marginal effects on the performance of the models and some had negative effects on the performance in some instances. The following important points were ascertained from the results:

i. The augmentation of a random crop had negative effects particularly on distresses where the location was important (Longitudinal cracking within the wheel path – LC2). This is rational as a crop would allow the distress not to appear in its precise location. However, it was originally considered as a positive as the augmentation was used successfully in the previous model in Palermo but in that set up the position of the distress was not important. This underscores the importance of establishing criteria based on specific site information and exact distresses.

ii. The effect of brightening seemed to be more effective than that of darkening which caused significant drops in performance. When examining photos, it could be seen that this augmentation showed mixed performance as some images appeared better when brightened whereas some in their original instance suffered from too much light and therefore darkening helped. This led to the consideration of exposure, contract and pixel value changes as these alterations focus on the particular allocation of pixels within the image and not a generic application to the entire dataset. These augmentations are however not natural and therefore particular attention has to be paid to their use.

iii. The use of horizontal and vertical flips appeared to provide a positive response to performance though it can also be considered marginal.

iv. A combination of flips with random changes to the contrast proved to be the best combination of augmentation for this exercise.

v. The augmentations generally had little positive effect on increasing the performance of the models to detect longitudinal cracking.

vi. It is simply not good enough to assume the positive effect of an augmentation and for practical implementation, testing must be done to determine the best combinations.

After all the testing, the best three models as defined by the combined metrics of precision, recall and the f1 score are given in the following section. Additionally, whilst these metrics provide a succinct performance, the confusion matrices and related positive and negative detections observed during the tests were also analysed as they provide the actual numbers of instances of false and missed detections. These are given below.

1. The **model using the base model of ssd_mobilenet_v2** and using a balanced dataset and augmentations of brightened images and random horizontal and vertical flips:

Table 7-6. Model results of best version of model based on ssd_mobilenet_v2 model

category	precision_@0.5IOU	recall_@0.5IOU	f1
RV	98%	68%	81%
TC	95%	29%	44%
LC1	91%	33%	49%
LC2	79%	28%	42%
BC1	92%	59%	72%

Table 7-7. Confusion matrix and corresponding positive and negative detections for ssd_mobilenet_v2 based model

RV	**TC**	**LC1**	**LC2**	**BC1**	
64	0	0	0	1	29
0	18	0	0	0	45
0	0	21	2	1	39
0	0	1	15	1	36
0	0	1	1	35	22
1	1	0	1	0	0

	TP	FP	FN	TN
RV	64	1	30	89
TC	18	1	45	135
LC1	21	2	42	132
LC2	15	4	38	138
BC1	35	3	24	118

2. With a **base model of base ssd_inception_v2** and using a balanced dataset and augmentations of brightened images along with random horizontal and vertical flips:

Table 7-8. Model results with the best version of the model based on ssd_inception_v2 model

category	precision_@0.5IOU	recall_@0.5IOU	f1
RV	95%	79%	86%
TC	96%	39%	55%
LC1	93%	21%	34%
LC2	82%	19%	31%
BC1	90%	90%	90%

Table 7-9. Confusion matrix and corresponding positive and negative detections for ssd_inception_v2 based model

RV	TC	LC1	LC2	BC1	
60	0	0	0	1	15
0	22	0	0	0	35
0	0	14	1	1	51
0	0	0	9	2	37
0	0	1	1	44	16
3	1	0	0	1	0

	TP	FP	FN	TN
RV	60	3	16	89
TC	22	1	35	127
LC1	14	1	53	135
LC2	9	2	39	140
BC1	44	5	18	105

3. With a **base model of faster_rcnn_inception_v2** and using a balanced dataset and augmentations of brightened images along with random horizontal and vertical flips.

Table 7-10. Model results with the best version of model based on faster_rcnn_inceptionv2 model

category	precision_@0.5IOU	recall_@0.5IOU	f1
RV	88%	86%	87%
TC	58%	86%	70%
LC1	60%	81%	69%
LC2	53%	52%	53%
BC1	76%	92%	83%

Table 7-11. Confusion matrix and corresponding positive and negative detections for faster_rcnn_inceptionv2 based model

RV	TC	LC1	LC2	BC1	
65	0	1	0	1	9
0	49	0	0	1	7
0	0	54	3	2	8
0	0	9	25	1	13
0	0	1	0	57	4
9	35	25	19	13	0

	TP	FP	FN	TN
RV	65	9	11	185
TC	49	35	8	201
LC1	54	36	13	196
LC2	25	22	23	225
BC1	57	18	5	193

From the tables, it can be shown that the models based on the SSD network with the inception and mobilenet configurations achieved greater levels of precision but lower levels of recall as compared to the faster-rcnn based model similar to the performance in the Italian models. It is also instructive to note that the first two are models which take a 'one-shot' look approach at determining the location of objects in the images, whereas the faster-rcnn one takes a region proposal approach making the case that for distress detection this plays a significant role considering the sizes of pavement distresses. The f1 scores for the models from the tables are visualized in Figure 7-10 where it can clearly be shown that the best overall model was the one based on the faster-rcnn model.

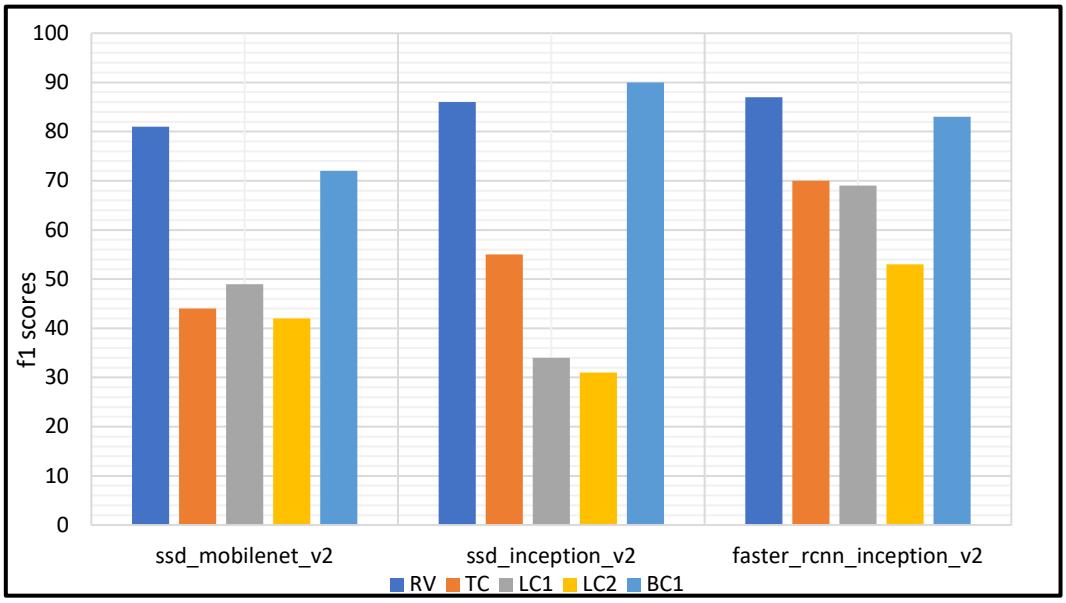

Figure 7-10. Comparison of f1 scores of the best three models

Furthermore, it should be noted that the first two models, therefore, produce lower levels of false positives – as high levels of precision imply – but in the same instance produce a larger number of false negatives (missed detections). The importance of this has to be decided by the stakeholder that the model is directed at, as some companies/authorities may value false detections higher than missed detections.

7.3.2 Effects of threshold and confidence on model

Once it was determined which three of the models had the highest performance, an investigation was carried out to determine the effects of the model with changes to the Intersection over Union (IOU) Threshold and the Confidence threshold. The IOU threshold is a value that is commonly used in object detection to measure the overlap of predictions versus the actual bounding box for an object. It has a range of 0 to 1, where one represents a perfect

overlap of detection and the ground truth. An illustration of what the IOU represents is given in Figure 7-11. It must be noted here as well that the models were trained with a minimum IOU Threshold of 0.5.

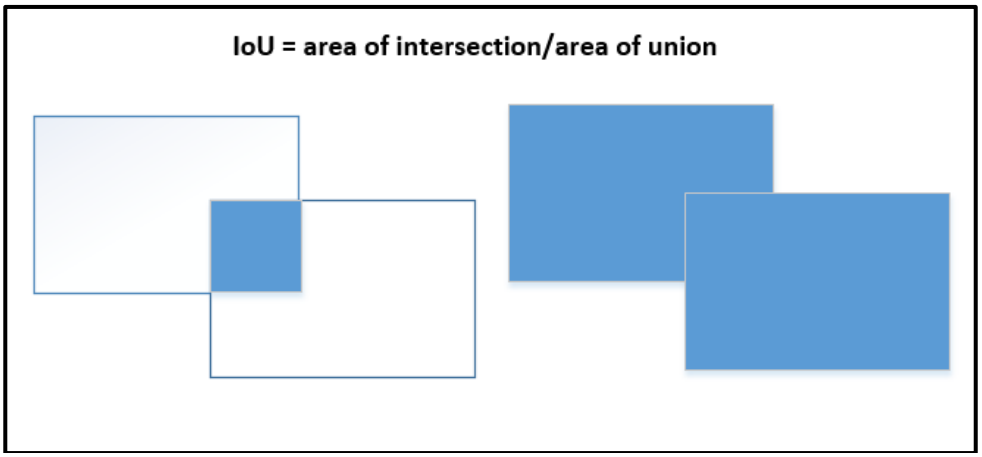

Figure 7-11. Visual representation of the Intersection over union principle

Confidence meanwhile refers to the score of the model in predicting the class, which is the 'sureness' the model has when making a prediction. The confidence threshold, therefore, sets the minimum value that the model score should be before returning a result of a detection in the results. For this task, a range of IOU thresholds was utilized from 0.10 to 0.95 with a fixed confidence threshold score of 0.50. Additionally, the confidence score was also altered with a range of 0.10 to 0.95 with a fixed IOU Threshold of 0.50. A third test case with equal values of IOU and confidence threshold was used with the same range. This process was tested on the three best model iterations of the ssd_mobilenet_v2, ssd_inceptionv2 and faster_rcnn_inceptionv2 models generated as referenced in the previous section. The results of each case study on the models are given below.

1. Effects on ssd_inceptionv2 based model

Controlling confidence and altering threshold – in the first case, the confidence level was controlled with varying levels of threshold applied from 10% to 95%. In this test, there was no effect on the general performance of the model (as characterized by the f1 score in Figure 7-12). After a threshold of 75% was applied however the f1 scores began to fall.

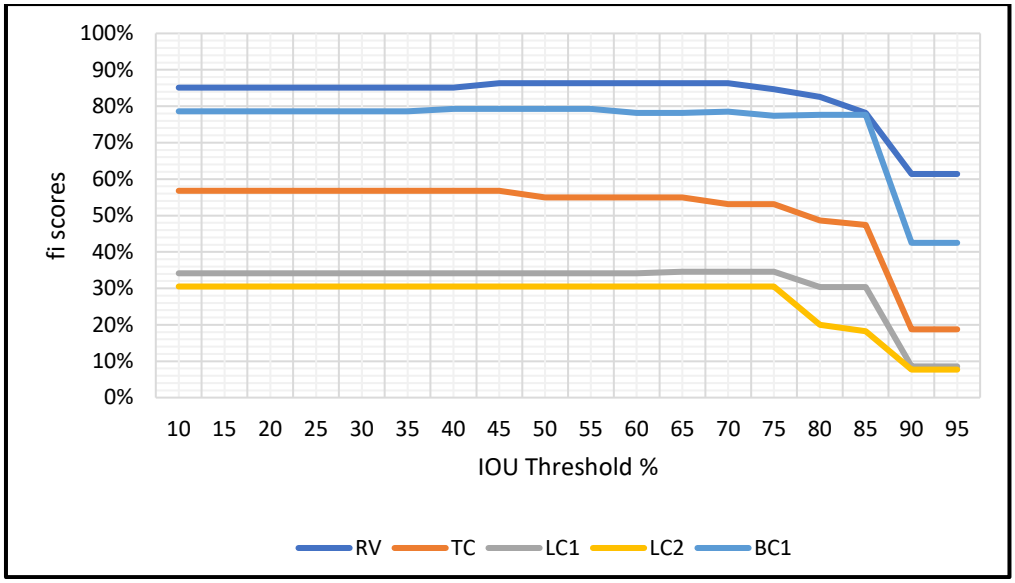

Figure 7-12. Variation of f1 scores with altering IOU Threshold

Controlling threshold and altering the confidence levels: in the second instance the IOU threshold was maintained at 50% and confidence levels were changed. With this in place, it was noted that the performance of the model dropped across categories incrementally as shown in Figure 7-13.

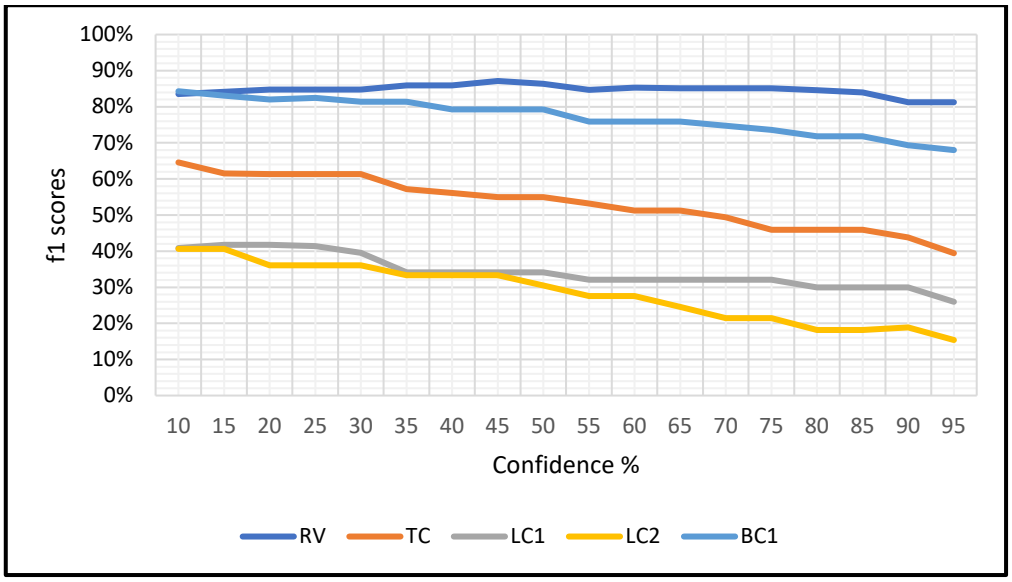

Figure 7-13. Variation of f1 scores with altering confidence threshold levels

Altering levels of confidence and threshold simultaneously – in the final case, both the threshold and confidence were varied. With this, there was a similar drop to that of Figure 7-12 with the performance diminishing after 75% in line with results in Figure 7-14.

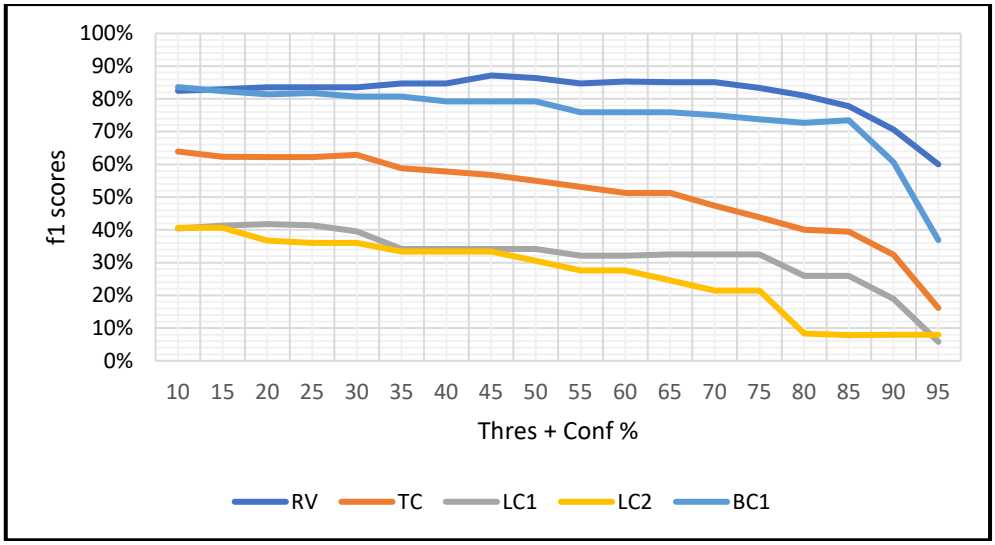

Figure 7-14. Variation of f1 scores with altering both confidence and IOU threshold levels

2. Effects on mobilenet based model

For the mobilenet-based model, the same tests were performed and the results mirrored that of inception as shown in Figure 7-15 when the threshold was varied with no effect until approximately 75% IOU threshold.

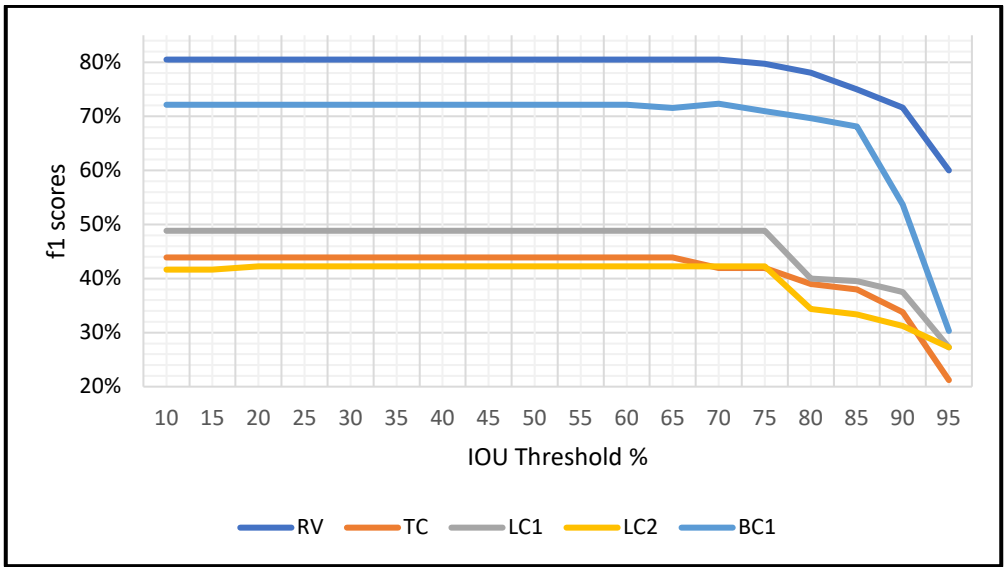

Figure 7-15. Variation of f1 scores with altering IOU threshold

The performance of the model however significantly fell after increasing the confidence below 50% controlling confidence and altering the threshold as shown in Figure 7-16.

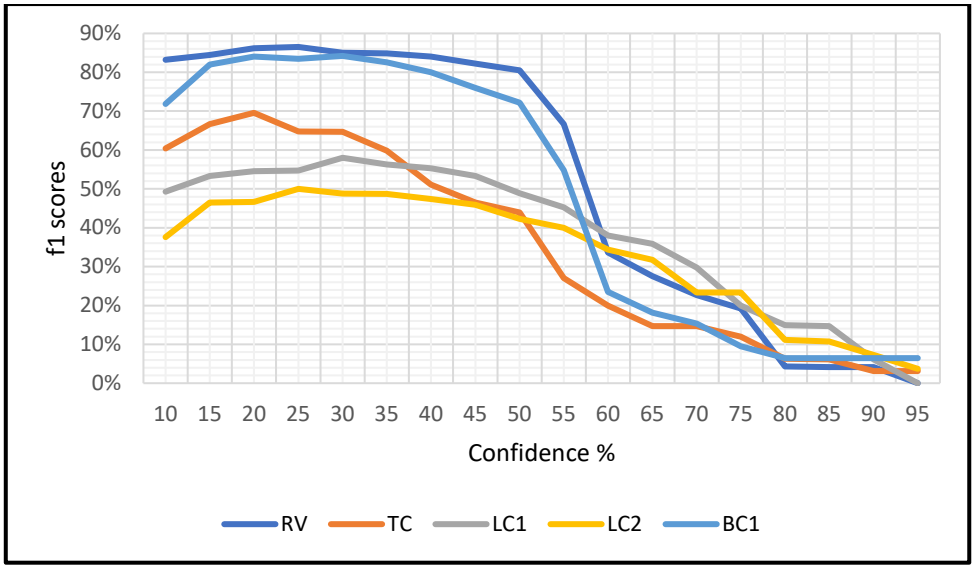

Figure 7-16. Variation of f1 scores with a confidence threshold

For the combined test, the results were again a combination of what was seen in Figure 7-15 and Figure 7-16 as given in Figure 7-17.

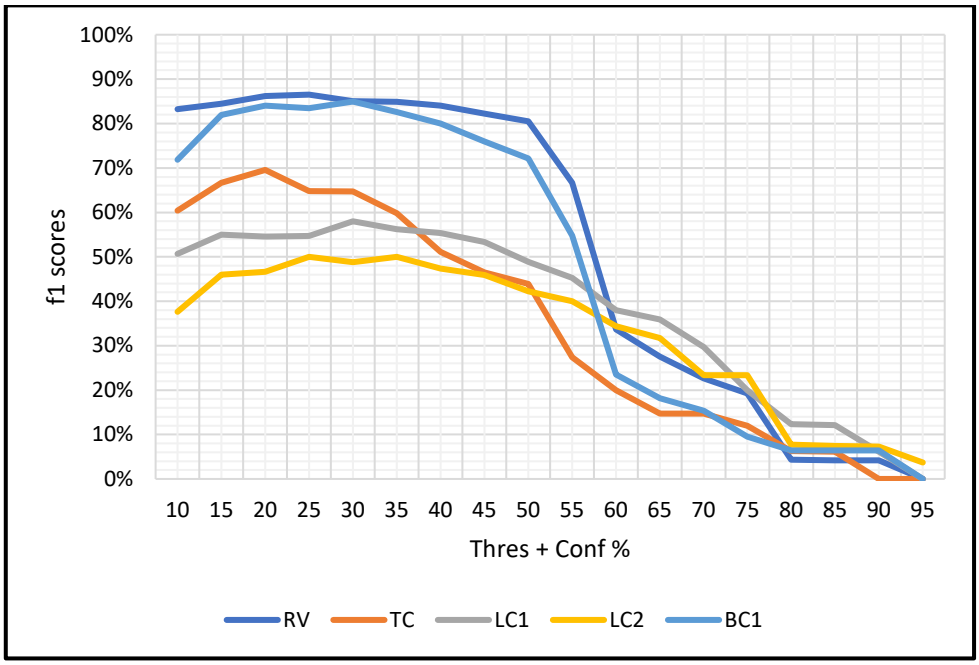

Figure 7-17. Variation of f1 scores when changing both confidence and IOU threshold

3. Effects on Faster rcnn based model

For the final model test, the performance of the model again was maintained until approximately 75% IOU threshold where its performance declined significantly and quickly as shown in Figure 7-18.

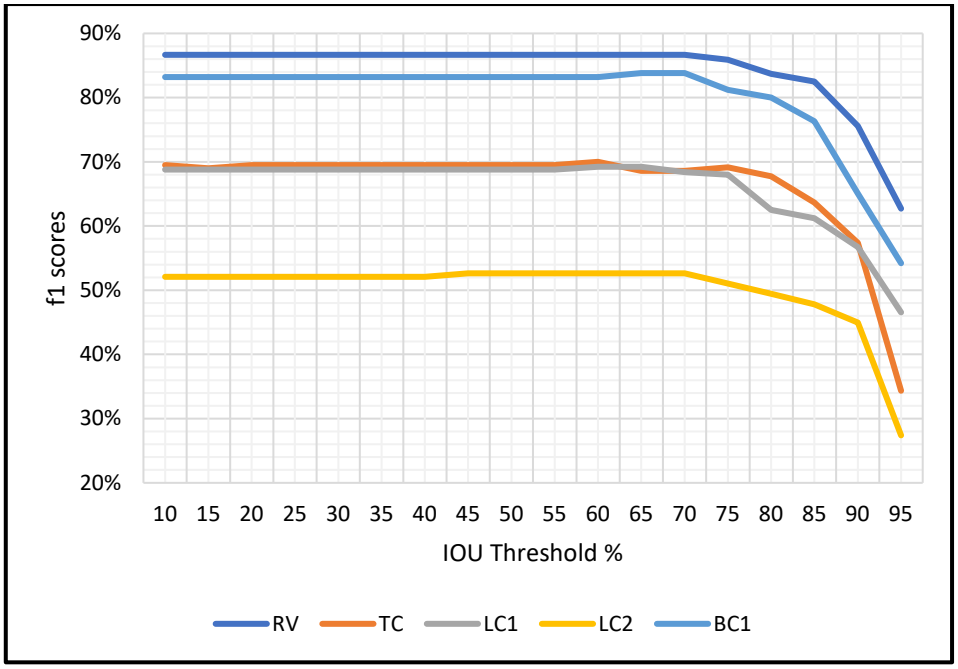

Figure 7-18. Variation of f1 scores when altering the IOU threshold

However, in the test of confidence threshold, the performance of the model increased incrementally as the confidence threshold was increased as shown in Figure 7-19.

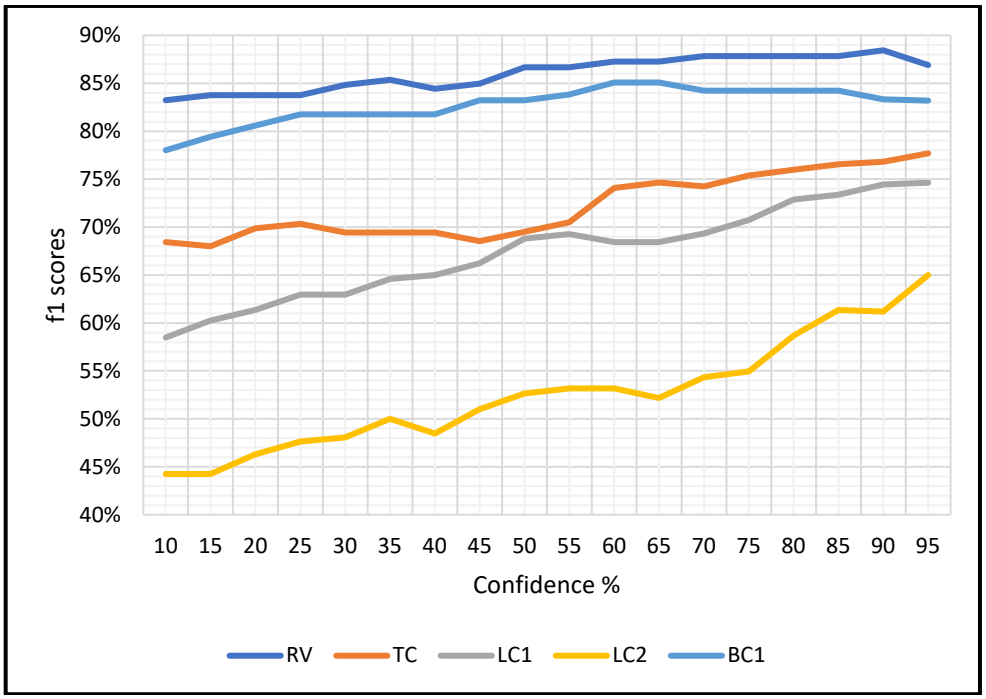

Figure 7-19. Variation of f1 scores when altering the confidence threshold

Similarly, the combination test showcased a similar pattern where performance levels fell significantly above 75% as seen in Figure 7-20.

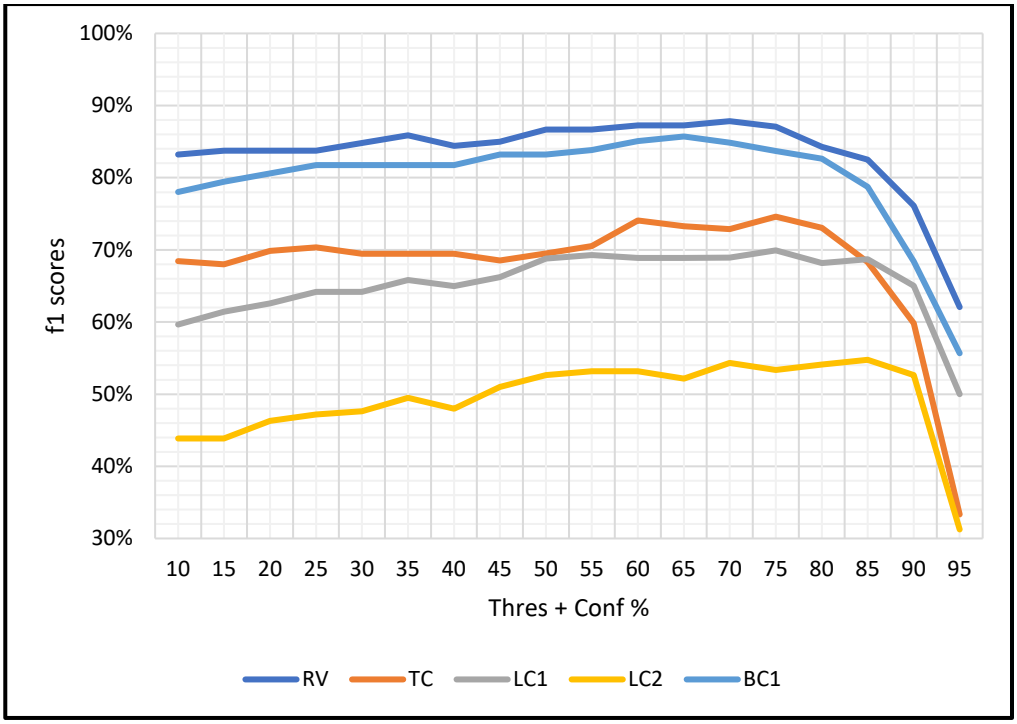

Figure 7-20. Variation of f1 scores while altering both confidence and IOU threshold

Given these results, it was concluded that the tuning of the confidence level does affect the models used. However, it appeared with the models based on inception and mobilenet, the overall performance of the models could not be increased even with the alterations to the confidence levels. To understand what could be causing these changes, the numbers of positives and negatives detected were similarly observed across the models with varying confidence levels. These graphs are shown in Figure 7-21 and Figure 7-22.

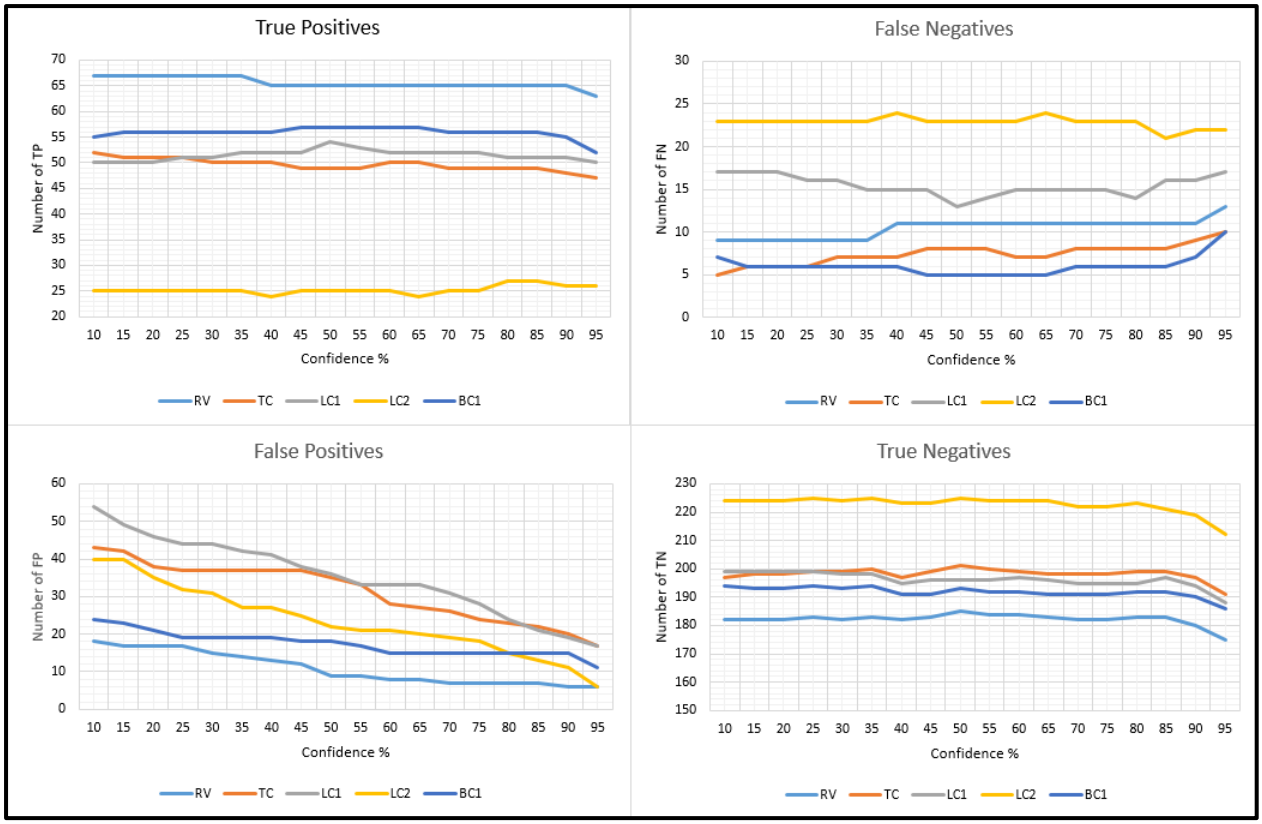

Figure 7-21. Variation of detected positives and negatives when tuning faster-rcnn based model

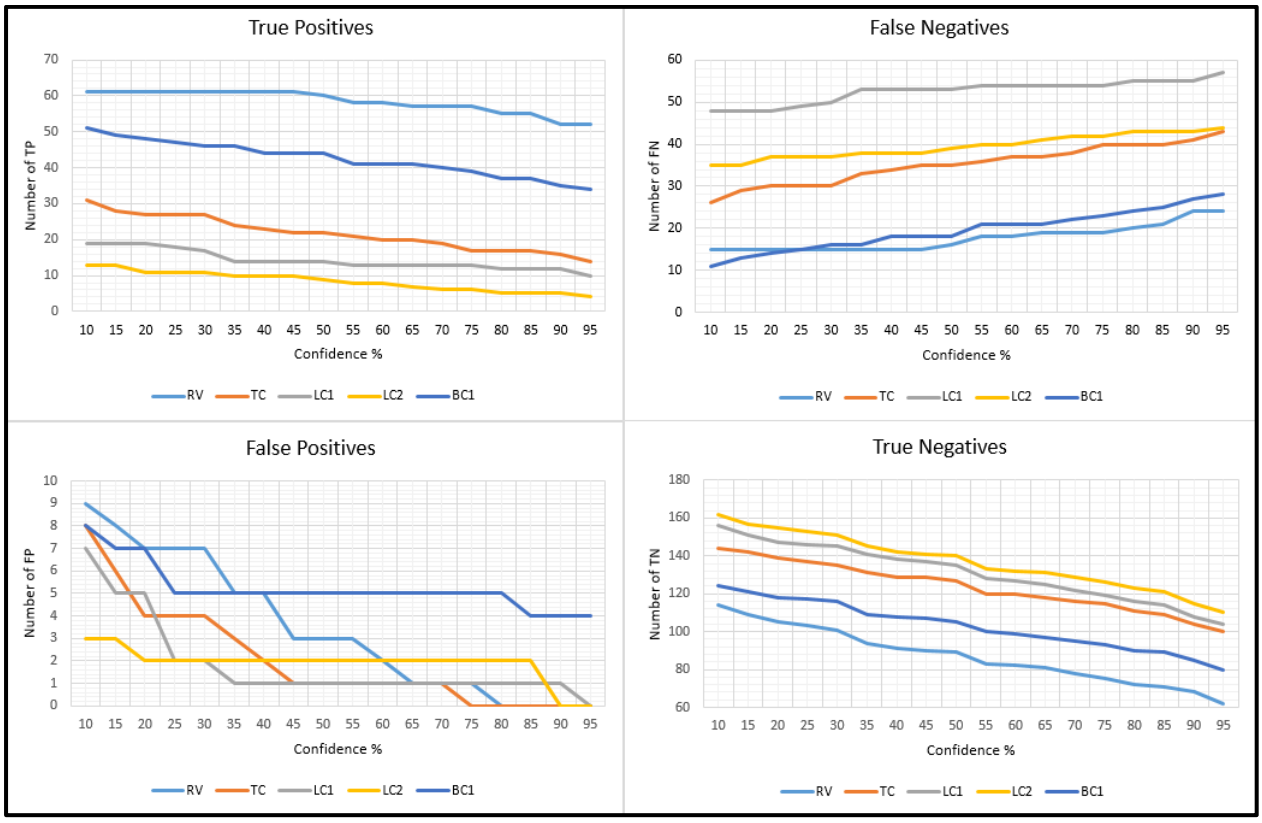

Figure 7-22. Variation of detected positives and negatives when tuning inception based model

As the inception and mobilenet model displayed similar trends, the inception model was used to compare to the faster-rcnn model. Concerning the positive and negative detections, a similar pattern is shown as seen in Figure 7-21 but because the numbers of false positives are substantially less, the effect of the confidence on the model does not produce better results.

Therefore, it is clear that when altering these values, the trained model itself must have the flexibility for any altering to be possible and effective. Essentially, there must be a higher number of false positives appearing in the results that could be filtered out with higher confidence levels. Whilst the inception model initially produced a higher level of precision, it also had a smaller number of false positives and therefore did not have much scope to be changed by the hypothesis of altering confidence.

On the other hand, the faster-rcnn based model had a lot of room for improvement in terms of the number of false positives and therefore increasing the confidence allowed the model to reduce the errors and thus produce a more robust model. It must be restated here that the models were all tested using the same test dataset, which was not revealed to the model until the testing phase and therefore represented a test akin to what could happen in practice. This is stated to establish that the effect was directly related to the models' performance on these types of images and detections.

7.3.3 Effects of location of distress category

In continuing to evaluate optimization techniques and trying to understand how models react to distress detection, a test was run to consider the use of a merged category for longitudinal cracking. This was done to understand if the precise location of the distress (lc1 being in the wheel path and lc2 being out of the wheel path) made a significant difference to the models. For this, a test was done considering a combination of the lc1 and lc2 categories into one merged category to be referred to as ‘lc1’. By doing this, all of the longitudinal cracking were consolidated into one category. Two tests were run using an inception based model and a faster-rcnn based model. The results of having one sole longitudinal cracking category showed performance was marginally increased. This is evidenced by the results in Table 7-12 and Table 7-13 and graphically represented in Figure 7-23.

Table 7-12. Confusion matrix and positive and negative detections for inception based model

	RV	TC	LC1	BC1	
	59	0	0	1	16
	0	27	1	1	28
	0	0	23	3	89
	0	0	1	47	14
	3	6	6	3	0

	TP	FP	FN	TN	Precision	Recall	F1 score
RV	59	3	17	97	95%	78%	86%
TC	27	6	30	129	82%	47%	60%
LC1	23	8	92	133	74%	20%	32%
BC1	47	8	15	109	85%	76%	80%

Table 7-13. Confusion matrix and positive and negative detections for faster rcnn based model

	RV	TC	LC1	BC1	
	64	0	1	1	10
	0	48	1	1	7
	0	0	87	3	25
	0	0	4	55	3
	8	15	26	4	0

	TP	FP	FN	TN	Precision	Recall	F1 score
RV	64	8	12	190	89%	84%	86%
TC	48	15	9	206	76%	84%	80%
LC1	87	32	28	167	73%	76%	74%
BC1	55	9	7	199	86%	89%	87%

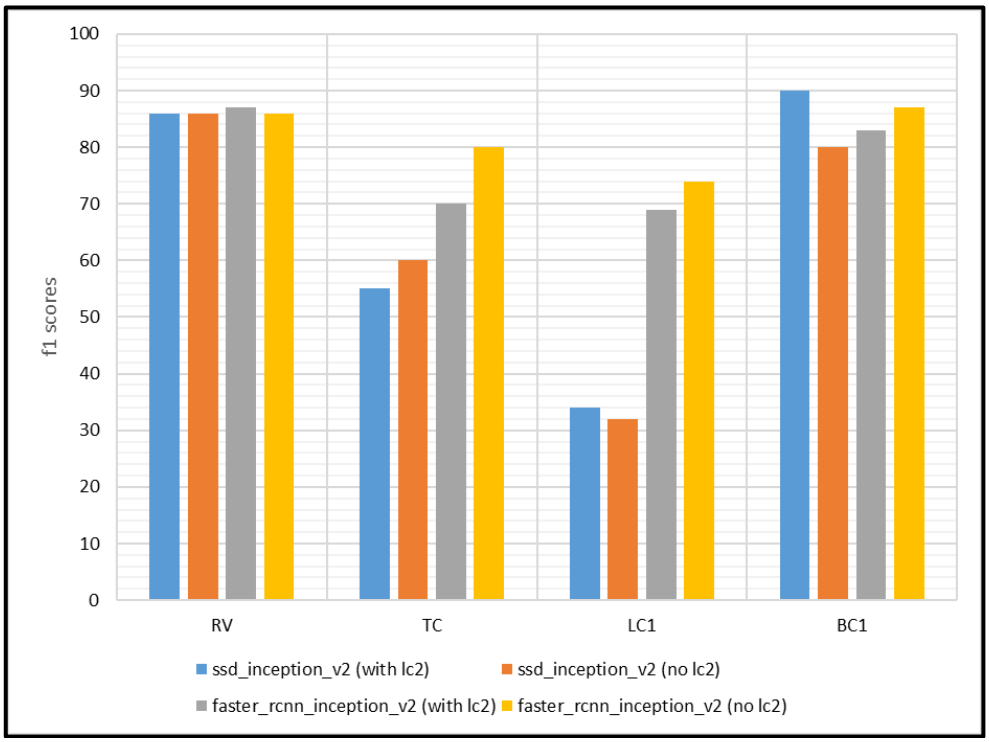

Figure 7-23. Comparison of models when merging LC1 and LC2 categories

As observed in Figure 7-23, there were marginal increases to the f1 scores. Further tests could be done with other models to see if there would be any significant differences or improvements possible with this consideration.

7.3.4 Testing images with no distress

As a further test on the robustness of the developed models, tests were carried out on blank images where there were no distresses were present. This was done as the performance of the models developed were based on test images where there were distresses present. To analyse what would happen with images with no distress another test set was used. The images within this test set had images of pavements with no distresses and involving situations where other methods would likely produce a false-positive result. Examples are given in Figure 7-24.

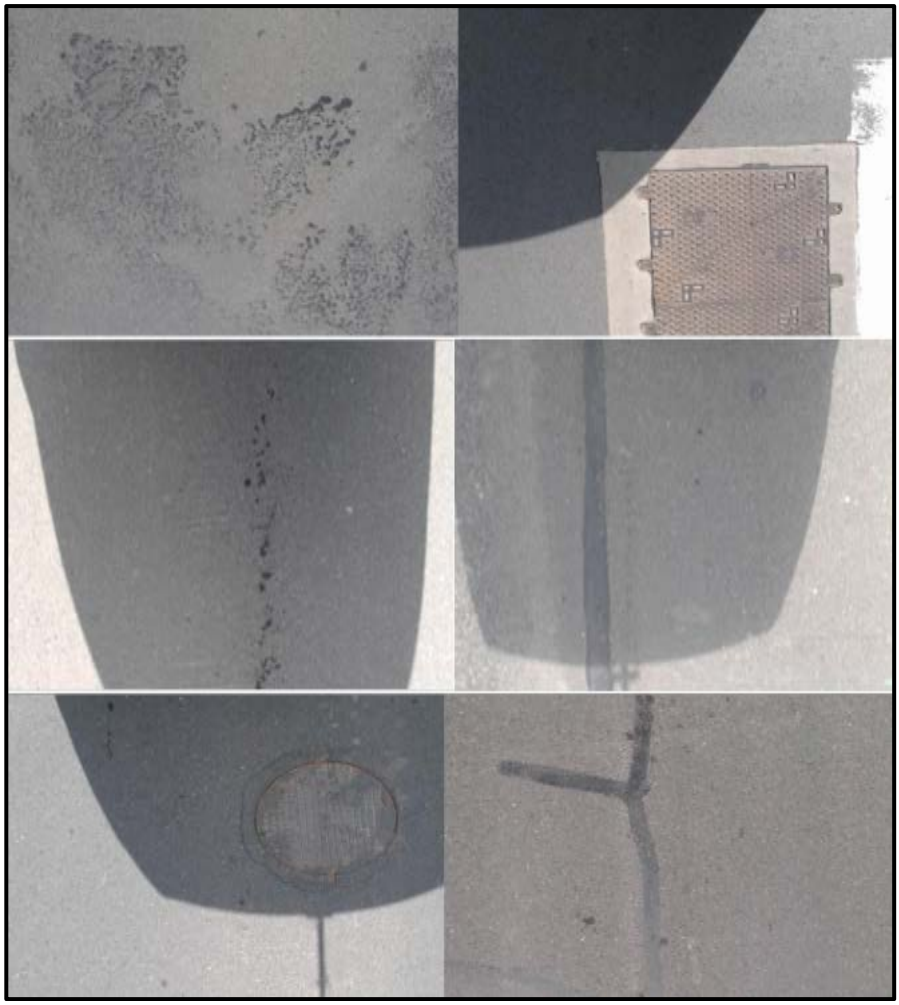

Figure 7-24. Examples of blank images used for the test

These included images with shadow projections, images with skid marks on the road, images with manhole covers and images with high contrast and brightness issues as shown. The test case tried to utilize images as shown where there were marks similar to cracks, manhole covers, discoloured sections and shadows created by the rod of the surveillance vehicle and marks from patches. A total of 210 images were used. The models were run over these images resulting in six cases of false detections representing a false rate of 2.86%. The instances where the model produced a false positive detection are given in Figure 7-25.

Figure 7-25. Instances of false detections during the blank image test

As shown, there are instances where there was a mark on the pavement similar to that of crack, two cases of discoloured surfaces being detected as ravelling and one case of a manhole cover being noted as a transverse crack. Given the small number of false detections, it should be considered as a positive outcome underlying the performance of the model. Additionally, the model did not suffer from the issues associated with other segmentation tools, which routinely produced false detections associated with shadows and markings on the road. None of the images showing the shadow of the surveillance vehicle were falsely detected as a pavement distress during the exercise. The images with false detections were ones with marks resembling a crack and of slightly discoloured roads where it appears that ravelling has not occurred but could appear in the future.

7.3.5 Understanding hyperparameter adjustments for different types of pavement images

As images obtained in real-world situations may differ (as evidenced in this study using smartphone and webcam images), the sizes of distresses within an image would change based on the camera perspective. A significant change in this perspective would be a change from a panoramic view using a camera within a vehicle to that of a camera positioned outside of the vehicle and directed vertically above the pavement. In these two situations, the number of pixels in the image where the distress occurs would change significantly. As a result of this, one of the key alterations that needs to be made while developing many detection models is the anchor box configuration.

During the modelling process, models make numerous predictions on where an object could be within the image space. Typically, thousands of boxes are generated on the image to assist in this process. These boxes should be consistent with the location, shape and size of the objects that the model is attempting to detect. This is important as the overlap between the boxes generated and the annotated training set is used for the model to understand the particular features of the annotations and their locations and shape.

As a result, it was important to establish a clearer understanding of the space occupied by the distresses in panoramic view images and top-down images to produce effective models. For this to be considered, images of each view were considered from similar road conditions on the same network in France so as to identify the differences. To this end, the CSV files generated from the annotated images containing the information on the bounding box location and sizes were analysed. As the images obtained in the two datasets were of different values, their sizes were normalized for comparative purposes using the resizing function ‘compute_new_static_size’ from the Tensorflow object detection API [355]. To this end, the distribution of the sizes and location of the bounding boxes width and height were calculated and are displayed in Figure 7-26 where the distributions on the left are of the images from the top-down database and on the right displays the boxes from the panoramic view.

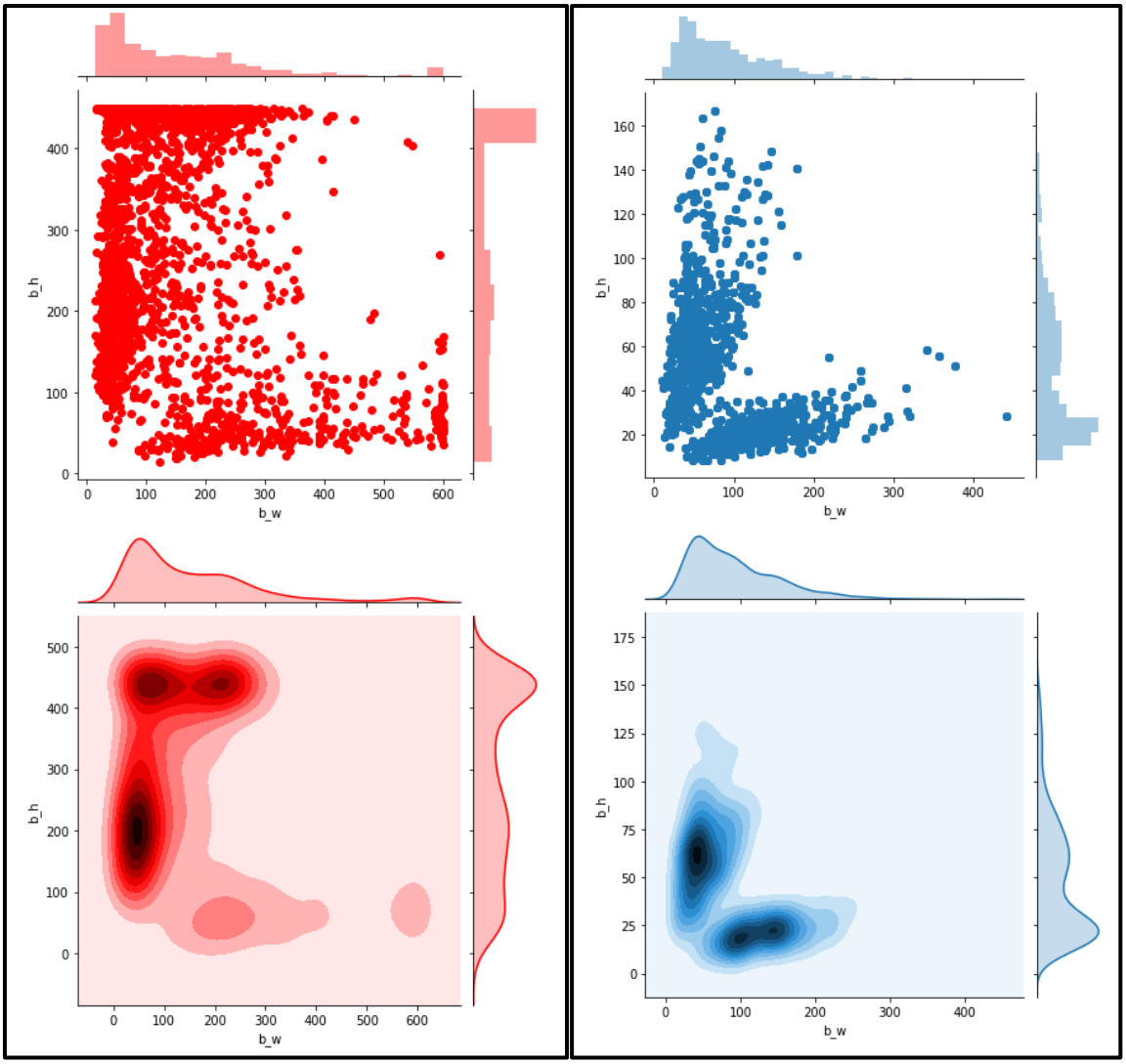

Figure 7-26. Distribution of bounding boxes of the annotated dataset (Left - boxes from the previous top-down model and Right - boxes from panoramic view)

As shown in Figure 7-26, the boxes within panoramic view are generally between a width of 0 to 200 and an average height of 100 to 500 as evidenced by the darker spots shown on the heatmap joint plots. These represent large differences in the sizes of the boxes which further explain why similar configurations of models are not transferrable based on location alone and the camera perspective is very important. To further explain this, generic examples of anchor box configurations used on the images are illustrated in Figure 7-27 and Figure 7-28 where the same anchor box configurations are shown on the images of different perspectives (one from a smartphone with a panoramic view and the other from a webcam looking down at the pavement. Within the figures, it can be observed that the anchor box configurations used for the top-down images are not suitable for the level and size of distress shown on the

panoramic images. As a result, this would make it more difficult for the model to pinpoint where the annotation is and subsequently understand the particular features of the distress.

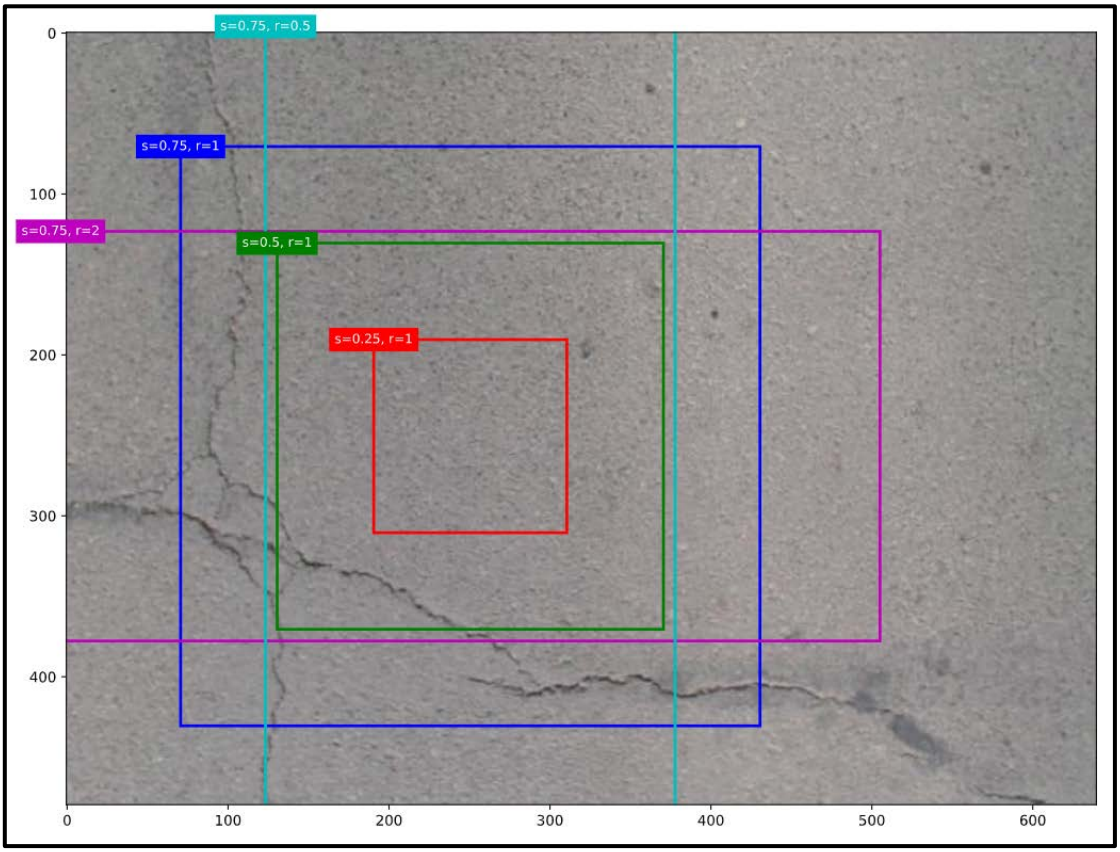

Figure 7-27. Example of anchor box configuration used on top-down images

Figure 7-28. Visualization of top-down anchor box configuration on panoramic images

As a result of these distributions, the decision was made to consider and use optimized anchor boxes sizes to be used to identify the locations of the distress annotations. This was done by carrying out calculations to determine more appropriate aspect ratio and scale sizes to be used in the training. The aspect ratio refers to the ratio of the width to the height of the box and the scale refers to the size of the box with respect to the size of the image being used.

A k-means clustering approach was utilized for this with four clusters applied for the bounding boxes in an attempt for the model to produce a greater IOU when creating the anchor boxes and searching for the location of the annotation during the training. The k-means clustering was considered suitable for this given the distribution shape of the boxes as shown in Figure 7-26. The algorithm is defined as shown below.

Algorithm 1 k-means algorithm

1: Specify the number k of clusters to assign.
2: Randomly initialize k centroids.
3: **repeat**
4: **expectation:** Assign each point to its closest centroid.
5: **maximization:** Compute the new centroid (mean) of each cluster.
6: **until** The centroid positions do not change.

The k means clustering approach was based on a calculation of the Intersection over Union (IOU) between the boxes and the 'k' number of clusters given in equation 7-1.

$$IOU = \frac{\text{intersection}}{\text{box\_area} + \text{cluster\_area} - \text{intersection}} \tag{7-1}$$

Following this, the average IOU between the boxes and clusters was obtained and then the k-means clustering was applied using the Euclidean distance to identify the nearest clusters in the process (K means code definition shown in Appendix C). A cluster of four was used to reproduce four numbers for the aspect and ratio and scale as in line with the previous number of scales and aspect ratios utilized for other models. Using this in python the clusters were returned in terms of an array featuring the width and height as follows:

[[52.5, 268.75][361.25, 81.25][285, 582.5][116.25, 505.]]

Once this was done, the aspect ratio was calculated and scale was also calculated based on the image size as shown in equations 7-2 and 7-3:

$$aspect\_ratio = \frac{clusterbox\_width}{clusterbox\_height} \tag{7-2}$$

$$scale = \frac{clusterbox\_height \times \sqrt{aspect\_ratio}}{height\ of\ grid\ anchor} \quad (7\text{-}3)$$

This resulted in the following aspect ratios: [0.76811594 1.11695906 7.35 0.59459459] and the following corresponding scale sizes: [0.37795709 0.56476108 0.33888604 0.22289598]. The differences between the optimized and the generic values are shown in Table 7-14.

Table 7-14. Differences between generic AR and scale size to optimized versions

Generic Aspect Ratio	Aspect Ratio after clustering	Generic Scale Size	Scale size after clustering
0.50	0.76811594	0.25	0.37795709
1.0	1.11695906	0.50	0.56476108
2.0	7.35	1.00	0.33888604
0.75	0.59459459	2.00	0.22289598

To demonstrate whether this change had any impact on the performance of the models, new models were then trained using the faster-rcnn and inception model bases. An example of the new anchor box configurations, when visualized on the image, is given in Figure 7-29. From this image, it can now be seen that the anchor boxes are more suitable to the shape and size of the annotated distress in the image as they appear similar in size.

Figure 7-29. Optimized anchor box configuration for panoramic images

To test the process, models using panoramic images captured on smartphone similar to the configuration used in Italy (as shown in chapter 6) were used in cloudy and sunny conditions. The dataset consisted of images with labels for longitudinal and transverse cracking only as described in Table 7-15.

Table 7-15. Details of panoramic images from French Network

Distresses	Number of annotations
LC1	1027
TC	642

The images were trained with the generic configurations first. However, these configurations were quickly shown to be not useful as detection results were extremely poor with little to no detections being achieved on the test set after over 200 – 600,000 training steps. With the changes to the anchor box configurations, not only were higher performances achieved but the number of training steps was also significantly decreased. The training time per step was however increased and this is understandable as the changes to the anchor box configurations meant that the scale and level of detail being examined was a lot smaller and therefore requiring more computational power. In both models, performance can be considered satisfactory with resulting high levels of precision and recall. The resulted performances are given below:

Table 7-16. Model results on panoramic images based on faster rcnn based model

category	Precision	Recall	f1
LC	81%	90%	85%
TC	78%	82%	80%

Table 7-17. Confusion matrix and corresponding positive and negative detections for faster rcnn based model

	LC	TC	
	70	1	7
	0	47	10
	16	12	0

	TP	FP	FN	TN
LC	70	16	8	47
TC	47	13	10	70

Table 7-18. Model results on panoramic images based on ssd inceptionv2 based model

category	Precision	Recall	f1
LC	88%	81%	84%
TC	76%	56%	65%

Table 7-19. Confusion matric and corresponding positive and negative detections for ssd inceptionv2 based model

	LC	TC	
	63	1	14
	1	32	24
	8	9	0

	TP	FP	FN	TN
LC	63	9	15	32
TC	32	10	25	63

The faster-rcnn model however had better performance with f1 scores as visualized in Figure 7-30. Two versions of the models were prepared as shown in the figure with the difference being the use of dataset with only images in sunny conditions, as opposed to the first version which included images in cloudy conditions. The performance of the models was marginally increased for the dataset features images with sunny background conditions.

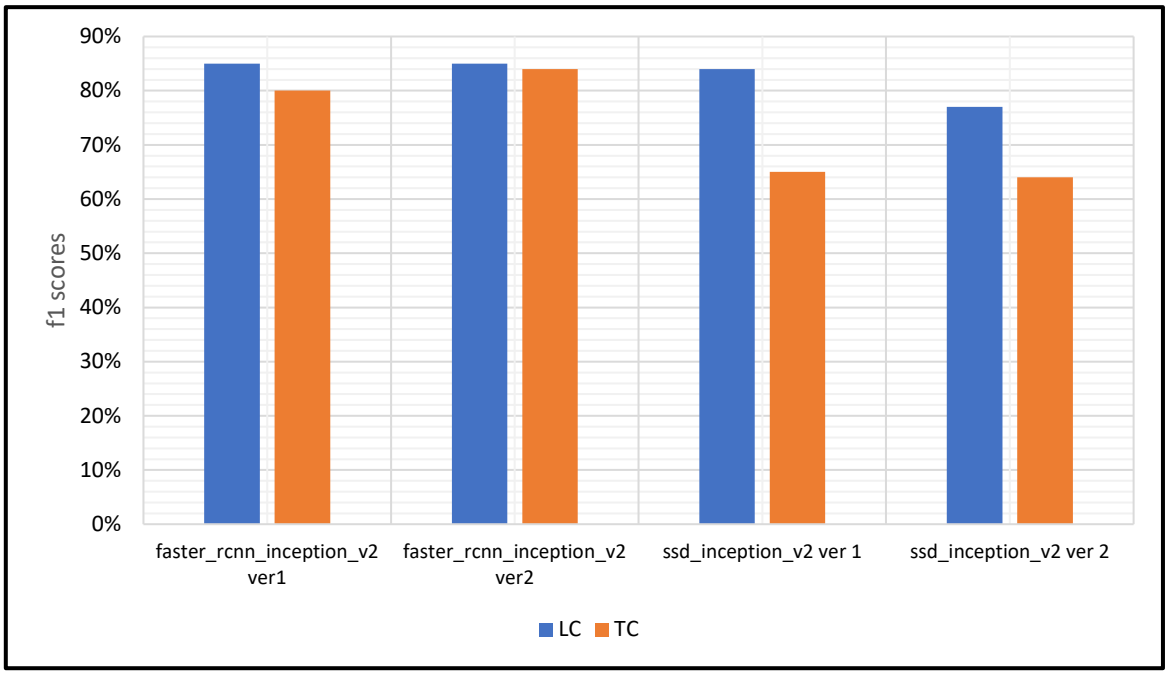

Figure 7-30. f1 scores of panoramic models

Also of note, was the fact that the transverse cracking was better detected with higher overall performance scores. For further examination, the positives and negatives also showed that the faster-rcnn model produced more true positives and less false negatives. Similar to the other results from the other work in the study, the inception model produced smaller numbers of false positives. Further to this, it was tested to see what the individual distributions of each category were with respect to width and height. This is shown in the jointplots for each distress category shown in Figure 7-31 and Figure 7-32. Within the distributions, the heatmaps are consistent with the expected locations of the distresses, e.g. transverse cracking having a heatmap in a vertical direction. This consistency validates the results of the distributions. From these distributions, optimizations for each category could be obtained using the same process as detailed earlier to optimize the anchor boxes. They could then be used in series to create a larger number of optimized anchor boxes. This however would require a lot of computational power as the process would entail four times the number of anchor boxes. It is however worth noting for other applications that this could result in higher performances.

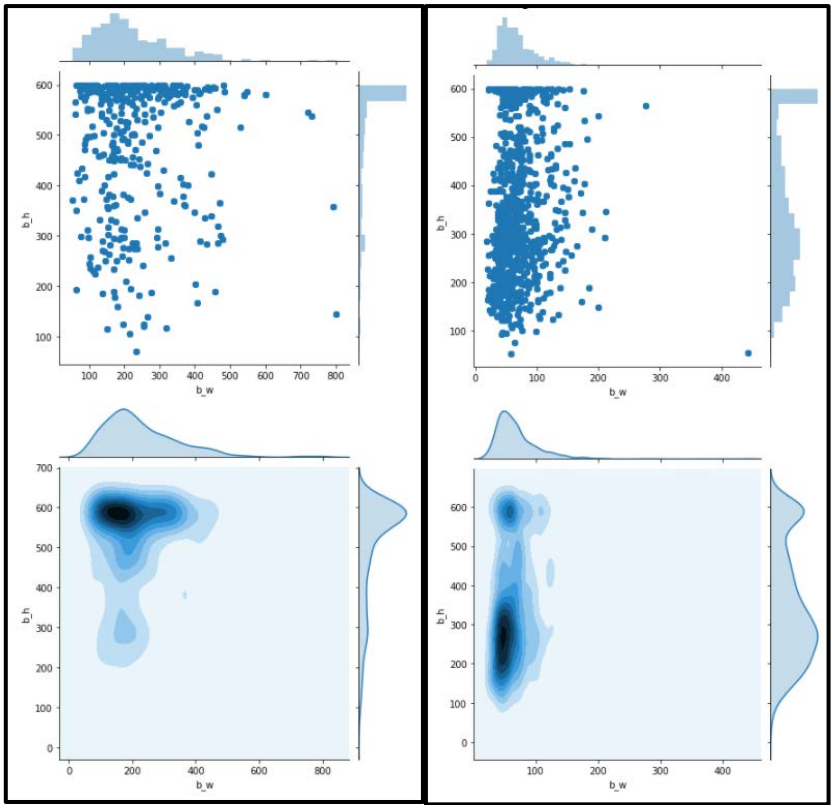

Figure 7-31. Distributions for Longitudinal cracking (right) and Block cracking (left)

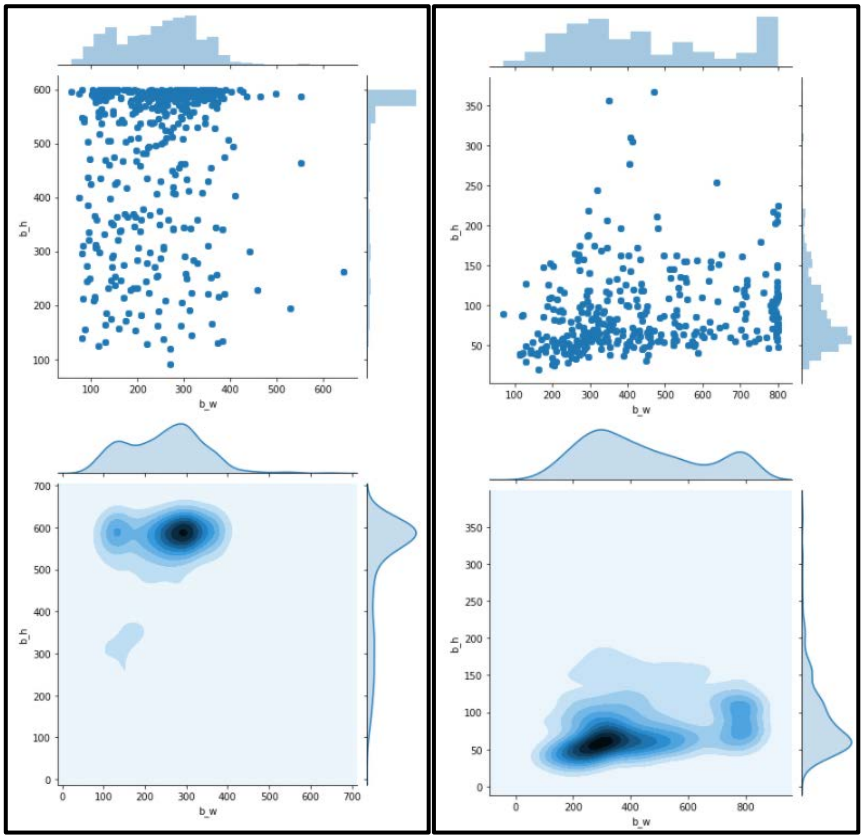

Figure 7-32. Distributions for Transverse cracking (right) and Ravelling (left)

7.4 Stability of Classification results for differing conditions

7.4.1 Implementing the model into a pavement monitoring system

For model implementation, several key points must be emphasized. The first is that the road network's location and environmental conditions play a major role in the tuning of DL models for detecting pavement distresses. Models are not transferable unless similar conditions are in place as the methods are not generalizable in different environmental conditions between different countries or types of networks. Models must be developed based on the unique conditions of distresses present in the particular network and the type of images that will be captured. Additionally, the metrics utilized to evaluate the performance of the models are subjective based on the needs of the stakeholder. Therefore, the confusion matrices must be developed and kept for evaluation as they provide the bases to use any of the available metrics. Concerning augmentations, tests are important to determine the effects on a case-by-case basis. It was shown that they also should only be used based on the specific conditions of the study as it was shown that not all augmentations are useful in some instances.

With respect to performance, models based on a region proposal system performed better than the quicker models that use one-shot approaches. This can be considered rational because of the small nature of the objects appearing in the images. The region-based models also showed a tendency to produce higher levels of recall vs the one-shot models showing a propensity to produce higher levels of precision. It was also shown that models produced few false detections when tested on images with no distresses. Whilst not perfect, the models coped better than the traditional methods and did not appear to produce errors such as the notable ones produced by earlier systems. Finally, when changing the perspective of the images, the configuration of the anchor boxes is critical as this helps the models to locate the annotated images during training especially when the boxes are very small as was the case with the panoramic database. It must also be noted that while the optimization tests were mainly carried out on the French models, the workflow to do so for other networks will remain the same as the methodology to optimize and calibrate results is the significant output.

Consequently, given the results of the models used both in Italy and France, a pipeline was developed where the models are integrated into planning processes, along with the data analytical approaches for maintenance predictions, and the 3D Modelling techniques utilized

in earlier chapters [132,158,356]. This pipeline is depicted in Figure 7-33, with the final goal being to produce better decisions on which M&R activities are done for a given road network.

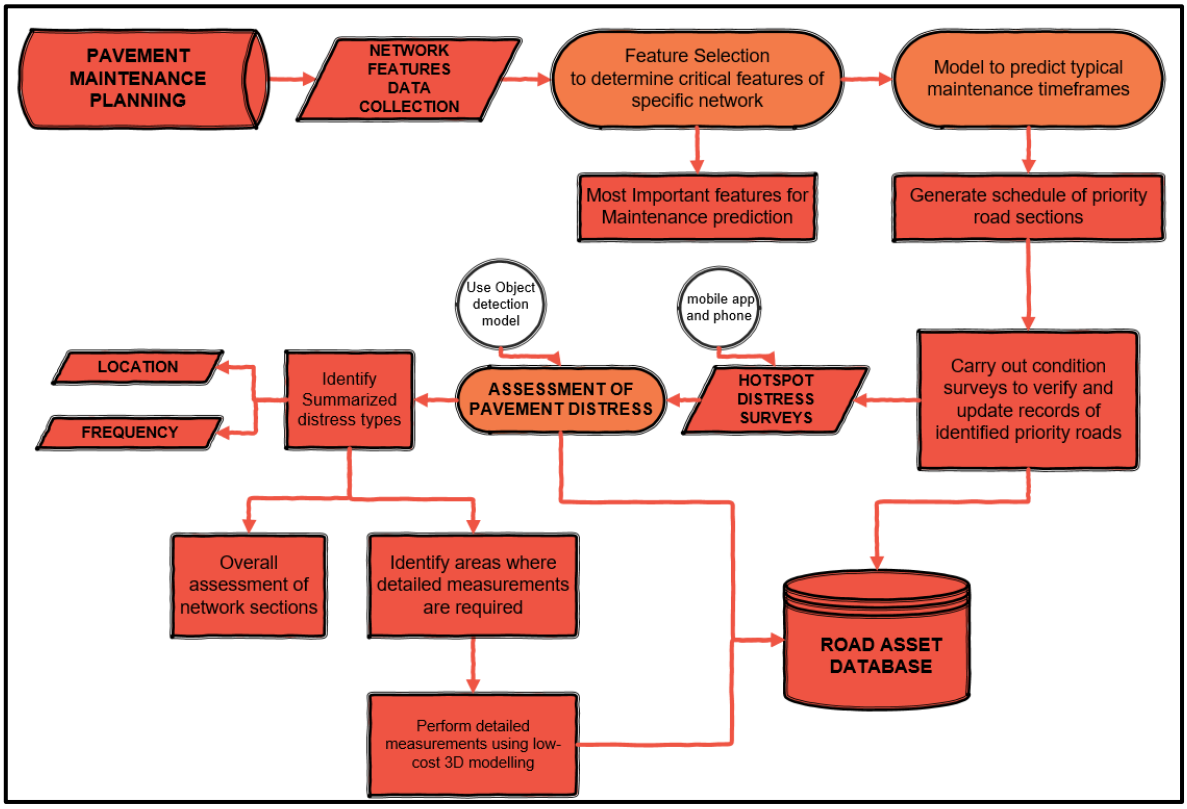

Figure 7-33. Pipeline for integrating techniques to be used in the road asset database

Within the pipeline, workflow integration is made starting with the data analytical methods used to identify the important features in a network and to predict typical maintenance timelines. Following this, the models using DL are considered for hotspot analyses and building distress databases. In the framework, the assessment utilizes smartphones. The DL models would be utilized in a smartphone application and used in rapid surveys to produce distress locations (GPS based) (which are detected in a box on the images) and an understanding of the structural defects at the locations. Then after the survey is performed over a network, the frequency of these two parameters can be produced and used as shown in section 7.1.2. This would help Road Authorities solve issues of monitoring the road network's condition in order to prioritize which roadways need rehabilitation and to continuously update their databases at a low cost. This would be possible as the data in their asset management system would be easily kept up to date, with easy access to sufficient monitoring data to make these decisions continuously over the pavement's life cycle. The use of 3D modelling could then be applied in situations where detailed metric information is required. The workflow combines the techniques to deliver vital information for road managers.

7.4.2 Limitations

Whilst the study into deep learning and the utilization of object detection modelling for detecting pavement distresses does show significant promise and use for industry, drawbacks to the techniques remain. These stem from the images that are used. During surveys, images can be blurry or overexposed and in these cases, no detection model would be able to detect the presence of a distress. This is particularly the case with images taken from smartphones in vehicles given the lower image quality level and the distance away from the road. Shadows caused by buildings or trees could also play a factor in missing detections during a survey. Additionally, with the angle of the camera that is used to carry out the surveys, it is difficult to get a metric evaluation of the distress and therefore metric evaluations would still be necessary to complement the work done by the distress detection applications. The use of a survey vehicle as shown in the case study could help with this as when the camera is focused directly onto the surface of a pavement metric evaluations through the use of segmentation can be done but this is a more complicated and expensive workflow.

Furthermore, some distress categories are more difficult to detect such as bleeding where there is a texture change and this is difficult for a model to detect. The weather could also impact this in scenarios where there are wet pavements making some detections harder to make. Whilst these types of distresses are more related to the functional characteristics of the pavement, they are still important in evaluations and the techniques are limited to tackling them. For these types, the use of 3D modelling and segmentation can be considered more applicable and this is why it was important to develop a pipeline exploiting these techniques in chapter four. The possibility also exists where some traditional machine learning techniques could be applied in conjunction with the deep learning models to help filter images and for labelling processes that could speed up the techniques and increase the accuracies.

Nevertheless, despite these limitations, the study has successfully shown the capacity of the deep learning models and pipeline to deliver valuable information to a road authority on road conditions. The costs of the data delivery are also low thereby addressing one of the most severe concerns. It also carried out novel experiments to test and optimize important aspects of the modelling process to ensure the robustness of the work.

The final chapter will now conclude on the full work of the project and explore future perspectives that can be tackled in future studies.

Chapter 8: Conclusions and Future outlook

The principal goal of this research was to develop a pipeline that would help simplify aspects of data collection and analysis practices within the pavement management system using low-cost tools and techniques. In pursuit of this goal, 3D image-based modelling, tabular data analysis and finally deep learning object detection modelling have been utilized to understand pavement networks, identify the location of distresses within networks and then to analyse the said distresses. At each level of the process, low-cost surveying methods have been used and the developed models have been done with a flexible nature to allow for easy and practical implementation in the real world.

The manuscript demonstrates how the state of art in data analysis, photogrammetry and deep learning can be combined to solve a major problem of a lack of data and data comprehension for road asset management. The approaches within the project help to reduce the subjectivity that currently plays a major role in manual survey methods by producing models with better accuracies and competencies than the typical systems utilized by struggling road authorities. In future studies, the models developed can be commercialized for specific use cases in these road authorities to ensure the pavement conditions are sustainably monitored.

The research within the PhD can be considered innovative because of the novel combination of data analysis techniques and the development of new models and workflows, which improve the data collection processes within the PMS and provide a path towards avoiding manual surveys and practices that result in unsustainable pavement management strategies.

This chapter will conclude the initial objectives that were highlighted in chapter 1 and will also explore the future perspectives of the pipelines developed within the project.

8.1 Overall Conclusions

Within the thesis, several different workflows and concepts were tackled. Despite the myriad of issues dealt with and the numerous case studies, the study can be summarized considering the key issue of acquiring data on pavements and analysing said data. The purpose of this is to give road managers a better chance of making better decisions for road maintenance and rehabilitation activities. Recalling the vital points from the typical data science workflow examined in Figure 1-5 in Chapter 1, it is key in these studies to understand: the specific problem at hand, what is the available data, how to prepare this data and finally how to iterate any models developed to obtain acceptable results. With these key points in mind, in Figure 8-1, two main questions are used to highlight the area of focus of the thesis and the general project to understand and conclude the purpose of the work.

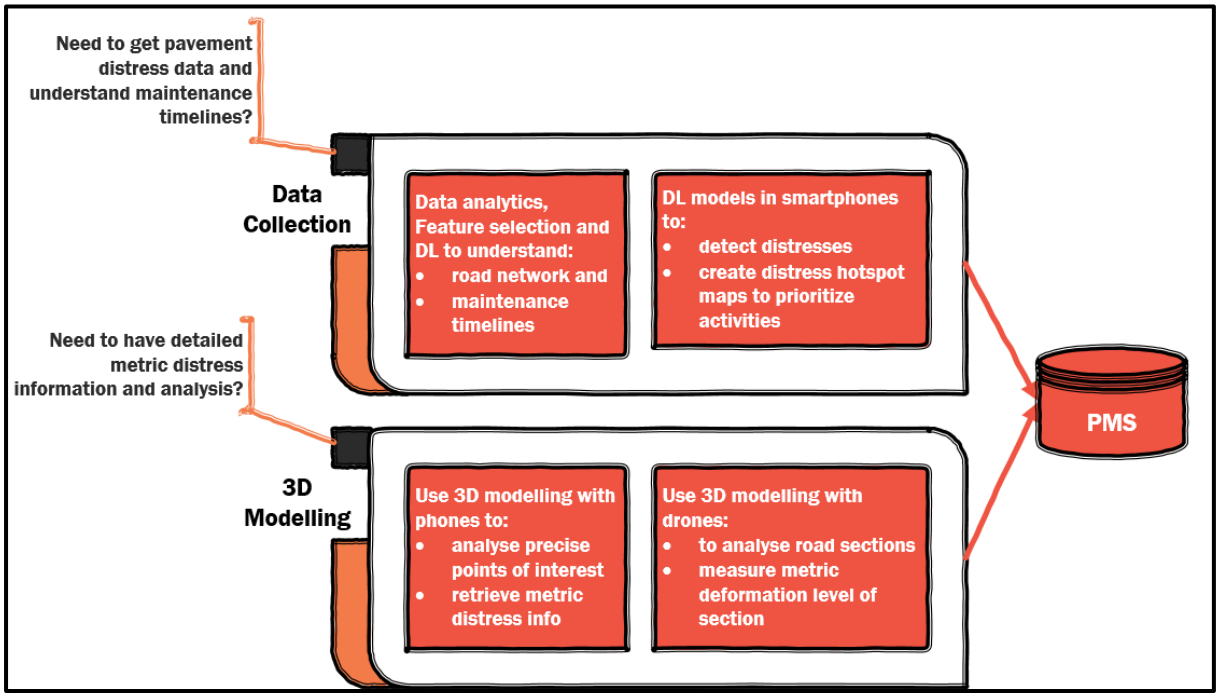

Figure 8-1. Summary of key issues tackled by study

In the figure, the first question expresses a need to acquire data on the network in terms of distresses present and on the maintenance approach used in the specific geographical location. To answer this need, the manuscript utilizes data analysis and deep learning, to model and innovatively predict future timelines, leveraging the combined power of several different modelling techniques. This included gradient boosting algorithms, tabular DL and feature selection techniques. Secondly, deep learning models and techniques were then used to pinpoint the location of distresses in networks for the purpose of generating hotspots distresses to help prioritize activities.

The second main question confronts the need to have detailed metric information on pavement distresses. To answer this, the manuscript relies on the use of low-cost and flexible 3D modelling approaches using smartphones, cameras and drones to produce metrically accurate 3D pavement models. These models were also segmented to retrieve the important and required information about deformation levels and the precise distress characteristics. All of the information, models and pipelines developed by answering these questions are valuable for road managers and can be used within the PMS. With the low-cost of the tools developed, this creates another pathway towards sustainable road management. Aside from these overall conclusions, the project at its inception aimed to answer specific key sub-objectives as highlighted in chapter 1. The conclusions for each of these are given below:

1. To review relevant processes and information

This objective was addressed in different aspects across chapters 1, 2, 3 and 5. In particular, chapters 3 and 5 provided extensive reviews of the current research fields and the state of art for 3D modelling and deep learning. Chapter 2 analysed the background of the situation within Palermo and the generic blocks within a PMS highlighting the data requirements and gaps that exist. Within the review, several techniques and tools are explained and a link is provided to demonstrate how they can be exploited to fill research gaps that exist within the data collection aspects of the PMS. The general structure of the pavement management system and then the structure and practices of detecting pavement distresses in a network or section were analysed. This was done to ensure the requirements of the data systems were well understood before the development of any models within the project. The industry standards and requirements were also explored to understand what is needed by road authorities to feed their databases.

The review of background information and the current state of art allowed for a contextualization of the models that were developed later in the study. This also allowed for the adequate development of case studies to show how the new techniques and workflows fit into the existing paradigms to make them practically implementable. The knowledge gained through the review formed the foundation of the developed project workflow and for the evaluation strategies exploited later in the project.

2. To develop suitable and practical workflows

This objective was assessed in chapters 4, 6 and 7. This involved carrying out several case studies to test and adapt the techniques that were developed in theory in real-world tests. In chapter 4, the techniques concerning photogrammetry and 3D modelling were tested and a pipeline was developed to model and analyse pavement distresses at particular points of interest along a road. This was done using different low-cost equipment including smartphones and the use of drones. The pipeline was tested using different devices to ensure the practicality of the processes. A pipeline was also established to use drone imagery with the 3D modelling to establish an overview of the pavement conditions and particular points where hand-cameras can be used for further assessments. The strategy also presented the development of equations to convert the data from the 3D model to a metric that could be used to describe the overall condition of the pavement. Different segmentation algorithms were also utilized to develop strategies for isolating distresses present within the pavement and steps needed to exploit them were examined. In chapters 6 and 7, the pipeline was further extended using DL, namely object detection modelling. Using the modelling process, a pipeline to carry out hot spot analyses of road networks was developed showing how the data obtained from the detection models could be utilized. Finally, models were also implemented in different environmental conditions to verify and validate the use of the workflows.

3. To evaluate and optimize the developed workflow and processes and combine the techniques explored in a suitable way

This objective was addressed in chapters 7 and 8. In chapter 7, workflows were combined using all the individual model combinations from the 3D modelling and the deep learning approaches to stress how each subset of the process can be used in conjunction with each other. The combination of techniques is innovative and based on the individual state of art approaches taken at each level of the study. Each level of the study also used approaches that could be easily used by road practitioners to have a hands-on pipeline ready for implementation. Additionally, the DL techniques were tested in different environments to ensure that the workflow could be translated in different situations. During these tests, different optimization techniques were used to show how different image types can be used and how to set up different models. This was done to ensure that the systems are flexible enough to be used by road practitioners. Different evaluations and tuning of model

parameters were carried out to validate the processes and show how changes in situations impact modelling decisions. Finally, chapter 8 represents a summary of the approaches used and the outlook of the work for future studies and implementation.

8.2 Future perspectives and outlook

The work presented in this project was motivated by the need to give road authorities helpful data on pavement conditions and maintenance strategies to deploy sustainable tactics. This is especially important for under-resourced and small road authorities, and the municipality in Palermo represents one of these, therefore creating the need for the project. In terms of data requirements, these authorities not only need low-cost systems but also systems that are flexible and adaptable, to ensure that practical implementation is possible. In discussions with the municipality and the larger SMARTI ETN project, it was clear that low-cost techniques are greatly needed to give road authorities the answers they need for maintenance systems.

This project, therefore, sought to understand how maintenance timelines and strategies should be set up by using data analytics and easily accessible datasets to give an authority a model that could successfully predict maintenance timelines. An innovative combination of deep learning and data analytics was utilized to create the models. This is key for municipalities such as those in Palermo who mostly rely on a standard timeline and do not change based on real-time changes in conditions in the network. For the implementation of the system, further validation should be done by attempting to build a wider database of the road network and then running the modelling techniques for the entire network to generate maintenance timelines for the entire network as opposed to only the section considered in this study. Additionally, the systems developed with the maintenance timeline were based on the limited data provided by the municipality and future work should try to replicate similar models using other datasets from different municipalities. Further discussions with the municipality should also be done to create a pipeline to store the information and for them to have a system in place that consistently utilizes the data sources exposed by this study. Whilst the study was able to use the limited data, it would be helpful for future work and future advances of maintenance strategies if more data is kept by the authority and the data is consolidated. Additional data also provides more testing data to validate the accuracies of models produced and this would be key to ensure that the models are robust. The role of the municipality and the agencies involved in maintenance also needs to be consistent, and

communication between the entities has to be clear to ensure that planning and strategy development is sustainable. The issue of the advanced skills required by personnel in the municipality is also important. It must be reiterated here that during the study, discussions were held with personnel from the municipality and at the research department at Université Gustave Eiffel. Firstly, the information obtained and utilized for the Italian models was obtained directly from communication with the local authorities in Palermo. This allowed the model to only consider the actual available resources and ensured that the process was relevant to the environmental context and resources. Additionally, while the model building required advanced skills in data analytics and modelling, the final model does not require substantial training to analyse its outputs. The hardest part of the process has been completed and what is required now is further validation with more test cases using the already constructed base model. This is also a reason why the local authority and municipality is one of the partners of the general project. Discussions will have to continue with them moving forward to allow practical implementation.

Concerning the French models, the models were built in discussion with research personnel and engineers who work directly with secondary road authorities and carry out monitoring and evaluation for these authorities. These personnel assist road agencies, who they have been contracted by, in monitoring network road conditions, which made their inputs critical. Therefore, the models were built with this in mind and the final models produced were done in a user-friendly manner to allow further validation. During this validation, the process could highlight some issues, which would require more optimization and again require the advanced skills used for model development. However, this should not be burdened on the road agency staff and it is intended that the models will be validated through research before practical implementation.

The public should also be kept in the loop for them to understand how money is being spent and to provide a good perspective on the rationale for maintenance activities. The public could also provide recommendations and assist in data collection through possible crowdsourcing avenues.

Using the timeline as the base, the next step was to create deep learning models that could be embedded into a smartphone application that could be used to carry out surveys across the network, to provide a hotspot analysis of the roads detecting the points where there are

distresses. Whilst the project was able to produce accurate models, further testing is needed with more test data from other roads from the rest of the network not covered within the study. Testing could also be done in simulators such as a pavement-testing carousel to observe the propagation of the distresses over time in a simulated environment. This would better enable the commercialization of the models that have been developed within the study. More categories of distress could also be incorporated into the analysis to have a wider overview of the road conditions. Crowdsourcing could also be used as a source for future datasets to have a larger training set. Another consideration to gain training data could be using Google maps imagery, whose resolution and quality continues to increase. In the pre-processing steps, the manual image annotation is also time-consuming, and it is expected that in the future, deep learning methods can be readily adapted to this stage, to provide some automation. However, research in the field is in its early stages and given the complexities of pavement distresses it could take some time before acceptable methods are available and thus manual approaches for this stage will have to remain. In future applications, other engineering features observed on the network such as the IRI could be used as a key to highlight images that should be labelled for future deep learning research. With respect to the detection modelling, image segmentation using the detection as a starter could be also be considered in order to better have a metric evaluation of the distresses. Whilst this would be highly dependent on the quality and resolution of images, it is worth considering for future applications and studies.

For implementations in industry, further substantive discussions are needed with stakeholders to determine the appropriate evaluation metrics and to ensure that the distress categories covered by the models are adequate. Discussions with the stakeholders should also consider the requirements of the phone application to be developed to ensure it is done in line with the needs of the road authority. It should also be mentioned that the field of deep learning is advancing very quickly as evidenced by the review of the state of art within the project. As a result of this, it is likely that new frameworks and models will be introduced in a short period of time and when this happens, the guidelines on developing models presented and optimized in this study becomes more important than the actual models developed by the study.

In the 3D image-based modelling aspect of the study, techniques were used to analyse pavement distresses by generating 3D models of them and segmenting the models and

metrically evaluating the distresses based on industry requirements. The work carried out in this aspect of the study demonstrated the accuracy of the techniques and different applications of the systems. For future work and implementation, more 3D model data is needed. Whilst the study did utilize some UAV imagery, this was limited during the project given equipment limitations and then finally the limitations introduced during the pandemic period. The results show great promise but more data is needed to further validate the assessments made using the 3D point cloud data. The current workflows are based on open-source systems and therefore they could be easily adapted to the new datasets and the generic workflow developed. Deep learning systems could also be applied to the 3D models to automatically measure the physical parameters of the distress in terms of dimensions of the distress created compared to the reference plane of the pavement.

With all of these considerations, the work in the study has produced several different models to tackle different problems along the PMS data collection and database pipeline. The techniques are connected and can be easily implemented given the practical and flexible nature of the systems developed and the discussions with the municipality during the project.

The work and discussions presented in the project present a synchronisation of theory, research using the theory and finally practical application. To successfully have this union, the project exploited data and image analysis, data science approaches, real-world case studies and thorough discussions with stakeholders.

Future work in the subject needs to continue to pursue a holistic view of the PMS and general pavement management to create systems that are diverse and capable of handling different conditions or situations. As Pavement Management is vital towards infrastructural development, the work and techniques provided in this study will aid future research and advancements providing a valuable step towards more sustainable pavement systems.

Bibliography

[1] B.R. Keeble, The Brundtland Report: "Our Common Future: the Report of the World Commission on Environment and Development," Oxford, United Kingdom, 1988. doi:10.1080/07488008808408783.

[2] Intergovernmental panel on climate change, Climate Change 2014: Synthesis Report, Geneva, Switzerland, 2014. https://www.ipcc.ch/site/assets/uploads/2018/05/SYR_AR5_FINAL_full_wcover.pdf.

[3] J. Zietsman, T. Ramani, National Cooperative Highway Research Program (NCHRP) Report 708: A Guidebook for sustainability performance measurement for transportation agencies, National Cooperative Highway Research Program (NCHRP), 2013. doi:10.17226/14598.

[4] H. Stripple, Life cycle assessment of Road, A Pilot Study for Inventory Analysis, 2001.

[5] A. Carlson, Life cycle assessment of roads and pavements- Studies made in Europe, VTI Rapp. 736A. (2011) 22.

[6] ECRPD, Energy Conservation in Road Pavement Design , Maintenance and Utilisation, (2010) 1–63.

[7] T.J. Vandam, J.T. Harvey, S.T. Muench, K.D. Smith, M.B. Snyder, I.L. Al-Qadi, H. Ozer, J. Meijer, P. V Ram, J.R. Roesier, A. Kendall, Towards Sustainable Pavement Systems: A Reference Document FHWA-HIF-15-002, Washington, DC, 2015. https://www.fhwa.dot.gov/pavement/sustainability/hif15002/hif15002.pdf.

[8] W. Waidelich, Guidance on Highway Preservation And Maintenance - Memorandum, U.S Department of transportation - Federal Highway Administration, Washington D.C, 2016. https://www.fhwa.dot.gov/preservation/memos/160225.pdf.

[9] International Road Federation (IRF), IRF World Road Statistics 2018 (Data 2011 -2016), Brussels, 2018.

[10] European Union Road Federation, Road Asset Management: An ERF Position paper for maintaining and improving a sustainable and efficient road network, Brussels, 2018. https://erf.be/wp-content/uploads/2018/07/Road-Asset-Management-for-web-site.pdf.

[11] S. Colonna, P. Fioretti, G. Fonzone, A. Sasso, New Approaches In Road Maintenance Planning: The Global Road Management System (GRMS), in: 13th Mini-Euro Conf. 9th Meet. EURO Work. Gr. Transp., Bari, Italy, 2002: pp. 752–756. http://www.iasi.cnr.it/ewgt/13conference/132_colonna.pdf.

[12] OECD, Road Infrastructure Maintenance (indicator) in Italy, (2021). doi:10.1787/c73dc965-en.

[13] N. Fernandes, Economic effects of coronavirus outbreak (COVID-19) on the world economy, SSRN. (2020) 0–29. doi:https://dx.doi.org/10.2139/ssrn.3557504.

[14] K.A. Zimmerman, D.G. Peshkin, Pavement management perspective on integrating preventive maintenance into a pavement management system, Transp. Res. Rec. (2003) 3–9. doi:10.3141/1827-01.

[15] K.L. Smith, D. Peshkin, A. Wolters, J. Krstulovich, J. Moulthrop, C. Alvarado, Guidelines for the Preservation of High-Traffic-Volume Roadways, National Academies of Sciences, Engineering,

and Medicine, Washington, D.C, 2011. doi:10.17226/14487.

[16] P. Rouse, T. Chiu, Towards optimal life cycle management in a road maintenance setting using DEA, Eur. J. Oper. Res. 196 (2009) 672–681. doi:10.1016/j.ejor.2008.02.041.

[17] X. Li, D.W. Goldberg, Toward a mobile crowdsensing system for road surface assessment, Comput. Environ. Urban Syst. 69 (2018). doi:10.1016/j.compenvurbsys.2017.12.005.

[18] S.C. Radopoulou, I. Brilakis, Improving Road Asset Condition Monitoring, Transp. Res. Procedia. 14 (2016) 3004–3012. doi:10.1016/j.trpro.2016.05.436.

[19] American Association of State Highway and Transportation Officials (AASHTO), Pavement Management Guide, 2012.

[20] M. Manosalvas-Paredes, R. Roberts, M. Barriera, K. Mantalovas, Towards more sustainable pavement management practices using embedded sensor technologies, Infrastructures. 5 (2020). doi:10.3390/infrastructures5010004.

[21] SMARTI ETN, SMARTI ETN website, (2017). www.smartietn.eu (accessed September 15, 2020).

[22] Scopus, Scopus Document Analysis - Artificial Intelligence and Pavements, (2020). https://www.scopus.com/term/analyzer.uri?sid=d649d8003648ad9ce274c7cecb69dbdc&origin=resultslist&src=s&s=%28TITLE-ABS-KEY%28artificial+intelligence%29+AND+TITLE-ABS-KEY%28pavement%29%29&sort=plf-f&sdt=b&sot=b&sl=68&count=309&analyzeResults=Analyze+results (accessed September 8, 2020).

[23] K.L. Wagstaff, Machine learning that matters, in: Proc. 29th Int. Conf. Mach. Learn. ICML 2012, 2012: pp. 529–534.

[24] A. Pantelias, G.W. Flintsch, J.W. Bryant, C. Chen, Asset management data practices for supporting project selection decisions, Public Work. Manag. Policy. 13 (2009) 239–252. doi:10.1177/1087724X08327574.

[25] T.B.J. Coenen, A. Golroo, A review on automated pavement distress detection methods, Cogent Eng. 4 (2017) 1–23. doi:10.1080/23311916.2017.1374822.

[26] A. Ragnoli, M. De Blasiis, A. Di Benedetto, Pavement Distress Detection Methods: A Review, Infrastructures. 3 (2018) 58. doi:10.3390/infrastructures3040058.

[27] M. Meocci, V. Branzi, A. Sangiovanni, An innovative approach for high-performance road pavement monitoring using black box, J. Civ. Struct. Heal. Monit. (2021). doi:10.1007/s13349-020-00463-8.

[28] S. Ahmed, P. Vedagiri, K. V. Krishna Rao, Prioritization of pavement maintenance sections using objective based Analytic Hierarchy Process, Int. J. Pavement Res. Technol. 10 (2017) 158–170. doi:10.1016/j.ijprt.2017.01.001.

[29] S. Sony, S. Laventure, A. Sadhu, A literature review of next-generation smart sensing technology in structural health monitoring, Struct. Control Heal. Monit. 26 (2019) 1–22. doi:10.1002/stc.2321.

[30] R. Mangiaracina, A. Perego, G. Salvadori, A. Tumino, A comprehensive view of intelligent transport systems for urban smart mobility, Int. J. Logist. Res. Appl. 20 (2017) 39–52. doi:10.1080/13675567.2016.1241220.

[31] Y. Ham, K.K. Han, J.J. Lin, M. Golparvar-Fard, Visual monitoring of civil infrastructure systems via camera-equipped Unmanned Aerial Vehicles (UAVs): a review of related works, Vis. Eng. 4

(2016). doi:10.1186/s40327-015-0029-z.

[32] K. Dick, L. Russell, Y. Souley Dosso, F. Kwamena, J.R. Green, Deep Learning for Critical Infrastructure Resilience, J. Infrastruct. Syst. 25 (2019) 05019003. doi:10.1061/(asce)is.1943-555x.0000477.

[33] I.C. Konstantakopoulos, A.R. Barkan, S. He, T. Veeravalli, H. Liu, C. Spanos, A deep learning and gamification approach to improving human-building interaction and energy efficiency in smart infrastructure, Appl. Energy. 237 (2019) 810–821. doi:10.1016/j.apenergy.2018.12.065.

[34] L. Inzerillo, G. Di Mino, R. Roberts, Image-based 3D reconstruction using traditional and UAV datasets for analysis of road pavement distress, Autom. Constr. 96 (2018) 457–469. doi:10.1016/j.autcon.2018.10.010.

[35] G. Di Mino, G. Salvo, S. Noto, Pavement management system model using a LCCA - microsimulation integrated approach, Adv. Transp. Stud. 1 (2014) 101–112. doi:10.4399/978885487354410.

[36] Y.U. Shah, S.S. Jain, M. Parida, Evaluation of prioritization methods for effective pavement maintenance of urban roads, Int. J. Pavement Eng. (2014). doi:10.1080/10298436.2012.657798.

[37] M. Mubaraki, A methodology for project-level maintenance for urban roads, Proc. Inst. Civ. Eng. - Transp. 168 (2015) 239–255. doi:10.1680/tran.13.00065.

[38] G. Loprencipe, A. Pantuso, A Specified Procedure for Distress Identification and Assessment for Urban Road Surfaces Based on PCI, Coatings. 7 (2017) 65. doi:10.3390/coatings7050065.

[39] D. Peterson, National Cooperative Highway Research Program Synthesis of Highway Practice Pavement Management Practices. No. 135., Transportation Research Board, Washington, DC, 1987. http://onlinepubs.trb.org/Onlinepubs/nchrp/nchrp_syn_135.pdf.

[40] Federal Highway Administration, PROJECT MANAGEMENT PLAN GUIDANCE FOR MAJOR PROJECTS, Washington D.C, 2017.

[41] American Association of State Highway and Transportation Officials (AASHTO), AASHTO Guidelines for Pavement Management Systems, American Association of State Highway and Transportation Officials, Washington, 1990. http://mail.tku.edu.tw/yinghaur/lee/pms/all-vu-graph/lc1-AASHTO Guidelines for PMS 1990.pdf.

[42] H.R.2950 - Intermodal Surface Transportation Efficiency Act of 1991, Public Law No 102-240. (n.d.). https://www.congress.gov/bill/102nd-congress/house-bill/2950 (accessed September 20, 2020).

[43] Congress of the United States of America, Safe, Accountable, Flexible, Efficient Transportation Equity Act: A Legacy for Users'' or '"SAFETEA–LU,"' (2005). https://www.transportation.gov/sites/dot.gov/files/docs/SAFETEA-LU_0.pdf.

[44] M. Irfan, M.B. Khurshid, Q. Bai, S. Labi, T.L. Morin, Establishing optimal project-level strategies for pavement maintenance and rehabilitation - A framework and case study, Eng. Optim. 44 (2012) 565–589. doi:10.1080/0305215X.2011.588226.

[45] G. Lamptey, S. Labi, Z. Li, Decision support for optimal scheduling of highway pavement preventive maintenance within resurfacing cycle, Decis. Support Syst. 46 (2008) 376–387. doi:10.1016/j.dss.2008.07.004.

[46] M.B. Khurshid, M. Irfan, S. Labi, Optimal performance threshold determination for highway asset interventions: Analytical framework and application, J. Transp. Eng. 137 (2010) 128–139.

doi:10.1061/(ASCE)TE.1943-5436.0000198.

[47] T.F. Fwa, W.T. Chan, K.Z. Hoque, Mulltiobjective Optimization for Pavement Maintenance Programming, J. Transp. Eng. 126 (2000) 367–374. doi:10.1061/(ASCE)0733-947X(2000)126:5(367).

[48] G. Bosurgi, F. Trifirò, A model based on artificial neural networks and genetic algorithms for pavement maintenance management, Int. J. Pavement Eng. 6 (2005) 201–209. doi:10.1080/10298430500195432.

[49] G. Di Mino, M. De Blasiis, F. Di Noto, S. Noto, An Advanced Pavement Management System based on a Genetic Algorithm for a Motorway Network, in: Third Int. Conf. Soft Comput. Technol. Civil, Struct. Environ. Eng., 2013.

[50] V. Donev, M. Hoffmann, Optimisation of pavement maintenance and rehabilitation activities, timing and work zones for short survey sections and multiple distress types, Int. J. Pavement Eng. 21 (2020) 583–607. doi:10.1080/10298436.2018.1502433.

[51] N.R. Tayebi, F.M. Nejad, M. Mola, Comparison between GA and PSO in Analyzing Pavement Management Activities, 140 (2014) 99–104. doi:10.1061/(ASCE)TE.1943-5436.0000590.

[52] S.A. Arhin, L.N. Williams, A. Ribbiso, M.F. Anderson, Predicting Pavement Condition Index Using International Roughness Index in a Dense Urban Area, J. Civ. Eng. Res. 5 (2015) 10–17. doi:10.5923/j.jce.20150501.02.

[53] G. Loprencipe, A. Pantuso, P. Di Mascio, Sustainable Pavement Management System in Urban Areas Considering the Vehicle Operating Costs, Sustain. 9 (2017) 453. doi:10.3390/su9030453.

[54] O. Elbagalati, M.A. Elseifi, K. Gaspard, Z. Zhang, Development of an Enhanced Decision-Making Tool for Pavement Management Using a Neural Network Pattern-Recognition Algorithm, J. Transp. Eng. Part B Pavements. 144 (2018) 04018018. doi:10.1061/jpeodx.0000042.

[55] L. Janani, R.K. Dixit, V. Sunitha, S. Mathew, Prioritisation of pavement maintenance sections deploying functional characteristics of pavements, Int. J. Pavement Eng. 0 (2019) 1–8. doi:10.1080/10298436.2019.1567923.

[56] K.T. Hall, C.E. Correa, S.H. Carpenter, R.P. Elliott, National Cooperative Highway Research Program Web Document - Rehabilitation Strategies for Highway Pavements Part B Appendix A, 2001. http://onlinepubs.trb.org/onlinepubs/nchrp/nchrp_w35-a.pdf.

[57] L. Bertrand, M. Boutonnet, J. Cazeneuve, J. Chabrol, M. Dauzats, J.. Griselin, A. Coquereau, J.. Poilane, B. Robert, P. Lepert, M. Siffert, Catalogue des degradations de surface des chaussees, Paris, 1998. http://www.ifsttar.fr/fileadmin/user_upload/editions/lcpc/MethodeDEssai/MethodeDEssai-LCPC-ME52.pdf.

[58] American Society for Testing and Materials. (ASTM), ASTM D 6433 -18 Standard Practice for Roads and Parking Lots Pavement Condition Index Surveys, West Conshohocken, 2018. doi:10.1520/D6433-18.

[59] Office of Materials and Road Research Pavement Management Unit, Minnesota Department of Transportation Pavement Distress Identification Manual, Minnesota, 2011. https://www.dot.state.mn.us/materials/manuals/pvmtmgmt/Distress_Manual.pdf.

[60] D.G. for I. and Mobility, “Catalogo dei dissesti delle pavimentazioni stradali,” Milan, 2005. http://www.ilsole24ore.com/art/SoleOnLine4/Speciali/2006/documenti_lunedi/30gennaio2006/Minicatalogo_Dissesti_ALLEGATO_B.pdf?cmd%3Dart.

[61] G. Jameson, Guide to Pavement Technology Part 5 : Pavement Evaluation and Treatment Design, 3rd ed., Austroads, Sydney, 2011. https://www.onlinepublications.austroads.com.au/items/AGPT05-11.

[62] J.S. Miller, W.Y. Bellinger, Distress Identification Manual for the Long-Term Pavement Performance Program (Fifth Revised Edition), Virginia, 2014. https://www.fhwa.dot.gov/publications/research/infrastructure/pavements/ltpp/13092/13092.pdf.

[63] British Columbia Ministry of Transportation and Infrastructure Construction Maintenance Branch, Pavement surface condition rating manual , Fifth edition, British Colombia, 2016. https://www2.gov.bc.ca/assets/gov/driving-and-transportation/transportation-infrastructure/highway-bridge-maintenance/pavement-marking/pavement-surface-condition-rating-manual.pdf.

[64] AASHTO, Mechanistic Empirical Pavement Design Guide: A Manual Practice, American Association of State Highway and Transportation Officials, Washington, DC, 2008.

[65] L. Inzerillo, G. Di Mino, S. Bressi, F. Di Paola, S. Noto, Image Based Modeling Technique for Pavement Distress surveys : a Specific Application to Rutting, Int. J. Eng. Technol. 16 (2016) 1–9. http://ijens.org/Vol_16_I_05/163705-2929-IJET-IJENS.pdf.

[66] L.M. Pierce, G. McGovern, K.A. Zimmerman, Practical Guide for Quality Management of Pavement Condition Data Collection, Washington, DC, 2013. https://www.fhwa.dot.gov/pavement/management/qm/data_qm_guide.pdf.

[67] W.D.O. Paterson, T. Scullion, Information Systems for Road Management: Draft Guidelines on System Design and Data Issues, Washington, DC, 1990. http://documents.worldbank.org/curated/en/196321468762908116/pdf/multi-page.pdf.

[68] R. Haas, W.R. Hudson, L.C. Falls, Pavement Asset Management, 1st Editio, Wiley-Scrivener, 2015. doi:10.1002/9781119038849.

[69] E. Schnebele, B.F. Tanyu, G. Cervone, N. Waters, Review of remote sensing methodologies for pavement management and assessment, Eur. Transp. Res. Rev. 7 (2015). doi:10.1007/s12544-015-0156-6.

[70] C.R. Bennett, A. Chamorro, C. Chen, H. De Solminihac, G.W. Flintsch, Data Collection Technologies for Road Management, Washington, DC, 2007. http://siteresources.worldbank.org/INTTRANSPORT/Resources/07-02-12DataCollectionTechnologiesReport-v20.pdf.

[71] W.N. Carey Jr, P.E. Irick, The pavement serviceability performance concept, Highw. Res. Board Bull. (1960) 40–58. http://onlinepubs.trb.org/Onlinepubs/hrbbulletin/250/250-003.pdf.

[72] W. Paterson, International roughness index: Relationship to other measures of roughness and riding quality, Transp. Res. Rec. J. Transp. Res. Board. (1986) 49–59. http://onlinepubs.trb.org/Onlinepubs/trr/1986/1084/1084-007.pdf.

[73] Y.U. Shah, S.S. Jain, D. Tiwari, M.K. Jain, Development of Overall Pavement Condition Index for Urban Road Network, Procedia - Soc. Behav. Sci. 104 (2013) 332–341. doi:10.1016/j.sbspro.2013.11.126.

[74] O. Swei, J. Gregory, R. Kirchain, Pavement management systems: Opportunities to improve the current frameworks, in: Transp. Res. Board 95th Annu. Meet., Transportation Research Board, Washington, DC, 2016. https://trid.trb.org/view/1393111.

[75] A.P. Singh, A. Sharma, R. Mishra, M. Wagle, A.K. Sarkar, Pavement condition assessment using soft computing techniques, Int. J. Pavement Res. Technol. 11 (2018) 564–581. doi:10.1016/j.ijprt.2017.12.006.

[76] A. Deluka-tiblja, B. Karleu, N. Dragi, A. Deluka-tiblja, R. Faculty, C. Engineering, A. Deluka-tiblja, B. Karleu, N. Dragi, B. Karleu, R. Faculty, C. Engineering, N. Dragi, Review of multicriteria-analysis methods application in decision making about transport infrastructure, J. Croat. Assoc. Civ. Eng. 65 (2013) 619–631. doi:10.14256/jce.850.2013.

[77] K.A. Zimmerman, Pavement Management Methodologies to select projects and recommend preservation treatments, (1995) 102. http://onlinepubs.trb.org/onlinepubs/nchrp/nchrp_syn_222.pdf.

[78] R. Haas, G. Felio, Z. Lounis, L.C. Falls, Measurable performance indicators for roads: Canadian and international practice, TAC/ATC 2009 - 2009 Annu. Conf. Exhib. Transp. Assoc. Canada Transp. a Clim. Chang. (2009).

[79] F. Humplick, W. Paterson, Framework of Performance Indicators for Managing Road Infrastructure and Pavements, in: 3rd Int. Conf. Manag. Pavements, World Bank, San Antonio, 1994: pp. 123–133. http://citeseerx.ist.psu.edu/viewdoc/download?doi=10.1.1.655.3713&rep=rep1&type=pdf.

[80] S. Sundin, C. Braban-Ledoux, Artificial intelligence-based decision support technologies in pavement management, Comput. Civ. Infrastruct. Eng. 16 (2001) 143-157. doi:10.1111/0885-9507.00220.

[81] S.M. Piryonesi, T. El-Diraby, Using Data Analytics for Cost-Effective Prediction of Road Conditions: Case of the Pavement Condition Index, McLean, VA, 2018. https://www.fhwa.dot.gov/publications/research/infrastructure/pavements/ltpp/18065/18065.pdf.

[82] H. Gong, Y. Sun, X. Shu, B. Huang, Use of random forests regression for predicting IRI of asphalt pavements, Constr. Build. Mater. 189 (2018) 890–897. doi:10.1016/j.conbuildmat.2018.09.017.

[83] J. Domitrović, H. Dragovan, T. Rukavina, S. Dimter, Application of an artificial neural network in pavement management system, Teh. Vjesn. 25 (2018) 466–473. doi:10.17559/TV-20150608121810.

[84] N.O. Attoh-Okine, Analysis of learning rate and momentum term in backpropagation neural network algorithm trained to predict pavement performance, Adv. Eng. Softw. 30 (1999) 291–302. doi:10.1016/S0965-9978(98)00071-4.

[85] J. Santos, A. Ferreira, G. Flintsch, An adaptive hybrid genetic algorithm for pavement management, Int. J. Pavement Eng. 20 (2019) 266–286. doi:10.1080/10298436.2017.1293260.

[86] M. Al Qurishee, W. Wu, B. Atolagbe, J. Owino, I. Fomunung, Creating a Dataset to Boost Civil Engineering Deep Learning Research and Application, Engineering. 12 (2020) 151–165. doi:10.4236/eng.2020.123013.

[87] R. Roberts, G. Giancontieri, L. Inzerillo, G. Di Mino, Towards Low-Cost Pavement Condition Health Monitoring and Analysis Using Deep Learning, Appl. Sci. 10 (2020) 319. doi:10.3390/app10010319.

[88] Federal Highway Administration, LTPP InfoPave, (2020). https://infopave.fhwa.dot.gov/ (accessed April 14, 2020).

[89] P. Marcelino, M. de Lurdes Antunes, E. Fortunato, Comprehensive performance indicators for

road pavement condition assessment, Struct. Infrastruct. Eng. 14 (2018) 1433–1445. doi:10.1080/15732479.2018.1446179.

[90] W. McKinney, Data Structures for Statistical Computing in Python, in: Proc. 9th Python Sci. Conf., 2010: pp. 51–56. http://conference.scipy.org/proceedings/scipy2010/mckinney.html.

[91] J. Hunter, D. Dale, E. Firing, M. Droettboom, Matplotlib Release 3.2.1, (2020) 2598.

[92] M. Waskom, Seaborn: statistical data visualization, (2020). doi:doi.org/10.5281/zenodo.592845.

[93] E.D. Sandru, E. David, Unified feature selection and hyperparameter Bayesian optimization for machine learning based regression, in: ISSCS 2019 - Int. Symp. Signals, Circuits Syst., IEEE, Iasi, Romania, 2019: pp. 1–5. doi:10.1109/ISSCS.2019.8801728.

[94] W. Koehrsen, feature-selector 1.0.0, (2019). https://pypi.org/project/feature-selector/.

[95] L. Prokhorenkova, G. Gusev, A. Vorobev, A.V. Dorogush, A. Gulin, Catboost: Unbiased boosting with categorical features, in: 32nd Conf. Neural Inf. Process. Syst. (NeurIPS 2018), Montreal, 2018: pp. 6638–6648.

[96] Y. Zhang, A. Haghani, A gradient boosting method to improve travel time prediction, Transp. Res. Part C Emerg. Technol. 58 (2015) 308–324. doi:10.1016/j.trc.2015.02.019.

[97] J.H. Friedman, Greedy function approximation: A gradient boosting machine, Ann. Stat. 29 (2001) 1189–1232. doi:10.2307/2699986.

[98] A. Natekin, A. Knoll, Gradient boosting machines, a tutorial, Front. Neurorobot. 7 (2013). doi:10.3389/fnbot.2013.00021.

[99] T. Chen, C. Guestrin, XGBoost: A scalable tree boosting system, in: Proc. ACM SIGKDD Int. Conf. Knowl. Discov. Data Min., 2016: pp. 785–794. doi:10.1145/2939672.2939785.

[100] Y. Freund, R.E. Schapire, A decision-theoretic generalization of on-line learning and an application to boosting BT - Computational learning theory, in: Proc. Second Eur. Conf. Comput. Learn. Theory, Springer-Verlag Berlin Heidelberg, Barcelona, 1995: pp. 23–37. doi:10.1007/3-540-59119-2.

[101] G. Ke, Q. Meng, T. Finley, T. Wang, W. Chen, W. Ma, Q. Ye, T.Y. Liu, LightGBM: A highly efficient gradient boosting decision tree, in: Proc. Adv. Neural Inf. Process. Syst. 30 (NIPS 2017), Long Beach, 2017: pp. 3147–3155. http://papers.nips.cc/paper/6907-lightgbm-a-highly-efficient-gradient-boosting-decision.

[102] E. Al Daoud, Comparison between XGBoost, LightGBM and CatBoost Using a Home Credit Dataset, Int. J. Comput. Inf. Eng. 13 (2019) 6–10.

[103] S. Jhaveri, I. Khedkar, Y. Kantharia, S. Jaswal, Success prediction using random forest, catboost, xgboost and adaboost for kickstarter campaigns, in: Proc. 3rd Int. Conf. Comput. Methodol. Commun. ICCMC 2019, IEEE, 2019: pp. 1170–1173. doi:10.1109/ICCMC.2019.8819828.

[104] G. Huang, L. Wu, X. Ma, W. Zhang, J. Fan, X. Yu, W. Zeng, H. Zhou, Evaluation of CatBoost method for prediction of reference evapotranspiration in humid regions, J. Hydrol. 574 (2019) 1029–1041. doi:10.1016/j.jhydrol.2019.04.085.

[105] A.V. Dorogush, V. Ershov, A. Gulin, CatBoost: gradient boosting with categorical features support, in: Work. ML Syst. NIPS 2017, 2018: pp. 1–7. http://arxiv.org/abs/1810.11363.

[106] S.M. Lundberg, S.I. Lee, A unified approach to interpreting model predictions, Adv. Neural Inf.

Process. Syst. 2017-Decem (2017) 4766–4775.

[107] J. Howard, S. Gugger, Fastai: A layered api for deep learning, Inf. 11 (2020) 1–26. doi:10.3390/info11020108.

[108] C. Guo, F. Berkhahn, Entity Embeddings of Categorical Variables, ArXiv E-Prints. (2016) 1–9. http://arxiv.org/abs/1604.06737.

[109] D. Chen, N. Mastin, Sigmoidal Models for Predicting Pavement Performance Conditions, J. Perform. Constr. Facil. 30 (2016) 1–8. doi:10.1061/(ASCE)CF.1943-5509.0000833.

[110] J. Fan, L. Wu, F. Zhang, H. Cai, W. Zeng, X. Wang, H. Zou, Empirical and machine learning models for predicting daily global solar radiation from sunshine duration: A review and case study in China, Renew. Sustain. Energy Rev. 100 (2019) 186–212. doi:10.1016/j.rser.2018.10.018.

[111] ISTAT, Istat Italy resident population 2020, (2020). http://dati.istat.it/Index.aspx?QueryId=18460&lang=en (accessed April 28, 2020).

[112] OECD, OECD Economic Surveys: Italy 2009, OECD Publishing, Paris, 2019. doi:https://doi.org/10.1787/369ec0f2-en.

[113] OECD, Tax Administration 2017: Comparative information on OECD and other advanced and emerging economies, Paris, 2018. doi:http://dx.doi.org/10.1787/tax_admin-2017-en.

[114] Istituto nazionale di statistica - ISTAT, Permanent Census - Italy 2011, Popul. Census. (2011). http://dati-censimentopopolazione.istat.it/Index.aspx?lang=en (accessed April 29, 2020).

[115] Citta di Palermo - Ufficio Traffico ed Authority, Piano Generale del Traffico Urbano, Palermo, 2010. https://www.comune.palermo.it/js/server/uploads/trasparenza_all/_17042014100136.pdf.

[116] Google Earth Pro v7.3.2.5776, 38° 07’ 18.69”N, 13° 19’ 42.81”E, Eye alt 19.55 mi. SIO, NOAA, U.S. Navy, NGA, GEBCO, Google. (2018). http://www.earth.google.com (accessed March 28, 2020).

[117] Città di Palermo, PANORMUS - Annuario di statistica del comune di palermo 2014, Palermo, 2014. https://www.comune.palermo.it/js/server/uploads/statistica/_28122015095300.pdf.

[118] Risorse Ambiente Palermo (RAP), Carta dei Servizi - Edizione 2019, Palermo, 2019. https://trasparenza.rapspa.it/pagina632_carta-dei-servizi-e-standard-di-qualit.html.

[119] Città di Palermo Servizio Trasporto Pubblico di Massa e Piano Urbano del Traffico, Piano Urbano della Mobilita Sostenibile Quadro Conoscitivo, Palermo, 2019. https://mobilitasostenibile.comune.palermo.it/pums/.

[120] Comune di Palermo, Portale Open data, Open Datasets. (2017). https://opendata.comune.palermo.it/opendata-ultimi-dataset.php (accessed March 28, 2020).

[121] Risorse Ambiente Palermo (RAP), Piano Industriale 2019-2021, (2019) 249. https://trasparenza.rapspa.it/archivio28_provvedimenti-amministrativi_-1_26221_725_1.html.

[122] J.L. Hintze, R.D. Nelson, Violin Plots: A Box Plot-Density Trace Synergism Statistical Computing and Graphics Violin Plots: A Box Plot-Density Trace Synergism, Source Am. Stat. 52 (1998) 181–184. http://www.jstor.org/stable/2685478%5Cnhttp://www.jstor.org/%5Cnhttp://www.jstor.org/action/showPublisher?publisherCode=astata.%5Cnhttp://www.jstor.org.

[123] L.N. Smith, Cyclical learning rates for training neural networks, in: Proc. - 2017 IEEE Winter Conf. Appl. Comput. Vision, WACV 2017, IEEE, 2017: pp. 464–472. doi:10.1109/WACV.2017.58.

[124] J. Cai, J. Luo, S. Wang, S. Yang, Feature selection in machine learning: A new perspective, Neurocomputing. 300 (2018) 70–79. doi:10.1016/j.neucom.2017.11.077.

[125] Z. Allah Bukhsh, I. Stipanovic, A. Saeed, A.G. Doree, Maintenance intervention predictions using entity-embedding neural networks, Autom. Constr. 116 (2020) 103202. doi:10.1016/j.autcon.2020.103202.

[126] F.J. Morales, A. Reyes, N. Caceres, L.M. Romero, F.G. Benitez, J. Morgado, E. Duarte, A machine learning methodology to predict alerts and maintenance interventions in roads, Road Mater. Pavement Des. 0629 (2020). doi:10.1080/14680629.2020.1753098.

[127] S.M. Piryonesi, T.E. El-Diraby, Data Analytics in Asset Management: Cost-Effective Prediction of the Pavement Condition Index, J. Infrastruct. Syst. 26 (2020) 04019036. doi:10.1061/(asce)is.1943-555x.0000512.

[128] VicRoads, Guide to Surface Inspection Rating For Pavements Surfaced with Sprayed Seals and Asphalt, 2009. https://www.vicroads.vic.gov.au/-/media/files/technical-documents-new/technical-reports-and-bulletins/technical-bulletin-tb-50--guide-to-surface-inspection-rating.ashx.

[129] F. Bernard, M. Boucher, M. Grondin, S. Lavoie, P.-P. Legare, N. Martel, Manuel d'identification des dégradations des chaussées flexibles, Quebec, 2002. https://ceriu.qc.ca/system/files/2018-06/Manuel-d-identification-des-degradations-des-chaussees-flexibles.pdf.

[130] Washington State Department of Transportation(WSDOT), Pavement Surface Condition Field Rating Manual for Asphalt Pavement, Washington, 1999. https://www.wsdot.wa.gov/publications/manuals/fulltext/m0000/AsphaltPavements.pdf.

[131] G. Di Mino, G. Salvo, S. Noto, Pavement management system model using a LCCA - microsimulation integrated approach, Adv. Transp. Stud. (2014). doi:10.4399/978885487354410.

[132] R. Roberts, L. Inzerillo, G. Di Mino, Developing a framework for using Structure-from-Motion techniques for Road Distress applications, Eur. Transp. /Transporti Eur. (2020) 1–11. http://www.istiee.unict.it/sites/default/files/files/2_5_ET_76.pdf.

[133] T.B.J. Coenen, A. Golroo, A review on automated pavement distress detection methods, Cogent Eng. 4 (2017). doi:10.1080/23311916.2017.1374822.

[134] K.C.P. Wang, W. Gong, Automated pavement distress survey: A review and a new direction, in: Pavement Eval. Conf., Roanoke, 2002: pp. 21–25. http://pms.nevadadot.com/2002presentations/43.Pdf.

[135] Q. Zou, Y. Cao, Q. Li, Q. Mao, S. Wang, CrackTree: Automatic crack detection from pavement images, Pattern Recognit. Lett. 33 (2012) 227–238. doi:10.1016/j.patrec.2011.11.004.

[136] A. Mancini, E.S. Malinverni, E. Frontoni, P. Zingaretti, Road pavement crack automatic detection by MMS images, 2013 21st Mediterr. Conf. Control Autom. MED 2013 - Conf. Proc. (2013) 1589–1596. doi:10.1109/MED.2013.6608934.

[137] H.S. Yoo, Y.S. Kim, Development of a crack recognition algorithm from non-routed pavement images using artificial neural network and binary logistic regression, KSCE J. Civ. Eng. 20 (2016) 1151–1162. doi:10.1007/s12205-015-1645-9.

[138] S. Miah, A. Uus, P. Liatsis, S. Roberts, S. Twist, M. Hovens, H. Godding, Design of

multidimensional sensor fusion system for road pavement inspection, in: 2015 22nd Int. Conf. Syst. Signals Image Process. - Proc. IWSSIP 2015, IEEE, 2015: pp. 304–308. doi:10.1109/IWSSIP.2015.7314236.

[139] S.K. Ryu, T. Kim, Y.R. Kim, Image-Based Pothole Detection System for ITS Service and Road Management System, Math. Probl. Eng. 2015 (2015). doi:10.1155/2015/968361.

[140] D. Joubert, A. Tyatyantsi, J. Mphahlehle, V. Manchidi, Pothole tagging system, in: 4th Robot. Mechatronics Conf. South Africa, 2011. http://hdl.handle.net/10204/5384.

[141] M. Quintana, J. Torres, J.M. Menéndez, A simplified computer vision system for road surface inspection and maintenance, IEEE Trans. Intell. Transp. Syst. 17 (2016) 608–619. doi:10.1109/TITS.2015.2482222.

[142] M. Gavilán, D. Balcones, O. Marcos, D.F. Llorca, M.A. Sotelo, I. Parra, M. Ocaña, P. Aliseda, P. Yarza, A. Amírola, Adaptive road crack detection system by pavement classification, Sensors. 11 (2011) 9628–9657. doi:10.3390/s111009628.

[143] L. Huidrom, L.K. Das, S.K. Sud, Method for Automated Assessment of Potholes, Cracks and Patches from Road Surface Video Clips, Procedia - Soc. Behav. Sci. 104 (2013) 312–321. doi:10.1016/j.sbspro.2013.11.124.

[144] G.M. Hadjidemetriou, S.E. Christodoulou, P.A. Vela, Automated detection of pavement patches utilizing support vector machine classification, Proc. 18th Mediterr. Electrotech. Conf. Intell. Effic. Technol. Serv. Citizen, MELECON 2016. (2016) 18–20. doi:10.1109/MELCON.2016.7495460.

[145] S.C. Radopoulou, I. Brilakis, Patch detection for pavement assessment, Autom. Constr. 53 (2015) 95–104. doi:10.1016/j.autcon.2015.03.010.

[146] C.W. Yi, Y.T. Chuang, C.S. Nian, Toward Crowdsourcing-Based Road Pavement Monitoring by Mobile Sensing Technologies, IEEE Trans. Intell. Transp. Syst. 16 (2015). doi:10.1109/TITS.2014.2378511.

[147] L.C. Lima, V.J.P. Amorim, I.M. Pereira, F.N. Ribeiro, R.A.R. Oliveira, Using crowdsourcing techniques and mobile devices for asphaltic pavement quality recognition, in: Brazilian Symp. Comput. Syst. Eng. SBESC, 2017. doi:10.1109/SBESC.2016.029.

[148] F. Seraj, B.J. Van Der Zwaag, A. Dilo, T. Luarasi, P. Havinga, Roads: A road pavement monitoring system for anomaly detection using smart phones, in: Lect. Notes Comput. Sci. (Including Subser. Lect. Notes Artif. Intell. Lect. Notes Bioinformatics), 2016. doi:10.1007/978-3-319-29009-6_7.

[149] H. Maeda, Y. Sekimoto, T. Seto, T. Kashiyama, H. Omata, Road Damage Detection Using Deep Neural Networks with Images Captured Through a Smartphone, (2018) 4–6. doi:10.3390/ijerph13010031.

[150] T. El-korchi, N. Wittels, Visual Appearance of Surface Distress in PCC Pavements : I . Crack Luminance, Transp. Res. Rec. (1990) 74–83.

[151] D.A. Casas Avellaneda, J.F. López-Parra, Detection and localization of potholes in roadways using smartphones, Dyna. 83 (2016) 156–162. doi:10.15446/dyna.v83n195.44919.

[152] C. Chiculita, L. Frangu, A low-cost pavement image acquisition system, 2016 IEEE 22nd Int. Symp. Des. Technol. Electron. Packag. SIITME 2016. (2016) 279–282. doi:10.1109/SIITME.2016.7777295.

[153] R. Wix, R. Leschinski, Cracking – a Tale of Four Systems, in: 25th Aust. Road Res. Board Conf.,

2012: pp. 1–20. http://114.111.144.247/Presto/content/Detail.aspx?ctID=MjE1ZTI4YzctZjc1YS00MzQ4LTkyY2UtMDJmNTgxYjg2ZDA5&rID=MzIxNw==&qrs=RmFsc2U=&ph=VHJ1ZQ==&bckToL=VHJ1ZQ==&rrtc=VHJ1ZQ==.

[154] S. Mathavan, K. Kamal, M. Rahman, A Review of Three-Dimensional Imaging Technologies for Pavement Distress Detection and Measurements, IEEE Trans. Intell. Transp. Syst. 16 (2015) 2353–2362. doi:10.1109/TITS.2015.2428655.

[155] A. Mahmoudzadeh, S.F. Yeganeh, A. Golroo, Kinect, a novel cutting edge tool in pavement data collection, in: Int. Arch. Photogramm. Remote Sens. Spat. Inf. Sci. - ISPRS Arch., 2015. doi:10.5194/isprsarchives-XL-1-W5-425-2015.

[156] A. Benedetto, F. Tosti, L. Bianchini Ciampoli, F. D'Amico, An overview of ground-penetrating radar signal processing techniques for road inspections, Signal Processing. 132 (2017) 201–209. doi:10.1016/j.sigpro.2016.05.016.

[157] G. Luis, C. Antunes, Road Rutting Measurement Using Mobile LiDAR Systems Point Cloud, Int. J. Geo-Information. 8 (2019) 404. doi:10.3390/ijgi8090404.

[158] L. Inzerillo, G. Di Mino, R. Roberts, Image-based 3D reconstruction using traditional and UAV datasets for analysis of road pavement distress, Autom. Constr. 96 (2018) 457–469. doi:10.1016/j.autcon.2018.10.010.

[159] I. Kertész, T. Lovas, Á. Barsi, Photogrammetric pavement detection system, Int. Arch. Photogramm. Remote Sens. XXXVII (2008) 897–902. doi:10.1201/9780203882191.ch85.

[160] I. Abdic, L. Fridman, D.E. Brown, W. Angell, B. Reimer, E. Marchi, B. Schuller, Detecting road surface wetness from audio: A deep learning approach, in: Proc. - Int. Conf. Pattern Recognit., 2016: pp. 3458–3463. doi:10.1109/ICPR.2016.7900169.

[161] R. Madli, S. Hebbar, P. Pattar, V. Golla, Automatic detection and notification of potholes and humps on roads to aid drivers, IEEE Sens. J. 15 (2015) 4313–4318. doi:10.1109/JSEN.2015.2417579.

[162] G. Erdogan, L. Alexander, R. Rajamani, Estimation of tire-road friction coefficient using a novel wireless piezoelectric tire sensor, IEEE Sens. J. 11 (2011) 267–279. doi:10.1109/JSEN.2010.2053198.

[163] H. Hasni, A.H. Alavi, K. Chatti, N. Lajnef, A self-powered surface sensing approach for detection of bottom-up cracking in asphalt concrete pavements: Theoretical/numerical modeling, Constr. Build. Mater. 144 (2017) 728–746. doi:10.1016/j.conbuildmat.2017.03.197.

[164] K.B. Singh, S. Taheri, Estimation of tire–road friction coefficient and its application in chassis control systems, Syst. Sci. Control Eng. 3 (2015) 39–61. doi:10.1080/21642583.2014.985804.

[165] A. Rahim, K.P. George, Falling weight deflectometer for estimating subgrade elastic moduli, J. Transp. Eng. 129 (2003) 100–107. doi:10.1061/(ASCE)0733-947X(2003)129:1(100).

[166] J.L.Y. Lee, D.H. Chen, K.H. Stokoe, T. Scullion, Evaluating potential for reflection cracking with rolling dynamic deflectometer, Transp. Res. Rec. (2004) 16–24. doi:10.3141/1869-02.

[167] N. Banks, D. Bayliss, S. Glaister, Motoring towards 2050 -Roads and Reality Technical Report, 2007. https://www.racfoundation.org/wp-content/uploads/2017/11/roads-and-reality-glaister-et-al-041207-technical-report.pdf.

[168] C. Zwerling, C. Peek-Asa, P.S. Whitten, S.W. Choi, N.L. Sprince, M.P. Jones, Fatal motor vehicle crashes in rural and urban areas: Decomposing rates into contributing factors, Inj. Prev. 11

(2005) 24–28. doi:10.1136/ip.2004.005959.

[169] Department for Transport, Reported road casualties in GB: 2016 annual report, (2017) 1–28. https://www.gov.uk/government/uploads/system/uploads/attachment_data/file/648081/rrcgb2016-01.pdf.

[170] J.W. Hall, K.L. Smith, L. Titus-Glover, J.C. Wambold, T.J. Yager, Z. Rado, Guide for Pavement Friction, Washington, DC, 2009. doi:10.17226/23038.

[171] J. Laurent, J.F. Hérbert, D. Lefebvre, Y. Savard, Using 3D laser profiling sensors for the automated measurement of road surface conditions (ruts, macro-texture, raveling, cracks)., in: 7th RILEM Int. Conf. Crack. Pavements, 2009: pp. 157–167.

[172] H. Oliveira, P.L. Correia, Automatic Road Crack Detection and Characterization, IEEE Trans. Intell. Transp. Syst. 14 (2013) 155–168. doi:10.1109/TITS.2012.2208630.

[173] Fugro Roadway, Fugro Roadware, Pavement Manag. Fly. (2014). https://www.fugro.com/docs/default-source/media-resources/pavement-management/pavement-management-flyer.pdf?Status=Master&sfvrsn=2.

[174] S. Cafiso, C. D'Agostino, E. Delfino, A. Montella, From manual to automatic pavement distress detection and classification, in: 5th IEEE Int. Conf. Model. Technol. Intell. Transp. Syst. MT-ITS 2017 - Proc., 2017. doi:10.1109/MTITS.2017.8005711.

[175] J. Landa, D. Prochazka, Automatic Road Inventory Using LiDAR, Procedia Econ. Financ. 12 (2014) 363–370. doi:10.1016/S2212-5671(14)00356-6.

[176] N. Sairam, S. Nagarajan, S. Ornitz, Development of Mobile Mapping System for 3D Road Asset Inventory, Sensors. 16 (2016) 367. doi:10.3390/s16030367.

[177] O.C. Puan, M. Mustaffar, T.-C. Ling, Automated Pavement Imaging Program (APIP) for Pavement Cracks Classification and Quantification, Malaysian J. Civ. Eng. (2007). http://eprints.utm.my/id/eprint/7828/1/LingTungChai2007_Automated_pavement_imaging_program_%28APIP%29.pdf.

[178] S. Chambon, J.M. Moliard, Automatic road pavement assessment with image processing: Review and Comparison, Int. J. Geophys. 2011 (2011). doi:10.1155/2011/989354.

[179] M. Russo, G. Guidi, F. Remondino, Principali tecniche e strumenti per il rilievo tridimensionale in ambito archeologico TT - Main techniques and tools for three-dimensional relief in the field of archaeology, Archeol. e Calc. 22 (2011) 169–198. http://www.archcalc.cnr.it/indice/PDF22/AC_22_Russo_et_al.pdf.

[180] K.C.P. Wang, Elements of automated survey of pavements and a 3D methodology, J. Mod. Transp. 19 (2011) 51–57. doi:10.1007/BF03325740.

[181] M. Ahmed, C.T. Haas, R. Haas, Toward low-cost 3D automatic pavement distress surveying: The Close Range Photogrammetry Approach, Can. J. Civ. Eng. 38 (2011) 1301–1313. doi:10.1139/L11-088.

[182] D. Allegra, G. Gallo, L. Inzerillo, M. Lombardo, F.L.M. Milotta, C. Santagati, F. Stanco, Low Cost Handheld 3D Scanning for Architectural Elements Acquisition, (2016). doi:10.2312/stag.20161372.

[183] K.C.P. Wang, W. Gong, Automated pavement distress survey: A review and a new direction, in: Pavement Eval. Conf., Roanoke, 2002: pp. 21–25. https://www.researchgate.net/profile/Kelvin_Wang3/publication/238694797_Automated_Pavement_Distress_Survey_A_Review_and_A_New_Direction/links/555c772808ae91e75e7740

88.pdf.

[184] C. Zhang, An UAV-based photogrammetric mapping system for road condition assessment, Int. Arch. Photogramm. Remote Sens. Spat. Inf. Sci. (2008).

[185] Y. Tan, Y. Li, UAV Photogrammetry-Based 3D Road Distress Detection, ISPRS Int. J. Geo-Information. 8 (2019) 409. doi:10.3390/ijgi8090409.

[186] C. Zhang, An UAV-based photogrammetric mapping system for road condition assessment, Int. Arch. Photogramm. Remote Sens. Spat. Inf. Sci. 37 (2008) 627–632. http://www.isprs.org/proceedings/XXXVII/congress/5_pdf/109.pdf.

[187] C. Zhang, A. Elaksher, 3D reconstruction from UAV-acquired imagery for road surface distress assessment, in: 31st Asian Conf. Remote Sens. 2010, ACRS 2010, 2010.

[188] S. Martínez, J. Ortiz, M.L. Gil, Geometric documentation of historical pavements using automated digital photogrammetry and high-density reconstruction algorithms, J. Archaeol. Sci. (2015). doi:10.1016/j.jas.2014.10.003.

[189] S. Sarsam, A. Daham, A.M. Ali, Implementation of Close Range Photogrammetry to Evaluate Distresses at Asphalt Pavement Surface, Int. J. Transp. Eng. Traffic Syst. 1 (2015) 31–44. http://civil.journalspub.info/index.php?journal=JTETS&page=article&op=view&path%5B%5D=25.

[190] L. Puzzo, G. Loprencipe, C. Tozzo, A. D'Andrea, Three-dimensional survey method of pavement texture using photographic equipment, Meas. J. Int. Meas. Confed. 111 (2017) 146–157. doi:10.1016/j.measurement.2017.07.040.

[191] C. Poullis, A. Gardner, P. Debevec, M. Del Rey, M. Del Rey, Photogrammetric Modeling And Image-Based Rendering For Rapid Virtual Environment Creation, Univ. South. Calif. Mar. DEL REY. (2004). https://pdfs.semanticscholar.org/4608/9bd9bc7a4754c16d1780c48e9799661bc1ec.pdf?_ga=2.89334619.1909118117.1531491307-2111245449.1530624312.

[192] G. Caroti, I. Martínez-Espejo Zaragoza, A. Piemonte, Accuracy assessment in structure from motion 3D reconstruction from UAV-born images: The influence of the data processing methods, in: Int. Arch. Photogramm. Remote Sens. Spat. Inf. Sci. - ISPRS Arch., 2015. doi:10.5194/isprsarchives-XL-1-W4-103-2015.

[193] M. Gaiani, F. Remondino, F.I. Apollonio, A. Ballabeni, An advanced pre-processing pipeline to improve automated photogrammetric reconstructions of architectural scenes, Remote Sens. (2016). doi:10.3390/rs8030178.

[194] F. Remondino, E. Nocerino, I. Toschi, F. Menna, A critical review of automated photogrammetric processing of large datasets, Int. Arch. Photogramm. Remote Sens. Spat. Inf. Sci. - ISPRS Arch. 42 (2017) 591–599. doi:10.5194/isprs-archives-XLII-2-W5-591-2017.

[195] G. Bitelli, M. Dubbini, A. Zanutta, Terrestrial laser scanning and digital photogrammetry techniques to monitor landslide bodies, XXth ISPRS Congr. Proc. Comm. V. (2004) 246–251. doi:10.1.1.1.9772.

[196] L. Wallace, A. Lucieer, Z. Malenovskỳ, D. Turner, P. Vopěnka, Assessment of forest structure using two UAV techniques: A comparison of airborne laser scanning and structure from motion (SfM) point clouds, Forests. 7 (2016) 1–16. doi:10.3390/f7030062.

[197] D.P. Andrews, J. Bedford, P.G. Bryan, A comparison of laser scanning and structure from motion as applied to the great barn at Harmondsworth, UK, Int. Arch. Photogramm. Remote Sens. Spat.

Inf. Sci. (2013). doi:10.5194/isprsarchives-XL-5-W2-31-2013.

[198] F. Fassi, L. Fregonese, S. Ackermann, V. De Troia, COMPARISON BETWEEN LASER SCANNING AND AUTOMATED 3D MODELLING TECHNIQUES TO RECONSTRUCT COMPLEX AND EXTENSIVE CULTURAL HERITAGE AREAS, ISPRS - Int. Arch. Photogramm. Remote Sens. Spat. Inf. Sci. (2013). doi:10.5194/isprsarchives-XL-5-W1-73-2013.

[199] E. Nocerino, F. Menna, D. Morabito, F. Remondino, I. Toschi, D. Abate, D. Ebolese, E. Farella, F. Fiorillo, S. Minto, P. Rodríguez-Gonzálvez, C. Slongo, M.G. Speraj, THE VAST PROJECT: VALORISATION of HISTORY and LANDSCAPE for PROMOTING the MEMORY of WWI, ISPRS Ann. Photogramm. Remote Sens. Spat. Inf. Sci. 4 (2017) 179–186. doi:10.5194/isprs-annals-IV-2-W2-179-2017.

[200] L. Inzerillo, G. Di Mino, R. Roberts, Image-based 3D reconstruction using traditional and UAV datasets for analysis of road pavement distress, Autom. Constr. 96 (2018) 457–469. doi:10.1016/j.autcon.2018.10.010.

[201] L. Inzerillo, G. Di Mino, F. Di Paola, S. Noto, The diagnosis of road surface distresses through image-based modeling techniques. Experimental survey on laboratory-rutted samples., Life Saf. Secur. 3 (2015) 31–35. http://www.iemest.eu/life-safety-and-security/images/Doc/ARTICOLI/2015/inzerillo_15/Inzerillo05.pdf.

[202] H. Su, S. Maji, E. Kalogerakis, E. Learned-Miller, Multi-view Convolutional Neural Networks for 3D Shape Recognition, in: Proc. IEEE Int. Conf. Comput. Vis. 2015, IEE, Santiago, Chile, 2015: pp. 945–953. https://www.cv-foundation.org/openaccess/content_iccv_2015/papers/Su_Multi-View_Convolutional_Neural_ICCV_2015_paper.pdf.

[203] R. Wang, J. Peethambaran, D. Chen, LiDAR Point Clouds to 3-D Urban Models : A Review, IEEE J. Sel. Top. Appl. Earth Obs. Remote Sens. 11 (2018) 606–627. doi:10.1109/JSTARS.2017.2781132.

[204] D. Maturana, S. Scherer, VoxNet: A 3D Convolutional Neural Network for real-time object recognition, IEEE Int. Conf. Intell. Robot. Syst. 2015-Decem (2015) 922–928. doi:10.1109/IROS.2015.7353481.

[205] W. Cao, Q. Liu, Z. He, Review of Pavement Defect Detection Methods, IEEE Access. 8 (2020) 14531–14544. doi:10.1109/aCCESS.2020.2966881.

[206] C. Santagati, L. Inzerillo, F. Di Paola, Image-Based Modeling Techniques for Architectural Heritage 3D Digitalization: Limits and Potentialities, ISPRS - Int. Arch. Photogramm. Remote Sens. Spat. Inf. Sci. XL-5/W2 (2013) 555–560. doi:10.5194/isprsarchives-XL-5-W2-555-2013.

[207] F. Remondino, M.G. Spera, E. Nocerino, F. Menna, F. Nex, State of the art in high density image matching, Photogramm. Rec. 29 (2014) 144–166. doi:10.1111/phor.12063.

[208] S. Zancajo-Blazquez, D. Gonzalez-Aguilera, H. Gonzalez-Jorge, D. Hernandez-Lopez, An automatic image-Based modelling method applied to forensic infography, PLoS One. 10 (2015) 1–15. doi:10.1371/journal.pone.0118719.

[209] J. Höhle, Oblique Aerial Images and Their Use in Cultural Heritage Documentation, ISPRS - Int. Arch. Photogramm. Remote Sens. Spat. Inf. Sci. XL-5/W2 (2013) 349–354. doi:10.5194/isprsarchives-xl-5-w2-349-2013.

[210] S. Zhang, C.D. Lippitt, S.M. Bogus, P.R.H. Neville, Characterizing pavement surface distress conditions with hyper-spatial resolution natural color aerial photography, Remote Sens. 8 (2016) 1–23. doi:10.3390/rs8050392.

[211] G. Salvo, L. Caruso, A. Scordo, Urban Traffic Analysis through an UAV, Procedia - Soc. Behav. Sci. 111 (2014) 1083–1091. doi:10.1016/j.sbspro.2014.01.143.

[212] D. Giordan, A. Manconi, F. Remondino, F. Nex, Use of unmanned aerial vehicles in monitoring application and management of natural hazards, Geomatics, Nat. Hazards Risk. 8 (2017) 1–4. doi:10.1080/19475705.2017.1315619.

[213] Ente Nazionel per l'Aviazione Civile - Italian Civil Aviation Authority, Regolamento (regulation) mezzi aerei a pilotaggio remoto (remotely piloted aerial vehicles), Rome, 2015. https://www.enac.gov.it/sites/default/files/allegati/2018-Lug/Regulation_RPAS_Issue_2_Rev_4_eng.pdf.

[214] Agisoft, Agisoft PhotoScan, (2017). www.agisoft.com.

[215] M.J. Westoby, J. Brasington, N.F. Glasser, M.J. Hambrey, J.M. Reynolds, "Structure-from-Motion" photogrammetry: A low-cost, effective tool for geoscience applications, Geomorphology. (2012). doi:10.1016/j.geomorph.2012.08.021.

[216] G. Verhoeven, Taking computer vision aloft -archaeological three-dimensional reconstructions from aerial photographs with photoscan, Archaeol. Prospect. 18 (2011) 67–73. doi:doi.org/10.1002/arp.399.

[217] P. Cignoni, M. Callieri, M. Corsini, M. Dellepiane, F. Ganovelli, G. Ranzuglia, MeshLab: An open-source mesh processing tool, in: 6th Eurographics Ital. Chapter Conf. 2008 - Proc., 2008: pp. 129–136. doi:10.2312/LocalChapterEvents/ItalChap/ItalianChapConf2008/129-136.

[218] Robert McNeel & Associates, Rhino3D, (2018). http://rhino3d.com/.

[219] F. Remondino, E. Nocerino, I. Toschi, F. Menna, A Critical Review of Automated Photogrammetric Processing of Large Datasets, ISPRS - Int. Arch. Photogramm. Remote Sens. Spat. Inf. Sci. XLII-2/W5 (2017) 591–599. doi:10.5194/isprs-archives-XLII-2-W5-591-2017.

[220] L. Inzerillo, Integrated Sfm Techniques Using Data Set From Google Earth 3D Model and From Street Level, ISPRS - Int. Arch. Photogramm. Remote Sens. Spat. Inf. Sci. XLII-2/W5 (2017) 361–367. doi:10.5194/isprs-archives-XLII-2-W5-361-2017.

[221] D. Panagiotidis, P. Surový, K. Kuželka, Accuracy of Structure from Motion models in comparison with terrestrial laser scanner for the analysis of DBH and height influence on error behaviour, J. For. Sci. 62 (2016) 357–365. doi:10.17221/92/2015-JFS.

[222] EDF R&D / TELECOM ParisTech (ENST-TSI), CloudCompare, (2016). https://www.danielgm.net/cc/.

[223] W. Hauser, B. Neveu, J.-B. Jourdain, C. Viard, F. Guichard, Image quality benchmark of computational bokeh, Electron. Imaging. 2018 (2018) 340-1-340–10. doi:10.2352/issn.2470-1173.2018.12.iqsp-340.

[224] Z.J. Arrospide E, Bikandi I, García I, Durana G, Aldabaldetreku G, Mechanical properties of polymer-optical fibres, in: B. Christian-Alexander, T. Gries, M. Beckers (Eds.), Polym. Opt. Fibres, Woodhead Publishing, 2017: pp. 201–216. doi:https://doi.org/10.1016/C2014-0-00562-X.

[225] M. Gaiani, F.I. Apollonio, A. Ballabeni, F. Remondino, Securing color fidelity in 3D architectural heritage scenarios, Sensors (Switzerland). 17 (2017). doi:10.3390/s17112437.

[226] Z. Li, C. Cheng, M.-P. Kwan, X. Tong, S. Tian, Identifying Asphalt Pavement Distress Using UAV LiDAR Point Cloud Data and Random Forest Classification, ISPRS Int. J. Geo-Information. 8 (2019) 39. doi:10.3390/ijgi8010039.

[227] D.B.A. Chacra, J.S. Zelek, Fully Automated Road Defect Detection Using Street View Images, in: Proc. - 2017 14th Conf. Comput. Robot Vision, CRV 2017, 2018: pp. 353–360. doi:10.1109/CRV.2017.50.

[228] D. Zhang, Q. Zou, H. Lin, X. Xu, L. He, R. Gui, Q. Li, Automatic pavement defect detection using 3D laser profiling technology, Autom. Constr. 96 (2018). doi:10.1016/j.autcon.2018.09.019.

[229] R. Gui, X. Xu, D. Zhang, H. Lin, F. Pu, L. He, M. Cao, A component decomposition model for 3D laser scanning pavement data based on high-pass filtering and sparse analysis, Sensors. 18 (2018) 2294. doi:10.3390/s18072294.

[230] B. Li, K.C.P. Wang, A. Zhang, Y. Fei, Automatic Segmentation and Enhancement of Pavement Cracks Based on 3D Pavement Images, J. Adv. Transp. 2019 (2019) 1–9. doi:10.1155/2019/1813763.

[231] A. Akagic, E. Buza, S. Omanovic, A. Karabegovic, Pavement crack detection using Otsu thresholding for image segmentation, in: 2018 41st Int. Conv. Inf. Commun. Technol. Electron. Microelectron. MIPRO 2018 - Proc., Croatian Society MIPRO, 2018: pp. 1092–1097. doi:10.23919/MIPRO.2018.8400199.

[232] S. Agnisarman, S. Lopes, K. Chalil Madathil, K. Piratla, A. Gramopadhye, A survey of automation-enabled human-in-the-loop systems for infrastructure visual inspection, Autom. Constr. 97 (2019) 52–76. doi:10.1016/j.autcon.2018.10.019.

[233] M. Li, L. Nan, N. Smith, P. Wonka, Reconstructing building mass models from UAV images, Comput. Graph. 54 (2016) 84–93. doi:10.1016/j.cag.2015.07.004.

[234] R. Schnabel, R. Wahl, R. Klein, Efficient RANSAC for point-cloud shape detection, Comput. Graph. Forum. 26 (2007) 214–226. doi:10.1111/j.1467-8659.2007.01016.x.

[235] E. Oniga, A. Breaban, F. Statescu, Determining the optimum number of ground control points for obtaining high precision results based on UAS images, Proceedings. 2 (2018). doi:10.3390/ecrs-2-05165.

[236] Agisoft LLC, Agisoft Metashape Professional, (2019). www.agisoft.com.

[237] J. Carballido, M. Perez-Ruiz, L. Emmi, J. Agüera, Comparison of positional accuracy between rtk and rtx gnss based on the autonomous agricultural vehicles under field conditions, Appl. Eng. Agric. 30 (2014) 361–366. doi:10.13031/aea.30.10342.

[238] J. Shan, Z. Hu, P. Tao, L. Wang, S. Zhang, S. Ji, Toward a unified theoretical framework for photogrammetry, Geo-Spatial Inf. Sci. 00 (2020) 1–12. doi:10.1080/10095020.2020.1730712.

[239] B. Tippetts, D.J. Lee, K. Lillywhite, J. Archibald, Review of stereo vision algorithms and their suitability for resource-limited systems, J. Real-Time Image Process. 11 (2016) 5–25. doi:10.1007/s11554-012-0313-2.

[240] Z. Wang, Review of real-time three-dimensional shape measurement techniques, Meas. J. Int. Meas. Confed. 156 (2020) 107624. doi:10.1016/j.measurement.2020.107624.

[241] L. De-Maeztu, A. Villanueva, R. Cabeza, Stereo matching using gradient similarity and locally adaptive support-weight, Pattern Recognit. Lett. 32 (2011) 1643–1651. doi:10.1016/j.patrec.2011.06.027.

[242] W. Liu, Z. Wang, X. Liu, N. Zeng, Y. Liu, F.E. Alsaadi, A survey of deep neural network architectures and their applications, Neurocomputing. 234 (2017) 11–26. doi:10.1016/j.neucom.2016.12.038.

[243] O. Russakovsky, J. Deng, H. Su, J. Krause, S. Satheesh, S. Ma, Z. Huang, A. Karpathy, A. Khosla, M. Bernstein, A.C. Berg, L. Fei-Fei, ImageNet Large Scale Visual Recognition Challenge, Int. J. Comput. Vis. 115 (2015) 211–252. doi:10.1007/s11263-015-0816-y.

[244] K. He, X. Zhang, S. Ren, J. Sun, Delving deep into rectifiers: Surpassing human-level performance on imagenet classification, Proc. IEEE Int. Conf. Comput. Vis. 2015 Inter (2015) 1026–1034. doi:10.1109/ICCV.2015.123.

[245] H. Zakeri, F.M. Nejad, A. Fahimifar, Image Based Techniques for Crack Detection, Classification and Quantification in Asphalt Pavement: A Review, Arch. Comput. Methods Eng. 24 (2017) 935–977. doi:10.1007/s11831-016-9194-z.

[246] Y. LeCun, Y. Bengio, G. Hinton, Deep learning, Nat. Methods. 521 (2015) 436. doi:doi:10.1038/nature14539.

[247] X. Feng, Y. Jiang, X. Yang, M. Du, X. Li, Computer vision algorithms and hardware implementations: A survey, Integr. VLSI J. 69 (2019) 309–320. doi:10.1016/j.vlsi.2019.07.005.

[248] N.J. Kwak, D.J. Kwon, Y.G. Kim, J.H. Ahn, Color image segmentation using edge and adaptive threshold value based on the image characteristics, in: Proc. 2004 Int. Symp. Intell. Signal Process. Commun. Syst. ISPACS 2004, IEEE, 2004: pp. 555–558. doi:10.1109/ispacs.2004.1439118.

[249] M. Sridevi, C. Mala, A Survey on Monochrome Image Segmentation Methods, 6 (2012) 548–555. doi:10.1016/j.protcy.2012.10.066.

[250] H. Kaiqi, W. Zhenyang, W. Qiao, Image enhancement based on the statistics of visual representation, Image Vis. Comput. 23 (2005) 51–57. doi:10.1016/j.imavis.2004.07.005.

[251] A.M.A. Talab, Z. Huang, F. Xi, L. Haiming, Detection crack in image using Otsu method and multiple filtering in image processing techniques, Optik (Stuttg). 127 (2016) 1030–1033. doi:10.1016/j.ijleo.2015.09.147.

[252] W. Wang, M. Wang, H. Li, H. Zhao, K. Wang, C. He, J. Wang, S. Zheng, J. Chen, Pavement crack image acquisition methods and crack extraction algorithms: A review, J. Traffic Transp. Eng. (English Ed. 6 (2019) 535–556. doi:10.1016/j.jtte.2019.10.001.

[253] E. Salari, G. Bao, Pavement distress detection and classification using feature mapping, 2010 IEEE Int. Conf. Electro/Information Technol. EIT2010. (2010). doi:10.1109/EIT.2010.5612119.

[254] A. Saxena, M. Prasad, A. Gupta, N. Bharill, O.P. Patel, A. Tiwari, M.J. Er, W. Ding, C.T. Lin, A review of clustering techniques and developments, Neurocomputing. 267 (2017) 664–681. doi:10.1016/j.neucom.2017.06.053.

[255] R.R. Yang, J.Q. Hiu, H.F. Meng, Pavement Crack Extraction Using Iterative Clustering Algorithm Based on Manifold Distance, Comput. Eng. 37 (2011) 212–214. https://www.scopus.com/record/display.uri?eid=2-s2.0-84894600568&origin=inward&txGid=c2b61a7617ddd681c64e519fef4ecaf4.

[256] N. Wang, S. Wang, H. Du, An iterative optimization clustering algorithm based on manifold distance, in: 2009 4th IEEE Conf. Ind. Electron. Appl. ICIEA 2009, IEEE, 2009: pp. 1565–1568. doi:10.1109/ICIEA.2009.5138457.

[257] A. Nasseri, M.J. Mohammadzadeh, S.H. Tabatabaei Raeisi, Fracture enhancement based on artificial ants and fuzzy c-means clustering (FCMC) in Dezful Embayment of Iran, J. Geophys. Eng. 12 (2015) 227–241. doi:10.1088/1742-2132/12/2/227.

[258] G. Zhao, T. Wang, J. Ye, Anisotropic clustering on surfaces for crack extraction, Mach. Vis. Appl.

26 (2015) 675–688. doi:10.1007/s00138-015-0682-1.

[259] A. Zhang, K.C.P. Wang, Y. Fei, Y. Liu, C. Chen, G. Yang, J.Q. Li, E. Yang, S. Qiu, Automated Pixel-Level Pavement Crack Detection on 3D Asphalt Surfaces with a Recurrent Neural Network, Comput. Civ. Infrastruct. Eng. 34 (2019) 213–229. doi:10.1111/mice.12409.

[260] M. Sikander Hayat Khiyal, A. Khan, A. Bibi, Modified Watershed Algorithm for Segmentation of 2D Images, Proc. 2009 InSITE Conf. 6 (2009). doi:10.28945/3349.

[261] R. Achanta, A. Shaji, K. Smith, A. Lucchi, SLIC Superpixels compared to State-of-the-Art Superpixel Methods, IEEE Trans. Pattern Anal. Mach. Intell. 34 (2012) 2274–2281. doi:10.1109/vr.2012.6180941.

[262] R.S. Adhikari, O. Moselhi, A. Bagchi, Image-based retrieval of concrete crack properties for bridge inspection, Autom. Constr. 39 (2014) 180–194. doi:10.1016/j.autcon.2013.06.011.

[263] I. Abdel-Qader, O. Abudayyeh, M.E. Kelly, Analysis of edge-detection techniques for crack identification in bridges, J. Comput. Civ. Eng. 17 (2003) 255–263. doi:10.1061/(ASCE)0887-3801(2003)17:4(255).

[264] Y. Adu-Gyamfi, C. Kambhamettu, N.O. Attoh-Okine, Performance Assessment of Flexible Pavements Using Active Contour Models, in: 2013 Airf. Highw. Pavement Conf., 2013. doi:10.1061/9780784413005.073.

[265] M. Avila, S. Begot, F. Duculty, T.S. Nguyen, 2D image based road pavement crack detection by calculating minimal paths and dynamic programming, 2014 IEEE Int. Conf. Image Process. ICIP 2014. (2014) 783–787. doi:10.1109/ICIP.2014.7025157.

[266] N. Attoh-Okine, A. Ayenu-Prah, Evaluating pavement cracks with bidimensional empirical mode decomposition, EURASIP J. Adv. Signal Process. 2008 (2008). doi:10.1155/2008/861701.

[267] H. Zhao, G. Qin, X. Wang, Improvement of canny algorithm based on pavement edge detection, Proc. - 2010 3rd Int. Congr. Image Signal Process. CISP 2010. 2 (2010) 964–967. doi:10.1109/CISP.2010.5646923.

[268] F. Cong, H. Hautakangas, J. Nieminen, O. Mazhelis, M. Perttunen, J. Riekki, T. Ristaniemi, Applying wavelet packet decomposition and one-class support vector machine on vehicle acceleration traces for road anomaly detection, Lect. Notes Comput. Sci. (Including Subser. Lect. Notes Artif. Intell. Lect. Notes Bioinformatics). 7951 LNCS (2013) 291–299. doi:10.1007/978-3-642-39065-4-36.

[269] C. Chen, S. Zhang, G. Zhang, S.M. Bogus, V. Valentin, Discovering temporal and spatial patterns and characteristics of pavement distress condition data on major corridors in New Mexico, J. Transp. Geogr. 38 (2014) 148–158. doi:10.1016/j.jtrangeo.2014.06.005.

[270] J. Chaki, N. Dey, A Beginner's Guide to Image Shape Feature Extraction Techniques, CRC Press, Boca Raton, 2019. doi:10.1201/9780429287794.

[271] G. Moussa, H. Hussain, A New Technique for Automatic Detection and Parameters Estimation of Pavement Crack, Proc. 4th Int. Multi- …. (2011) 1–6. doi:10.13140/2.1.3191.2001.

[272] A.M. Khan, S. Ravi, Image Segmentation Methods : A Comparative Study, Int. J. Soft Comput. Eng. 3 (2013).

[273] B. Basavaprasad, M. Ravi, A COMPARATIVE STUDY ON CLASSIFICATION OF IMAGE SEGMENTATION METHODS WITH A FOCUS ON GRAPH BASED TECHNIQUES, Int. J. Res. Technol. 3 (2014) 310–315.

[274] Y.-C. Tsai, V. Kaul, R.M. Mersereau, Critical Assessment of Pavement Distress Segmentation Methods, J. Transp. Eng. 136 (2010) 11–19. doi:10.1061/(ASCE)TE.1943-5436.0000051.

[275] A. Krizhevsky, I. Sutskever, G.. Hinton, ImageNet classification with deep convolutional neural networks, in: 26th Annu. Conf. Neural Inf. Process. Syst. 2012, NIPS 2012, Lake Tahoe, 2012: pp. 1097–1105.

[276] K. Simonyan, A. Zisserman, Very deep convolutional networks for large-scale image recognition, in: 3rd Int. Conf. Learn. Represent. ICLR 2015 - Conf. Track Proc., 2015: pp. 1–14. https://arxiv.org/pdf/1409.1556.pdf.

[277] C. Szegedy, W. Liu, Y. Jia, P. Sermanet, S. Reed, D. Anguelov, D. Erhan, V. Vanhoucke, A. Rabinovich, Going deeper with convolutions, in: Proc. IEEE Comput. Soc. Conf. Comput. Vis. Pattern Recognit., 2015. doi:10.1109/CVPR.2015.7298594.

[278] K. He, X. Zhang, S. Ren, J. Sun, Deep residual learning for image recognition, in: Proc. IEEE Comput. Soc. Conf. Comput. Vis. Pattern Recognit., IEEE Computer Society, 2016: pp. 770–778. doi:10.1109/CVPR.2016.90.

[279] G. Huang, Z. Liu, L. van der Maaten, K.Q. Weinberger, Densely connected convolutional networks, in: IEEE Conf. Comput. Vis. Pattern Recognit. (CVPR), 2017, 2017: pp. 4700–4708. http://openaccess.thecvf.com/content_cvpr_2017/html/Huang_Densely_Connected_Convolutional_CVPR_2017_paper.html.

[280] J. Hu, L. Shen, G. Sun, Squeeze-and-Excitation Networks, in: IEEE Conf. Comput. Vis. Pattern Recognit. (CVPR), 2018, 2018: pp. 7132–7141. http://openaccess.thecvf.com/content_cvpr_2018/html/Hu_Squeeze-and-Excitation_Networks_CVPR_2018_paper.html.

[281] B. Zoph, V. Vasudevan, J. Shlens, Q. V. Le, Learning Transferable Architectures for Scalable Image Recognition, in: IEEE Conf. Comput. Vis. Pattern Recognit. (CVPR), 2018, 2018: pp. 8697–8710. doi:10.1109/CVPR.2018.00907.

[282] F.N. Iandola, S. Han, M.W. Moskewicz, K. Ashraf, W.J. Dally, K. Keutzer, SqueezeNet: AlexNet-level accuracy with 50x fewer parameters and <0.5MB model size, (2016) 1–13. http://arxiv.org/abs/1602.07360.

[283] A.G. Howard, M. Zhu, B. Chen, D. Kalenichenko, W. Wang, T. Weyand, M. Andreetto, H. Adam, MobileNets: Efficient Convolutional Neural Networks for Mobile Vision Applications, (2017). http://arxiv.org/abs/1704.04861.

[284] X. Zhang, X. Zhou, M. Lin, J. Sun, ShuffleNet: An Extremely Efficient Convolutional Neural Network for Mobile Devices, in: IEEE Conf. Comput. Vis. Pattern Recognit. (CVPR), 2018, 2018: pp. 6848–6856. http://openaccess.thecvf.com/content_cvpr_2018/html/Zhang_ShuffleNet_An_Extremely_CVPR_2018_paper.html.

[285] B. Wu, A. Wan, X. Yue, P. Jin, S. Zhao, N. Golmant, A. Gholaminejad, J. Gonzalez, K. Keutzer, Shift: A Zero FLOP, Zero Parameter Alternative to Spatial Convolutions, in: Proc. IEEE Comput. Soc. Conf. Comput. Vis. Pattern Recognit., 2018: pp. 9127–9135. doi:10.1109/CVPR.2018.00951.

[286] W. Chen, D. Xie, Y. Zhang, S. Pu, All you need is a few shifts: Designing efficient convolutional neural networks for image classification, in: Proc. IEEE Comput. Soc. Conf. Comput. Vis. Pattern Recognit., 2019: pp. 7234–7243. doi:10.1109/CVPR.2019.00741.

[287] M. Everingham, S.M.A. Eslami, L. Van Gool, C.K.I. Williams, J. Winn, A. Zisserman, The Pascal

Visual Object Classes Challenge: A Retrospective, Int. J. Comput. Vis. 111 (2014) 98–136. doi:10.1007/s11263-014-0733-5.

[288] T.Y. Lin, M. Maire, S. Belongie, J. Hays, P. Perona, D. Ramanan, P. Dollár, C.L. Zitnick, Microsoft COCO: Common objects in context, Lect. Notes Comput. Sci. (Including Subser. Lect. Notes Artif. Intell. Lect. Notes Bioinformatics). 8693 LNCS (2014) 740–755. doi:10.1007/978-3-319-10602-1_48.

[289] J. Huang, V. Rathod, C. Sun, M. Zhu, A. Korattikara, A. Fathi, I. Fischer, Z. Wojna, Y. Song, S. Guadarrama, K. Murphy, Speed/accuracy trade-offs for modern convolutional object detectors, Proc. - 30th IEEE Conf. Comput. Vis. Pattern Recognition, CVPR 2017. 2017-Janua (2017) 3296–3305. doi:10.1109/CVPR.2017.351.

[290] M. Abadi, P. Barham, J. Chen, Z. Chen, A. Davis, J. Dean, M. Devin, S. Ghemawat, G. Irving, M. Isard, M. Kudlur, J. Levenberg, R. Monga, S. Moore, D.G. Murray, B. Steiner, P. Tucker, V. Vasudevan, P. Warden, M. Wicke, Y. Yu, X. Zheng, G. Brain, I. Osdi, P. Barham, J. Chen, Z. Chen, A. Davis, J. Dean, M. Devin, S. Ghemawat, G. Irving, M. Isard, M. Kudlur, J. Levenberg, R. Monga, S. Moore, D.G. Murray, B. Steiner, P. Tucker, V. Vasudevan, P. Warden, M. Wicke, Y. Yu, X. Zheng, TensorFlow: A System for Large-Scale Machine Learning This paper is included in the Proceedings of the TensorFlow : A system for large-scale machine learning, in: 12th USENIX Conf. Oper. Syst. Des. Implement., 2016.

[291] W. Liu, D. Anguelov, D. Erhan, C. Szegedy, S. Reed, C.Y. Fu, A.C. Berg, SSD: Single shot multibox detector, in: Eur. Conf. Comput. Vis. ECCV 2016, 2016: pp. 21–37. doi:10.1007/978-3-319-46448-0_2.

[292] C. Szegedy, V. Vanhoucke, S. Ioffe, J. Shlens, Z. Wojna, Rethinking the Inception Architecture for Computer Vision, Proc. IEEE Comput. Soc. Conf. Comput. Vis. Pattern Recognit. 2016-Decem (2016) 2818–2826. doi:10.1109/CVPR.2016.308.

[293] J. Dai, Y. Li, K. He, J. Sun, R-FCN: Object Detection via Region-based Fully Convolutional Networks, in: Adv. Neural Inf. Process. Syst., 2016: pp. 379–387. http://papers.nips.cc/paper/6465-r-fcn-object-detection-via-region-based-fully-convolutional-networks.pdf.

[294] S. Ren, K. He, R. Girshick, J. Sun, Faster R-CNN: Towards Real-Time Object Detection with Region Proposal Networks., IEEE Trans. Pattern Anal. Mach. Intell. 39 (2017) 1137–1149. doi:10.1109/TPAMI.2016.2577031.

[295] J. Redmon, S. Divvala, R. Girshick, A. Farhadi, You only look once: Unified, real-time object detection, in: Proc. IEEE Comput. Soc. Conf. Comput. Vis. Pattern Recognit. 2016, IEEE, Las Vegas, 2016: pp. 779–788. doi:10.1109/CVPR.2016.91.

[296] T. Lin, P. Doll, R. Girshick, K. He, B. Hariharan, S. Belongie, F. Ai, C. Tech, Feature Pyramid Networks for Object Detection, in: Proc. IEEE Conf. Comput. Vis. Pattern Recognit. (CVPR), 2017, IEEE, Honolulu, Hawaii, 2017: pp. 2117–2125. https://openaccess.thecvf.com/content_cvpr_2017/papers/Lin_Feature_Pyramid_Networks_CVPR_2017_paper.pdf.

[297] P. Jin, V. Rathod, X. Zhu, Pooling Pyramid Network for Object Detection, ArXiv E-Prints. (2018). https://arxiv.org/pdf/1807.03284.pdf.

[298] E. Shelhamer, J. Long, T. Darrell, Fully Convolutional Networks for Semantic Segmentation, IEEE Trans. Pattern Anal. Mach. Intell. 39 (2017) 640–651. doi:10.1109/TPAMI.2016.2572683.

[299] A. Garcia-Garcia, S. Orts-Escolano, S. Oprea, V. Villena-Martinez, J. Garcia-Rodriguez, A Review

on Deep Learning Techniques Applied to Semantic Segmentation, (2017) 1–23. http://arxiv.org/abs/1704.06857.

[300] J.P. Sinno, Y. Qiang, A Survey on Transfer Learning, IEEE Trans. Knowl. Data Eng. 22 (2010) 1345–1359. doi:10.1109/TKDE.2009.191.

[301] C. Shorten, T.M. Khoshgoftaar, A survey on Image Data Augmentation for Deep Learning, J. Big Data. 6 (2019). doi:10.1186/s40537-019-0197-0.

[302] A. Canziani, E. Culurciello, A. Paszke, An Analysis of Deep Neural Network Models for Practical Applications., ArXiv Prepr. (n.d.). doi:arXiv:1605.07678v4.

[303] M. Oquab, L. Bottou, I. Laptev, J. Sivic, Learning and transferring mid-level image representations using convolutional neural networks, in: Proc. IEEE Comput. Soc. Conf. Comput. Vis. Pattern Recognit., 2014: pp. 1717–1724. doi:10.1109/CVPR.2014.222.

[304] A. Ahmed, K. Yu, W. Xu, Y. Gong, E. Xing, Training Hierarchical Feed-Forward Visual Recognition Models Using Transfer Learning from Pseudo-Tasks, in: Eur. Conf. Comput. Vis. 2008, Marseille, 2008: pp. 69–82. doi:10.1007/978-3-540-88690-7_6.

[305] J. Yosinski, J. Clune, Y. Bengio, H. Lipson, How transferable are features in deep neural networks?, in: Proc. 27th Int. Conf. Neural Inf. Process. Syst., 2014: pp. 3320–3328.

[306] K. Zhang, H.D. Cheng, B. Zhang, Unified Approach to Pavement Crack and Sealed Crack Detection Using Preclassification Based on Transfer Learning, J. Comput. Civ. Eng. 32 (2018) 04018001. doi:10.1061/(ASCE)CP.1943-5487.0000736.

[307] H. Ceylan, M.B. Bayrak, K. Gopalakrishnan, Neural networks applications in pavement engineering: A recent survey, Int. J. Pavement Res. Technol. 7 (2014). doi:10.6135/ijprt.org.tw/2014.

[308] K. Gopalakrishnan, Deep Learning in Data-Driven Pavement Image Analysis and Automated Distress Detection: A Review, Data. 3 (2018) 28. doi:10.3390/data3030028.

[309] F. Zantalis, G. Koulouras, S. Karabetsos, D. Kandris, A Review of Machine Learning and IoT in Smart Transportation, Futur. Internet. 11 (2019) 94. doi:10.3390/fi11040094.

[310] C. Koch, K. Georgieva, V. Kasireddy, B. Akinci, P. Fieguth, A review on computer vision based defect detection and condition assessment of concrete and asphalt civil infrastructure, Adv. Eng. Informatics. (2015). doi:10.1016/j.aei.2015.01.008.

[311] N.N. Eldin, A.B. Senouci, A Pavement Condition-Rating Model Using Backpropagation Neural Networks, Comput. Civ. Infrastruct. Eng. 10 (1995) 433–441. doi:https://doi.org/10.1111/j.1467-8667.1995.tb00303.x.

[312] Hamdi, S.P. Hadiwardoyo, A.G. Correia, P. Pereira, P. Cortez, Prediction of surface distress using neural networks, AIP Conf. Proc. 1855 (2017). doi:10.1063/1.4985502.

[313] M.S.R. Amin, L.E. Amador-Jiménez, Pavement management with dynamic traffic and artificial neural network: a case study of Montreal, Can. J. Civ. Eng. 43 (2015) 241–251. doi:https://doi.org/10.1139/cjce-2015-0299.

[314] S. Terzi, Modeling the pavement serviceability ratio of flexible highway pavements by artificial neural networks, Constr. Build. Mater. 21 (2007) 590–593. doi:10.1016/j.conbuildmat.2005.11.001.

[315] A. Bianchini, P. Bandini, Prediction of pavement performance through neuro-fuzzy reasoning, Comput. Civ. Infrastruct. Eng. 25 (2010) 39–54. doi:10.1111/j.1467-8667.2009.00615.x.

[316] F. Gu, X. Luo, Y. Zhang, Y. Chen, R. Luo, R.L. Lytton, Prediction of geogrid-reinforced flexible pavement performance using artificial neural network approach, Road Mater. Pavement Des. 19 (2018) 1147–1163. doi:10.1080/14680629.2017.1302357.

[317] C. Plati, P. Georgiou, V. Papavasiliou, Simulating pavement structural condition using artificial neural networks, Struct. Infrastruct. Eng. 12 (2016) 1127–1136. doi:10.1080/15732479.2015.1086384.

[318] G. Sollazzo, T.F. Fwa, G. Bosurgi, An ANN model to correlate roughness and structural performance in asphalt pavements, Constr. Build. Mater. 134 (2017) 684–693. doi:10.1016/j.conbuildmat.2016.12.186.

[319] L. Yao, Q. Dong, J. Jiang, F. Ni, Establishment of Prediction Models of Asphalt Pavement Performance based on a Novel Data Calibration Method and Neural Network, Transp. Res. Rec. 2673 (2019) 66–82. doi:10.1177/0361198118822501.

[320] N. Rakesh, A.K. Jain, M.A. Reddy, K.S. Reddy, Artificial neural networks - Genetic algorithm based model for backcalculation of pavement layer moduli, Int. J. Pavement Eng. 7 (2006) 221–230. doi:10.1080/10298430500495113.

[321] A.B. Goktepe, E. Agar, A.H. Lav, Advances in backcalculating the mechanical properties of flexible pavements, Adv. Eng. Softw. 37 (2006) 421–431. doi:10.1016/j.advengsoft.2005.10.001.

[322] G.H. Shafabakhsh, O.J. Ani, M. Talebsafa, Artificial neural network modeling (ANN) for predicting rutting performance of nano-modified hot-mix asphalt mixtures containing steel slag aggregates, Constr. Build. Mater. 85 (2015) 136–143. doi:10.1016/j.conbuildmat.2015.03.060.

[323] K. Gopalakrishnan, S.K. Khaitan, A. Choudhary, A. Agrawal, Deep Convolutional Neural Networks with transfer learning for computer vision-based data-driven pavement distress detection, Constr. Build. Mater. 157 (2017). doi:10.1016/j.conbuildmat.2017.09.110.

[324] S. Chatterjee, P. Saeedfar, S. Tofangchi, L. Kolbe, Intelligent Road Maintenance: a Machine Learning Approach for Surface Defect Detection, ECIS 2018 Proc. Res. Pap. 194. (2018) 1–16. https://aisel.aisnet.org/ecis2018_rp/194.

[325] H. Nhat-Duc, Q.L. Nguyen, V.D. Tran, Automatic recognition of asphalt pavement cracks using metaheuristic optimized edge detection algorithms and convolution neural network, Autom. Constr. (2018). doi:10.1016/j.autcon.2018.07.008.

[326] L. Zhang, F. Yang, Y. Daniel Zhang, Y.J. Zhu, Road crack detection using deep convolutional neural network, in: Proc. - Int. Conf. Image Process. ICIP, 2016. doi:10.1109/ICIP.2016.7533052.

[327] T. Saar, O. Talvik, Automatic asphalt pavement crack detection and classification using neural networks, BEC 2010 - 2010 12th Bienn. Balt. Electron. Conf. Proc. 12th Bienn. Balt. Electron. Conf. (2010) 345–348. doi:10.1109/BEC.2010.5630750.

[328] B. Li, K.C.P. Wang, A. Zhang, E. Yang, G. Wang, Automatic classification of pavement crack using deep convolutional neural network, Int. J. Pavement Eng. (2018) 1–7. doi:10.1080/10298436.2018.1485917.

[329] Y. Liu, J. Yao, X. Lu, R. Xie, L. Li, DeepCrack: A deep hierarchical feature learning architecture for crack segmentation, Neurocomputing. 338 (2019). doi:10.1016/j.neucom.2019.01.036.

[330] Y.J. Cha, W. Choi, O. Büyüköztürk, Deep Learning-Based Crack Damage Detection Using Convolutional Neural Networks, Comput. Civ. Infrastruct. Eng. 32 (2017). doi:10.1111/mice.12263.

[331] Z. Tong, J. Gao, Z. Han, Z. Wang, Recognition of asphalt pavement crack length using deep convolutional neural networks, Road Mater. Pavement Des. 19 (2018) 1334–1349. doi:10.1080/14680629.2017.1308265.

[332] H. Oliveira, P.L. Correia, CrackIT - An image processing toolbox for crack detection and characterization, 2014 IEEE Int. Conf. Image Process. ICIP 2014. (2014) 798–802. doi:10.1109/ICIP.2014.7025160.

[333] D. Seichter, M. Eisenbach, R. Stricker, H.M. Gross, How to Improve Deep Learning based Pavement Distress Detection while Minimizing Human Effort, IEEE Int. Conf. Autom. Sci. Eng. 2018-Augus (2018) 63–70. doi:10.1109/COASE.2018.8560372.

[334] M. Eisenbach, R. Stricker, D. Seichter, K. Amende, K. Debes, M. Sesselmann, D. Ebersbach, U. Stoeckert, H.M. Gross, How to get pavement distress detection ready for deep learning? A systematic approach, in: Proc. Int. Jt. Conf. Neural Networks, 2017. doi:10.1109/IJCNN.2017.7966101.

[335] R. Stricker, M. Eisenbach, M. Sesselmann, K. Debes, H.M. Gross, Improving Visual Road Condition Assessment by Extensive Experiments on the Extended GAPs Dataset, in: Proc. Int. Jt. Conf. Neural Networks, IEEE, Budapest, Hungary, 2019: pp. 1–8. doi:10.1109/IJCNN.2019.8852257.

[336] L. Some, Automatic image-based road crack detection methods, KTH Royal Institute of Technology, 2016. http://www.diva-portal.org/smash/record.jsf?pid=diva2%3A945233&dswid=-7141%0Ahttp://kth.diva-portal.org/smash/record.jsf?pid=diva2%3A945233&dswid=1058%0Ahttp://www.diva-portal.org/smash/get/diva2:945233/FULLTEXT03.pdf.

[337] H. Majidifard, P. Jin, Y. Adu-Gyamfi, W.G. Buttlar, Pavement Image Datasets: A New Benchmark Dataset to Classify and Densify Pavement Distresses, Transp. Res. Rec. J. Transp. Res. Board. 2674 (2020) 328–339. doi:10.1177/0361198120907283.

[338] H. Majidifard, Y. Adu-Gyamfi, W.G. Buttlar, Deep machine learning approach to develop a new asphalt pavement condition index, Constr. Build. Mater. 247 (2020) 118513. doi:10.1016/j.conbuildmat.2020.118513.

[339] G. Ciaparrone, A. Serra, C. Vito, P. Finelli, C.A. Scarpato, R. Tagliaferri, A Deep Learning Approach for Road Damage Classification, Adv. Multimed. Ubiquitous Eng. Notes Electr. Eng. 518 (2019). doi:10.1007/978-981-13-1328-8_84.

[340] A. Geiger, P. Lenz, C. Stiller, R. Urtasun, Vision meets robotics: The KITTI dataset, Int. J. Rob. Res. 32 (2013) 1231–1237. doi:10.1177/0278364913491297.

[341] and Y.J.Z. Lei Zhang , Fan Yang , Yimin Daniel Zhang, ROAD CRACK DETECTION USING DEEP CONVOLUTIONAL NEURAL NETWORK Lei Zhang , Fan Yang , Yimin Daniel Zhang , and Ying Julie Zhu, Icip. (2016).

[342] H. Maeda, Y. Sekimoto, T. Seto, T. Kashiyama, H. Omata, Road Damage Detection and Classification Using Deep Neural Networks with Smartphone Images, Comput. Civ. Infrastruct. Eng. 33 (2018). doi:10.1111/mice.12387.

[343] Y.J. Wang, M. Ding, S. Kan, S. Zhang, C. Lu, Deep Proposal and Detection Networks for Road Damage Detection and Classification, Proc. - 2018 IEEE Int. Conf. Big Data, Big Data 2018. (2019) 5224–5227. doi:10.1109/BigData.2018.8622599.

[344] A. Alfarrarjeh, D. Trivedi, S.H. Kim, C. Shahabi, A Deep Learning Approach for Road Damage Detection from Smartphone Images, Proc. - 2018 IEEE Int. Conf. Big Data, Big Data 2018. (2019)

5201–5204. doi:10.1109/BigData.2018.8621899.

[345] J. Singh, S. Shekhar, Road Damage Detection And Classification In Smartphone Captured Images Using Mask R-CNN, (2018). http://arxiv.org/abs/1811.04535.

[346] J. Hale, Deep Learning Framework Power Scores 2018, Towar. Data Sci. Artic. (2018). https://towardsdatascience.com/deep-learning-framework-power-scores-2018-23607ddf297a (accessed March 20, 2019).

[347] J. Hale, Which Deep Learning Framework is Growing Fastest?, Towar. Data Sci. Artic. (2019). https://towardsdatascience.com/which-deep-learning-framework-is-growing-fastest-3f77f14aa318 (accessed May 20, 2019).

[348] Tzutalin, labelImg, (2015). https://github.com/tzutalin/labelImg.

[349] W. Paterson, International roughness index: Relationship to other measures of roughness and riding quality, Transp. Res. Rec. J. Transp. Res. Board. (1986) 49–59.

[350] T. Fawcett, An introduction to ROC analysis, Pattern Recognit. Lett. 27 (2006) 861–874. doi:10.1016/j.patrec.2005.10.010.

[351] D. Chicco, G. Jurman, The advantages of the Matthews correlation coefficient (MCC) over F1 score and accuracy in binary classification evaluation, BMC Genomics. 21 (2020) 1–13. doi:10.1186/s12864-019-6413-7.

[352] l'Observatoire National de la Route, Rapport Observatoire National de la Route (ONR) 2019, Paris, 2019. https://www.idrrim.com/ressources/documents/11/7102-IDRRIM_Rapport_ONR-2019.pdf.

[353] L. Bertrand, P. Lepert, Relevé des dégradations de surface des chaussées : Méthode d'essai LPC n°38-2, Paris, 1997. https://www.ifsttar.fr/fileadmin/user_upload/editions/lcpc/MethodeDEssai/MethodeDEssai-LCPC-ME38_2.pdf.

[354] L. BERTRAND, M. Boutonnet, J. Cazeneuve, J. Chabrol, M. Dauzats, J.F. Griselin, A. Coquereau, J.P. Poilane, B. Robert, P. Lepert, others, Catalogue des degradations de surface des chaussees-Version 1998, Tech. METHODES DES Lab. DES PONTS CHAUSSEES-METHODE D'ESSAI LPC, Complement LA METHODE D'ESSAI NO 38-2. (1998).

[355] TensorFlow, TensorFlow 1 Detection Model Zoo, (2020). https://github.com/tensorflow/models/blob/master/research/object_detection/g3doc/tf1_detection_zoo.md (accessed July 21, 2020).

[356] R. Roberts, L. Inzerillo, G. Di Mino, Exploiting Low - Cost 3D Imagery for the Purposes of Detecting and Analyzing Pavement Distresses, Infrastructures. 5 (2020) 6. doi:10.3390/infrastructures5010006.

Appendix A

FastAI Model Setup:

Parameter setups:

```
dep_var = 'year'
cat_vars = ['zone', 'commercial_activities', 'unemployment' ,
'circ_road_den', ‘public_buildings’, ‘street_category’]
cont_vars = ['area','length', 'traffic_rate','tz_pop', 'tz_pop_den
','tz_workers', 'tz_arrivals', 'tz_depatures', 'tz_perdays_rt']
procs = [FillMissing, Categorify, Normalize]
test = TabularList.from_df(test_df,cat_names=cat_names, cont_names
=cont_vars, procs=procs)
valid = TabularList.from_df(val_df,cat_names=cat_vars, cont_names=
cont_vars, procs=procs)
data = (TabularList.from_df(train_df, path='.', cat_names=cat_vars
, cont_names=cont_vars,
procs=procs).split_by_rand_pct(valid_pct = 0.2, seed = 47)
                        .label_from_df(cols = dep_var, label_cls =
 FloatList, log = True)
                        .add_test(test)
                        .databunch())
```

Model setup:

```
learn = tabular_learner(data,layers=[50,10,1],ps=[0.01,0.01,0.1],m
etrics=rmse,emb_drop=0.05, callback_fns=ShowGraph)
```

Learning rate set up: `learn.fit_one_cycle(80, lr, wd=0.2)`

Catboost diagram:

```
shap_values = model.get_feature_importance(Pool(X_valid, label=y_vali
d,cat_features=categorical_features_indices), type="ShapValues")
expected_value = shap_values[0,-1]

shap_values = shap_values[:,:-1]

shap.initjs()

shap.force_plot(expected_value, shap_values[3,:], X_valid.iloc[3,:])
```

Summary of layers of Fastai model used:

```
TabularModel
==========================================================================
Layer (type)         Output Shape         Param #    Trainable
==========================================================================
Embedding            [3]                  12         True
__________________________________________________________________________
Embedding            [3]                  9          True
__________________________________________________________________________
Embedding            [5]                  40         True
__________________________________________________________________________
Embedding            [10]                 260        True
__________________________________________________________________________
Embedding            [5]                  40         True
__________________________________________________________________________
Dropout              [26]                 0          False
__________________________________________________________________________
BatchNorm1d          [9]                  18         True
__________________________________________________________________________
Linear               [50]                 1,800      True
__________________________________________________________________________
ReLU                 [50]                 0          False
__________________________________________________________________________
BatchNorm1d          [50]                 100        True
__________________________________________________________________________
Dropout              [50]                 0          False
__________________________________________________________________________
Linear               [10]                 510        True
__________________________________________________________________________
ReLU                 [10]                 0          False
__________________________________________________________________________
BatchNorm1d          [10]                 20         True
__________________________________________________________________________
Dropout              [10]                 0          False
__________________________________________________________________________
Linear               [1]                  11         True
__________________________________________________________________________
ReLU                 [1]                  0          False
__________________________________________________________________________
BatchNorm1d          [1]                  2          True
__________________________________________________________________________
Dropout              [1]                  0          False
__________________________________________________________________________
Linear               [1]                  2          True
__________________________________________________________________________

Total params: 2,824
Total trainable params: 2,824
Total non-trainable params: 0
```

Appendix B

Table showing distresses across different global manuals, Note: ø = Diameter, Des. = Descriptive definition

Distress	Manual 1	Manual 2	Manual 3	Manual 4	Manual 5	Manual 6	Manual 7	Manual 8
Longitudinal and Transverse cracking	L: width< 10mm M:10mm≥ width≥ 75mm H:width≥76mm	L:Mean width ≤ 6 mm M:Mean width > 6 mm and ≤ 19 mm or any crack with mean width ≤ 19 mm H- Mean width > 19 mm or any crack with mean width ≤ 19 mm	L:mean unsealed crack width < 5mm M:mean unsealed crack width 5-20mm H:mean unsealed crack width >20mm	L: Des. – slight noticeable cracks M: Des. – more perceivable larger cracks H: Des. – large distinct cracks	L:Width <2mm M:2mm> Width <10mm H:width> 10mm	L: affecting < 10% of area. M: affecting 10 – 20% of area. H: affecting > 20% of area	L: < 5mm width M: 5mm≥ width≥ 20mm H: >20mm width	L: < 1/4 in. width M: > ¼ in. width with no spalling H: >¼ in. width with spalling
Edge Cracking	L: Des. low cracking with no breakup M: Des. Medium cracking with some breakup and ravelling H: Des. significant breakup or ravelling at edge	Cracks located within 0.6m of edge L: Desc. - cracks with no breakup M: Des. Cracks with some breakup with material loss of up to 10% H: Cracks with breakup with material loss > 10%	Single cracks within 300mm of edge L: no spalling; mean unsealed crack width < 5mm M: moderate spalling; mean unsealed crack width 5-20mm H: severe spalling; mean unsealed crack width >20mm	No specific levels defined	Not mentioned	L: affecting < 10% of area. M: affecting 10 – 20% of area. H: affecting > 20% of area	L: < 5mm width M: 5mm≥ width≥ 20mm H: >20mm width	Not covered
Alligator Cracking (Fatigue cracking)	L: Desc. – observations of longitudinal cracks that are not spalled M: Desc. – observation of further development of light cracks H:Desc. – network of cracks that are well defined	L: Desc. – observations of longitudinal cracks that are not spalled M: Desc. – observation of further development of light cracks H:Desc. – network of cracks that are well defined and spalled	L: no L severity defined M: Desc. – observation interconnected cracks forming blocks H: Desc. – network of cracks that are well defined and spalled	L: set of cracks or meshes (thin meshes inferior to 30cm), forming a series of polygons and localized in the treads M: Significant cracks and meshs without fine rising L: excessive cracking with fines rising and material removal	L:Width <2mm M:2mm> Width <10mm H:width> 10mm	L: affecting < 10% of area. M: affecting 10 – 20% of area. H: affecting > 20% of area	Not mentioned	L: Desc. – observations of thin longitudinal cracks that are not spalled M: Desc. – observation of further development of light connected cracks H:Desc. – network of cracks that are well defined and spalled

Distress	Manual 1	Manual 2	Manual 3	Manual 4	Manual 5	Manual 6	Manual 7	Manual 8
Block cracking	L: Blocks defined by low level of longitudinal and transverse cracks M: blocks defined by med level of longitudinal and transverse cracks H: blocks defined by high level of longitudinal and transverse cracks	L: blocks with cracks with average width < 6mm M: blocks with cracks with average width > 6 mm and ≤ 19 mm H: blocks with cracks with average width > 19mm	Not covered	L: longitudinal and transversal cracks joining to form a network less than 2m M: network of cracks (mesh between 1 and 2m) H: significant network cracking >2m	L:Width <2mm M:2mm> Width <10mm H:width> 10mm	L: affecting < 10% of area. M: affecting 10 – 20% of area. H: affecting > 20% of area	Not mentioned	L: Block size 9ft^2 or greater with cracks < ¼ in. M: Block size 5ft^2 to 8ft^2 with cracks > ¼ in. H: Block size 4ft^2 or less with spalled cracks
Slippage cracking	L: Average crack width < 10 mm M: average crack width is > 10 and < 40 mm or surrounding area is spalled L: average crack > 40mm or surrounding area is broken into movable pieces	Not covered	Not covered	Not mentioned	Not mentioned	L: affecting < 10% of area. M: affecting 10 – 20% of area. H: affecting > 20% of area	Not mentioned	Not covered
Joint Reflective cracking (happens when asphalt has been laid over PCC)	L: non filled crack < 10mm or filled crack with any width M: non filled crack >10mm but <75mm or filled crack with secondary cracking H: non filled crack >75mm, or any crack filled or, a crack of any width where 100 mm approx.. of pavement around crack is severely raveled or broken	L: non filled crack < 6mm or filled crack with any width M: non filled crack >6mm but <19mm or filled crack with secondary cracking H: non filled crack >19mm, or any crack filled or, a crack of <19mm and adjacent pavement is severely cracked	L: crack width < 5mm M: mean unsealed crack width 5-20mm H: unsealed crack width >20mm	L: noticeable open seal M: open seal with cracks forming near L: open joint with excessive surrounding cracks	L: initial visible at joint cracking M: Locally open joints; initial secondary cracks and loss of material H: Open joints; extension of secondary cracks; aggregates fall apart.	L: affecting < 10% of area. M: affecting 10 – 20% of area. H: affecting > 20% of area	Not mentioned	Not covered

Distress	Manual 1	Manual 2	Manual 3	Manual 4	Manual 5	Manual 6	Manual 7	Manual 8
Ravelling or weathering	L: Desc. Aggregate started to wear away M: Desc. Worn away aggregate with rough surface texture H: significant worn away aggregate and very rough texture	No severity levels defined, measured in terms of affected surface area	L: no L severity defined M: Desc. - Worn away aggregate with rough surface texture H: Desc. - significant worn away aggregate and very rough texture	No specific severity levels defined	L: Desc. - loss of bitumen; some surface material loss M: Desc. - Open weaving; material loss; possible presence of thin cracks. H: Desc. - Disrupted surface; formation of holes. Aggregates can also detach into groups.	Considered as loss of surface texture L: Binder is between 2/3 up the aggregate and just below the top of the aggregate M: Binder just below the top of the aggregate L: Binder over the top of the aggregate	L: Desc. - Slight coarse aggregates loss, mainly In wheelpath M: Desc. – Very visible aggregate loss H: Desc. - Fully eroded surface and degradation in wheel paths	L: Desc. – aggregate/binder has begun to wear M: Desc. – aggregate/binder has worn away and texture is rough L: Desc. – significant aggregate/binder wear away with very rough texture
Depression	L: max depth of 13 – 25mm M: max depth of 25 – 50mm H: max depth > 50mm	Not covered as an individual distress	Not covered as an individual distress	No specific levels defined	L: Desc. - Barely visible deformations M: Desc. - Distortions clearly visible H: Desc. – substantial distortions to ride quality and Drainage compromised.	L:affecting < 10% of area M:affecting 10 – 30% of area H:affecting > 30% of area	L: depth < 20mm M: depth >20mm and <40mm H: depth >40mm	Not covered
Bumping/ Sagging	L: Desc. – causing low severity ride quality M: Desc. – causing med severity ride quality H: Desc. – causing high severity ride quality	Not covered	Not covered	L: depth of 0.5cm to 1.5cm M: depth of 1.5cm to 3cm H: depth > 3cm	Similar to depressions	Not covered but could be counted as a deformation with measurements as rutting	Not mentioned	L: 1/8 in. to 2in. per 10ft. M: 2in. to 4in. per 10ft. L: > 4in. per 10ft.

Distress	Manual 1	Manual 2	Manual 3	Manual 4	Manual 5	Manual 6	Manual 7	Manual 8
Shoving	L: Desc. – causing low severity ride quality M: Desc. – causing med severity ride quality H: Desc. – causing high severity ride quality	No severity levels defined, measured in number of occurrences and affected surface area	L: Desc. – causing low severity ride quality M: Desc. – causing med severity ride quality H: Desc. – causing high severity ride quality	Not mentioned	Not mentioned	L:affecting < 10% of area M:affecting 10 – 30% of area H:affecting > 30% of area	Not mentioned	Not covered
Swelling	L: Desc. – causing low severity ride quality M: Desc. – causing med severity ride quality H: Desc. – causing high severity ride quality	Not covered	Not covered	L: swell of 1-3 cm M: swell of 3-5 cm H: swell > 5cm	Not mentioned	Not covered but could be counted as a deformation with measurements as rutting	Not mentioned	Not covered
Lane/shoulder drop off	L: difference in elevation between the pavement edge and shoulder is > 25 mm and< 50 mm M: difference in elevation is > 50 mm and < 100 mm H: difference in elevation is > 100 mm	No severity levels defined, not measured but just a note of distress presence is made	Not covered	No specific levels defined	Not mentioned	Not covered	Not mentioned	L: Desc. - ravelling at edge M: Desc. - patching at edge H: Desc. - edge lane < 10ft.
Rutting	L:depth of 6 to 13 mm M:depth >13 to 25 mm H:depth >25 mm	No severity levels defined and measurements of depth recorded	L:depth < 10 mm M:depth of 10 to 20 mm H:depth > 20 mm	L:noticeable depth of 5 to 15 mm M:significant depth of 15 to 30 mm H:deep rut depth > 30 mm	L:depth<15mm M: depth>15 to <30mm H:depth> 30mm	L:affecting < 10% of area M:affecting 10 – 30% of area H:affecting > 30% of area	L: < 10mm depth M: 10mm≥ depth≥ 20mm H: >20mm depth	L: ¼ in. to ½ in. depth M: ½ in. to ¾ in. depth H: over ¾ in. depth
Corrugation	L: Desc. – causing low severity ride quality M: Desc. – causing med severity ride quality H: Desc. – causing high severity ride quality	Not covered	Not covered	No severity levels defined	Not mentioned	L:affecting < 10% of area M:affecting 10 – 30% of area H:affecting > 30% of area	Not mentioned	L: 1/8 in. to 2 in. per 10 ft. M: 2in. to 4in. per 10 ft. L: > 4in per 10ft.

Distress	Manual 1	Manual 2	Manual 3	Manual 4	Manual 5	Manual 6	Manual 7	Manual 8
Potholes	L:depth: 13 to ≤25mm and ø <450mm or depth: 25 to ≤50mm and ø <200mm M:depth 13 to ≤25mm and 450mm>ø>750mm **or** depth >25mm to ≤50mm and 200mm<ø<450mm **or** depth:>50mm and 200mm<ø<450mm H:depth > 25mm and ≤50mm and 450mm< ø <750mm or depth:> 50mm and 450mm< ø<750mm	L: < 25 mm deep. M: 25 to 50 mm deep. H: > 50 mm deep.	L:area > 175 cm² (~150mm ø) and < 25mm deep M:area > 175 cm² (~150mm ø) and 25 to 50mm deep H:area > 175 cm² (~150mm ø) and > 50mm deep	L: ø < 150mm M: ø > 150mm H: -	L:ø<100mm and depth <50mm M:100<ø<300mm and depth <25mm H:ø>300mm and depth >25mm	Measured in terms of the area affected but grouped under current required 'maintenance patching'	L: <200mm diameter M: 200mm≥ diameter≥ 300mm H: >300mm diameter	Potholes are considered as high severity alligator cracking and need to be noted in the comments area of field forms.
Bleeding and Pumping/ Flushing	L:Desc. – slight degree with no sticking asphalt M: Desc. Asphalt sticking to shoes/vehicle for short periods H: Desc. Asphalt sticking to shoes/vehicle for long periods	No severity levels defined, measured in terms of affected surface area	L: no L severity defined M: Desc. Clear observation of free excess asphalt H: Desc. Pavement has wet look with clear tyre marks	L: area of degradation less than 0.5m square (isolated phenomenon) M: area of degradation between 0.5m square and 5m square, localized and random on tread L: surface greater than 5 m square and generalized to the two treads (the rise of the binder is accompanied by degradations of the deformation type)		Not covered	L: < 25% of affected surface. M: < 50% of affected surface H: > 50% of affected surface	L: Desc. – minor amount of aggregate covered by excess asphalt M: Desc. – significant amount of surface aggregate covered with excess asphalt L: Desc. – most of the surface aggregate covered with excess asphalt
Polished Aggregate	No levels defined, measured in terms of surface area affected	No severity levels defined, measured in terms of affected surface area	Not covered	No severity levels defined	Not mentioned	Not covered	Not mentioned	Not covered

Distress	Manual 1	Manual 2	Manual 3	Manual 4	Manual 5	Manual 6	Manual 7	Manual 8
Stripping	Not covered	Not covered	Not covered	L: low amplitude resulting in an increase in macro texture M: covering pavement whose depth can reach 1 to 2 cm H: covering pavement whose depth can reach 2 to 4 cm	Not mentioned	L: Desc. – minor loss aggregate particles M: Desc. – loss of aggregate particles in pockets L: Desc. – significant and widespread loss of aggregate particles	L: Desc. - Slight loss of coarse aggregates, mainly in the wheelpath M: Desc. – Very visible loss of large aggregates Leaving reg. holes H: Desc. - Fully eroded surface & degradation in wheel paths	Not covered
Patching/ Utility cuts	L: Des. – good condition path M: Des. - med deterioration of patch H: Des. – badly deteriorated patch	L: low severity distress of any type including rutting < 6 mm M: Patch has moderate severity distress of any type or rutting from 6 to 12 mm H: Patch has high severity distress of any type including rutting > 12 mm	Not covered	Not mentioned	L: Desc. – slight Intact patches, M: Desc. – larger patches noted near joint and edge H: Patches with excessive Cracking and distress	L: patching affecting < 10% of area M: patching affecting 10-20% of area L: patching affecting >20% of area	Not mentioned	L: Desc. - patch with any low severity distress M: Desc. - patch with any Med severity distress H: Desc. - patch with any high severity distress

Appendix C

- Kmeans coding used to carry out kmeans clusters based on IOU

```
- def kmeans(distress_detections, k, dist=np.median):
-     rows = distress_detections.shape[0]
-
-     distances = np.empty((rows, k))
-     last_clusters = np.zeros((rows,))
-
-     np.random.seed()
-
-     clusters = distress_detections[np.random.choice(rows, k,
- replace=False)]
-
-     while True:
-         for row in range(rows):
-             distances[row] = 1 - iou(distress_detections[row],
-  clusters)
-         nearest_clusters = np.argmin(distances, axis=1)
-
-         if (last_clusters == nearest_clusters).all():
-             break
-
-         for cluster in range(k):
-             clusters[cluster] = dist(distress_detections[nearest_
  clusters == cluster], axis=0)
-
-         last_clusters = nearest_clusters
-
-     return clusters
-
```